SMALL-SCALE HEAT-DRIVEN ADSORPTION COOLING

A Dissertation

Presented to

The Academic Faculty

by

Thomas Ryan Robbins

In Partial Fulfillment

of the Requirements for the Degree

Doctorate of Philosophy in Mechanical Engineering in the

School of The George W. Woodruff School of Mechanical Engineering

Georgia Institute of Technology

December 2014

SMALL-SCALE HEAT-DRIVEN ADSORPTION COOLING

Approved by:

Dr. Srinivas Garimella, Advisor

G.W. Woodruff School of Mechanical Engineering

Georgia Institute of Technology

Dr. William Koros

School of Chemical and Biomolecular Engineering

Georgia Institute of Technology

Dr. Samuel Graham

G.W. Woodruff School of Mechanical Engineering

Georgia Institute of Technology

Dr. Krista Walton

School of Chemical and Biomolecular Engineering

Georgia Institute of Technology

Dr. Sheldon Jeter

G.W. Woodruff School of Mechanical Engineering

Georgia Institute of Technology

Date Approved: June 26, 2014

ACKNOWLEDGEMENTS

I would like to thank my partner, Sophia for her patience and support. I would also like to recognize the many members of the Sustainable Thermal Systems Laboratory, who provided insight and guidance throughout my time on this project. Additionally, I would also like to thank the members of my committee, Dr. Samuel Graham, Dr. Sheldon Jeter, Dr. William Koros, and Dr. Krista Walton. And finally, I would like to acknowledge my advisor, Dr. Srinivas Garimella.

TABLE OF CONTENTS

LIST OF TABLES

LIST OF FIGURES

NOMENCLATURE

Symbols

A	Area [m^2]
c_p	Specific heat [J kg^{-1} K]
COP	Coefficient of performance [-]
D	Constant in the DA equation [-]
Diff	Change in diffusion coefficient [m^2 s^{-1}]
Dia	Diameter [m]
$\frac{dw_{ad}}{dt}$	Time rate of change of specific adsorption [kg kg^{-1} s^{-1}]
dx	Half the thickness of the node in the x direction [m]
E_0	Energy of interaction term [J kg^{-1}]
f_D	Friction coefficient [-]
F_o	LDF shape factor [-]
Fo	Fourier number [-]
ht	Convection coefficient [W m^{-2} K^{-1}]
h	Enthalpy [J kg^{-1} K^{-1}]
k	Thermal conductivity [W m^{-1} K^{-1}]
K_{ev}	Constant for evaporator heat transfer [W s kg^{-1} K^{-1}]
K_{valve}	Head loss term for valves [-]
K_{ldf}	Linear driving force coefficient [s^{-1}]
$l_{f,ad}$	Assumed conduction length from fins to adsorbent [m]
L_{press}	Length for pressure drop [m]

L_{short}	Length that heat from thermal shorting penetrates into wall [m]
m	Mass [kg]
$\dot{m}$	Mass flow rate [kg s^{-1}]
n	Constant in the DA equation [-]
P	Pressure [kPa]
q	Quality [-]
Q	Heat transfer [J]
r	Radius [m]
R	Thermal resistance [K W^{-1}]
SCC	Specific cooling capacity [W kg^{-1}]
T	Temperature [ºC]
t	Time [s]
u	Internal energy [J kg^{-1} K^{-1}]
UA	Heat transfer conductance [W K^{-1}]
V	Volume [m^3]
Vel	Velocity [m s^{-1}]
V_{pore}	The pore volume [m^3 kg^{-1}]
w	Specific adsorption [kg kg^{-1}]
y	Width of node [m]
z	Height of node [m]

Greek Symbols

α	Thermal diffusivity [m^2 s^{-1}]

β	Interaction coefficient [K]
Δ	Change from one step to another [-]
η	Effectiveness [-]
σ	Stephan-Boltzmann constant [W m^{-2} K^{-4}]
ρ	Density [kg m^3]
ν	Specific volume [m^3 kg]

Subscripts and Superscripts

ad	Adsorbent
alum	Aluminum portion of the float
am	Ammonia
amb	Surrounding air temperature
c	Condenser fluid
cf	Coupling fluid
cooling	Total heat transferred into the evaporator
cond	Condenser structure
conv	Convection
e	Evaporator fluid
elec	Electrical heater
es	End structure
evap	Evaporator structure
f	Fin
finsl	The foam insulation of the float

fl	The fluid channel
g	Source temperature
half,cycle	The half cycle time
heat,in	Heat added to the adsorbent bed
hb	Heating block
hp	Heating pad
i	The spatial index in the model
i.d.	Inner diameter
ideal	Carnot efficiency
inf	The surroundings
ins	Insulation
interaction	Interaction between adsorbent and wall
is	The internal structure of the adsorbent bed
J	The time index in the model
K	Absolute temperature
mid	Middle of a node
node	Within a model node
o.d.	Outer diameter
os	Outer structure
plate	Heat transfer plates
rad	Radiation
reservoir	The fluid reservoir used in the float valve system
s	Heat sink

sad	Adsorbent bed heat sink
sat	At saturation conditions
shell	The outer wall of the float valve system
sp	Vapor space in the adsorbent bed
spreader	The heat spreader in the float valve system
surr	At the surrounding conditions

B1,B2 Two node names separate by a comma denotes transfer between those nodes

SUMMARY

There is more than 10^{10} GJ yr^{-1} of energy available as low temperature (50-150°C) waste heat in the United States, with similar amounts of heat available globally. At large scales, some of this heat is used in thermally driven cooling processes. However, many of the heat sources in this temperature range are too small to be used economically with existing technologies. This work investigates scaling heat driven adsorption heat pumps from 10s of kW to 10s W - 100s W of heat input. Utilization of heat sources at these scales opens up mobile adsorption cooling applications, solar cooling, and small-scale cooling off the grid. The activated carbon and ammonia adsorbent refrigerant pair is investigated in this work. From the literature, it is known that adsorption system performance degrades as the system scale is decreased. The present work seeks to identify and address the causes of that degradation with improved small-scale adsorbent bed designs. Detailed heat and mass transfer models are developed to aid in this design process. Small-scale adsorbent beds are designed to utilize heat input that ranges from 10-100 W and fabricated using the insight gained from these models. These prototype systems, the smallest adsorption heat pumps to date, are evaluated on an experimental facility designed and constructed as part of this work. Several iterations of bed designs are explored, with two concepts being identified as the most promising.

The first adsorbent bed has heat introduced into the center of the bed and is cooled on the external surface of the bed with natural convection. This allows the cooling coupling loop to be removed from the system, reducing the complexity and pumping power required. This center heated externally cooled (CHEC) system contains 35 g of

adsorbent material and is designed to use heat inputs ranging from 50 - 100 W. The bed has a volume of 85 cm^3 and the mass of the bed is less than 0.4 kg. The COPs for this adsorbent bed range from 0.002 - 0.007, while the specific cooling capacities (SCC) for the CHEC bed are 0.5 – 3.8 W kg^{-1}. An additional loss, due to condensation of the refrigerant outside the condenser, was identified in this design.

The second adsorbent bed uses a flat disc shaped bed (Flat Bed) that is alternately heated and cooled using a thermal switching technique developed in this work. This bed is designed so that it can operate autonomously using only the heat input without additional electronic control. The Flat Bed has 10 g of adsorbent, has a total mass of ~170 g, and operates on heat inputs ranging from 10 - 20 W. For the Flat Bed system, the COPs range from 0.01 - 0.03, the SCCs range from 9 – 30 W kg^{-1}, and the peak cooling is 4 W. For both systems, the average ambient temperatures are ~25°C and the evaporator temperature is 1-5°C below the ambient during cooling. The evaporator coupling fluid inlet temperature is ~0.3-0.4^oC below ambient. Lower cooling temperatures could be achieved with lower coupling fluid flow rates.

From the experimental and modeling work, four scaling factors are identified as the causes for reduced system performance: thermal shorting of heat around the adsorbent material that is then lost to the surroundings, increased inert masses due to fabrication limits at small scales, refrigerant condensation in undesired locations, and increased interaction between the adsorbent and chamber wall. Thermal shorting and undesired refrigerant condensation are identified as the primary causes for the lost performance. As much as 70% of the heat input can circumvent the adsorbent through thermal shorting and the cooling can be reduced by as much as 50% by condensation in connections. Some

strategies for addressing these limitations are discussed and recommendations are made for future improvements to systems at the 10-100 W heat input scale.

To allow adsorption technology to be easily adapted to the available heat sources, reductions in system complexity are explored. To remove the coupling fluid systems and pumps, the adsorbent bed designs investigated here are directly air coupled for cooling. Heat driven controls are investigated to eliminate the electrical load for the system entirely. Modeling and proof of concept testing is performed for these alternative heat driven controls and a thermal switching technique driven by adsorption bed weight is identified as the most promising approach. This control approach is tested in the Flat Bed system, and found to perform very close to the design conditions.

CHAPTER 1

INTRODUCTION

A considerable amount of thermal energy (>10^{10} GJ yr^{-1} in the U.S.) in temperatures ranging from 50-150ºC is discarded to the ambient each year (Rattner and Garimella, 2011). The amount of thermal energy in this low thermodynamic availability range is approximately twice as large as the amount of heat used for residential space heating in the U.S. annually (U.S. Energy Information Administration, 2009), but the use of this low availability, specially diffuse energy is extremely limited at this time, and the vast majority of this energy is rejected into the environment, serving no useful purpose. The potential for upgrading this low grade thermal energy to high exergy forms like electricity is limited by the second law of thermodynamics to low efficiencies. Instead, these thermal energy resources can be used more efficiently in thermally driven cooling cycles. Thermally driven cycles have been considered in other applications, where they have been used to provide chilled water, air conditioning, ice making or process heating through heat transformers. Thermally driven systems have been shown to yield total facility improvements in efficiency greater than 10%, by reducing the primary energy consumption that would be used for refrigeration systems (Garimella *et al.*, 2011). Unfortunately, the technologies and designs that are suitable for these applications are not useful for the majority of the available thermal energy resources. The more widely available designs require heat sources at a scale of >10 kilowatts, while there are many heat sources in the 50-100°C temperature range that can supply only tens or hundreds of watts.

To utilize these vast thermal resources, several technological hurdles must be overcome. Costs must be minimized, because the potential savings from any individual source are small. Cost reductions can be achieved by eliminating complex moving parts and expensive controls from thermally driven systems. Electrical inputs should be eliminated entirely to allow application to a broad range of heat sources and to eliminate the cost of batteries, circuitry, and/or electrical connections. Versatile, drop-in solutions must be developed that can be applied to a broad range of conditions, because customization for each source at these scales is simply not economical. Finally, systems should be designed in modular fashion to allow quick and simple scaling to a range of heat sources.

This work seeks to address these technological hurdles with the development of a thermally driven cooling system utilizing adsorption cooling technology. In this chapter, thermal resources are explored to demonstrate just a few of the possible applications of small-scale heat driven cooling. Then a comparison of available heat driven technologies, and the justification for the selection of adsorption cycles for this work is made. Some fundamental limits for a small-scale adsorption system's size, cooling capacity, and efficiency are established. Finally, an outline of this work is presented.

1.1 Small-Scale-Cooling Applications

Waste heat in the transportation sector represents more than half of the available energy in the low temperature range (Rattner and Garimella, 2011). There is a large amount of thermal energy available in transportation because more than half the energy of the fuel in automobiles and other transportation systems is transformed into heat rather than useful work. Meanwhile, automobiles require cooling for passenger comfort in the

summer and for dehumidifying the air for defrosting/defogging of windows in the winter. The coolant line exiting the engine is at an appropriate temperature to power heat driven cooling systems and, coupled with appropriate controls, the convection cooling already available in a moving vehicle can provide the cooling necessary to an adsorbent bed. In this way, air conditioning can be delivered to the vehicle by using waste heat, instead of by drawing power from the drive train. The proposed use of adsorption cooling for automobiles has been explored by several researchers (Boatto *et al.*, 2000; Lambert and Jones, 2006; Tamainot-Telto *et al.*, 2008).

Cooling technology increases quality of life in a number of important ways. The preservation of food is possible with refrigeration, greatly increasing the storage life and nutritional value of foods available to a community. A wide range of medical technologies become available with cooling because medicine, vaccines, and biological samples must be stored and transported in low temperature environments. Air conditioning can improve the comfort and air quality within buildings in a community. Conventional technologies for meeting these cooling needs require electricity, either as the primary driver of the cooling or for the operation of secondary systems (such as pumps). A system powered solely by low quality heat, without the use of electricity, expands the potential to meet the cooling needs in developing communities, where access to electricity is limited. Heat sources are already commonly available for cooking and heating, or may be provided by simple solar collectors that can provide sustainable heat sources. Additionally, a thermally driven system can be made mobile with reduced weight and cost to the system when the battery system can be replaced with a fuel heat source with much greater energy density.

In the cooling of electronics, large amounts of heat must be removed from processors and other sensitive components (Phelan *et al.*, 2002). Active cooling of electronics has been considered, but a conventional refrigeration system driven by compressors does not scale effectively to mobile electronic devices. There are also associated problems of vibrations from compressor based cooling systems, which can damage sensitive electronics. Heat driven heat pumps are well matched to meeting the low vibration needs of electronics, and secondary heat sources with lower heat fluxes in the same device can provide the heat necessary to drive these systems.

1.2 Thermal System Comparison and Limits

There are several technologies that allow thermal energy to be used to provide for cooling needs and a survey of appropriate technologies was conducted to identify the best candidate for small-scale applications. The candidate technologies considered in this survey are: conventional absorption heat pumps, the passive fully thermally driven Einstein diffusion absorption cycle, adsorption cooling, and thermoelectric devices. The advantages and disadvantages of these candidate technologies are discussed here. Several technologies are eliminated from consideration due to fundamental limitations that prevent them from being low-cost drop-in solutions at small scales. The remaining technologies are assessed and ultimately, adsorption is chosen as the best candidate for further investigation.

The evaluation of these systems was based on the overall system footprint, including such components as the control system, auxiliary systems, and coupling fluid pumps, which have typically not been included in theoretical assessments of such

systems. In many situations, these auxiliary systems are the determining factors in successful small-scale applications of these concepts.

An absorption cycle was examined first. In this system, refrigerant vapor is absorbed into a liquid at low temperature and low pressure. Heat is removed from the liquid to allow the absorption process to continue. The saturated liquid is then pumped to a high pressure, where it is heated and the refrigerant desorbs from the liquid. The refrigerant condenses in the condenser, as in a vapor compression system, before flowing through an expansion valve to the evaporator. From the desorber, the liquid with the lower concentration of refrigerant is pumped to the absorber where it absorbs the evaporated refrigerant to continue the cycle. Absorption systems often have high COPs compared to other heat driven systems. Large-scale systems delivering several hundred kW of cooling can have COPs in the range of 0.7 to 1.1 (Ryan, 2004). Small-scale systems have achieved COPs of 0.4 (Determan and Garimella, 2010). Another advantage is that absorption systems operate continuously, rather than periodically, and therefore deliver a constant cooling duty. However, an absorption system requires a pump for circulating fluid from the low pressure side to the high pressure side. Despite the high COPs, the necessity of the circulating pump prevents the system from being entirely heat driven and as the system is scaled down, it becomes increasingly difficult to eliminate complexity and reduce cost, because pumping systems are still necessary.

The Einstein cycle is an entirely heat driven cycle. It is very similar to the conventional absorption cycle, but operates at a single pressure with a carrier gas to achieve different partial pressures at different locations in the cycle. Absorption of ammonia into water is controlled by a surrounding vapor of hydrogen or helium that

changes the partial pressure of the refrigerant in the system, forcing it to condense or evaporate. The cycle uses a heat driven bubble pump to circulate fluids and requires no electric inputs. As such, it can operate solely on a thermal input. However, the efficiency of the Einstein cycle is very low. Current systems achieve a COP of about 0.1, despite ideal systems being predicted to deliver much greater COPs of around 0.4 (Delano, 1997). In some cases, COPs as high as 0.2 have been observed (Delano, 1998). A small-scale system delivering 50 to 70 watts of cooling using this cycle was demonstrated in previous work (Delano, 1998). The system weighed several kilograms. The Einstein cycle has been demonstrated to operate solely on a thermal input; however, the COPs are low and the system footprint is fairly large for the delivered cooling compared to other systems.

Adsorption cycles function very similarly to absorption systems; however, they differ in two significant ways: the adsorption system uses a solid sorbent rather than a liquid sorbent, and adsorption systems operate in a periodic manner. The solid sorbent and periodic operation increase the dynamic losses of the adsorption system compared to an absorption system. COPs for single-effect adsorption systems are in the 0.5-0.6 range (Critoph, 1996). The periodic nature also means that the delivered cooling fluctuates over time, which is usually undesirable. Adsorptions systems also have larger footprints than conventional systems, because adsorbent materials have a low density, requiring a large volume per unit mass of refrigerant. Additionally, void space is required to allow refrigerant flow, which further increases system size. They do not however require pumps or electrical input and a few examples of autonomous adsorption system have been proposed and demonstrated (Critoph, 1994a; Headley *et al.*, 1994; Hassan *et al.*, 2011).

Adsorption systems can use the lowest temperature sources of any of the technologies considered with driving temperatures as low as 45°C for some adsorbents.

Thermoelectric devices were also considered. Thermoelectric systems operate on the Seebeck effect, using sets of dissimilar conducting materials to convert a temperature difference between junctions into an electrical potential. Thermoelectrics can also operate in reverse using the Peltier effect, converting an electric current into a temperature difference by moving heat from one set of junctions to the other. A set of thermoelectric devices can then be used with a temperature source to act as a heat pump. Unfortunately, the performance of such devices is limited by the materials used to construct them (DiSalvo, 1999). With currently available materials, COPs for the cooling mode are limited to approximately 0.3 and when coupled with a thermoelectric generator capable of only 10% efficiency to provide the electricity, the overall COP for such a system would therefore be 0.03 in the ideal case (Tellurex, 2013).

Table 1.1 provides a summary of the different technologies considered. Based on a comparison of these heat-driven technologies, adsorption heat pump systems were chosen as the most viable candidate technology for the development of a small-scale drop in cooling solution. Absorption was ruled out due to the electrical requirements for pumps within the system. The COPs of thermoelectric devices are deemed too low to be viable for these applications. Compared with the Einstein cycle, adsorption systems offer better COPs and a smaller potential footprint. Adsorption systems are however not without disadvantages and a more in-depth introduction is provided in the following section.

Table 1.1 Technology Comparison

Technology	COPs	Scale	Footprint	Heat Only
Absorption	0.7-1.1	> 300 W	Moderate	No
Einstein Cycle	0.2 <	> 50 W	Large	Yes
Adsorption	0.5-0.6	> 1 kW	Large	Yes
Thermoelectric	0.03*	> 1 W	Small	Yes

*When heat driven

1.3 Overview of Adsorption Heat Pumps

Adsorption is used with waste heat to produce cooling on a large scale and has many appealing system properties. Figure 1.1 shows the Clausius-Clapeyron diagram of the ideal adsorption process. Adsorption systems operate cyclically and the cooling produced is periodic, occurring during the adsorption phase of system operation. The addition of multiple beds operating out of phase with one another can deliver nearly continuous cooling. Starting from state point 1, the adsorbent bed is cool and the refrigerant concentration is low in the adsorbent. The bed is at the same pressure as the evaporator and is continually cooled. As the temperature of the bed drops, refrigerant from the evaporator is adsorbed. The adsorption process releases heat, which is rejected to the heat sink. Adsorption continues until the minimum bed temperature is reached, state point 2, after which refrigerant transfer ceases and isosteric heating of the bed begins. The temperature and pressure of the bed increase until the condenser pressure is reached, state point 3. Isobaric heating at the condenser pressure begins and refrigerant is desorbed as the temperature increases. The refrigerant is transferred to the condenser during this phase, until the maximum bed temperature is reached and the refrigerant concentration in the adsorbent is low at state point 4. When the desorption phase ends, the bed is cooled isosterically until the bed reaches the evaporator pressure and is once again at state point 1.

In large scale adsorption systems, pumps and timed valves are used to control the heating and cooling of beds. These pumps are used only to increase the heat transfer rate to the bed; thus, the system function does not require pumps for the working fluid in a manner similar to what an absorption system requires. Due to its periodic nature, adsorption system performance is decreased due to dynamic losses as excess thermal mass is heated and cooled with each cycle. Therefore, limiting the thermal mass is essential for high performance.

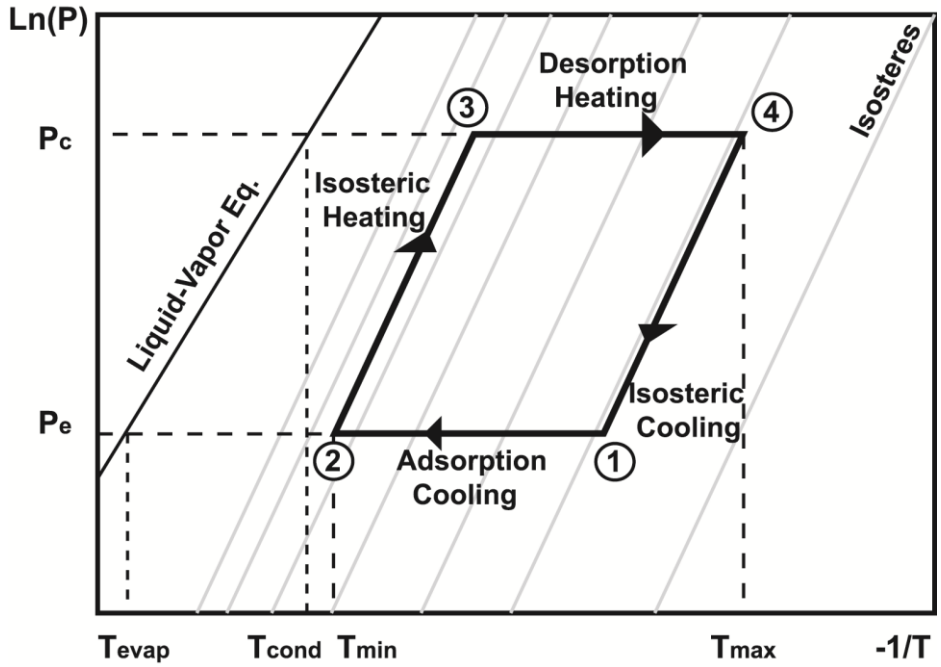

Figure 1.1 The ideal Clausius-Clapeyron equation based operation of an adsorption

Entirely heat driven operation has been demonstrated with solar driven adsorption systems, discussed in Section 2. Other advantages include having very few moving parts, high reliability, usability over a wide range of driving temperatures with proper adsorbent/refrigerant pair selection, and environmentally benign refrigerants (Wang and Oliveira, 2006).

The focus of the present study is to develop a small-scale cooling system driven by low quality heat using an adsorption cycle. Control techniques are proposed and investigated to provide the periodic heating required for the adsorbent system without electrical input. Modeling and experiments are conducted to characterize this system. The tools developed in this work can be used to scale adsorption systems over a large range of applications and for future designs of adsorption systems.

1.4 Design Size Approximation

Before investigating adsorption technology for small-scale drop in cooling, it is necessary to set some theoretical bounds upon the expected operation to justify the feasibility of this technology. Specifically, it is necessary to estimate the limits for the operating conditions because as the system is scaled down from MW and kW of cooling, the relative magnitude of the dynamic losses increases. The increase in dynamic losses is due to a number of factors. First, the shell or chamber of the adsorbent bed is almost entirely thermally isolated from the adsorbent in a large scale system, but as the system is scaled down the thermal resistance between the adsorbent and the bed shell decreases because the distance is greatly decreased and heat transfer through connections into the bed is significant. The contribution of the shell loss is significant, because it has a relatively large volume of material. This loss is mitigated somewhat by not undergoing the full temperature swing as many of the other thermal masses in the system do. Related to the losses due to the system bed are the increases in the end effects and the impact of connections on system performance. The decreased thermal resistance from the point of heat input through the bed means that heat can spread from connections into the bed around the ends of the system to the shell simultaneously with the heating of the

adsorbent. Finally, as the system is scaled down, the size of the components is limited not by the system pressure requirements, but by what is available commercially. This means that the system components are frequently thicker than is necessary, increasing the thermal mass and dynamic losses.

The cooling that an adsorbent system can deliver is limited by the mass of the adsorbent within the system. The considered adsorbent-refrigerant pairs are discussed in detail in Section 2.1.4. The adsorbent pair chosen for this work is activated carbon and ammonia. Critoph and Metcalf (2004) estimated the limit of the specific cooling capacity (SCC) of activated carbon to be approximately 2,000 W kg^{-1}. This SCC limit implies that a minimum of 25 grams of adsorbent are required to deliver the desired 10-50 W of cooling for this system. Measurements of activated carbon pellet packing density performed in the present study provide an estimated volume for this mass of adsorbent of approximately 32 cm^3, including the void space between the particles. The adsorbent bed structure undergoes some or all of the thermal swing of the cycle. The volume of the bed structure is of the same order of magnitude as the adsorbent and for this estimation the bed structure is assumed to be the same volume as the adsorbent material.

Based on these estimates, the maximum coefficient of performance (COP) that can be expected for a chosen bed structure material can be determined. For a volume of 32 cm^3, the mass of the structure of the bed will be 86.4 grams for aluminum and 256 grams for stainless steel. For these masses, the bed structure heat capacities are 77.8 J K^{-1} and 128 J K^{-1}, respectively. For preliminary estimates, it is assumed that the adsorbent and structure material undergo a temperature swing of 50ºC over the course of the cycle, which yields the energy input required to heat the structure in each cycle (and

subsequently, the amount of heat that must be removed) of 3,900 J for an aluminum bed and 6,400 J for a stainless steel bed.

The adsorbent is assumed to undergo a swing of approximately 50% of the total capacity seen in experimental work (Critoph, 1996) from 0.1 kg kg^{-1} to 0.25 kg kg^{-1} during the cycle. This means that the adsorbent bed will adsorb and desorb 3.75 grams in each cycle, allowing for 5140 J of heat to be removed from the evaporator in each cycle. The heat of adsorption is assumed to be 300 kJ kg^{-1}, and the sensible heating of the adsorbent is neglected for this approximation. The resulting heat input for the adsorbent bed in each cycle is approximately 10,200 J for an aluminum system and 12,700 J for a stainless steel system. The ideal COP for the small-scale system can be predicted based on these estimates to be approximately 0.51 for an aluminum system, and 0.41 for a stainless steel system. With these upper bounds for an adsorption system COP and SCC established, further examination of small scale systems is justified, although the actual system performance will be much lower due to heat transfer limits and the thermal mass of the structure and components.

1.5 Dissertation Organization

The organization of this work is as follows:

- Chapter 2. Literature pertaining to adsorption cooling system is reviewed. The focus here is on adsorption pairs, adsorption cooling technology, and autonomous adsorption cooling systems. Research needs are identified based on this review.
- Chapter 3. The system design and modeling approach for the adsorption system under consideration here is described. The results of the modeling effort and the influences on the development of the adsorption system are discussed.

- Chapter 4. The experimental facility and testing procedures are described. The evolution of the experimental system design is outlined.
- Chapter 5. The finalized adsorbent bed design and development is discussed.
- Chapter 6. The control system design is explained. Proof of concept testing and modeling are discussed. Conclusions are drawn from this testing and their impact upon system design is explained.
- Chapter 7. The testing of the experimental beds is described and system performance is evaluated.
- Chapter 8. The important conclusions from this work are presented and recommendations for future work are made.

CHAPTER 2

LITERATURE REVIEW

A review of the literature on adsorption was conducted to assess the present state of adsorption technology and to determine the areas where additional development is required to enable adsorption to be applied effectively to distributed low-temperature heat sources. First, refrigerant/adsorbent pairs were investigated to identify appropriate working pairs for the applications under consideration here. Next, adsorbent system designs were reviewed, with a focus on novel and autonomous systems. System and heat transfer control techniques were also investigated. Finally, relevant modeling approaches were investigated to guide and justify the modeling work done as part of the present study.

2.1 Adsorbent Pairs

The choice of refrigerant and adsorbent impact the operation range and performance of an adsorption system. Important properties for refrigerants include heat of vaporization, thermal conductivity, boiling point, reactivity and stability, toxicity, environmental impact, and freezing point. A high heat of vaporization is desirable because it allows the adsorption system size to be minimized and higher specific cooling capacity to be achieved by reducing the amount of refrigerant and adsorbent required for a given heat load. A low boiling temperature is desirable to allow the refrigerant to be used over a wide range of cooling applications; process cooling, air conditioning, refrigeration, or freezing. A low boiling point is also preferable because it leads to higher

operating pressures, which reduces the impact of pressure drop within the system and decreases the chance of system contamination due to air ingress from the surroundings. Chemical stability increases system life and allows a wider range of system materials to be used. Low toxicity and environmental impacts are important for user safety and life cycle impacts. A low freezing point is desirable because it prevents crystallization in the system that can clog or damage components.

Although it is important to optimize the properties of the refrigerant, it is crucial to choose an appropriate adsorbent because its properties generally determine the performance of a system. Important adsorbent properties are specific adsorption capacities, thermal properties, stability, susceptibility to contamination, and mass transfer properties (Wang *et al.*, 2010). The adsorption capacity establishes the amount of refrigerant that can be adsorbed in a cycle, which directly determines the cooling capacity of the system and indirectly affects the relative impact of dynamic losses for the system. In this work, the adsorption capacity is defined as the specific adsorption (kg kg^{-1}), kilograms of refrigerant adsorbed per kilograms of adsorbent. A good adsorbent should have high thermal conductivity to facilitate heat transfer, but a low specific heat to reduce the thermal mass, which contributes to dynamic losses. Adsorbent materials are susceptible to contaminants because of their adsorptive nature; during handling and preparation, they may be exposed to moisture or other contaminants that will be readily absorbed. It is necessary that the adsorbent does not bind strongly to these contaminants, because system performance will be degraded by their presence. Diffusion of refrigerant through the adsorbent is essential for the adsorption process, and good mass transfer is necessary to allow short cycles, which yield high cooling capacities.

There are different classes of adsorbents and the literature on the three types of common adsorbents used for heat pumps, physical adsorbents, chemical adsorbents, and composite adsorbents is discussed here. Some representative specific adsorption values are presented at the end of this section in Table 2.1.

2.1.1 Physical Adsorbents

Physical adsorption is a surface phenomenon, which relies on the interaction between the adsorbent surface and the condensing refrigerant molecules. For physical adsorbents to be effective, they must be porous and have large surface areas per mass, typically greater than 10^5 m^2 kg^{-1}. These large surface areas are present in materials that have appropriate structures such as zeolite and silica gel structures, or can be induced in a material through pyrolysis or chemical treatment, as with activated carbon. Because of their surface area interactions, physical adsorbents tend to be compatible with a large number of refrigerants.

Based on the results of numerous studies (Danica and Sing, 1961; Critoph, 1989b; Do, 1998; Sumathy *et al.*, 2003; Demir *et al.*, 2008; Wang *et al.*, 2009b), three adsorbent pairs are generally considered to be the best available: silica-gel/water for source temperatures of 45-100ºC, activated carbon/ammonia for applications with source temperatures of 70-130ºC, and zeolite/water for applications with source temperatures greater than 120ºC. The focus of this work is on activated carbon, because the temperature ranges match well with the intended sources.

Critoph (1988, 1989) numerically investigated refrigerant and activated carbon pairs. He determined that the two best refrigerants to pair with activated carbon are methanol and ammonia. Methanol was found to yield higher COPs, but ammonia has a

higher operating pressure, can achieve lower cooling temperatures, and higher heat of vaporization. Critoph concluded that the advantages of ammonia outweighed the higher COPs of methanol and he concluded that ammonia was the best refrigerant for use with activated carbon. Critoph (1996) later investigated activated carbon monoliths with ammonia, butane, and R32. Critoph found ammonia to be the best refrigerant among those he investigated. In a recent review of carbon adsorbent work, Askalany *et al.* (2012b), observed performance trends similar to those observed by Critoph (1989b, 1996) and concluded that methanol and ethanol refrigerants yielded the highest COP in activated carbon adsorption systems. Diethyl ether has also been investigated for use with activated carbon as a refrigerant. In one study, Al-Ghouti *et al.* (2010), concluded that diethyl ether would be a good refrigerant for adsorption heat pumps without any clear substantiation of this finding; however, the observed specific adsorption capacities were less than 0.01 kg kg^{-1}, which is too low to be effective.

Activated carbon comes from biological carbon sources that are activated through a number of thermal and chemical treatments. Many conventional activated carbon materials are derived from wood, but investigation into better activated carbons continues into other biological materials. Saha *et al.* (2008) investigated n-butane adsorption in activated carbon derived from pitch (Maxsorb III). They measured high pore volumes 1.79 x 10^{-3} m^3 kg^{-1} and surface areas of 3.25 x 10^6 m^2 kg^{-1}, and very high specific adsorption rates in this material approaching 0.8 kg kg^{-1}. This activated carbon was also investigated by El-Sharkaway with ethanol (2008) and with methanol (2009). Very high specific adsorptions were also observed for ethanol with a maximum near 1 kg kg^{-1} and the results matched very closely with modeling using the Dubinin-Astakhov equation

(Dubinin and Astakhov, 1971). Habib *et al*. (2010) also investigated adsorption of R134a and R507A into Maxsorb III activated carbon. Very large specific adsorption values were found for these refrigerants as well, over 1 kg kg^{-1}. Zeolite with water and activated carbon with methanol were compared by Cacciola and Restuccia (1995). They found that the zeolite performed better than the activated carbon for higher temperatures with sources approaching 200ºC because heating activated carbon to temperatures greater than 130ºC does not significantly increase the amount of desorption that occurs.

Related to activated carbon is activated carbon fiber. Activated carbon fiber has also been evaluated for use with cooling systems. The advantage of this adsorbent is that is can improve heat transfer and cooling capacity, because the fibers are more continuous than activated carbon pellets and so have better effective thermal conductivities. Attan *et al.* (2011) conducted a review of a broad range of activated carbon fiber and refrigerant pairs, including ammonia, acetone, methanol, water, CO_2, and ethanol. They concluded that although all of the refrigerants investigated can be used with activated carbon fiber, the highest COP is achieved when paired with ethanol.

Defining the limits for cooling capacity from adsorbent pairs is important. Glaznev and Aristov (2010) investigated the effects of adsorbent grain size on the cooling capacity of silica gel. They investigated the adsorption kinetics during very fast changes in temperature for silica gel grains of various sizes. Based on their experimental results, they predicted very high maximum cooling capacities (approaching 10 kW kg^{-1}) for grains bound directly to a metal plate in the adsorbent bed. Critoph and Metcalf (2004) investigated a flat-plate adsorption system design with very rapid heating and cooling of

the adsorbent material. They found that the upper limits of the specific cooling capacity achievable with activated carbon is of the order of 2,000 W kg^{-1} of adsorbent.

2.1.2 Chemical Adsorbents

Chemical adsorbents function differently than physical adsorbents. The adsorption action is achieved by chemical binding or dissolution of the refrigerant into the adsorbent material. Common chemical adsorbents are alkali metal-chloride salts paired with ammonia or water, such as $CaCl_2$/ammonia (Wang *et al.*, 2010). The uptake in the chemical adsorbents is not limited by the surface area of the material, which generally leads to higher specific adsorption rates when compared to physical adsorbents. Chemical adsorbents also have distinct transition regions where the equilibrium specific adsorption changes rapidly. This change reduces the dynamic losses and improves system efficiency (Wang *et al.*, 2009a).

The specific adsorption equilibrium values of alkali metal-chloride adsorbents were experimentally measured by Wang *et al.* (2009a) for use in adsorption systems with ammonia. Very large uptakes were observed for these adsorbents, with specific adsorptions approaching 1 kg kg^{-1} in some cases. Desorption temperatures varying from 40-80ºC were observed for these adsorbents. One of the most promising, $CaCl_2$, exhibited a change in specific adsorption of more than 70% of the maximum in a 10ºC range. An adsorption system utilizing $BaCl_2$ and $NiCl_2$ was modeled by Goetz *et al.* (1997). This system utilized a bed-to-bed design and displayed relatively low cooling capacities.

Less common chemical pairs including metal-hydride hydrogen pairs and a sodium-sulfur adsorbent system are discussed in the review by Srivastava and Eames (1998). These alternatives are not competitive with metal-chloride systems because the

specific adsorptions of these alternatives are much lower, yielding lower cooling capacities. There has been limited research on them for heat pumping.

Although chemical adsorbents do have distinct advantages, physical adsorbents usually have better heat and mass transfer properties and do not exhibit adsorption swelling and agglomeration, which is common in chemical adsorbent beds. The reduced heat and mass transfer limits the cooling capacities of chemical adsorbents. Mass transfer is further impeded by agglomeration over multiple cycles of adsorbent particles. Swelling during the adsorption process may damage or clog components or lead to adsorbent migration to undesirable locations (Wang *et al.*, 2005a). Because of these disadvantages, heat-driven chillers utilizing these adsorbents have been less common than those using physical adsorbents.

2.1.3 Composite Adsorbents

A number of composite adsorbents have been developed to address the performance limitations of pure adsorbents. Typically, these composites consist of a physical adsorbent and a chemical adsorbent. Physical adsorbents improve the heat and mass transfer properties of the chemical adsorbents while also limiting the swelling characteristics of the chemical adsorbents, while the chemical adsorbents improve the refrigerant uptake of the adsorbent pair. Many composite adsorbents have been identified and although experimental work is currently limited, there is increasing interest in investigating these materials.

Wang *et al.* (2005a) experimentally and numerically investigated metal chloride adsorbents and hybrid activated carbon/metal chloride adsorbents (Wang *et al.*, 2004a; Wang *et al.*, 2004b; Wang *et al.*, 2006) for ice-making applications with ammonia as the

refrigerant. They found that the activated carbon helped to limit the swelling problems normally experienced by the chemical adsorbents. They also noted significant improvements in COP and specific cooling capacity (SCC) for the composite adsorbents with improvements in SCC as high as a factor of ten. Zhong *et al.* (2007) similarly measured the adsorption of a $BaCl_2$/vermiculite hybrid and modeled the performance of a system using this hybrid adsorbent. Their model predicted a COP between 0.5-0.7 for driving temperatures between 56-67 ºC.

Chan *et al.* (2012) recently investigated zeolite impregnated with different concentrations of $CaCl_2$. The adsorbent performance was experimentally measured, and the system performance was modeled. When comparing the results to pure 13X zeolite, they found a nearly three-fold increase in specific adsorption capacity and a four-fold increase in the swing in specific adsorption. They also found an 80% increase in COP and a 34% increase in SCC compared with pure 13X.

Table 2.1 Some Representative Adsorbent Classification Studies

Author and Year	**Adsorbent**	**Refrigerant**	**Temperature Range**	**Specific Adsorption (kg kg^{-1})**
Zhong *et al.* (2007)	$BaCl_2$ in a Vermiculite host	Ammonia	42-55 ºC	0.05-0.4
El-Sharkawy *et al.* (2006)	Activated carbon fiber	Ethanol	25-55 ºC	0.2-0.7
Chan *et al.* (2012)	13X Zeolite with $CaCl_2$	Water	25-175 ºC	0.3 for 10% by weight solutions to 0.85 for 46% by weight solutions.
Aristov *et al.* (2002)	SWS (Silica Gel with LiBr and $CaCl_2$)	Water	70-130 ºC	0.7
Aristov *et al.* (2008)	SWS (Silica Gel $CaCl_2$)	Water	35-90 ºC	0.3
Wang *et al.* (2004b)	Activated carbon, $CaCl_2$, and composite activated carbon $CaCl_2$	Ammonia	30-60 ºC	Activated Carbon 0.3, $CaCl_2$ 0.9, and Composite 0.8
El-Sharkawy *et al.* (2008)	Activated carbon	Ethanol	20-60 ºC	0.18-1.0
Habib *et al.* (2010)	Activated carbon	R134a and R507A	20-60 ºC	R134a 1.6-1.0 and R507a 1.3-0.9
El-Sharkawy *et al.* (2009)	Activated carbon	Methanol	20-60 ºC	0.1-1.1
Saha *et al.* (2008)	Activated carbon	Butane	25-55 ºC	0.2-0.7

The temperature range represents the values at which the adsorbent classification was performed

Selective water sorbents (SWS) have also been developed by mixing chemical adsorbents with silica compounds. The silica compound is impregnated with the chemical adsorbent salt. Calcium-chloride and lithium-bromide were investigated as additives to micro and mesoporous silica (Aristov *et al.*, 2002) and were found to have improved water uptakes compared to pure silica materials. More recently, similar work from the same group (Aristov *et al.*, 2008) investigated SWS, a silica-$CaCl_2$ composite material, for adsorption with a 33.7% by weight $CaCl_2$ content. They predicted uptakes

approaching 0.3 kg kg^{-1} for this adsorbent material with maximum cooling capacities of 1 kW kg^{-1}, but with lower driving temperatures than previously observed for similar compounds.

Tso *et al.* (2012) modeled a composite adsorbent consisting of two physical adsorbents. They combined silica-gel and activated carbon and modeled its use in an adsorbent system for water chilling from 14 to 9 ºC. They found improved COP, 0.65, and SCC, 380 W kg^{-1}, compared with either of the pure silica-gel (0.49 COP and 245 W kg^{-1} SCC) and the pure activated carbon (0.41 COP and 189 W kg^{-1} SCC).

2.2 Adsorbent System Design

There are many design considerations for an adsorbent system. The majority of the studies on adsorption system designs have focused on a single- or double-bed system with an evaporator and a condenser. Considerations for such systems include: bed and heat exchanger design, system operation parameters, and heat and mass recovery mechanisms.

2.2.1 Heat Exchanger Design

Heating and cooling mechanics are of fundamental interest to improving the cooling capacity and size of adsorption systems. Many adsorbents are granular in nature and adsorbent beds are frequently packed with adsorbent pellets (Demir *et al.*, 2008). These beds exhibit poor heat transfer properties because void spaces between the adsorbent particles and contact resistances decrease heat transfer (Restuccia *et al.*, 2005). Adsorbent particles can be mechanically compacted or held together with a porous binder to create monolithic adsorbent materials that have improved heat transfer properties at the

expense of mass transfer properties (Tamainot-Telto and Critoph, 1997; Ziegler, 2002; Wang *et al.*, 2003; Critoph and Metcalf, 2004; Restuccia *et al.*, 2005; Chang *et al.*, 2009). Generally, an improvement in overall system performance is observed with the use of monolithic materials.

Many adsorbent systems incorporate heat transfer tubes interspersed with the adsorbent pellets or material in the beds. A common approach to improve the heat transfer performance of adsorbent beds is to include metal fins or extensions on the heat exchanger tubes, which improves the effective thermal conductivity of the bed (Hajji and Khalloufi, 1996; Demir *et al.*, 2008; Chang *et al.*, 2009; Demir *et al.*, 2010; Raymond, 2010; Rezk and Al-Dadah, 2012). There is a trade-off between the increased dynamic losses due to the fin mass and the increased heating and cooling rates of the adsorbent. When properly implemented, fins can increase both the COP and the SCC.

A less commonly used approach to improve heat transfer into the adsorbent material uses external heat transfer and internal refrigerant transfer. This has been achieved, for example, by packing the adsorbent into tubes of a shell-and-tube heat exchanger (Al-Ghouti *et al.*, 2010). This method does increase the heat transfer, but can increase the overall bed size and reduces mass transfer to the adsorbent.

Research has also been conducted to improve the heat transfer on the adsorbent side with convection. To overcome the limitations of the heat and mass transfer within the adsorbent bed, Critoph (1994b) investigated forced convection of the refrigerant vapor. This yielded only modest returns for the activated carbon and ammonia system, and lower returns would be expected for lower pressure refrigerants. In another attempt to capitalize on convective heat transfer, Wang *et al.* (2012) experimentally investigated

fluidized systems, where the adsorbent particles circulate through the bed. They measured rates of adsorption and desorption that were eight times higher than conventional systems, implying a drastic increase in cooling capacity. Fluidizing the bed, however, introduces a range of other technical challenges, such as reinforcing the bed and circulating the solid particles. This has limited their use so far; however, if these challenges can be overcome, fluidized beds could offer significant increases in system performance.

2.2.2 System Operation

In addition to investigation of heat exchanger design, a number of studies have been conducted on the operation of adsorption systems. A number of authors have investigated the effect of cycle length on two-bed adsorption system performance. Alam *et al.* (2000) studied a silica-gel/water system numerically. They found distinct peaks in COP and cooling capacities as the switching times are varied. Miyazaki *et al.*(2009) found that as the heat capacity is reduced, the optimum cycle times for both COP and SCC are shortened. Similarly, faster heat transfer also leads to a reduction in cycle times required to achieve peak COP and SCC (Saha *et al.*, 1995).

Wang *et al.* (2008) investigated the effect of variable temperature sources on the performance of a solar driven silica-gel/water system. They saw significant changes, between 3.7-7%, in the COP depending on how the temperature of the system and the source varied compared to the operation where the temperature was constant. Li and Wu (2009; 2009) investigated varying temperature sources and found that lower source temperatures during the desorption phase decreased the cooling capacity, but occasionally yielded higher COPs, while increasing the temperature over the desorption

phase led to a decrease in both cooling capacity and COP. Variations in cooling load were also considered and the average cooling load over a cycle was found to be more important for predicting system performance than the variations in the cooling load over time. Transient effects on system performance were modeled and experimentally validated by Chua *et al.* (2004) for a two-bed silica-gel water chiller system. It was found that regardless of the initial mass distribution within the system, it reached periodic steady state performance within five cycles. The cycle time was also investigated, and SCC and COP trends similar to those noted by other researchers were observed.

2.2.3 Heat and Mass Recovery

Gains in system performance can be achieved with mass and heat transfer recovery between adsorbent beds. Mass recovery is achieved by allowing the pressure between beds to equalize before changing phases, which increases the desorption in one bed while increasing the adsorption in the other. Heat recovery is achieved by transferring heat from the hot bed to the cold bed, usually with an additional heat transfer loop between the beds, before switching phases. This achieves a pre-heating and pre-cooling of the bed before external heat input begins, and also helps to limit the effects of dynamic losses on system performance. Leong and Liu (2004) investigated a zeolite/water system with heat and mass recovery. Their models predicted COP improvements of over 45% in a two-bed system, but predicted a reduction in system cooling capacity due to the additional time required for heat recovery. An increase in COP and SCC by 6% and 7%, respectively, were predicted with just mass recovery. The mass recovery took less than 1% of the total cycle time in this system. The same authors later extended their work with a parametric investigation of heat and mass recovery

(Leong and Liu, 2006). They again found that heat recovery improves COP while decreasing the SCC of the system, and established a degree of recovery to evaluate the percentage of total available energy recovered. They concluded that energy recovery beyond 90% caused a severe reduction in SCC with limited increases in COP. Wang and Chua (2007a) experimentally and numerically investigated two different heat recovery methods for a two-bed silica-gel water system. This system employed both a hot and a cold water reservoir for the heating and cooling of the adsorbent beds. The first heat recovery method circulates water from the cooling reservoir through the hot bed before returning the water to the hot water reservoir and vice versa during the heat recovery for the phase. During normal operation, the water returns to the same reservoir from which it was drawn. The second method flows water through the hot bed and then through the cold bed when the system phase changes. The two methods increased the system COP without significantly decreasing the SCC.

Heat and mass recovery in a four-bed system was investigated by Ng *et al.* (2006). This work found that the additional beds allowed heat recovery to improve the system COP without reducing the SCC. An approximately 30% improvement in efficiency was achieved in this system and because of the nature of the system, heat recovery was achieved with only minor modification to the valve control system. A two-bed, two-condenser, and two-evaporator heat and mass recovery process was explored experimentally by Chen *et al.* (2010). They removed the check valves usually used in a system to regulate the flow from the evaporator and condenser and instead actively controlled the valve to improve the heat and mass recovery. They noted improved system performance but did not quantify the amount of improvement.

Heat recovery has also been investigated using a thermal wave that propagates through the adsorbent bed by various authors (Shelton *et al.*, 1990; Pons *et al.*, 1996; Sun *et al.*, 1997; Critoph, 1998; Ziegler, 1999; Sward *et al.*, 2000). The thermal wave causes one portion of the bed to reach the full desorption temperature before the next portion of the bed begins to be heated. Because the heat transfer fluid and bed have a distinct temperature front and the fluid leaves at very near the initial bed temperature until very near the end of the phase, a reheat process may be used on the heat transfer fluid so that the only heat required is to make up for the differences in the desorption and adsorption energy, as well as losses. Some researchers have reported a near doubling of system COPs from comparative systems without a thermal wave (Shelton *et al.*, 1990; Pons *et al.*, 1996). However, this increase in system performance is hard to achieve, because very high heat transfer rates are required to create an effective thermal wave, which typically decreases the cooling capacity. Additionally, re-adsorption in the unheated portion of the bed can dampen the effectiveness of this approach.

2.3 Novel Adsorbent System Designs

A number of novel adsorbent systems have been proposed and investigated. Such systems use designs that differ from the standard system through the number and arrangement of beds. They may also differ due to the arrangement of heat exchangers or operation of adsorbent beds. These system designs are discussed below.

2.3.1 Multi-Bed and Multi-Stage System Design

A number of different design approaches have been implemented to limit the cyclic losses in adsorption systems. Typically, two or three beds operating in alternating

cycles are used to limit cooling fluctuations over time. Some systems have investigated larger numbers of beds or staging of system levels where the evaporator of one system level provides cooling for the condenser of the next system level.

A novel three-bed, two-evaporator system was proposed and modeled by Miyazaki *et al.* (2010). The dual evaporator allows two beds to be adsorbing simultaneously, while a third is desorbing. A bed is connected to a low pressure evaporator and then when reaching near saturation conditions for that bed, it is connected to a high pressure evaporator and adsorption continues. COP for this system design increased by 70%, while SCC increased by 50% for this system design compared to a standard adsorption chiller working at the same conditions.

As the number of beds is increased progressively, an adsorption system approaches continuous operation. Large numbers of beds can be implemented with an adsorbent bed wheel where individual adsorbent chambers are rotated continuously. This set up was investigated numerically by Critoph (2002) for an activated carbon/ammonia system based on measurements from a single chamber with heat and mass recovery between the chambers. COPs approaching 0.9 were predicted for this arrangement.

Multi-stage adsorption systems frequently aim to improve efficiency with multiple cooling cycles arranged in cascading stages that transfer heat or refrigerant from one to another. The use of stages allows more efficient use of the adsorbent and reduces re-adsorption during the desorption processes. The improvement in efficiency is counterbalanced by increased cost and increased system complexity due to the additional beds and components. Akahira *et al.* (2005) investigated a two-stage, four-bed silica gel-water system with a detailed system model. They utilized a mass recovery phase in their

system and were able to improve the system performance compared to a similarly sized single-stage system. A two stage activated carbon cycle using R134a and R507A refrigerants in the two stages was investigated by Habib *et al.* (2011). The evaporator of the R134a cycle was connected to the condenser of the R507a system. The performance in this cycle was comparatively low, achieving COPs of only 0.04-0.1.

2.3.2 Bed-to-Bed Adsorption Systems

Some adsorption systems utilize mass transfer between adsorption beds, not for mass recovery, but for cooling or heating. In such systems, adsorbent beds replace the evaporator and/or condenser. Staging effects may also be achieved with bed-to-bed adsorption. Different adsorbents are used in each bed and as conditions change, the refrigerant equilibrium differences between adsorbents cause refrigerant movement throughout the system.

Alyousef *et al.* (2012) investigated a system using three beds with two different types of activated carbon-metal chloride composite adsorbents. Two different adsorbents allowed a step-wise adsorption process from one adsorbent to another. A similar two-stage chemisorption system was investigated by Xu *et al.* (2011). The system utilized two beds, one filled with manganese chloride, and the other with barium chloride with ammonia as the refrigerant. Cooling was delivered both at the evaporator and at the barium chloride bed. Heating of the manganese chloride desorbed the ammonia in the high temperature bed and exposure to the manganese chloride allowed desorption in the barium chloride bed. This system achieved a COP of 0.7 and a SCC of 225 W kg^{-1}, higher than what is normally observed for these adsorbents, but the delivered cooling was at two different temperatures, which was not accounted for in the calculation of the COP.

Several configurations were investigated by Li *et al.* (2012), including a bed-to-bed re-adsorption process. It was found that using a bed-to-bed system improved the cooling capacity of the system by delivering cooling at both the evaporator and first adsorbent bed, although at different cooling output temperatures. The bed-to-bed design was also made adaptable so that the process could incorporate internal heat recovery, depending on the desired output, or operate as a conventional system. The COP doubled when operating in bed-to-bed mode compared to conventional operation.

2.3.3 Hybrid Adsorption Systems

Hybrid adsorption systems that combine the adsorption cycle with other cycles have also been investigated. Such hybrid systems have been largely limited to the research realm. Early work at the end of the 19th century was done in this area by coupling an adsorption system with a compression system with heat and compressors providing power, but there has been limited work on such a pairing recently (Ziegler, 2002). More recent work on vapor compression systems has focused on in-line pairings of adsorbent materials and compressors with a common refrigerant (Askalany *et al.*, 2012a). These cycles operate primarily through a pressure swing process rather than a temperature swing, and will therefore not be discussed further in this work.

More recent work has considered pairing adsorption with thermoelectric systems. The thermoelectric system pumps heat between the adsorbent beds using an electrical input. Gordon *et al.* (2002) predicted COPs of 1.2 with a system model for this pair. A similar system was later experimentally investigated by Sinha and Joshi (2010). The system used a zeolite/water pair to cool electronics in high temperature applications. The thermoelectric device pumps heat between the beds, acting as a form of heat recovery.

This work achieved a relatively low COP (0.35) compared to what has been predicted by Gordon *et al.* (2002). These systems however are not heat driven, and depend upon an electrical input to the thermoelectric device.

2.3.4 Dual-Use Adsorption Systems

Adsorption systems have also been investigated as dual-use systems, which provide cooling and heating (Askalany *et al.*, 2012a). Thus far, these systems have been studied for simultaneous water heating and air conditioning. In these systems, the cooling of the adsorbent bed is used to provide water heating while heat is still rejected to the surroundings by a condenser. Several authors investigated this application and found improved overall energy utilization with these systems (Wang *et al.*, 2000; Chang *et al.*, 2009; Li *et al.*, 2012). There has also been interest in using adsorption systems for residential combined heating, cooling, and power generations systems. These systems are coupled to a gas-powered generator. A number of authors have investigated this implementation, both numerically (Leong and Liu, 2004, 2006; Jiang-Jiang *et al.*, 2010; Deng *et al.*, 2011) and experimentally (Kong *et al.*, 2005; Li and Wu, 2009). These systems have been found to be cost effective and to improve energy utilization from the primary energy source, but the present author is unaware of any successful commercial implementation.

2.4 System Control

The control of adsorption systems in aspects other than cycle time has not received much attention. System control is primarily achieved through actuation of valves

that switch heat transfer fluid paths through the system at fixed times. Some research has been done recently to investigate alternate system control criteria.

2.4.1 Autonomous Control

Normal adsorption system operation requires electronic controls and electrical power for heat transfer fluid pumping; however, research efforts have attempted to remove all electrical input. Using only heat inputs for control builds upon the appeal of the heat driven nature of adsorption technologies. However, due to the difficulties of achieving heat driven operation, there has been limited work on entirely heat driven systems.

One autonomous control method is to use the cyclic heating and cooling provided by solar radiation. Headley *et al.* (1994) examined a concentrated solar adsorption system with a half-cycle time of approximately 8 hours. The solar cycle provided the cyclic heating of the bed and the bed was allowed to cool in the evening and through the night. One kilogram of ice was produced daily with this process. The long cycle time and relatively small bed caused the specific cooling capacity of the system to be small, because the desorption process goes nearly to completion long before the heating phase stops. The COP of the system, including the collector efficiency, was between 0.007-0.02.

Critoph (1994a) also investigated a similar diurnal system with directly heated activated carbon. This system averaged approximately 20 Watts for 17 kilograms of adsorbent with COPs of approximately 0.05. More recently, Hassan *et al.* (2011) investigated a solar flat plate single-bed system that also used the solar cycle for system control. The adsorbent was heated directly by solar radiation to address some of the heat

transfer limitations of these systems. This bed had better efficiency than the value reported by Headley *et al.* (1994), but averaged only two Watts of cooling with very low specific cooling capacities.

2.4.2 Alternative Control Methods

Another control strategy implemented in adsorption systems is to use differing heating and cooling times for the adsorption bed. In a standard bed, the two phases are of equal lengths. Especially in two-bed systems, this allows the two beds to operate 180 degrees out of phase with one another to deliver more regular operation. Because the amount of heat duty and heat transfer rates are similar in both phases, equal phase lengths is an effective method for two-bed systems. However, if the heat transfer rates are very different for the two phases, it may be advantageous to change the relative lengths. Additionally, if the heating or cooling temperature is much beyond the range necessary for effective adsorption/desorption, additional heating or cooling may only increase dynamic losses. Fixed cycle times with equal phase lengths and differing phase lengths were investigated by Sapienza (2011). For the zeolite system investigated, it was found that for some cases, significant increases in COP and SCC, by as much as 15%, can be achieved by adjusting the ratio of adsorption/desorption times in this system.

Another investigation considered more directly controlling the system operation (Gräber *et al.*, 2011). This was done by actively monitoring several system parameters and determining the optimum cycle times for those conditions. This has the possibility of eliminating off-design operation losses, but does not consider the effects of variable source temperatures and makes the system susceptible to faulty readings.

2.4.3 Thermal Switching

Thermal control is commonly achieved using fluid circulation systems to increase the convection-side heat transfer coefficient. The forced convection greatly increases the convection coefficient, and bulk movement of the fluid movement allows heat to removed quickly (Incropera and DeWitt, 1996). The disadvantage of this approach is the need for constant energy input to circulate the fluid. Because this work explores directly coupling the system to the surroundings, system control through pumps was eliminated and alternatives were investigated. Investigation of alternate heat switching mechanisms has been largely limited to cryogenic and MEMS applications, usually on a small scale. In such systems, normal fluid heat exchangers cannot be applied.

Several types of heat switches have been investigated. Gas gap switches, developed for cryogenic applications, utilize a physical gap into which a conducting gas is pumped or from which gas is evacuated to achieve the desired thermal conductivity (Prina *et al.*, 1999; Catarino *et al.*, 2008). Experiments have determined that the thermal resistance ratio of the "on"/"off" for these switches must be between 150 and 200. Bimetallic temperature controlled switches have also been investigated for use as heat switches (Milanez and Mantelli, 2003). These systems use the different thermal expansion coefficients of the two metals to break thermal contact and increase thermal resistance. The "on"/"off" ratio for these systems is approximately 60. Bimetallic switches require relatively high driving temperatures to achieve switching. Microscale heat switches have been developed utilizing the induced deflection of gold beams to complete and break a thermal circuit. They achieve a change in thermal resistance of a factor of six (Hyeun-Su *et al.*, 2008). Xiaobao *et al*. (2010) also investigated a MEMS

variable resistor device utilizing the thermal expansion of low-melting-point alloy arrays to make and break a thermal connection. The change in thermal resistance observed in this work was not quantified. Thermoelectric materials with the electrical conduction path in parallel with the thermal conduction path have also been investigated as variable thermal resistors; however, they are limited by the figure of merit of the material. Current materials can achieve a change in thermal resistance of a factor of two (Min and Yatim, 2008). A similar concept utilizes the Peltier effect to pump heat and produce a large apparent thermal conductivity through the cell. A change in thermal resistance of a factor of 100 is observed using this technique (Szekely and Mezosi, 2006).

2.5 Small-Scale Adsorption

Generally, only adsorption systems that have capacities greater than 20 kW are considered "mature" adsorption technologies, although this is largely due to economic constraints (Gupta *et al.*, 2008). These larger scale commercial systems can achieve COPs of approximately 0.6-0.7. For the purposes of this work, small-scale systems are defined as adsorption systems specifically designed to delivering 10 kilowatts of cooling or less. Many systems in the literature meet the cooling criteria for a small-scale system, but have been used primarily to investigate other aspects of adsorption systems, such as new adsorbent materials. Because the focus of those works is not on the scaling effects and design of small-scale adsorption systems, they will not be discussed here. There are few investigations of smaller scale adsorption systems for air conditioning for residential or vehicular applications (Askalany *et al.*, 2012a). These systems do approach the SCCs observed in large-scale commercial systems, but there seems to be a transition range at the low end, where the cooling capacity drops as observed in small-scale laboratory

systems testing adsorption system components (Restuccia *et al.*, 2005; Yang *et al.*, 2006). The lack of data in this range makes it hard to confirm this observation, because the variations at these small scales could also be attributed to other design factors. The system performance also tends to decrease as the amount of cooling delivered decreases, which is most probably due to an increase in dynamic losses.

One of the first investigations of small-scale adsorption systems was conducted by Suzuki (1993), who modeled a zeolite-water system for automobile cooling. The modeled system consisted of 2 kilograms of absorbent and was driven by engine coolant fluid as the heat source. The model predicted that the system would deliver 2300 W of cooling; however, large volumetric heat transfer rates were assumed (on the order of 100 kW m^{-3} K^{-1}), which may be difficult to achieve in a real system. Residential adsorption systems utilizing solar heat to provide air-conditioning have been investigated by a number of authors. Clausse *et al.* (2008) investigated an activated carbon/methanol system for such an application. A maximum COP of 0.55 was achieved for this pair, which compares favorably with a large-scale system, but relatively high source temperatures were used to achieve this (130ºC), and the average COP for the system was only 0.49 due to the startup time and the solar-coupled nature of the system.

Restuccia *et al.* (2004) analytically and experimentally investigated a small-scale silica gel/$CaCl_2$ adsorption system with water as the refrigerant. The system had 1.1 kilograms of adsorbent and delivered 50-100 watts of cooling. This composite adsorbent achieved COPs between 0.1-0.6, but had cycles longer than 2 hours, implying long start up times.

Adsorption systems used in combined heating, cooling and power generation are considered small-scale by most authors. These systems use scaled down adsorption chillers that deliver ~10 kW of cooling with designs that are fundamentally the same as the large scale systems, but with lower capacities. Kong *et al.* (2005) experimentally investigated a combined cooling, heating, and power system that utilizes a small-scale adsorption system to provide cooling. This system had a cooling capacity of 6-10 kW, and was specifically intended for use in a combined cycle. With mass recovery, COPs between 0.3 and 0.34 for the cooling portion of the system were achieved. Similar results were obtained by Li and Wu (2009), with COPs in the range of 0.3-0.45 for cooling capacities ranging from 6-10 kW. Huangfu *et al.* (2007) experimented with another combined cooling and power system in a similar range, delivering 6-7 kW of cooling with COPs between 0.3 and 0.45.

An investigation of the effect of the system scale on system performance was conducted by Khan *et al.* (2007) for a two-stage silica-gel water system. The effect of system scale was investigated by varying the mass of adsorbent material within the adsorber beds from 4 kg to 80 kg, while maintaining the ratio of structural mass to adsorbent mass. In this study, the method used to calculate UA for heat transfer into the adsorbent leads to the UA being relatively high for lower adsorbent masses. Thermal losses and the adsorbent chamber mass were neglected in this model, which also leads to higher COPs at lower adsorbent masses, rather than lower COPs as would be expected with losses considered. The performance of the chiller still increases sharply as the adsorbent mass is increased until a maximum performance is reached, after which the efficiency slowly decreases.

A thorough consideration of adsorption system scaling effects could not be identified, therefore the scale of adsorption system effects on performance has been analyzed based on a survey of COP values available in literature. To better identify scaling effects, the system effectiveness was also considered. Considering the effectiveness helps to mitigate the impact of systems operating conditions by comparing the achieved COP with the ideal COP for a system at the same system operating conditions. The system effectiveness is calculated as follows:

$$\eta = \frac{COP}{COP_{ideal}} \tag{2.1}$$

The COP_{ideal} is determined for these systems using:

$$COP_{ideal} = \frac{\left(T_{g,K} - T_{s,K}\right)}{T_{g,K}} \frac{T_{e,K}}{\left(T_{sad,K} - T_{e,K}\right)} \tag{2.2}$$

Where $T_{g,K}$ represents the absolute temperature of the heat source, $T_{s,K}$ represents the absolute temperature of the cooling water to the condenser, $T_{sad,K}$ represents the absolute temperature of the cooling water to the adsorption bed, and $T_{e,K}$ represents the absolute temperature of the evaporator. In many systems $T_{sad,K}$ and $T_{s,K}$ are nominally the same because a common cooling source is used. Over time, these temperatures may fluctuate, especially the temperature of the evaporator, therefore the design delivered chilling temperature was used when possible. The ideal COP may be considered to be the thermal efficiency and does not account for pumping power or other power uses. The COP used for this calculation was the one stated by the authors or supplied by manufacturers for commercial systems. Therefore, the COP may or may not include additional system power usage and there may be some other variations in definitions used by different authors. When a range of values was presented for a system, average values were used.

Only data from experimental and commercial systems are included in this analysis. Modeling data were excluded because they often did not have a specific scale that was considered, and frequently exclude losses or thermal masses. Additionally, some modeling results found were concerned primarily with establishing upper bounds on performance for a pair and did not estimate achievable performance for a real system. Most of the data available at a range of scales were from silica-gel/water systems, because such systems have been extensively developed and are the most widely available commercial systems. The activated carbon data have been included to show that other physical adsorbents follow a trend similar to that observed for silica-gel/water and it is expected that similar analyses could be conducted if a broader range of data were available for these other adsorbents. Additionally, it is expected that similar trends exist in chemical and composite adsorbent pairs, but they would be shifted due to the higher average performance of those adsorbents overall. These type of systems were not considered in this analysis; therefore, the impact of heat and mass recovery, multiple-stages, and other differences in system design were not identified. Figure 2.1 shows the COP vs. cooling scale for the three working substance pairs considered. A clear trend can be observed for the silica gel/water system. A logarithmic regression was performed on the data to identify the relationship between the system scale and efficiency, as shown in Figure 2.1. The coefficient of determination value for this relationship was found to be 0.64. The COP decreases by approximately 0.07 for every order of magnitude reduction in system scale. This is an overall trend, and it is expected that eventually the system performance would plateau at the extremes of higher and lower scales. In general, for systems within two orders of magnitude of one another, differences in system type and

operating conditions play a larger role than scaling effects. It should be noted that the activated carbon/ammonia pair appears to have larger COPs than those for similarly sized silica-gel/water systems. This is partially explained by the difference in the ideal system COP due to the different operating temperatures of the two types of systems.

System effectiveness was also considered. The results for the effectiveness comparison are shown in Figure 2.2. The trend is very similar to the trend seen in the COP comparison, but has a smaller slope. Additionally, qualitatively it appears that the other physical adsorbents more closely match the effectiveness scaling trends observed in the silica-gel/water systems, but there are insufficient data to compare the pairs effectively. A regression was also performed for the effectiveness, and the coefficient of determination was found to be 0.58.

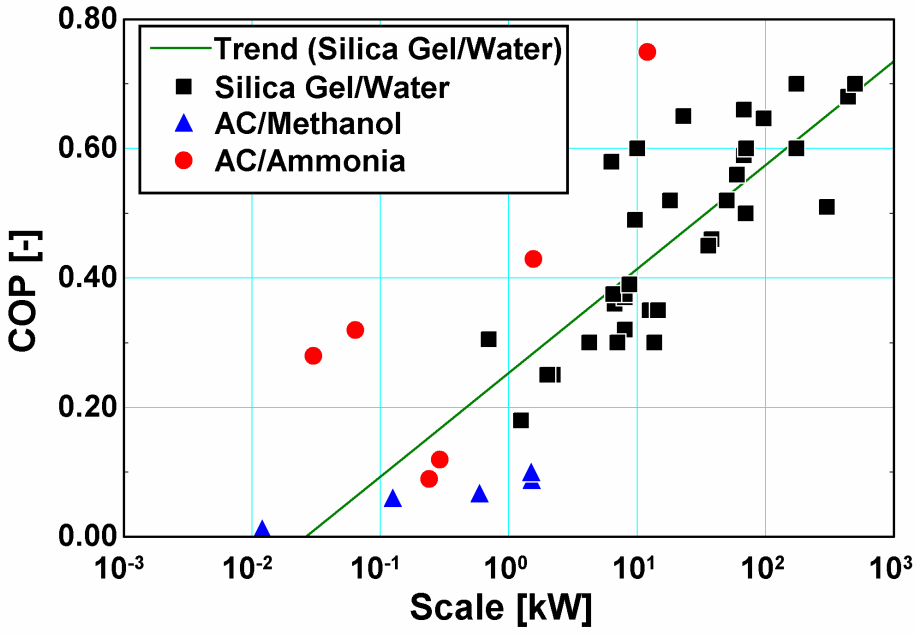

Figure 2.1 Scaling trends in adsorption systems. The trend line shows the scaling relationship for silica gel/water systems.

The additional variations in system performance are most probably due to differences in system design, materials, and whether the authors included auxiliary power systems in the calculation of COP. There is also some variation in how authors report system temperatures, with some reporting average temperatures and others reporting inlet temperatures. The variation in temperature reporting may help explain why the effectiveness is not as strongly correlated with scale as COP. Another source of variation is related to the system optimization approach, because a system designed to maximize the cooling capacity may be expected to operate at lower COPs than systems designed to optimize the COP. For a given system, the trend in COP is usually the opposite of the trend in cooling capacity observed for all systems.

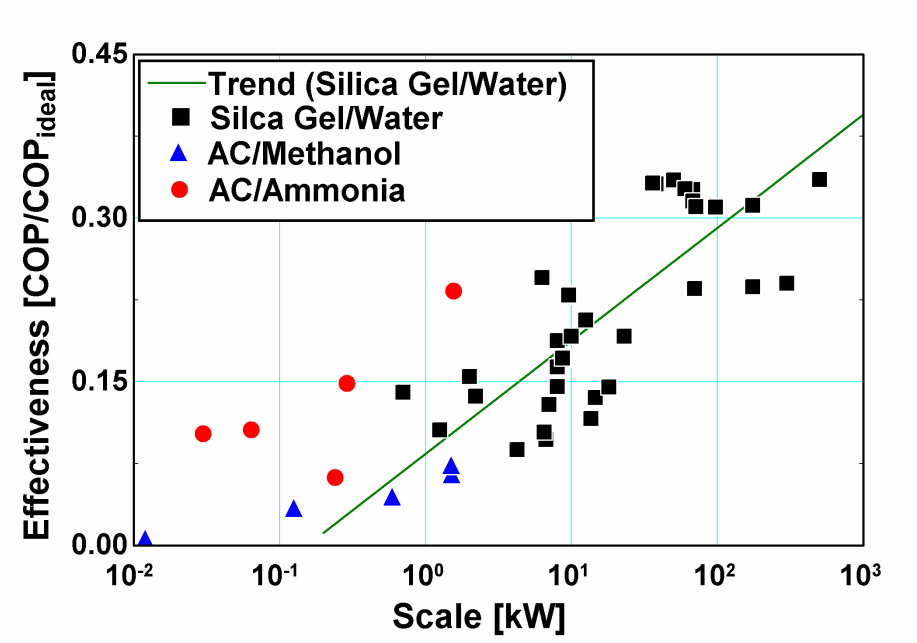

Figure 2.2 Scaling trends in adsorption systems. The trend line shows the scaling relationship for silica gel/water systems.

2.6 Adsorbent System Modeling

The modeling of adsorption systems is fundamental to the understanding of the process of adsorption, in system design, and in performance prediction. Because of the transient nature of the system, it is necessary to model adsorption systems on a transient basis, which is not as straightforward as in conventional refrigeration systems. This simplification and experimental validation of adsorption models are discussed in this section.

2.6.1 Linear Driving Force Analysis

The linear driving force model for adsorption dynamics has been employed in the models developed in the present study. The appropriateness of this model has been established by other authors previously. Scott (1994) developed the linear driving force (LDF) model to accurately approximate the transient adsorption process. The LDF model greatly simplifies the modeling of the system, allowing a mass transfer coefficient to be developed from the adsorbent geometry and properties. Raymond and Garimella (2009) compared the linear driving force model with a finite difference model for the adsorption kinetics. They developed an adsorption time coefficient for which the linear driving force method is valid and found good agreement for longer times. El-Sharkawy (2011) also evaluated the accuracy of the LDF equation and compared it with Fickian diffusion for silica-gel/water and $CaCl_2$/silica gel composites with water. He also confirmed good agreement between the two approaches and the time scale effects for short cycle times. The modified shell-core method and the general driving force model were compared with the LDF method by Yao and Tien (1998). They found that at low dimensionless times, the alternative methods are superior to the driving force method for all geometries, but at

higher dimensionless times, the LDF method is more accurate for slabs, the general driving force method is more accurate for cylinders, and the modified shell-core method is more accurate for spheres. The characteristic time for the system also affects the performance of the different models.

2.6.2 Experimental Validation

To ensure the reliability of models, it is important to experimentally validate the model results. Through experimental validation, the important parameters for accurate modeling of adsorption systems can be determined. Wang and Chua (2007b) compared experimental results for a two-bed silica gel-water system with lumped and distributed parameter models. Both models use the LDF mass transfer method and demonstrated good agreement with the experimental results. The computationally less intensive lumped parameter model was also demonstrated to be an effective means of modeling adsorption systems.

2.7 Research Needs

Table 2.2 presents a summary of many of the investigations discussed above with the corresponding system scale, operating temperatures and working pairs. Adsorbent pairs have been widely studied and characterized. There are still advances being made and recently introduced composite materials are likely to be more commonly used in future adsorption systems. The established adsorbent materials are capable of providing efficient adsorbent system operation and should meet the needs of small-scale, low-temperature cooling systems. Therefore, adsorbent materials are not identified as a research need for the present study.

As seen in the investigation of scaling effects in adsorption systems, low COPs are expected for the heating source considered in this study. Nevertheless, for 1 to 10 W of cooling, it is possible with good system design, the right operating conditions, and appropriate adsorbent pair selection to achieve COPs approaching 0.2. Despite the establishment of scaling trends discussed above, there has been limited research on adsorption systems at the very low end of cooling capacities. Most of the work investigating cooling in the 10 to 100 watt range found in the literature have been larger systems designed to test other facets of the system, or operating with cycle times well outside the optimized operation for such systems. These systems often have adsorbent loads of a kilogram or more with very low SCC. Such large adsorbent beds lead to systems that have large space requirements and increased complexity that make them unsuitable for drop-in cooling. Therefore, even though these test systems provide cooling at the same scale as could be achieved with available distributed heat sources in the 80-130ºC range, they are not appropriate for use with these heat sources. Systems specifically designed to operate with heat sources less than 1 kW while simultaneously minimizing the system size have not yet been developed. Therefore, research that demonstrates the performance of systems at this scale is needed.

Finally, autonomous adsorption systems have been demonstrated, but these systems had poor performance and did not effectively use the available heat. There is an opportunity to improve such systems. If successful, the gains made in this area will not be limited to small-scale systems, but can be applied over all system scales, particularly solar powered or other varying temperature source applications.

Based on the research needs discussed above, the present study seeks to demonstrate adsorption cooling at miniature scales. In conjunction with this, techniques for autonomous operation of adsorption systems are developed.

Table 2.2 Summary of System Performance Studies from Literature

Investigations and Comparisons of Adsorbent Pairs								
Author and Year	**Adsorbent**	**Refrigerant**	**COP**	**Scale**	**Temperatures ^{o}C**	**Experimental**	**Model**	**Notes**
Critoph (1988)	Activated carbon	Ammonia, Methanol, Others	0.5-0.6	N/A	T_g 80-140 T_s 25-30 T_e (-10)-(-5)		X	Theoretical limits of adsorbent pairs refrigeration. Some of this work republished in the 1989 article.
Critoph (1989b)	Activated carbon	Ammonia, Methanol, NO_2, SO_2, C_2NH_3, HCHO	0.2-0.6	N/A	T_g 80-140 T_s 25-30 T_e (-10)-(-5)		X	Concludes that methanol has the highest COP, but the best super atmospheric refrigerant is Ammonia
Cacciola and Restuccia (1995)	Zeolite 4A, Zeolite 13X, Activated carbon	Water (Zeolite) Methanol (AC)	0.5-0.8 (Zeolite) 0.2-0.6 (AC)	N/A	T_g 100 (AC) 175 (Zeolite) T_s 55 T_e 5		X	Numerically models different adsorbent pairs.
Critoph (1996)	Monolithic activated carbon	R32, Butane, Ammonia	0.4-0.6 (Am) 0.1-0.25 (R32)	N/A	T_g 100-250 T_s 30-60 T_e (-5)		X	Modeling of different refrigerants with monolithic carbon to assess performance.
Critoph and Metcalf (2004)	Activated carbon	Ammonia	0.25-0.35	N/A	T_g 200 T_s 30 T_e 15		X	Investigates a flat plate monolithic carbon design looking for the highest specific heats that could be achieved
Lu *et al.* (2006)	4:1$CaCl_2$ /Activated carbon	Ammonia	0.1-0.43	1.5 kW*	T_g 76-114 T_s 16-30 T_e (-20)-(-13)	X		They demonstrate higher specific cooling capacities than observed with other chloride salt adsorption pairs. Solar coupled heating.
Zhong *et al.* (2007)	$BaCl_2$ in vermiculite matrix	Ammonia	0.5-0.7	N/A	T_g 56-67 T_s 25-45 T_{sad} 20-37 T_e (-10)-10		X	Theoretical modeling of the performance of the system based upon the measured properties.

Table 2.2 (Cont.) Summary of System Performance Studies from Literature

Author and Year	Adsorbent	Refrigerant	COP	Scale	Temperatures °C	Experimental	Model	Notes
Saha *et al.* (2009)	Silica-gel/$CaCl_2$	Water	0.4	8 kW	T_g 80* T_s 30* T_e 10		X	A numerical comparison of a silica gel composite and pure silica gel. An improvement in COP and a significant improvement in SCC is observed.
Habib *et al.* (2011)	Activated carbon	R134a and R507A	0.04-0.08	1 kW	T_g 70 T_s 30 T_e -5		X	Exploration of activated carbon with refrigerant systems for cooling purposes.
Tso *et al. (2012)*	Activated carbon/Silica	Water	0.65	N/A	T_g 85 T_s 30 T_e 9		X	Modeled a composite adsorbent and predicted better performance than silica gel or AC by themselves
Studies of Adsorption System Operation and Design								
Saha *et al.* (1995)	Silica Gel	Water	0.14-0.22	0.25-2.20 kW	T_g 40-60 T_s 25 T_e 12	X	X	Investigates cycle time as well as silica gel water performance
H.T. Chua *et al.* (1999)	Silica-gel	Water	0.2-0.5	14.6 kW	T_g 86.3 T_s 31.1 T_e 14		X	Basic modeling of a two-bed silica gel/water system. Investigated the effects of cycle time and the effects of switching time.
Alam *et al.* (2000)	Silica-gel	Water	0.1-0.45	N/A	T_g 80 T_s 20 T_e 14		X	Analysis of switching frequency and heat exchanger design of a silica gel/water system, shows difference in peak COP and peak SCC.
Critoph (2002)	Activated carbon	Ammonia	0.44-0.91	300 W	T_g 170 T_s 36 T_{sad} 51 T_e 8.9		X	Modeling of a directly air coupled adsorbent wheel system. Very high COPs were achieved.
Akahira *et al.* (2005)	Silica-gel	Water	0.2-0.5	5-20 kW	T_g 70 T_s 30 T_e 7-14		X	Two-stage silica gel system, fixed cycle time.
Khan *et al.* (2007)	Silica-gel	Water	0.2-0.4	1.5-7 kW	T_g 60,80 T_s 30 T_e 14		X	An exploration of the effect of absolute adsorbent mass on the system performance.

Table 2.2 (Cont.) Summary of System Performance Studies from Literature

Author and Year	Adsorbent	Refrigerant	COP	Scale	Temperatures °C	Experimental	Model	Notes
Wang and Chua (2007b)	Silica-gel	Water	0.2-0.4	4-13 kW	T_g 70-85 T_s 30 T_e 10-17	X	X	Validation of lumped modeling parameters using experimental data and a comparison with distributed modeling parameters.
Khan *et al.* (2008)	Silica-gel	Water	0.2-0.3	1-4 kW	T_g 60 T_s 30 T_e 14		X	Investigates a 3-stage, 6-bed adsorption system. Remarkably low COP for such a system. Cycle times show operation much closer to peak cooling capacity.
Kubota *et al.* (2008)	Silica-gel	Water	0.2-0.3	1.8-2.6 kW	T_g 75 T_s 30 T_e 10	X		Investigates impact of a fin tube bed design on system performance.
Wang *et al.* (2008)	Silica-gel	Water	0.29-0.44	5.6-7.5 kW	T_g 60,70-77 T_s 30 T_e 20	X		Solar-driven system with varied cycle times and a time varying temperature source. When the rate of change of the temperature source is greater than a given value, the COP drops steeply (19% largest observed drop).
Miyazaki and Akisawa (2009)	Silica-gel	Water	0.58	6.3 W*	T_g 85 T_s 30 T_e 9-14		X	An investigation of heat exchanger design on the optimum switching time. Faster heat transfer results in shorter optimum cycle times, and reduced heat capacity leads to shorter cycle times.
Sapienza *et al.* (2011)	Zeolite	Water	0.2-0.6	140 W*	T_g 75-90 T_s 35 T_e 15	X		An experimental investigation of the effects of varying the ratio of adsorption/desorption phases.
Rezk and Al-Dadah (2012)	Silica-gel	Water	0.68	439 kW	T_g 79.7 T_s 33.4 T_e 5.8	X	X	An investigation of the impact of fin spacing and cycle time in a commercial scale system. A large focus on modeling with limited experimental validation

Table 2.2 (Cont.) Summary of System Performance Studies from Literature

Author and Year	Adsorbent	Refrigerant	COP	Scale	Temperatures °C	Experimental	Model	Notes
Raymond (2010)	Silica-gel Activated carbon fiber	Water (Silica-gel) Methanol (ACF)	0.53 (Silica) 0.41 (ACF)	1.94 kW (Silica-gel) 1.93 kW (ACF)	T_g 90 T_s 35 T_e 5		X	A detailed analysis of particle and bed sizing effects on system performance.
Heat and Mass Recovery Studies								
Shelton *et al.* (1990)	Zeolite	Ammonia	1.3-1.75 (heating) 0.3-0.75*	N/A	T_g 316 T_s 49 T_e 5		X	Modeling assessment of a thermal wave system design for a heat pump in heating mode.
Critoph (1994b)	Activated carbon	Ammonia	1.2-1.3	N/A	T_g 250 T_s 55 T_e 0		X	Investigates the efficiency of thermal wave systems.
Miles and Shelton (1996)	Activated carbon	Ammonia	0.48-1.0	5 kW 12 kW	T_g 230 T_s 38-30 T_{sad} 31-28 T_e 2-10	X		A gas-fired two-bed adsorption system with a focus on cost effectiveness and a thermal wave approach. High cooling COPs are achieved with very low cooling rates. Neglects electrical requirements.
Sun *et al.* (1997)	-	Ammonia*	0.2-0.85	N/A	T_g 260 T_s 40 T_{sad} 20 T_e 5		X	Modeling approach to a thermal wave system. They do not specify their working pair, but based on assumptions appear to be examining an ammonia refrigerant.
Sward *et al.* (2000)	Zeolite	Water	1.2	N/A	T_g 120 T_s 30 T_e 5		X	Modeling of a thermal wave system.
Leong and Liu (2004)	Zeolite	Water	w/out recovery 0.44 w/ 0.65	N/A	T_g 120 T_s 45 T_{sad} 25 T_e 6		X	Investigation of heat and mass recovery in a two bed system.

Table 2.2 (Cont.) Summary of System Performance Studies from Literature

Author and Year	Adsorbent	Refrigerant	COP	Scale	Temperatures °C	Experimental	Model	Notes
Leong and Liu (2006)	Zeolite (13X)	Water	0.4-0.65	N/A	T_g 120 T_s 25 T_{sad} 45 T_e 6		X	A parametric study of the effect of heat transfer rates and bed dimensions on heat and mass recovery. An extension of their previous work.
Ng *et al.* (2006)	Silica-gel	Water	0.25-0.35	10.2-17 kW	T_g 85 T_s 29.4 T_e 12.2	X		An experimental investigation of a four bed system with heat and mass recovery.
Wang and Chua (2007a)	Silica-gel	Water	0.2-0.4	4-13 kW	T_g 86.3 T_s 31 T_e 14.8	X	X	Investigated two schemes for heat recovery. One directs flow first through the hot bed then through the cool bed before being rejected. The second uses a pre-heating/cooling phase in which rejected water goes to a reservoir. Also modeled different system-level effects.
Chen *et al.* (2010)	Silica-gel	Water	0.49	9.6 kW	T_g 82.1 T_s 31.6 T_e 12.6	X		A novel heat and mass recovery scheme involving two condensers and evaporators at different temperatures.
Dual Use/Coupled Adsorption System Studies								
Kong *et al.* (2005)	Silica-gel	Water	0.3-0.34	6-10 kW	T_g 60-95 T_s 32 T_e 13	X		A combined heating, cooling, and power system. Utilizes a very standard two-bed silica gel-water system.
Huangfu *et al.* (2007)	Silica-gel	Water	0.3-0.45	6-7 kW	T_g 85 T_s 32 T_e 20	X		Investigation of a combined power, heating and cooling system. Similar results as other authors. Note the higher evaporator temperature.
Li and Wu (2009)	Silica-gel	Water	0.3-0.45	6-10 kW	T_g 56-80 T_s 30 T_e 20	X	X	Investigation of a combined power and heating system with adsorption cooling. Also investigated variable heat input.

Table 2.2 (Cont.) Summary of System Performance Studies from Literature

Author and Year	Adsorbent	Refrigerant	COP	Scale	Temperatures °C	Experimental	Model	Notes
Sinha and Joshi (2010)	Activated carbon	R134a and R507A	0.04-0.1	1 kW	T_g 70 T_s 30 T_e -10		X	Modeling of a two-stage cooling system using two different refrigerants for each stage to achieve freezing temperatures.
Adsorption System Evaluations								
Wang *et al.* (2000)	Activated carbon	Methanol	0.14 (Model) 0.06 (Exp.)	125W*	T_g 85-100 T_s 15-35 T_{sad} 10-25 T_e -10	X	X	Solar driven water heating and ice making adsorption system. The adsorption process provides heating for water. Cooling is averaged over an eight hour period, peak cooling is much higher.
Wang *et al.* (2003)	Activated carbon	Methanol	0.022-0.074	0.4-1.5 kW	T_g 110 T_s 30* T_e (-7)	X		A comparison of three different adsorbent beds. One has granulated carbon and the other two have consolidated carbon.
Restuccia *et al.* (2004)	Silica-gel/$CaCl_2$	Water	0.3-0.6	50-100 W	T_g 95 T_s 40 T_{sad} 20 T_e 10	X	X	Compares a small-scale experiment with a model. The cooling capacity is small, but they use 1.1 kg of adsorbent. The high COPs are due to the composite adsorbent.
Clausse *et al.* (2008)	Activated carbon	Methanol	0.49	2 kW	T_g 130 T_s 20-30 T_e 5-20		X	Model of a solar driven residential adsorption cooling system. Significant variations in efficiency and cooling capacity during the day.
Chang *et al.* (2009)	Silica-gel	Water	0.37	9 kW	T_g 80 T_s 30 T_e 14	X		A solar powered adsorption chiller system for Taiwan.
Xia *et al.* (2009)	Silica-gel	Water	0.39	8.7 kW	T_g 82.5 T_s 30.4 T_e 12	X		A comparison of two-bed adsorption chillers.

Table 2.2 (Cont.) Summary of System Performance Studies from Literature

Author and Year	Adsorbent	Refrigerant	COP	Scale	Temperatures °C	Experimental	Model	Notes
Miyazaki *et al.* (2010)	Silica-gel	Water	0.3-0.8	2.0-7.5 kW	T_g 75 T_s 30 T_e 7		X	A novel two evaporator water chiller system that utilizes two evaporator pressures to increase the amount of adsorption in a given bed. The evaporators step down the temperature of the incoming water.
Xu *et al.* (2011)	$MnCl_2$ and $BaCl_2$	Ammonia	0.7	2-3 kW	T_g 90-160 T_s 30 T_e 15		X	A two-bed system that uses desorption from the $BaCl_2$ to the MnCl to deliver cooling in two spots with a single heat input.
Alyousef *et al.* (2012)	Activated carbon fiber/$BaCl_2$ Activated carbon fiber/$MnCl_2$	Methanol	-	-	T_g 90* T_s 20* T_e -5*	X		Two $MnCl_2$ composites beds with a $BaCl_2$ composite bed. Ammonia is exchanged between the beds and cooling is performed at the $BaCl_2$ bed. The experimental results and conditions are not entirely clear.
Li *et al.* (2012)	$MnCl_2$ and NaBr	Ammonia	Bed-to-bed 0.72 Double-effect 0.61 Two stage 0.33	~700 W*	T_g 124,152 T_s 30 T_e -35, 3	X	X	Investigates an adaptable solar system utilizing two adsorbent beds loaded with different dessicant salts. Bed-to-bed, two-stage, and double-effect operation can be achieved depending on the system configuration.
Autonomous Adsorption System Investigations								
(Headley *et al.*, 1994)	Charcoal	Methanol	0.007-0.02*	1 kg of ice/ 8 hours, 12W*	T_g 74-154 T_s 26-32 T_e (-6)-6	X		Solar system that works on a daily cycle that is controlled by the sun. COP includes efficiency of the collector.
Critoph (1994a)	Activated carbon	Ammonia	0.32 (constant heating) 0.28 (solar)	64 W (constant) 30 W (solar)	T_g 103 (constant) T_g 93 (solar) T_s 20* T_e 0		X	Testing of a solar powered cooling device. Various insulations tested as well as steady heat inputs.

Table 2.2 (Cont.) Summary of System Performance Studies from Literature

Author and Year	Adsorbent	Refrigerant	COP	Scale	Temperatures °C	Experimental	Model	Notes
Hassan *et al.* (2011)	Activated carbon	Methanol	0.211	N/A	T_g Direct Solar Heat (120*) T_s 14-26* T_e 0*		X	Investigates direct solar heating of activated carbon. A model using real world solar irradiance values. Very low specific cooling capacity and very long cycle times.
Small-Scale Adsorption System Studies								
Tamainot-Telto and Critoph (1997)	Activated carbon	Ammonia	0.06-0.12	240 W*	T_g 91-110 T_s 20-40 T_e (-18)-11.8	X		Experimental investigation of monolithic carbon vs. standard carbon. A single bed experimental system is used, coupled to cooling systems and steam to maintain constant temperatures.
Restuccia *et al.* (2005)	Zeolite	Methanol	0.1-0.12	100 W	T_g 90 T_s 40 T_e 10	X		Experimental investigation of a compacted adsorbent in a bed. Small-scale testing for a several kiloton system.
Yang *et al.* (2006)	Silica-gel	Water	0.31	700 W	T_g 85 T_s 30 T_e 10	X		Design of a 1 kW adsorption room air conditioner. Experimental output lower than design.

*Estimated based upon information provided within the paper, but not explicitly stated by the author.
When a "normal" or "standard" case was provided by the author, those are the temperature and COP values listed. Otherwise the range of values tested in the work is provided. T_g, temperature of the heat source or desorption temperature, $T_{s,}$ temperature of the heat sink or cooling fluid stream, T_{sad}, temperature of the heat sink for the adsorbent bed if it is different than the condenser sink temperature, T_e, temperature of the evaporator or chilled water stream.

CHAPTER 3

ADSORPTION SYSTEM DESIGN

The methodology used for the design of the adsorption system is described here. To aid the design, a detailed heat and mass transfer model was been developed and is described here. The model structure description starts with a broad system level overview. Then the model is described more specifically on a component-by-component basis, and finally, the mechanics of fluid movement and mass transfer within the system are discussed. The designs developed during this investigation are then presented, and the results from the modeling of these designs are presented. Finally, the modeling is used to explore and develop the experimental procedure discussed in Chapter 4.

3.1 Design Methodology

The primary goal of this study is to demonstrate a working small-scale adsorption system (<100 g of adsorbent material) suitable for application to small-scale heat sources (<100 W) for the recovery of energy as useful cooling. To achieve that goal, it is necessary that the system be able to operate solely on a thermal input, as well as being economic, scalable, and easily fitted to existing systems. The design methodology weighs these factor more heavily than efficiency. Several design elements are proposed and tested to achieve the system goals including, direct air-coupled convective cooling the adsorbent bed to eliminate the cooling loop, and heat driven controls for the system.

In designing this system, it is necessary to consider several constraints of adsorption cooling technology and develop methods for addressing those issues. It is also

necessary to develop a detailed understanding of the system operation, particularly at the small scales being considered here, and to develop design tools to aid in system development. As established in the previous section, there is limited understanding of adsorption systems at this scale and a decrease in system efficiency is observed as the capacity of adsorption systems are reduced. Therefore, a detailed heat and mass transfer model of the adsorption system at the small-scale considered is necessary. First, a system was modeled using common adsorption design elements scaled down to act as a baseline for the design of the system. Then a variety of new system elements were tested using these common adsorption models, including directly convection coupling the bed to the surrounding and alternative control methods. Further discussion of the proposed control elements may be found in Chapter 6. The models developed here will be validated with experimental results.

3.1.1 Design Envelope

The design envelope is chosen to be representative of small-scale thermal resources (≤100W). The design conditions are used to choose both the modeling and experimental conditions. Temperature sources in the range from 70-100ºC are considered with heat fluxes from 10-100 W. Environmental temperatures in the range of 20-30ºC are considered for the heat sink for the adsorption bed and the condenser. The total adsorbent mass considered for the system is less than 100 g, so that a total system mass less than 1 kg can be achieved. An adsorbent bed that fits in an envelope ($50 \times 100 \times 200$ mm^3) is chosen to facilitate implementation of easily transportable units in modular fashion. It is expected that the performance will necessarily be significantly lower than the ideal

calculated in Section 1 due to limitations in heating and cooling the adsorbent, but the goal is to deliver cooling rates in the 5-10 W range.

3.1.2 Pair Selection

Activated carbon/ammonia was chosen as the working pair for this investigation. This pair has operation temperatures that fit well with the desired temperature source range and perform best in the temperature range from 80-150ºC (Critoph, 1989b). The activated carbon/ammonia working pair can operate at low evaporator temperatures and is therefore useful for a range of cooling conditions from sub-zero refrigeration to air conditioning. Activated carbon/ammonia pairs reviewed in literature demonstrated better performance than silica-gel/water at the lower scales, as described in Chapter 2, and tend to have higher cooling capacities, making them better suited for scaling a system down. Additionally, the above-atmospheric operating pressure means that the potential for ingress of air is reduced, and the effects of pressure drops between components are reduced compared to sub-atmospheric pressure refrigerants. The corrosive nature of the ammonia refrigerant with some materials of construction does pose some difficulty in the design of the system, but the corrosion is outweighed by the potential for better performance and higher operating pressure.

3.1.3 Adsorbent Bed Design Focus

The focus for the system design is placed on the adsorbent bed, as this is the component that governs the size of the system both in weight and volume. The evaporator and condenser are not explored extensively in this work. While the evaporator and condenser play important roles in the system, they are fundamentally two-phase heat

exchangers that are not unique to this system in operation. Because of the focus on the adsorbent bed, in the modeling, UA values are assumed for the evaporator and condenser, and in the experimental facility, tube-in-tube heat exchangers are used for the evaporator and condenser to make measurement of heat transfer rates more accurate. In an actual application, the evaporator and condenser would ideally be liquid-to-air heat exchangers.

The proposed changes and controls of the system as well as the testing focused on the adsorbent bed as well. The heat transfer into and out of the adsorbent material is vital to system operation and largely limits the system performance. Designs with new approaches to solving the heating and cooling problem in the adsorbent bed are explored. To allow the system to operate on only thermal energy, the reconsideration of the design of the control system for bed operation is also necessary. The main changes investigated for the adsorbent bed design are methods to directly air couple the adsorbent bed and methods to achieve the cyclic heating and cooling necessary for the bed using only actuation methods that are driven by system operation.

3.2 Modeling

The model used for design and evaluation of the system is discussed here. Three different adsorbent bed designs are considered in this work. The system model is explained using the baseline model that most closely resembles existing adsorption systems. The baseline system replaces the many heat transfer channels of a large scale system with a single heat transfer channel. In this small scale system, the outer structure of the adsorbent bed is in direct contact with the adsorbent, but is insulated using a layer of polymer insulation to limit the heat loss from the adsorbent. Also modeled are two alternative designs that have not been investigated in previous studies. The first is a

periodically heated bed where the bed is heated in the center and cooled on the external surface of the bed (hereafter referred to as the center heated externally cooled (CHEC) design), while the second is a thermal switch controlled adsorbent system (hereafter referred to as the Flat Bed system due to the bed geometry). The model framework was built for the baseline bed configuration. Section 3.7 explains how the alternate system models differ from those for the baseline.

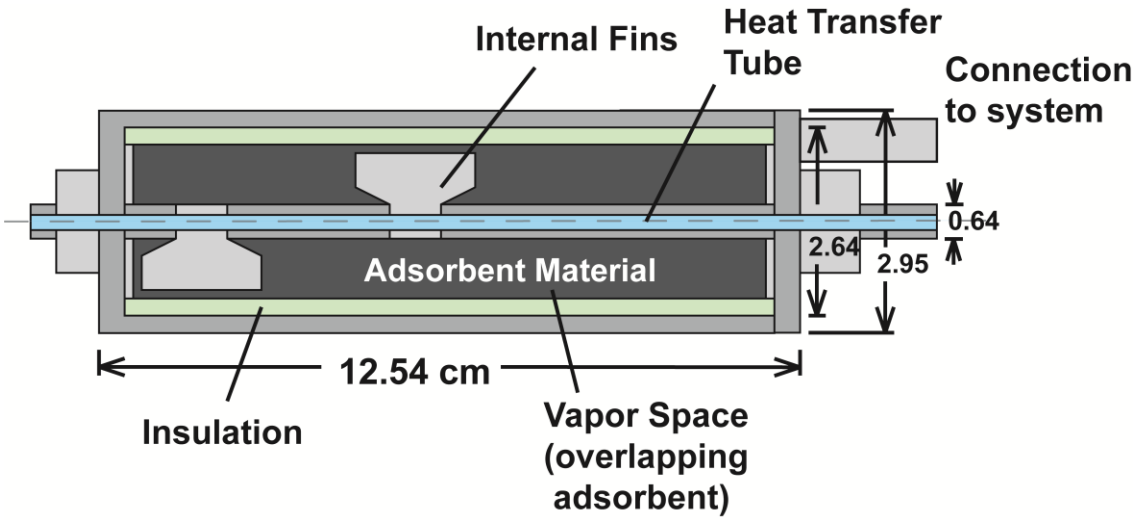

Figure 3.1 Schematic of the baseline system

3.2.1 System Overview

The system design envelope established the conditions for which the system is designed. For the model, the following specific conditions are considered as the baseline. Unless stated otherwise, the models presented use these conditions. The source temperature is 100ºC, while the sink temperature is 25ºC. The sink temperature is used for cooling of the adsorbent bed, cooling of the condenser in fluid coupling lines, as well as the ambient temperature condition to which losses from the system occur. The system model is developed for a baseline system design that is based on a representative unit of a conventional system with liquid coupling for the bed. This system geometry is based on

what can be achieved experimentally, and the model was refined to match the experimental geometries described in Chapter 5. The schematics for this bed are shown in Figure 3.1. A representative step from the system model is presented throughout this chapter to illustrate the model operation. This representative step is at approximately 750 seconds into the simulation, as the system switches from the desorption mode to the adsorption mode. The adsorption and desorption phases are 750 s in this sample case.

3.2.2 Model Structure

The adsorption system model is developed on the Engineering Equation Solver (Klein, 2009) platform. Figure 3.2 shows a diagram of the operation of the adsorption system model. As a transient system, information from the previous system state is used as the input for the following time step. In this model, the specific inputs are the previous temperature and refrigerant mass distribution. In each node, the volume is specified, and the mass of refrigerant in the node volume is divided by the node volume to determine the specific volume of the refrigerant in the node. The inert nodes representing the bed structure and walls do not contain any refrigerant mass. The adsorbent material and the vapor surrounding it occupy the same volume and the volume for these nodes is determined by the void fraction of the adsorbent material. The specific volume and temperature are used to determine the rest of the properties of the node, including the pressure, enthalpy, and internal energy. The property calculation is done using the Ammonia_MH function in EES which calculates properties for ammonia using the Martin-Hou Equation of State (Martin and Hou, 1955).

The properties are communicated to the equilibrium adsorption model, which determines the equilibrium uptake value within the adsorbent nodes. The equilibrium

model outputs and properties are passed onto the mass transfer section of the code that determines the transfer of ammonia within the system and the new mass distribution. The node property information is also used along with the initial temperature information and a thermal resistance network and the relevant thermal masses to determine the heat transfer during the time step.

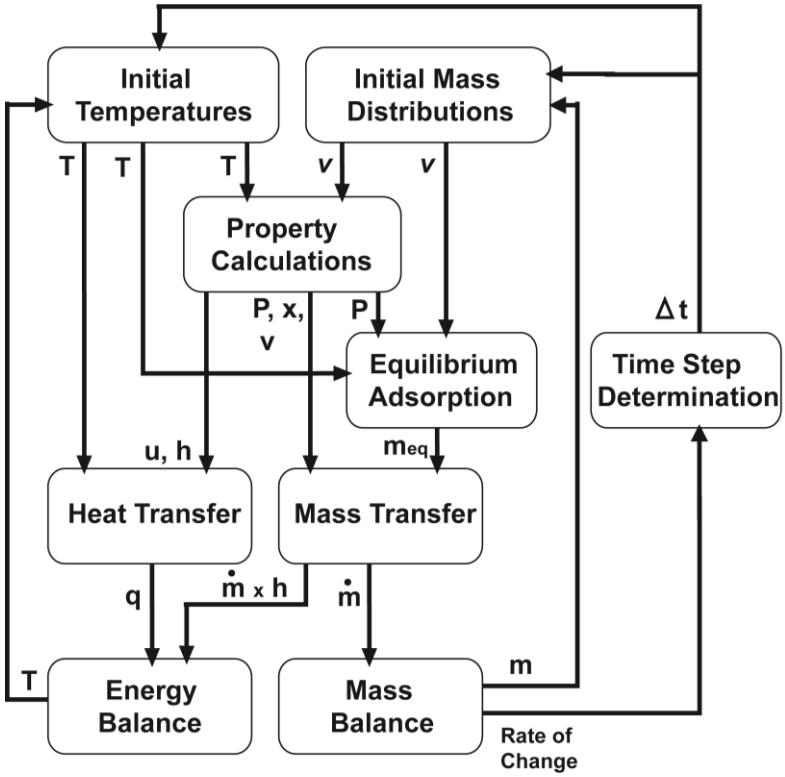

Figure 3.2 Modeling diagram showing the different sections of code and how they communicate with one another

The resistance network is shown in Figures 3.5 and 3.6. These values are described in more detail in the following section. Energy balances are performed and the heat transfer and enthalpy transfer information is used to determine the new temperatures for the system. At the end of the process, the rate of change of the variables over the last two steps is used to determine the time step size for the next iteration. The adaptive time

stepping improves computational efficiency while also ensuring stability when the bed transfers from adsorption to desorption.

Although this work focuses on a single bed system, the model is developed using modular components to allow consideration of different system configurations. Figure 3.3 shows the modular structure of the model. The adsorbent bed or beds, evaporator, and condenser are all individual components that transfer ammonia mass and enthalpy between components based on the operation of the valves between them. Within the components, each node is subdivided into a finite volume nodal network. Inputs and outputs from each component are tracked, including heat losses to the environment. Additional components, such as an additional adsorbent bed, can be added to the system by connecting the component to the rest of the system with valve components.

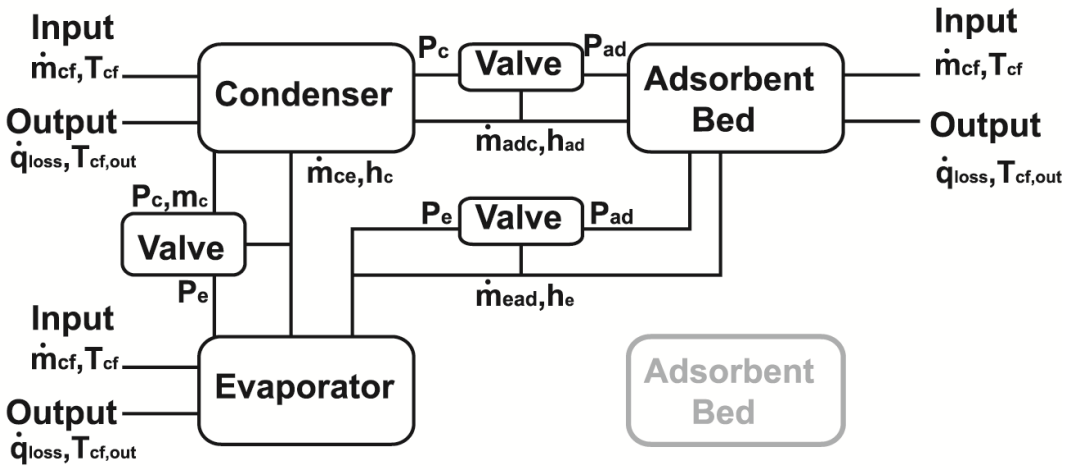

Figure 3.3 Modular structure of the system components. Each box is a separate component within the model.

3.2.2.1 Property Calculations

The refrigerant properties are determined at the start of each time step, using Ammonia_MH, as mentioned above. The volume of each node is fixed by the system

geometry and is specified within the code. The volume is used with the mass distribution to determine the specific volume of the refrigerant within the node as shown in Equation 3.1

$$v_{node}^{i} = \frac{V_{node}}{m_{node}^{i}} \tag{3.1}$$

The specific volume of the refrigerants in the node is used to determine the properties because many of the nodes contain two phase refrigerant and the specific volume allows the properties for the node to be defined by two properties even when two phases exist. The specific volume and temperature are then used to determine the pressure, internal energy, quality, and enthalpy of the ammonia in the node.

For the refrigerant space around the adsorbent example point (the innermost node closest to the coupling fluid outlet), the volume of this space is 4.48 $\times 10^{-5}$ m^3. The initial refrigerant mass is 0.4248 g, while the temperature is 70.1ºC. Using these values the pressure of the adsorbent bed space is 1017 kPa, the specific internal energy is 1432 kJ kg^{-1}, and the specific enthalpy is 1588 kJ kg^{-1}.

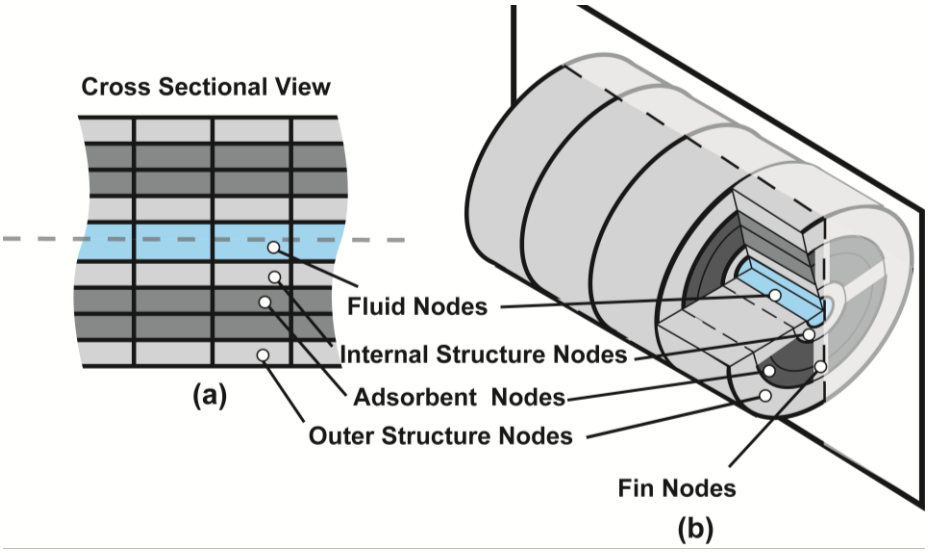

Figure 3.4 Nodal structure of the adsorbent bed component

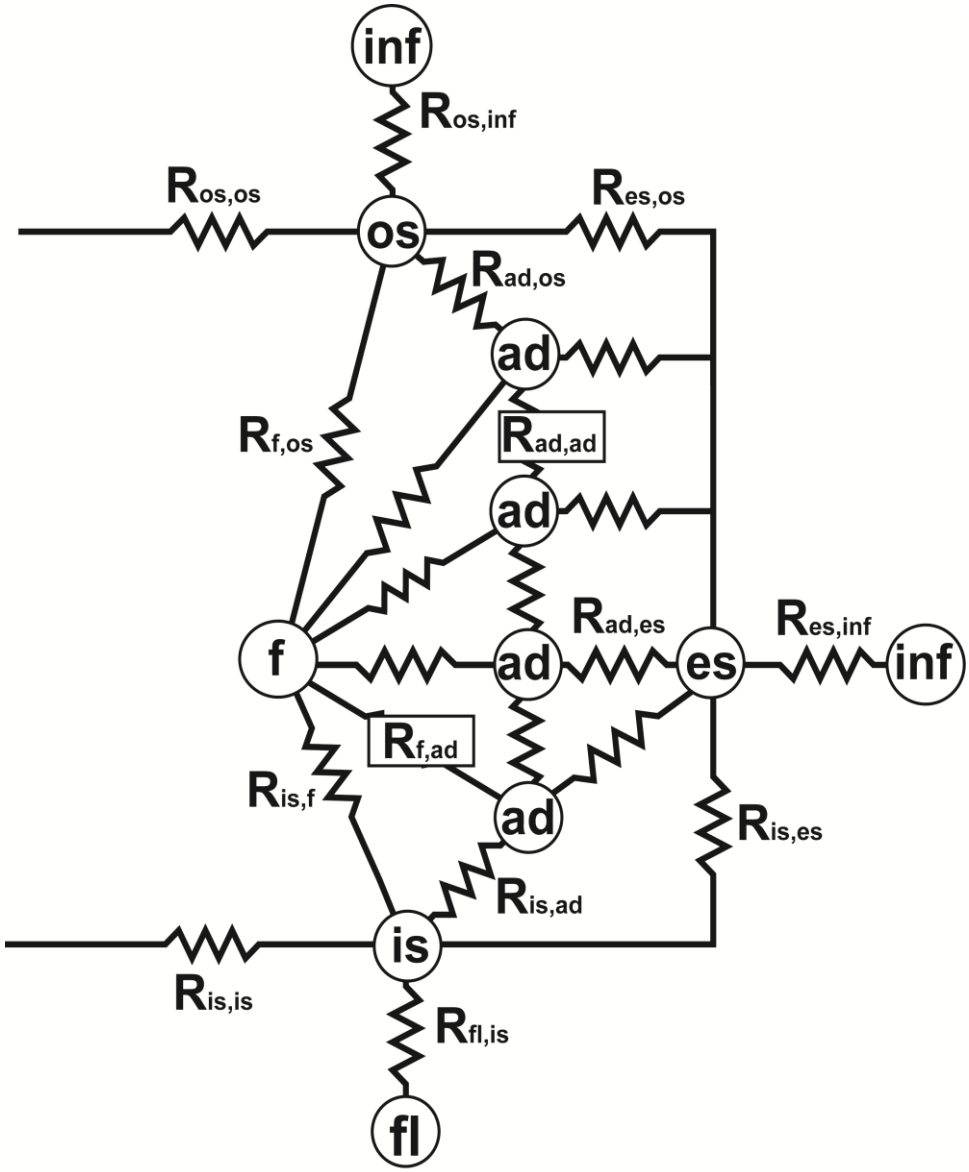

Figure 3.5 Close-up of one axial section of the resistance network. The nodes are labeled with the subscripts corresponding to the different materials and sections of the bed

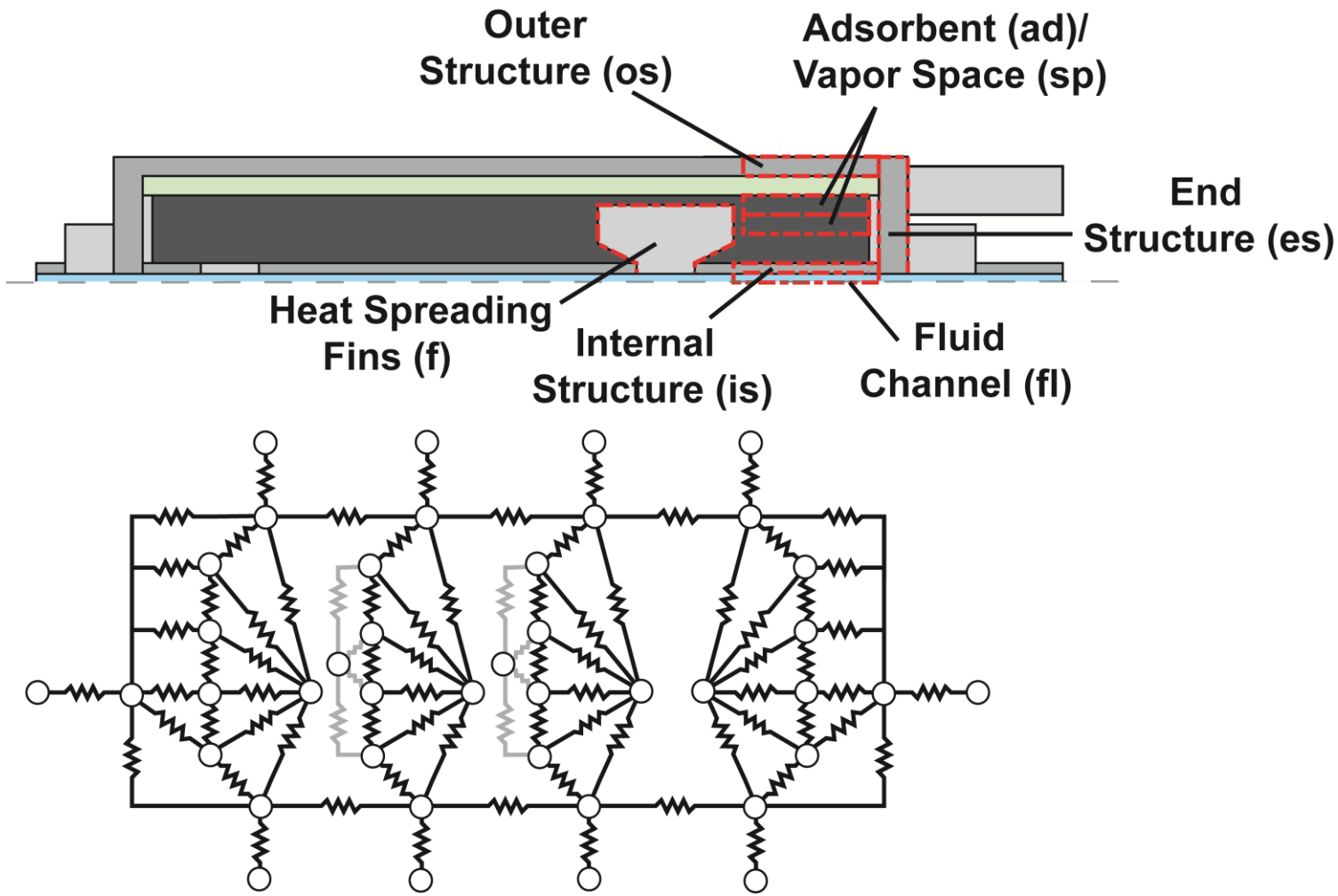

Figure 3.6 Bed schematic with the nodes outlined by dashed lines. These nodes correspond with the circles in the resistance network for the adsorbent bed. The gray connections represent the overlapping space nodes. The subscripts used to label each type of node are indicated on the schematic.

3.2.3 Adsorbent Bed

In approaching the adsorbent bed to develop an understanding of system operation, the fundamental unit of a large scale conventional bed is replicated at a smaller scale as a baseline. This baseline model is developed and then modified to accommodate alternative designs. Rather than multiple fluid tubes running through the adsorbent in this small-scale bed, a single heat transfer tube is used. Fins are used for spreading heat through the adsorbent, as in larger systems.

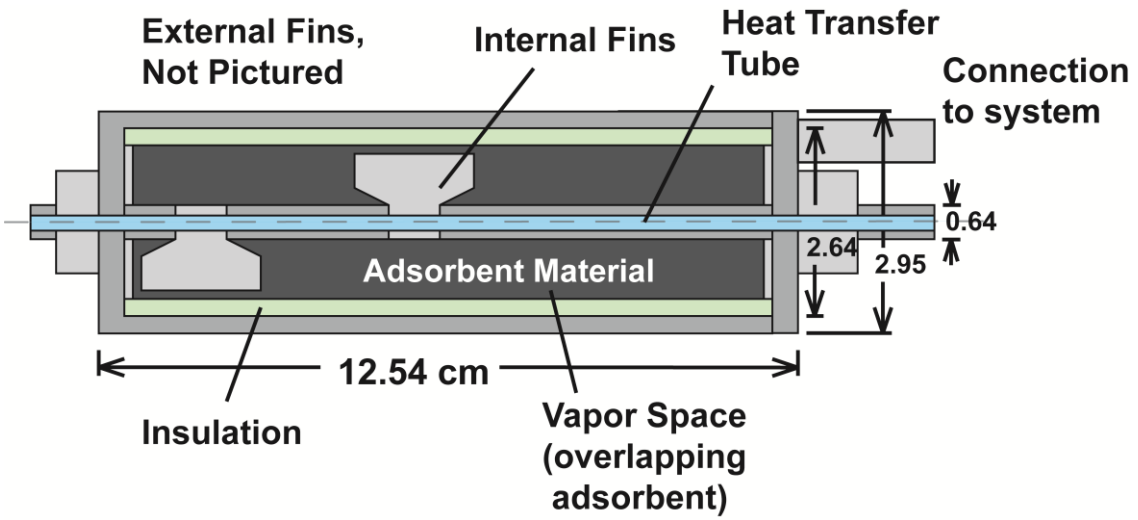

Figure 3.7 Schematic of the Baseline System

For the small-scale bed under consideration, the commonly used assumption that there is no heat transfer between the adsorbent and adsorbent bed outer structure cannot be used. In a large-scale system, there is usually a vapor-filled region between the adsorbent and chamber wall; however, providing a large enough vapor area to eliminate losses results in a significant increase in bed size at this scale. There is also significant thermal short circuiting from the heat transfer channel to the outer bed structure that is usually neglected in large scale models. Therefore, both these loss terms are accounted

for in the adsorbent bed model and design process in the present study. A layer of insulation around the adsorbent is used in the baseline model to limit these losses.

The adsorbent bed is assumed to be cylindrical, with the heat transfer channel in the center of the bed. The adsorbent is segmented into four radial sections and four axial sections. Figure 3.4 shows a schematic of the bed and a representation of the nodal structure. The fin and adsorbent space nodes are not shown. A schematic of the CHEC adsorbent bed is shown in Figure 3.7 for reference, and a schematic of the Flat Bed system is shown in Figure 3.23.

The CHEC system uses the same adsorbent bed model as the baseline model, but with different UA values. The Flat Bed system also uses four discretizations through the thickness of the adsorbent, however the uniform heating of the Flat Bed surface eliminates the need for axial discretization. The volumes and thermal masses are also changed to match the flat geometry of the bed.

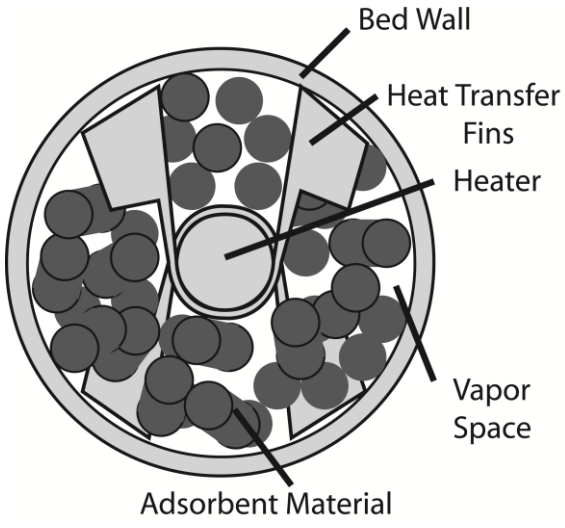

Figure 3.8 End view of the adsorbent bed with adsorbent pellets and vapor space

As seen in Figure 3.8, due to the void space around particles within the adsorbent bed, each adsorbent node is also coupled with a vapor space node that shares the same

volume. Refrigerant entering the bed from the evaporator enters this vapor space volume during adsorption (shown in Figure 3.9) and leaves this volume to enter the condenser during the desorption process. Additionally, ammonia is exchanged with this volume during the adsorption and desorption phases and the pressure of this space is used in both the equilibrium uptake calculations and the mass exchange modules for the valves.

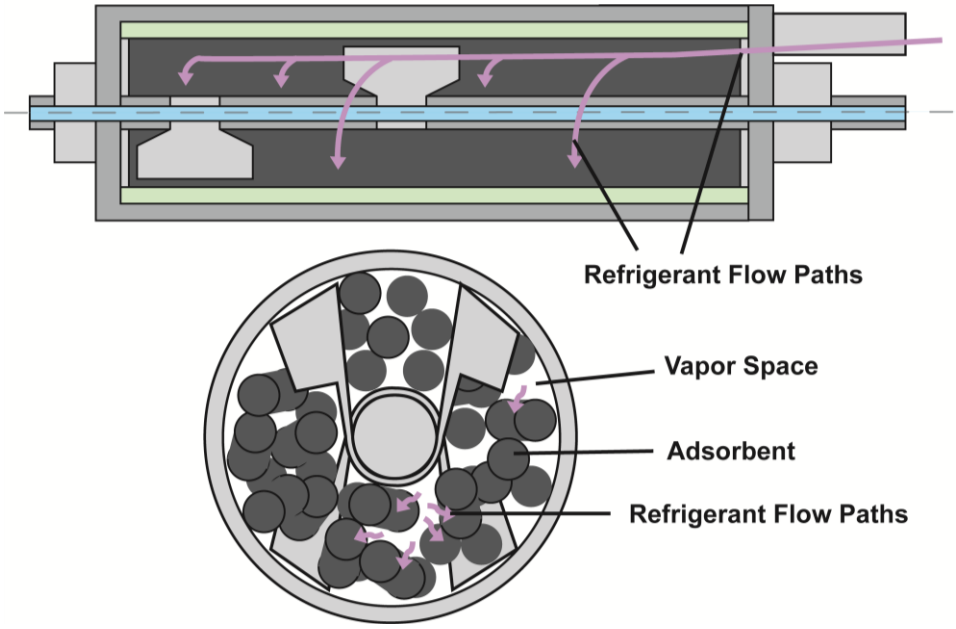

Figure 3.9 Refrigerant flow path into the bed vapor space and then the adsorbent

The size of this bed was initially based on a target total volume of the adsorbent bed that would be less than 130 cm^3 (8 in^3). As an initial assumption, one-half of that volume was assumed to be adsorbent material. Measurement of the adsorbent being used in this work yielded a density for loose particles of 0.75 g cm^{-3}, which for the chosen volume results in 48.75 g of adsorbent material. Therefore, 50 g of adsorbent was chosen for the initial modeling work.

Preliminary experiments with different geometries showed that the initial assumption about the adsorbent-to-structure volume ratio was optimistic at these scales. Additionally, axial losses were found to be significant and additional losses were

accounted for in later models. The bed design limits the adsorbent thickness so that thermal resistance through the bed is kept as low as possible, allowing faster heating and cooling. To achieve a uniform adsorbent thickness, and therefore uniform heating, a cylindrical bed was chosen with the adsorbent arranged in a uniform thickness around a central heat transfer tube. The cylindrical design also has the advantage of being easy to manufacture. The heat transfer tube allows fluid to pass through it to heat and cool the adsorbent. The diameter of the heat transfer tube was chosen to be 0.636 cm (0.25 inches) based on available cartridge heaters that were to be used in the experimental work. The adsorbent layer thickness is limited to 1 cm to limit the thermal resistance of the adsorbent material. This leads to a total diameter for the adsorbent and heat transfer tube combination of 2.636 cm. To contain the target adsorbent mass of 50 g, the required bed length is 12.45 cm. Such a system can be scaled effectively to deliver a larger amount of cooling by increasing the system length. Doubling the bed length doubles the cooling capacity for an ideal system. Eventually, the length would lead to pressure drop problems through the bed and refrigerant distribution that would prevent the length from being fully effective, but with the current dimensions, these factors are not limiting. The thickness of the outer wall of the adsorbent bed is chosen to be 1.59 mm (0.0625 in) as are the ends of the adsorbent bed.

The adsorbent bed is shown in the Figure 3.7 The bed is segmented and there are several different types of nodes used in the adsorbent bed: the central fluid channel, the heat transfer tube wall (internal structure), the adsorbent layer, heat spreader fins that go through the adsorbent, the vapor space surrounding the adsorbent, the end caps of the adsorbent bed (end structure) and the adsorbent bed wall (outer structure). Both stainless

steel and aluminum materials were considered over the course of the work; the final model uses aluminum. Each type of node is explained below along with the heat transfer and energy balance within the adsorbent bed.

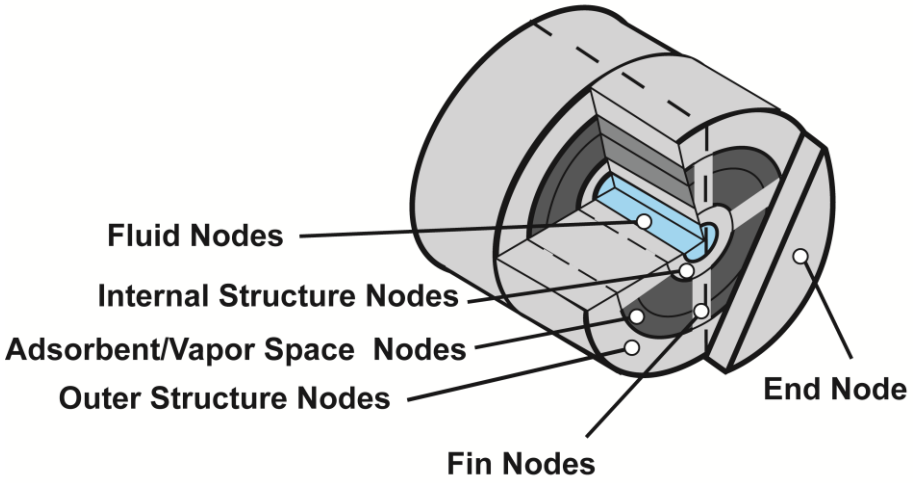

Figure 3.10 Modeling diagram of the adsorbent bed with different node types marked

3.2.3.1 Fluid Channel

The center of bed is the heat transfer fluid channel. The fluid node is highlighted in Figure 3.10. In the baseline system, the heat transfer fluid provides both the heating and cooling to the adsorption system. In modeling the fluid channel, a mass flow rate and entrance temperature for the fluid is specified. The fluid is contained within the internal structure and no mass transfer occurs between the fluid nodes and the rest of the bed. The properties of the heat transfer fluid are assumed to be constant and equal to the properties of water at 20ºC.

The fluid enters the first node at a rate of 0.265 g s^{-1} and at the source temperature or the ambient cooling temperature based upon the system phase. The internal structure has a wall thickness of 0.794 mm (0.03125 in), so that the fluid volume in each node is

0.556 cm^3 and the fluid mass per channel is 0.555 g. Fluid leaves the node at the node temperature to the downstream fluid node. Heat is transferred from the fluid node to the first internal structure node of the bed.

The expected Reynolds number for this flow is 78, and therefore, the flow is expected to be laminar in this channel. The channel flow is considered to be laminar flow through a pipe and a constant temperature wall condition is assumed, which yields a Nusselt number of 3.66. The expected convection coefficient of the heat transfer fluid, h_{tf}, is 520 W m^{-2} K^{-1}. The $UA_{fl,is}$ is calculated using Equation 3.2

$$UA_{fl,is} = \frac{1}{R_{fl} + R_{is}} = \left(\frac{1}{2\pi r_{fl}\, dx\, h_{tf}} + \frac{\ln \frac{r_{is-mid}}{r_{is-i.d.}}}{2\pi k_{is} dx} \right)^{-1} \tag{3.2}$$

Here, r_{fl} is the outer radius of the fluid channel, k_{is} is the thermal conductivity of the internal structure, $r_{is\text{-}mid}$ is the radius to the middle of the internal structure node, and $r_{is\text{-}i.d.}$ is the radius to the inner edge of the internal structure node. This leads to a $UA_{fl,is}$ from the fluid to the internal structure of 0.201 W K^{-1} for each node. The temperature of the fluid changes as it flows through the bed and there is temperature lag before the fluid temperature begins to change in the channel immediately following switching. The flow through the channel helps to limit axial differences in temperature. In each time step an energy balance is performed on each of the heat transfer fluid nodes using the heat transfer to the wall as well as flow down the length of the tube. An energy balance is used to determine the change in temperature of the fluid over time and is given by Equation 3.3

$$m_{fl}c_p\frac{\left(T_{fl,i}^{\,j+1}-T_{fl,i}^{\,j}\right)}{\Delta t}=\underbrace{-UA_{fl,is,i}\left(T_{fl,i}^{\,j}-T_{is,i}^{\,j}\right)}_{\dot{q}_{fl,is,i}}+\dot{m}_{fl}c_pT_{fl,i-1}^{\,j}-\dot{m}_{fl}c_pT_{fl,i}^{\,j} \qquad (3.3)$$

In Equation 3.3, the left side of the equation is the forward time stepping portion of the model representing the change in node temperature with time; m_{fl} is the mass of liquid in the node, c_p is the specific heat of the fluid node, T_{fl} is the temperature of the fluid node, Δt is the change in time for the time step. The first term on the right side of the energy balance is the heat transfer into the adjacent internal structure, T_{is} is the temperature of the adjacent internal structure node. The second and third terms are the energy of the mass transfer into and out of the node, respectively, and $\dot{m}_{fl}$ is the mass flow rate of the fluid.

Numerical diffusion down the tube was tested for the various time steps being considered by tracking the temperature front vs. the increase in the fluid temperature due to numerical diffusion. Numerical diffusion occurs immediately following the change of phase, but in less than 2% of the half-cycle time the results converge to within 5% of the actual temperature. The small temperature drop of the fluid through the bed implies that only a small portion of the thermal capacity of the fluid is utilized. The heat input for the system is the total heat transfer from all of the fluid nodes to all of the internal structure nodes. This heat transfer term is underlined in Equation 3.3.

The last fluid node is used to illustrate for the sample time step. The temperature of the node at the start of the time step is 86.5ºC. The heat transfer from the fluid to the adjacent internal structure is 4.26 W. The incoming fluid is at 90.3ºC, while the exiting fluid is at 86.5ºC. The time step is determined by the change in the previous step to be 0.083 s. This time step is used for all of the sample calculations.

3.2.3.2 Internal Structure

The internal structure is the heat transfer tube containing the heat transfer fluid. Figure 3.11 shows the internal structure node. The outer diameter is 0.635 cm (0.25 in) while the wall thickness is 0.794 mm (0.03125 in). The volume of the nodes representing the tube wall that makes up the internal structure of the bed is 0.433 cm^3. Two materials are considered for the adsorbent system structure, stainless steel and aluminum. The properties for stainless steel (AISI 304 steel) and aluminum are evaluated at 77°C using EES property functions. The mass of these nodes for a stainless steel structure is 3.46 g, while with aluminum it is 1.16 g. The heat transfer resistance in the internal structure radially is very small compared to the convection resistance (~1%) and the conduction resistance into the adsorbent material (~1%); therefore, the thermal resistance in the radial direction is neglected. The heat transfer conductance between the internal structure nodes and the first adsorbent, $UA_{is,ad}$, is calculated using Equation 3.4

$$UA_{is,ad} = \frac{1}{R_{is} + R_{ad}} = \left(\frac{\ln \frac{r_{is-o.d.}}{r_{is-mid}}}{2\pi k_{is} dx} + \frac{\ln \frac{r_{ad-mid}}{r_{ad-i.d.}}}{2\pi k_{ad} dx} \right)^{-1} \tag{3.4}$$

The heat transfer conductance is calculated from the thermal resistance through half of the internal structure and half of the adjacent adsorbent layer. In Equation 3.4, $r_{is\text{-}o.d.}$ is the radius of the outer diameter of the internal structure, $r_{is\text{-}mid}$ is the radius to the middle of the internal structure, k_{is} is the thermal conductivity of the internal structure material, dx is the axial length of the node, $r_{ad\text{-}mid}$ is the radius to the middle of the first adsorbent layer, $r_{ad\text{-}i.d.}$ is the radius to the inner edge of the adsorbent layer, and k_{ad} is the thermal conductivity of the adsorbent layer. $UA_{is,ad}$ is 0.0918 W K^{-1}, this low UA value is

due to the low thermal conductivity of the adsorbent material. The heat transfer conductance, $UA_{is,f}$, from the structure to the fins, which are assumed to be aluminum for this case, is 0.0889 W K^{-1}. The fins are assumed to be 0.3 mm thick and extend through the full adsorbent thickness.

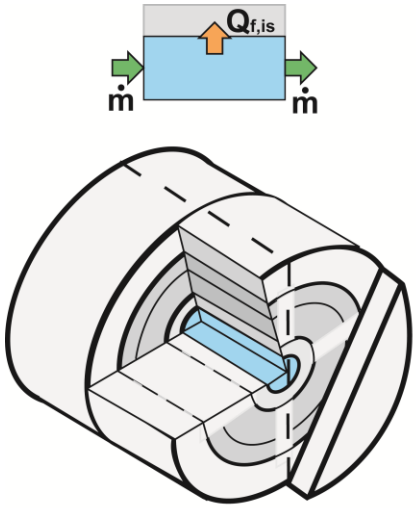

Figure 3.11 Fluid enters the node from one side of the node to the other side of the node. Heat is transferred to the internal structure.

Heat transfer from the internal structure is primarily in the radial direction between the internal structure and the heat transfer fluid, the adsorbent material, and the fins, but there is also axial conduction in the internal structure because of its high thermal conductivity compared with the surrounding materials. This is especially important at the first and last nodes, where heat is transferred axially to the adsorbent bed end structure and contributes strongly to losses from the system, especially for higher thermal conductivity materials. The axial heat transfer conductance for the internal structure, $UA_{is,is}$, is 0.0089 W K^{-1} for stainless steel and 0.089 W K^{-1} for aluminum. The heat transfer conductance, $UA_{is,es}$ from these internal structure nodes to the ends is 0.2125 W K^{-1} for stainless steel and 2.125 W K^{-1} for aluminum. The large heat transfer rates to the

end structure highlights one of the fundamental limitations of a small-scale thermal system. The conduction losses to the system wall become more and more dominant at the smaller scale. These losses can be reduced by decreasing the thickness of the wall and using different materials with lower thermal conductivities, but the improvement is limited because of the limited options in system materials.

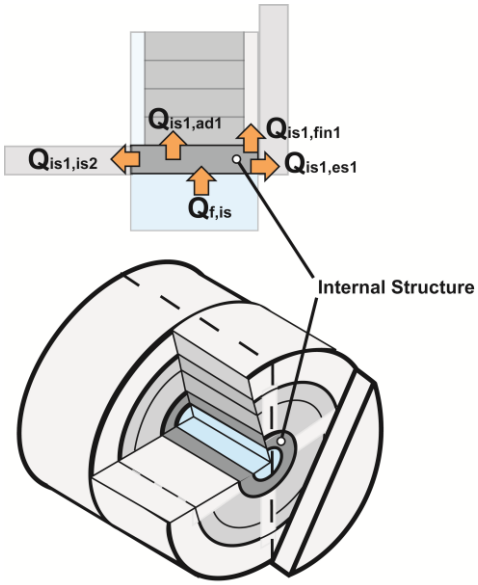

Figure 3.12 Heat enters the node from the fluid nodes and is transferred to the adsorbent, fin, adjacent internal structure nodes, and the adsorbent shell nodes.

The heat transfer from the internal structure to the refrigerant vapor space is assumed to be negligible. This assumption is justified due to the relatively small surface area for heat transfer to the vapor space compared to the adsorbent material (< 1%) and the very low convection coefficient (< 10 W m^{-2} K^{-1}). There is no mass transfer in the structure nodes. The energy balance on the internal structure nodes is given by Equation 3.5

$$m_{is}c_{p,is}\frac{\left(T_{is,i}^{\,j+1}-T_{is,i}^{\,j}\right)}{\Delta t}=UA_{fl,is,i}\left(T_{fl,i}^{\,j}-T_{is,i}^{\,j}\right)-UA_{is,ad,i}\left(T_{is,i}^{\,j}-T_{ad,i}^{\,j}\right)-UA_{is,f,i}\left(T_{is,i}^{\,j}-T_{f,i}^{\,j}\right)$$
$$+UA_{is,i-1,is,i}\left(T_{is,i-1}^{\,j}-T_{is,i}^{\,j}\right)-UA_{is,i,is,i+1}\left(T_{is,i}^{\,j}-T_{is,i+1}^{\,j}\right) \quad (3.5)$$

In the above equation, m_{is} is the mass of the internal structure node, $c_{p,is}$ is the specific heat capacity of the node, T_{is} is the temperature of the internal structure, Δt is the change in time for the time step, $UA_{fl,is}$ is the heat transfer conductance between the fluid and the internal structure, T_{fl} is the temperature of the fluid node, $UA_{is,ad}$ is the heat transfer conductance between the internal structure node and the adjacent adsorbent node, T_{ad} is the temperature of the adsorbent node, *i* is the spatial index, *j* is the temporal index, and $UA_{is,is}$ is the heat transfer conductance axially from one internal structure node to the next.

Equation 3.6 is the energy balance for the internal structure nodes at the end where they connect to the end structure nodes.

$$m_{is}c_{p,is}\frac{\left(T_{is,i}^{\,j+1}-T_{is,i}^{\,j}\right)}{\Delta t}=UA_{fl,is,i}\left(T_{fl,i}^{\,j}-T_{is,i}^{\,j}\right)-UA_{is,ad,i}\left(T_{is,i}^{\,j}-T_{ad,i}^{\,j}\right)-UA_{is,f,i}\left(T_{is,i}^{\,j}-T_{f,i}^{\,j}\right)$$
$$+UA_{is,i-1,is,i}\left(T_{is,i-1}^{\,j}-T_{is,i}^{\,j}\right)-UA_{is,es}\left(T_{is,i}^{\,j}-T_{es,i}^{\,j}\right) \quad (3.6)$$

The left hand side of the equation represents the change in internal energy of the internal structure node, while each term on the right side represents heat transfer between the internal structure and surrounding nodes. The end node is very similar to the axial nodes, but there is heat transfer to the end structure rather than to other internal structure nodes on one side. Here, $UA_{is,es}$, is the heat transfer conductance from the internal structure to the end structure nodes and T_{es} is the temperature of the end structure. For the internal structure nodes, the sample node under consideration is the structure node closest to the fluid outlet. The starting temperature of this node is 65.2ºC. The heat

transfer from the internal structure to the adsorbent is 0.767 W, while the heat transfer from the internal structure to the fin node is 0.766 W. The final temperature in the node is 65.2ºC. The temperature change in this time step is negligible.

3.2.3.3 Adsorbent

The adsorbent is the divided both axially and radially. An axial section of the adsorbent bed is shown in Figure 3.13. Radially, the adsorbent is divided into four nodes of equal thickness. Because of the cylindrical nature of the adsorbent bed, the volume and mass of adsorbent in these nodes varies radially. Each layer is 2.38 mm (0.0938 in) thick. The adsorbent node mass for the first, second, third, and fourth layers are 1.72 g, 2.66 g, 3.59 g, and 4.53 g, respectively. The adsorbent is in thermal contact with the heat transfer fins, the internal structure, the refrigerant vapor space, other adsorbent nodes, the end structure and the outer bed structure. The refrigerant vapor space occupies the same volume as the adsorbent nodes. The adsorbent is assumed to have a void fraction of 0.4, i.e. 60% of the volume is occupied by adsorbent material, while the other 40% is occupied by refrigerant vapor. The specific heat of the adsorbent is assumed to be 900 J kg^{-1} K^{-1} based on literature values for activated carbon specific heat (Wang *et al.*, 2006). The heat capacity of the adsorbent due to the sensible heating of the adsorbent compared to the heat capacity due to adsorption and desorption (~10^6 J per kg of adsorbed material) is very small.

The heat transfer between the adsorbent material and rest of the system is dominated by the low thermal conductivity within the adsorbent material. Individual pellets are not heated evenly, with the individual pellets forming numerous heat transfer pathways. Within the adsorption system model, the adsorbent is considered to be a

homogeneous material. The heat transfer coefficients in this model are estimated based on a thermal conductivity of 0.2 W m^{-1} K^{-1} for the packed adsorbent material (Critoph and Turner, 1995). The outer structure is insulated from the adsorbent to prevent losses to the surroundings and the heat transfer conductance from the adsorbent to the outer shell, $UA_{ad,os,}$ is 0.005 W K^{-1}. The heat transfer conductance from the adsorbent to the end structure, $UA_{ad,es}$, varies from 0.0004 to 0.001 W K^{-1} through the adsorbent thickness. The intra-adsorbent heat transfer conductances are: $UA_{ad1,ad2}$ = 0.101 W K^{-1}, $UA_{ad2,ad3}$ = 0.145 W K^{-1}, and $UA_{ad3,ad4}$ = 0.189 W K^{-1}. Due to the very low thermal conductivity, axial conduction through the adsorbent material is neglected.

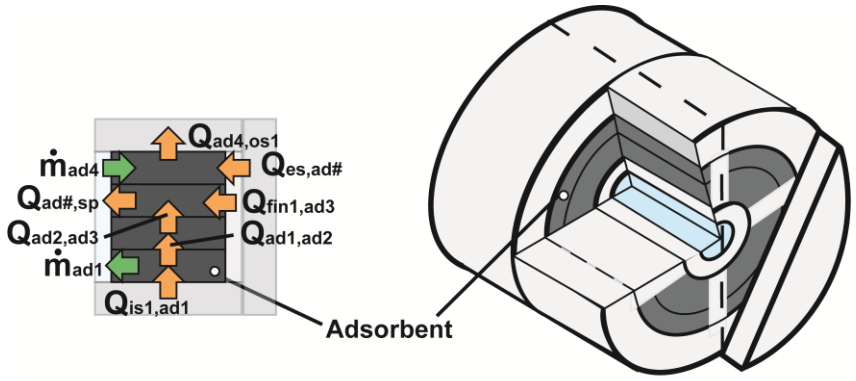

Figure 3.13 Heat enters the node from the fluid nodes and is transferred to the adsorbent, fin, adjacent internal structure nodes, and the adsorbent shell nodes

The fins increase the heat transfer into the adsorbent and help limit the temperature gradient through the adsorbent. The heat transfer conductance between the fins and adsorbent nodes, $UA_{f,ad}$, is 0.064 W K^{-1} calculated using Equation 3.7

$$UA_{f,ad} = \frac{1}{R_f + R_{ad}} \underset{\to 0}{=} \left(\frac{l_{f,ad}}{k_{ad} A_f} \right)^{-1} \tag{3.7}$$

The thermal resistance for heat transfer from the fin surface to the adsorbent is dominated by the adsorbent resistance, because of the much higher thermal conductivity of the metal fins (200 W m^{-1} K^{-1} vs. 0.2 W m^{-1} K^{-1}), and therefore, only the adsorbent resistance is considered. With a fin thickness of 0.3 mm, the thermal resistance through the thickness of the fin is 0.0009 K W^{-1} compared to 15.6 K W^{-1} for the adsorbent layer. The ratio of the heat transfer length from the fin into the adsorbent, $l_{f,ads,}$ and the surface area of the fin for transfer, A_f, is assumed to be constant, 0.32 m, for the model, because the fins widen further from the central heating channel so that they have more surface area for heat transfer as the radius increases, as shown in Figure 3.9, to compensate for the larger volume of adsorbent as the radius increases. This is equivalent to an average heat transfer path length of 2.5 mm and a fin surface area of 8 cm^2.

The heat transfer coefficient in the refrigerant vapor space is assumed to be constant throughout the adsorbent system operation and despite the low convection coefficient, because of the large adsorbent surface area, approximately 0.03 m^2, the heat transfer conductance for the adsorbent to the refrigerant vapor, $UA_{ad,sp}$, is 0.01 W K^{-1}. In addition to heat transfer with the adsorbent, there is also mass transfer between the adsorbent nodes and the refrigerant vapor space. There is also an associated heat of adsorption, which is assumed to be independent of temperature in this model, because it varies little with temperature and the heat released through adsorption is dominated by the heat of vaporization of the refrigerant vapor.

The adsorbent material in this model is based on the Norit RB3 activated carbon adsorbent that was used in the tests. The pore volume per mass of adsorbent is 0.00041 m^3 kg^{-1} based on measurements made on the adsorbent used in the experiments. The

specifics of the mass transfer are discussed in Sections 3.4 and 3.5. The energy balance for the adsorbent nodes is given by Equation 3.8

$$m_{ad\#}c_{p,ad}\frac{\left(T_{ad\#,i}^{\ j+1}-T_{ad\#,i}^{\ j}\right)}{\Delta t}+\frac{\left(m_{ad\#,i}^{\ j+1}u_{ad\#,i}^{\ j+1}-m_{ad\#,i}^{\ j}u_{ad\#,i}^{\ j}\right)}{\Delta t} = UA_{ad\#-1,ad\#}\left(T_{ad\#-1,i}^{\ j}-T_{ad\#,i}^{\ j}\right)-UA_{ad\#,ad\#+1}\left(T_{ad\#,i}^{\ j}-T_{ad\#+1,i}^{\ j}\right) +UA_{ad\#,sp}\left(T_{ad\#,i}^{\ j}-T_{sp,i}^{\ j}\right)+UA_{f,ad}\left(T_{f,i}^{\ j}-T_{ad\#,i}^{\ j}\right) \dot{m}_{ad\#}\left[h(T_{ad\#},x=0)_i^j-h\left(T_{sp},v=v_{sp}\right)\right]+\dot{m}_{ad\#}H_{ad} \quad (3.8)$$

The first term is the sensible heating of the adsorbent material and the second term is change in internal energy due to the changing temperature and mass of the adsorbed ammonia. On the right side of the equation, the first two terms are the heat transfer between adsorbent layers, the next term is the heat transfer with the surrounding void space ammonia, and the last heat transfer term is the heat transfer between the adsorbent node and the heat spreading fins. The energy balance equation changes for the nodes around the edges of the bed, which would also have heat transfer terms for the structure nodes. The last two terms represent the energy transfer due to adsorption/desorption. The first is the energy adsorbed or released as the refrigerant transfers between the state within the adsorbent and the conditions of the surrounding space, by calculating the enthalpy of the ammonia at the two states. The last term is the heat of adsorption representing the energy released or absorbed caused by interaction of the two materials. A mass balance on the adsorbent nodes is performed simultaneously.

For the sample adsorbent node, the one closest to the fluid heat transfer channel outlet is chosen. The adsorbed mass at the start of the time step is 0.8571 g and the initial node temperature is 57.0ºC. The heat transfer rate to the next layer of adsorbent material is 0.371 W and the adsorbent transfers heat into the fin at a rate of 0.020 W in this time step. The rate of energy transferred out of the node by refrigerant desorption is 0.307 W.

The heat transfer out of the adsorbent into the end node is 0.00648 W. This leads to a new adsorbed refrigerant mass of 0.857 and a new temperature of 57.0ºC .

3.2.3.4 Vapor Space

A single vapor space node is modeled over the entire adsorbent bed. Only a single vapor node is used because the mass transfer in the space around the adsorbent occurs much more quickly than into the particle (~10^{-4} vs. ~10^{-7}); therefore, the vapor space is assumed to be uniform compared to the adsorbent particles. The vapor space receives refrigerant mass from the evaporator and transfers mass to the condenser. Heat and mass transfer also occurs between the vapor space and the adsorbent material. The heat transfer with the other surfaces is neglected for the vapor space because of the low thermal conductivity of the vapor and the low surface area for heat transfer. The vapor space temperature and pressure are determined at the beginning of every time step, based on the internal energy and specific volume of the refrigerant in the vapor space at the start of the time step. The energy balance on the vapor space is

$$\frac{\left(u_{sp}{}^{j+1} m_{sp}^{j+1} - u_{sp}{}^{j} m_{sp}^{j}\right)}{\Delta t} = \sum_{\#=1}^{k} UA_{ad,sp}\left(T_{ad\#,i}{}^{j} - T_{sp}{}^{j}\right) + \sum_{n=1}^{k} h_{ad,spn}{}^{j} \dot{m}_{ad,sp}{}_{n}^{j} - h_{sp}{}^{j} \dot{m}_{sp,c}{}^{j} + h_{e}{}^{j} \dot{m}_{e,sp}{}^{j} \quad (3.9)$$

The left hand side of the equation represents the change in internal energy for the node. The internal energy of the space u_{sp}, the initial mass of refrigerant in the space is m_{sp}, the temporal index is represented by j, with the initial values being at j and the final values being at $j+1$. The first set of terms on the right is the heat transfer between the adsorbent surface and the space, which depend upon the temperature difference between the vapor space and each adsorbent node. The second set of terms represents enthalpy transferred into or out of the vapor space due to mass transfer between the adsorbent and

vapor space. The mass transfer from the adsorbent to the space is represented by $\dot{m}_{ad,sp\ n}$ and the enthalpy of the ammonia that is transferred is given by $h_{ad,sp\ n}{}^{j}$, which is equal to the enthalpy of vapor at the pressure and temperature conditions of the vapor space. The final two terms are the energy transfer between adsorbent bed and the condenser and the evaporator respectively. In these terms, $\dot{m}_{sp,c}$ is the mass transfer to the condenser, h_{sp} is the enthalpy of the space, $\dot{m}_{e,sp}$ is the mass transfer from the evaporator into the vapor space, and h_e is the enthalpy of the saturated vapor at the evaporator pressure. This is solved simultaneously with the mass balance on the vapor space

$$\frac{\left(m_{sp}^{j+1}-m_{sp}^{j}\right)}{\Delta t}=\sum_{n=1}^{k}\dot{m}_{ad,sp\ n}{}^{j}-\dot{m}_{sp,c}{}^{j}+\dot{m}_{e,sp}{}^{j} \tag{3.10}$$

The temperature for the next step in the vapor space is calculated from the internal energy using the Internal Energy function in EES. For the sample time step, the vapor space initially contains 0.4218 g and the temperature of the space is 68.7ºC. Heat is transferred from the space to the adsorbent at a rate of 4.77 W in this time step. There is no mass transfer from the evaporator in this time step and the mass transfer rate to the condenser is 0.016 g s^{-1}. The final temperature of the adsorbent space is 69ºC, and the final refrigerant mass is 0.4223 g.

3.2.3.5 Fin

The fins spread heat from the internal structure more evenly through the adsorbent. The heat transfer for fin nodes is shown in Figure 3.14. The fin primarily transfers heat with the adsorbent and internal structure, but there is some loss to the outer

structure. The heat transfer conductance between the two, $UA_{f,os}$, is 0.005 W K^{-1}. The energy balance for the fin is given by Equation 3.11

$$m_{fin,i} c_{p,st} \frac{\left(T_{f,i}^{\,j+1} - T_{f,i}^{\,j}\right)}{\Delta t} = UA_{is,f}\left(T_{is,i}^{\,j} - T_{f,i}^{\,j}\right) - \sum_{n=1}^{4} UA_{f,ad}\left(T_{f,i}^{\,j} - T_{ad,n,i}^{\,j}\right) - UA_{f,os}\left(T_{f,i}^{\,j} - T_{os,i}^{\,j}\right) \quad (3.11)$$

The left side of the equation represents the internal energy change of the fin node. The mass of the node is given by, m_{fin} and the specific heat of the node, $c_{p,st}$, is the same as that of the other structural nodes. In addition to the heat transfer from the internal structure and the adsorbent that has been previously defined, the fin also transfers heat to the outer structure of the bed which is at temperature T_{os}.

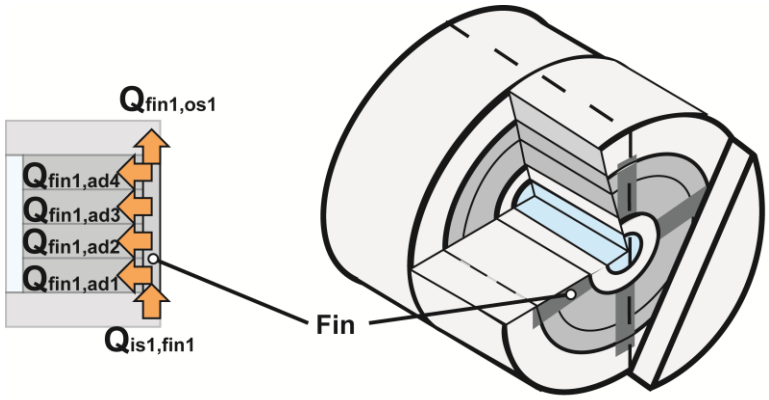

Figure 3.14 Heat enters the node from the fluid nodes and is transferred to the adsorbent, fin, adjacent internal structure nodes, and the adsorbent shell nodes.

At the start of the sample time step, the fin temperature is 56.66ºC. The loss to the outer structure is 0.0291 W, and the heat transfer from each of the adsorbent nodes to the fin is 0.0195 W. This leads to a new fin temperature in the following step of 56.67ºC.

3.2.3.6 Bed End Structure

The bed end structure is the material making up the end cap of the adsorbent bed. The end structure is illustrated in Figure 3.15. The end cap is 1.588 mm (0.0625 in) thick

and extends from the internal structure to the outer structure with a radius of 1.587 cm (0.625 in). The end structure nodes have a mass of 9.66 g for the stainless steel and a mass of 3.26 g in the case of aluminum. The end structure transfers heat with an internal structure node, with an external structure node, to the surroundings, and with the adsorbent on the end. Heat is transferred from the center of the end structure node to the center of the outer structure node by conduction, calculated using the thermal resistance from the edge of each node to the node center point. The heat transfer coefficient between the end structure and the outer structure, $UA_{es,os}$, is 0.2125 W K^{-1} for stainless steel and 2.125 W K^{-1} for aluminum.

The surface area that interacts with the surroundings is 0.008 m^2, and for this area, the heat transfer coefficient is estimated to be 10 W m^{-2} K^{-1}. The natural convection portion of this coefficient is calculated using the correlation for heat transfer from a vertical plate from Churchill and Chu (1975b) and yields a convection coefficient of 8.3 W m^{-2} K^{-1}. The radiation heat transfer is accounted for in this convection coefficient using the radiation heat transfer coefficient from Incropera and DeWitt (1996) which linearizes the radiation heat transfer.

$$ht_{es,rad} = \varepsilon\sigma(T_{os} + T_{\inf})(T_{os}^2 + T_{\inf}^2) \tag{3.12}$$

The emissivity is assumed to be 0.2 based on emissivity for a partially oxidized aluminum surface (Incropera and DeWitt, 1996). The temperature of the outer structure for Equation 3.12 is assumed to be 77°C (350 K) in the above equation. The radiation heat transfer coefficient from Equation 3.12 is 1.6 W m^{-2} K^{-1}. The total heat transfer coefficient for this surface is

$$ht_{es} = ht_{es,conv} + ht_{es,rad} \tag{3.13}$$

The heat transfer conductance is then found using Equation 3.14

$$UA_{es,\inf} = ht_{es} A_{es} \tag{3.14}$$

The heat transfer conductance to the surroundings, $UA_{es,inf}$, is 0.0076 W K^{-1}. There are losses from the end material to the ambient, but it primarily transfers heat from the internal structure to the external structure, which in turn loses that heat to the surroundings. The energy balance for the end nodes is given in Equation 3.15

$$\begin{aligned} c_{p,st} m_{es} \frac{\left(T_{es,1}^{\,j+1} - T_{es,1}^{\,j}\right)}{\Delta t} = {} & UA_{is,es}\left(T_{is,1}^{\,j} - T_{es,1}^{\,j}\right) - UA_{es,\inf}\left(T_{es,1}^{\,j} - T_{\inf}\right) \\ & - UA_{es,os}\left(T_{es,1}^{\,j} - T_{os,1}^{\,j}\right) - \sum_{n=1}^{4} UA_{ad,es}\left(T_{es,1}^{\,j} - T_{ad,n,1}^{\,j}\right) \end{aligned} \tag{3.15}$$

For the sample point, the end node closest to the fluid inlet is considered. At the start of the time step, the node temperature is 67.58ºC. The heat transfer from the internal structure is 5.24 W. The loss to the surroundings is 0.324 W. The new temperature of the end structure node is 67.59ºC.

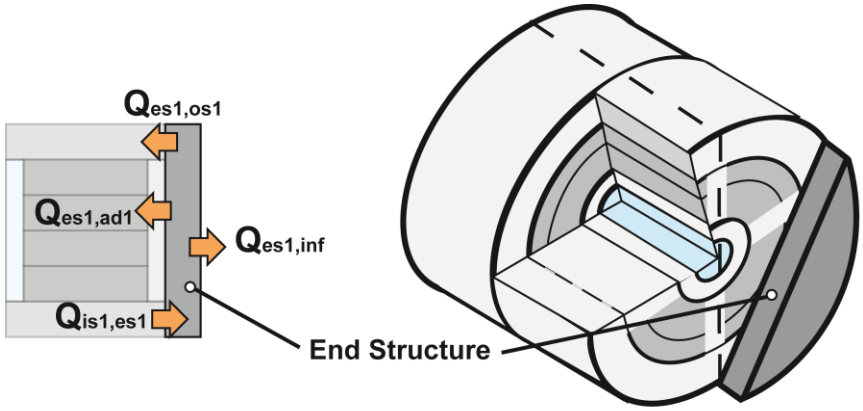

Figure 3.15 Heat enters the node from the fluid nodes and is transferred to the adsorbent, fin, adjacent internal structure nodes, and the adsorbent shell nodes.

3.2.3.7 Outer Structure

The outer bed structure is the area that surrounds the adsorbent material. In a large-scale system there is usually a wire mesh that holds the adsorbent material around the heat transfer tubes and the outer structure is separated by a vapor gap. However, in this small-scale system, there is no gap and the outer structure serves to hold the adsorbent against the heat transfer tube as well as contain the bed. The direct contact increases the dynamic losses of the system, but decreases the volume of the adsorbent bed significantly at this scale. To achieve the same gap used in larger systems, the volume of the bed would have to be at least doubled. The outer structure is 1.588 mm (0.0625 in) thick and runs the entire length of the bed. The mass of the outer structure node is 37.6 g for the stainless steel case and 12.69 g for the case of aluminum. The outer structure is in thermal contact with the adsorbent material, the heat transfer fins, the end structure, and the surroundings. The outer structure also transfers heat axially. The heat transfer conductance along the outer structure axially, $UA_{os,os}$, is 0.773 W K^{-1} and the heat transfer conductance for losses from the outer structure to the surroundings, $UA_{os,inf}$, is 0.050 W K^{-1}, calculated using the correlation developed by Churchill and Chu for flow over a horizontal cylinder (Churchill and Chu, 1975a). Radiation is accounted for here in the same manner as for the end structure. The energy balance for the outer structure nodes is given by Equation 3.16

$$m_{os}c_{p,st}\frac{\left(T_{os,i}^{\,j+1}-T_{os,i}^{\,j}\right)}{\Delta t}=UA_{f,os}\left(T_{f,i}^{\,j}-T_{os,i}^{\,j}\right)+UA_{os,os}\left(T_{os,i-1}^{\,j}-T_{os,i}^{\,j}\right) \\ -UA_{os,os}\left(T_{os,i}^{\,j}-T_{os,i+1}^{\,j}\right)+UA_{ad,os}\left(T_{ad\#,i}^{\,j}-T_{os,i}^{\,j}\right)-UA_{os,\inf}\left(T_{os,i}^{\,j}-T_{\inf}\right) \tag{3.16}$$

As with the internal structure, the outer structure nodes at the ends of the bed transfer heat to the end structure node rather than axially to the next outer structure node. For the sample point, the outer structural node closest to the exit is considered. The

starting temperature is 62.48ºC. The heat transfer from the fin is 0.759 W, the heat transfer from the adjacent adsorbent is 0.0529 W, and the loss to the surroundings is 1.879 W. The new adsorbent structure temperature is 62.48ºC.

3.2.4 Evaporator and Condenser

Less emphasis was placed on scaling down the evaporator and condenser components when it became obvious in the design process that the scaling effects for the system would have the greatest impact on the adsorbent bed operation. For this reason, the evaporator and condenser are modeled as simple tube-in-tube heat exchangers. A diagram of the evaporator is shown in Figure 3.17. The evaporator and condenser are both assumed to be 40.6 cm (16 in) long. The internal refrigerant tubes have an outer diameter of 6.35 mm (0.25 in) with a wall thickness of 0.794 mm (0.0313 in). The outer coupling fluid tube has an outer diameter of 1.27 cm (0.5 in) with a wall thickness of 0.794 mm (0.0313 in). The walls of these tubes are considered to be stainless steel in all models.

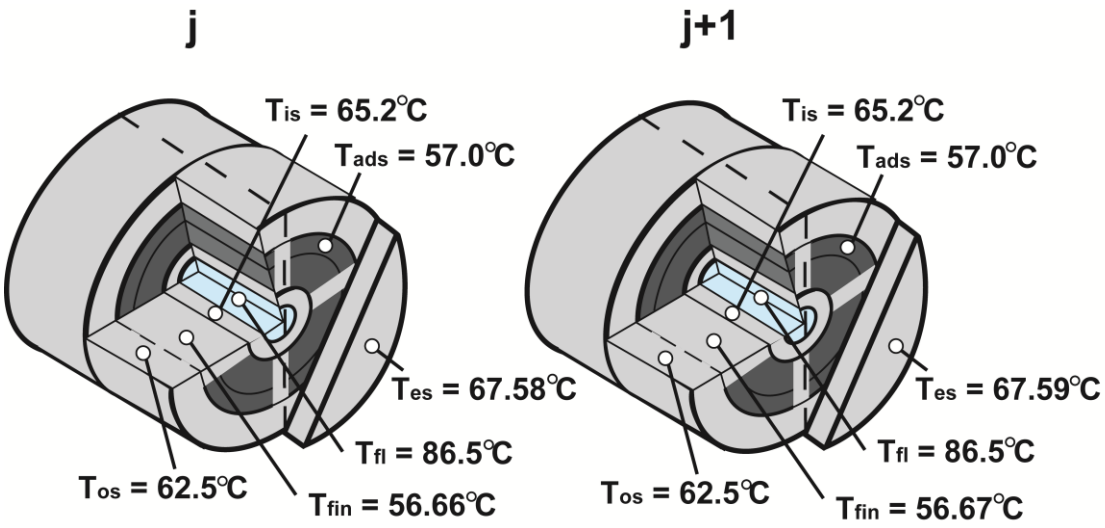

Figure 3.16 Temperatures throughout the bed for the sample time step

Table 3.1 UA values for the baseline model

Name	Value [W K^{-1}]	Name	Value [W K^{-1}]	Name	Value [W K^{-1}]
$UA_{fl,is}$	0.201	$UA_{ad,es4}$	0.001	$UA_{os,os}$	0.773
$UA_{is,ad}$	0.0918	UA_{ad1ad2}	0.101	$UA_{os,inf}$	0.050
$UA_{is,f}$	0.0889	UA_{ad2ad3}	0.145	$UA_{stc,cf}$	4.5
$UA_{is,is}$	0.089	UA_{ad3ad4}	0.189	$UA_{ste,ef}$	4.5
$UA_{is,es}$	2.125	$UA_{f,ad}$	0.064	$UA_{stc,inf}$	0.050
$UA_{ad,os}$	0.005	$UA_{ad,sp}$	0.100	$UA_{ste,inf}$	0.050
$UA_{ad,es1}$	0.0004	$UA_{f,os}$	0.005	$UA_{ef,inf}$	0.002
$UA_{ad,es2}$	0.0006	$UA_{es,os}$	2.125	$UA_{cf,inf}$	0.002
$UA_{ad,es3}$	0.0008	$UA_{es,inf}$	0.0076		

The pressure drop in the system is small compared to the large pressure swing that occurs over the system cycle, therefore the evaporator and condenser are assumed to be at a uniform pressure. Because the nodes in these components are always in a two-phase state when the system operates at design conditions, the refrigerant inside the evaporator and the condenser is at a uniform temperature. Initial models segmented the refrigerant nodes in these components, but segmenting was found not to affect the model results and made the program less stable. Therefore, the refrigerant space in each of these components is modeled as a single node. The evaporator and condenser nodes exchange heat with the tube wall, which in turn transfers heat to the coupling fluid loop. The surrounding nodes are axially segmented to better resolve the heat transfer in the evaporator.

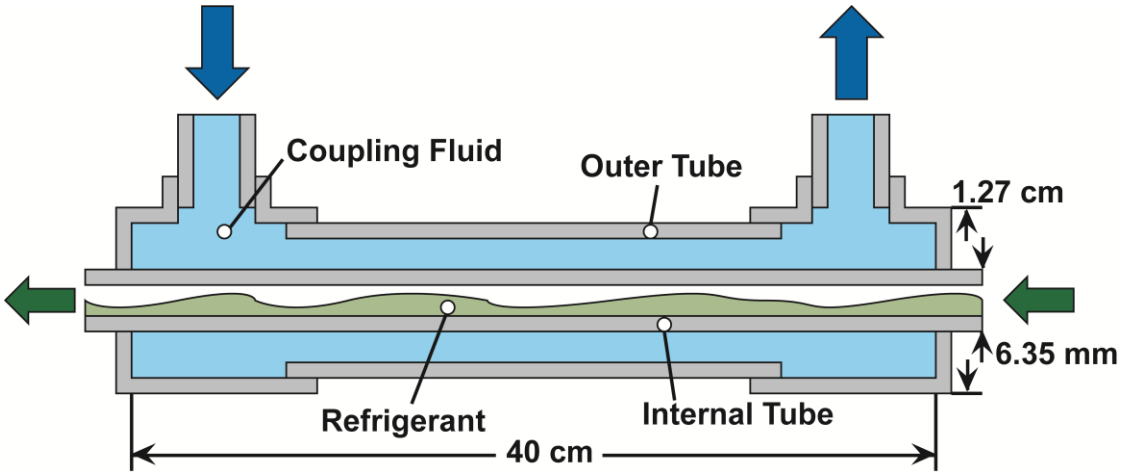

Figure 3.17 Tube-in-tube evaporator used in the model (not to scale)

For each node of the evaporator and condenser, an energy balance is performed. A mass balance is also necessary for these nodes, as refrigerant is entering and exiting them throughout the system operation. Equation 3.17 gives the energy balance for the evaporator refrigerant node

$$\frac{\left(m_{ev}{}^{j+1}u_{ev}{}^{j+1}-m_{ev}{}^{j}u_{ev}{}^{j}\right)}{\Delta t}=\sum_{n=1}^{k}UA_{ev,ste}\left(T_{ste,n}{}^{j}-T_{ev}^{j}\right)+\dot{m}_{co,ev}{}^{j}h_{co}{}^{j}-\dot{m}_{ev,bed}{}^{j}h\left(T_{ev}^{j},x=1\right) \quad (3.17)$$

The change in internal energy for the node is determined using the change in refrigerant mass and specific internal energy for the time step on the left hand side of the equation. The internal energy is then used to calculate the temperature of the evaporator for the following time step. Heat is transferred into the refrigerant from the evaporator wall. The heat transfer conductance between the refrigerant and evaporator wall, $UA_{ev,ste}$, is variable, to account for the change in heat transfer rate when ammonia transfers from the evaporator to the adsorbent bed. The heat transfer conductance varies linearly with temperature from a minimum of 0.05 W K^{-1} to a maximum of 4 W K^{-1}. These conductance values correspond to convection coefficients of 30 W m^{-2} K^{-1} and 2600 W m^{-2} K^{-1}. Because of the highly transient two-phase nature of this process, an appropriate

correlation could not be identified and the typical convection coefficient value ranges from Incropera and Dewitt (1996) were used. The peak convection coefficient when the valve is first opened is expected to be larger than the value used, but a larger value leads to numerical instability and the conductance value was capped. Because the external annulus resistance is the dominant resistance for heat transfer to the coupling fluid stream when the convection coefficient increases, capping the UA value for the refrigerant heat transfer coefficient should not lead to large errors. The model stays near the lower value for much of the cycle, because the evaporation rate is slow. The enthalpy of the fluid coming from the condenser is equal to the enthalpy of liquid at the condenser temperature, unless the condenser has reached dry-out conditions where no liquid is present in the condenser. The enthalpy of the refrigerant leaving the evaporator is equal to the enthalpy of the refrigerant vapor at the saturation temperature of the evaporator. The evaporator is assumed to only pass vapor and no liquid to the adsorbent bed. The specifics of the mass transfer between the evaporator, condenser, and bed are discussed in Section 3.2.6. A mass balance is also performed for the evaporator node given in Equation 3.18

$$\frac{\left(m_{ev}^{j+1} - m_{ev}^{j}\right)}{\Delta t} = \dot{m}_{co,ev}{}^{j} - \dot{m}_{ev,bed}{}^{j} \tag{3.18}$$

The mass and energy balance are solved simultaneously. The condenser is modeled in a manner similar to that used for the evaporator. The energy balance for the condenser is given in Equation 3.19

$$\frac{\left(m_{co}{}^{j+1}u_{co}{}^{j+1} - m_{co}{}^{j}u_{co}{}^{j}\right)}{\Delta t} = \sum_{n=1}^{k} UA_{co,stc}\left(T_{stc,n}{}^{j} - T_{co}^{j}\right) - \dot{m}_{co,ev}{}^{j}h_{co}{}^{j} + \dot{m}_{bed,co}{}^{j}h\left(T_{sp}^{j}, v_{sp}^{j}\right) \tag{3.19}$$

A mass balance is also performed for the condenser node. The left hand side of the equation is the internal energy of the condenser, because the internal energy property calculation includes the specific volume initially and in the next step, the heat of vaporization is accounted for here. The heat transfer conductance between the condenser refrigerant and condenser tube wall, $UA_{co,stc}$, is also varied linearly with the temperature difference between the condenser refrigerant temperature and the coupling fluid temperature as was done in the evaporator. The maximum value is 4 W K^{-1} and the minimum value is 0.05 W K^{-1}, as in the evaporator.

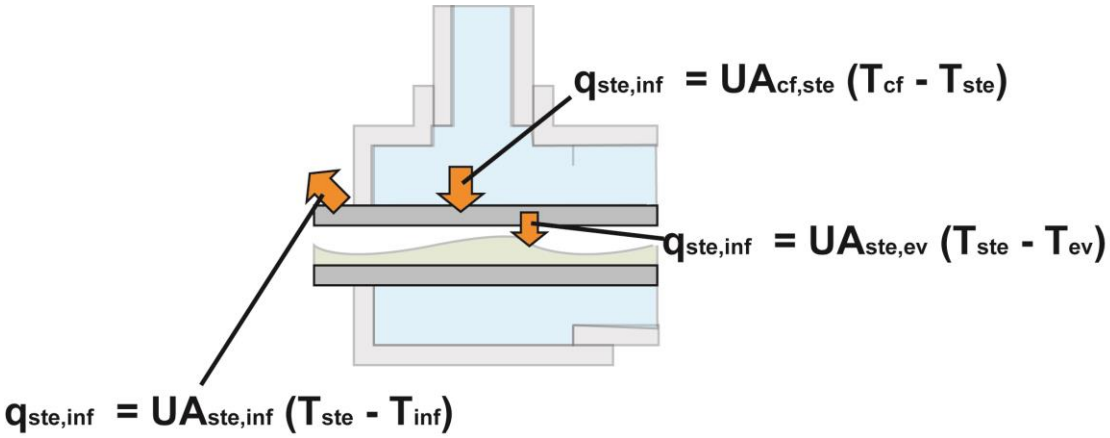

Figure 3.18 Energy balance for evaporator structure node

The evaporator and condenser tube walls are modeled in the same way. The first and last nodes for the wall have losses to the surroundings to account for heat transfer to surrounding connections. The energy balances for the nodes closest to the adsorbent bed in both the evaporator and condenser are shown in Equations 3.20 and 3.21, respectively

$$m_{ste,1}c_{p,st}\left(T_{ste,1}^{\,j+1}-T_{ste,1}^{\,j}\right)=UA_{ste,ef}\left(T_{ef,1}^{\,j}-T_{ste,1}^{\,j}\right)-UA_{ev,ste}\left(T_{ste,1}^{\,j}-T_{ev}^{\,j}\right)-UA_{ste,\inf}\left(T_{ste,1}^{\,j}-T_{\inf}\right) \quad (3.20)$$

$$m_{stc,1}c_{p,st}\left(T_{stc,1}^{\,j+1}-T_{stc,1}^{\,j}\right)=UA_{stc,cf}\left(T_{cf,1}^{\,j}-T_{stc,1}^{\,j}\right)-UA_{co,stc}\left(T_{stc,1}^{\,j}-T_{co}^{\,j}\right)-UA_{stc,\inf}\left(T_{stc,1}^{\,j}-T_{\inf}\right) \quad (3.21)$$

Figure 3.20 illustrates this energy balance. The middle nodes are calculated the same way as in Equations 3.16 and 3.17, but without the final loss term. The convection

coefficient for the inner surface of the outer fluid annulus is determine assuming laminar flow using the adjusted Nusselt numbers for concentric tubes from Kays and Perkins (1972). The Nusselt number for this case with D_o = 12.7 mm and D_i = 6.35 mm is 5.56. The convection coefficient on the inner surface is 550 W m^{-2} K^{-1}. The heat transfer conductances of the coupling fluid, $UA_{stc,cf}$ and $UA_{ste,ef}$, are both 4.5 W K^{-1}. The convection coefficient for the fluid to the outer wall of the evaporator and condenser is 425 W m^{-2} K^{-1}; however, the thermal resistance to the surroundings is dominated by the insulation around the outside of the tube-in-tube heat exchanger and the UA is calculated based on that insulation. The insulation is chosen to be a 1.87 cm (3/4 in.) thick layer of foam insulation with an effective thermal conductivity of 0.03 W m^{-1} K^{-1}. The heat transfer coefficient for the outer surface is calculated based on natural convection and radiation heat transfer. For the natural convection, the correlation for natural convection over a horizontal tube from Churchill and Chu (1975a) is used again. The temperature difference between the surface and the surroundings is assumed to be 1°C and the natural convection coefficient is found to be 2.2 W m^{-1} K^{-1}. The radiation heat transfer coefficient is calculated using Equation 3.12 with the insulation emissivity assumed to be 0.9 (rubber) (Engineering Toolbox, 2013). The radiation heat transfer coefficient is found to be 2.5 W m^{-2} K^{-1}. The total heat transfer coefficient for the outer surface of the insulation is rounded to 5 W m^{-2} K^{-1}. The heat transfer conductance values for losses to the surrounding are then $UA_{ste,inf}$ and $UA_{stc,inf}$, are 0.05 W K^{-1}. The energy balance for one of the evaporator coupling fluid stream nodes is given by Equation 3.22

$$m_{ef} c_{p,f} \frac{\left(T_{ef,i}^{\,j+1} - T_{ef,i}^{\,j}\right)}{\Delta t} = UA_{ste,ef}\left(T_{ef,i}^{\,j} - T_{ste,i}^{\,j}\right) - UA_{ef,\inf}\left(T_{ef,i}^{\,j} - T_{\inf}\right) + \dot{m}_{ef} c_{p,f}\left(T_{ef,i}^{\,j-1} - T_{ef,i}^{\,j}\right) \quad (3.22)$$

The mass flow rate of the coupling fluid through the evaporator and the condenser is 1 g s^{-1} and each of the nodes contains 6.6 g of water. The coupling fluid enters the evaporator at 20ºC, to match with the expected experimental results, and the condenser at 25ºC. The last term represents the loss from the fluid stream to the surroundings at the ends of the tube-in-tube heat exchanger. The heat transfer conductance for this loss term, $UA_{ef,inf}$, is 0.002 W K^{-1}. For this value, it is assumed that the refrigerant transfers heat effectively out to the tube wall that is conducted at the ends and that the area of these tubes that are transferring is effectively ~4% of the tube area (about 0.5 inches of tube length on either side). The same insulation thickness and natural convection value are used for this loss. The condenser coupling fluid stream is analyzed in the same way, with similar heat transfer conductances. The amount of heat removed or added to the coupling fluid stream is used to determine the cooling rate in the evaporator and the heat rejection rate in the condenser.

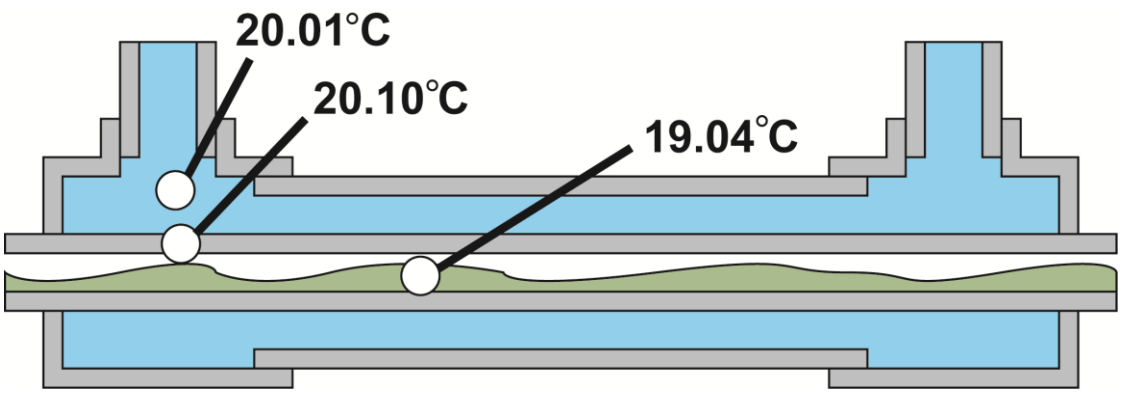

Figure 3.19 Temperatures in the evaporator at the sample time step

For the sample point, the evaporator refrigerant space, the tube wall closest to the adsorbent bed, and the fluid inlet point are considered. Initially these nodes are at 19.04ºC, 20.10ºC, and 20.01ºC, respectively. The mass of refrigerant in the evaporator space is 14.5 g. The heat transfer from the tube wall to the coupling fluid loop is 0.459 W

and the heat transfer from the tube wall to the evaporator refrigerant 0.196 W. The loss to the surroundings from the tube wall is 0.240 W and the loss from the coupling fluid to the surroundings is 0.009 W. There is no mass transfer from the condenser or to the evaporator in this time step, because the adsorbent bed is lower in pressure than the condenser and higher in pressure than the evaporator, so the check valves prevent flows. Therefore, the mass of refrigerant in the evaporator is the same at the end of the time step. The final temperature for each of the nodes is 24.26ºC, 20.10ºC, and 20.01ºC, respectively.

3.2.5 Equilibrium Model

The equilibrium specific adsorption is determined using the Dubinin-Astakhov (DA) equilibrium model (Do, 1998). The DA model uses the available pore volume, the absolute temperature of the adsorbent, and the pressure of the refrigerant vapor surrounding the adsorbent to determine the equilibrium specific adsorption, the mass of refrigerant adsorbed per mass of adsorbent. The adsorbent is defined by constants for activated carbon taken from Critoph (1996). The DA equilibrium equation is given by

$$w_{eq} = \rho V_{pore} \exp\left(-D\left(\frac{T_{adK}}{\beta} \ln\left(\frac{P_{sat}}{P_{surr}} \right) \right)^{n} \right) \tag{3.23}$$

where w_{eq} is the equilibrium concentration in the adsorbent, ρ is the density of the ammonia as a saturated liquid at the temperature of the adsorbent, V_{pore} is the specific volume of pores, β is the interaction coefficient between the activated carbon and ammonia, T_{adK} is the absolute temperature of the adsorbent, P_{surr} is the pressure of the vapor surrounding the adsorbent, P_{sat} is the saturation pressure at the temperature of the adsorbent, D is a constant for carbon, β is a constant for carbon taken from Critoph

(1989a), and n is a constant set by the DA as 2. With each time step, the new equilibrium concentration is calculated for the section of adsorbent, assuming that it is at a uniform temperature. The uniform temperature adsorbent assumption is justified because thermal diffusivity in the adsorbent is approximately three orders of magnitude larger than the mass diffusivity in the adsorbent.

In addition to the equilibrium adsorption calculation, it is also important to determine the amount of energy the adsorption process releases or absorbs. The heat released or adsorbed can be attributed to two sources; the heat of vaporization of the ammonia being adsorbed as the ammonia transitions from vapor to liquid on the adsorbent surface, and the heat of adsorption caused by the interaction of the refrigerant with the activated carbon surface. The heat transfer component from adsorption is

$$-H_{ad} = h_{fg} + \beta E_0 \left(\ln \tfrac{1}{\theta}\right)^{1/n} \tag{3.24}$$

The heat of vaporization, h_{fg}, is the enthalpy released by the ammonia condensing from the vapor state in the space around the adsorbent to a liquid state at the temperature of the adsorbent. The second term varies with temperature, but is not strongly dependent on temperature and depends most heavily on the interaction energy term E_0. This term is taken from Chua *et al.* (2004).

3.2.6 Mass Transfer Model

Two types of mass transfer occur in the model, inter-component and adsorbent mass transfer. The inter-component mass transfer is regulated by the valves between the components. The adsorbent mass transfer is determined using the linear driving force method. Both modes are discussed here.

3.2.6.1 Mass Flow Between Components

The fluid movement between the system components is driven by the pressure changes between the components and is regulated by valves between components. The intra-component pressure drop is less than 0.1% of the inter-component pressure drop and it is therefore assumed that the pressure within a component is uniform and all pressure drops occur between components. The hydraulic diameter for flow between components is less than 10% of the hydraulic diameters in components. The Darcy-Weisbach equation can be used to show that the intra-component pressure drop can be neglected

$$\Delta P = f_D \frac{L_{pipe}}{Dia} \frac{\rho Vel^2}{2} \tag{3.25}$$

Assuming the friction factor, density, mass flow rate, and pipe lengths are similar, a factor of 10 reduction in diameter results in a factor of 100 increase in fluid velocity, which results in an increase in the pressure drop of ~10^5 for these more narrow portions of the system. Some fundamental assumptions are made about the nature of the mass flow, based on the design of the system. The expansion valve is placed at the bottom of the condenser and it is assumed that the refrigerant leaving the condenser is in a liquid state as long as there is liquid present in the condenser. Similarly, it is assumed that only vapor passes between the adsorbent bed and the other system components. This is a reasonable assumption because the orientation of the system components ensures separation of the liquid and vapor. The valves between system components are separate subprograms in the model. The valve models take the pressure and the refrigerant quality in each component as inputs and return the mass transfer rate for the time step.

In each valve, the mass transfer rate is determined by setting the pressure drop through the valve equal to the pressure difference between the components. The mass flow rate is calculated as shown in Equation 3.26

$$\dot{m} = K_{valve} A_{space} \sqrt{2|\Delta P| / v}\, sign(\Delta P) \tag{3.26}$$

The driving pressure difference is ΔP, the difference in pressure between the components of the system, and the sign of the pressure difference determines the direction of the flow rate. K_{valve} is the pressure drop coefficient for the valve as well as for the connections between the components. Between the adsorbent bed and the other system components is also a filter preventing adsorbent material from leaving the adsorbent bed. The filter is accounted for by a decrease in the valve coefficient. A_{space} is the area through which the refrigerant flows within the valve. v is the specific mass of the refrigerant within the component from which the refrigerant flows. To prevent instability, the maximum pressure difference is set to 20 kPa. For most of the system operation, the pressure difference between components is much lower than this. The values of K_{valve} and A_{space} for each of the valves are found in Table 3.2.

The calculation of the flow from the condenser to the evaporator for the time step in question is described here. At the sample time, the pressure in the condenser, P_{cond}, is 997.6 kPa and in the evaporator, P_{evap}, is 995.1 kPa. This gives a ΔP value of 2.5 kPa and the sign of this pressure difference indicates that the flow will be from the condenser to the evaporator. The specific volume of the liquid within the condenser is 0.00166 m^3 kg^{-1}. The smallest value of the expansion valve, A_{space}, has a fixed value of 0.0024 cm^2 for this model and K_{valve} for this model is held at 0.55. The mass flow rate between the

condenser and evaporator is then calculated to be 1.44×10^{-7} kg s^{-1} for the sample time step.

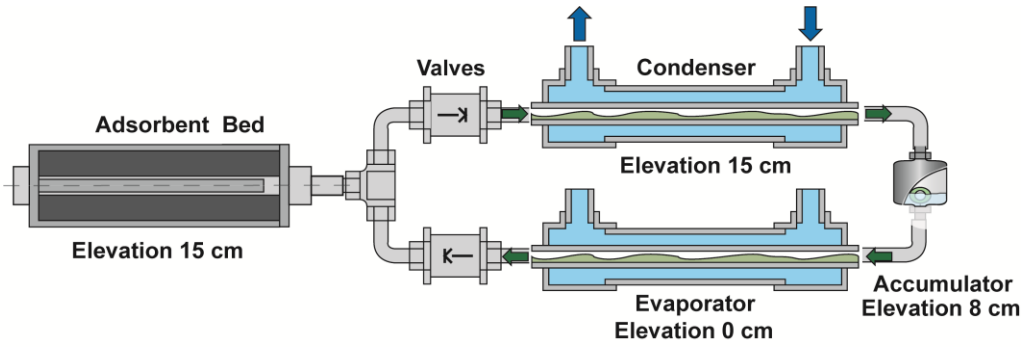

Figure 3.20 System component elevations with a float valve accumulator

The system design calls for a float valve controlled expansion valve that maintains a constant refrigerant level within the condenser, shown in Figure 3.20. This prevents the dry out of the condenser and flooding of the evaporator that can lead to performance degradation. As the level of refrigerant increases in the condenser, the float opens the valve and allows refrigerant transfer. As discussed in the experimental section in Chapter 4, it was not feasible to use a float valve in the experimental facility because a compatible float valve of an appropriate size could not be found. Appendix C demonstrates that it is possible to access the operation of the facility accurately without a float valve until a dry-out or flooding condition is reached. The model uses a float valve that opens when the condenser contains 12 grams of ammonia. When the mass of refrigerant is less than this, the mass flow rate is set to zero regardless of the pressure difference between the condenser and evaporator.

The connections between the evaporator and the adsorbent bed and between the adsorbent bed and the condenser are modeled as check valves. Flow is only allowed in

one direction in the system, if mass would be transferred into evaporator or from the condenser into the adsorbent bed, the mass flow rate is set to zero.

3.2.6.2 Adsorbent

Refrigerant transfer into and out of the adsorbent is calculated using the linear driving force approximation (LDF). The equilibrium concentration used in the LDF equation is calculated using the DA model as described in Section 3.2.5. The change in concentration is calculated using the linear driving force approximation is shown in 3.25

$$\frac{dw_{ad}}{dt} = K_{ldf}(w_{eq} - w_{ad}) \tag{3.27}$$

The change in concentration in the adsorbent is equal to the difference between the equilibrium concentration and the current concentration multiplied by the linear driving force mass transfer coefficient, K_{ldf}, which is obtained from the properties of the adsorbent material as follows:

$$K_{ldf} = \frac{F_o Diff}{r_{ad}^2} \tag{3.28}$$

where F_0 is a geometric parameter based on the shape of the adsorbent, r is the radius of the adsorbent, and D is the effective diffusivity of the refrigerant within the material.

Raymond and Garimella (2009) investigated the range of dimensionless times over which the linear driving force (LDF) method was an appropriate approximation for the mass transfer occurring in the system. They found that for dimensionless half cycle times greater than 0.12, the LDF method is accurate for modeling mass transfer. In the present study the dimensionless half cycle time varies from 0.4 to 0.7; therefore, it is acceptable to use this approximation. The LDF assumes that the resistance to mass transfer is entirely in the solid phase; therefore, mass transfer is uniform throughout the

bed. This is justified, because the mass transfer in the gas phase is approximately three orders of magnitudes faster than in the solid phase.

For the sample point being considered, the equilibrium uptake was determined to be 0.4967 kg kg^{-1} and the current uptake is 0.5013 kg kg^{-1}. The driving concentration difference for this time step is 0.00457 kg kg^{-1}. The radius, *r*, of the adsorbent particles is assumed to be 0.001 m in this model based on the particle size used in the experimental work. The shape factor, F_o, for the adsorbent in this system is 15, and the effective diffusion coefficient of the refrigerant in the adsorbent taken from literature (Do, 1998) is 3×10^{-9} m^2 s^{-1}. The K_{ldf} is then 0.045 s^{-1} for the adsorbent in this system. To determine the amount of refrigerant transferred into or out of the adsorbent for this time step, the time rate of change of specific adsorption is multiplied by the mass of adsorbent in the node

$$\Delta m_{am\,j}^{\ i} = \frac{dw_{ad}}{dt}_{j}^{\ i} m_{ad\,j} \Delta t \tag{3.29}$$

For the node being considered the starting ammonia mass is 0.8625 g. The change in refrigerant in the adsorbent is 2.77×10^{-7} kg for this time step. The change in refrigerant mass is then used to determine the new refrigerant mass for the next time step:

$$m_{am\,j}^{\ i+1} = m_{am\,j}^{\ i} + \Delta m_{am\,j}^{\ i} \tag{3.30}$$

The resulting new refrigerant mass for the adsorbent node is 0.8623 g.

3.3 Alternate Designs

Alternative designs were developed with the goal of simplifying the system operation, directly air coupling the adsorbent bed, and eliminating or limiting electrical requirements for fluid coupling pumps and control systems. Models were used to test

various design ideas for overcoming the limits of current adsorption technology and evaluate their performance. This modeling, coupled with experimental evaluation, led to the development of two final adsorbent beds for comparison and testing. The two alternative design concepts are discussed here. A more detailed discussion of the experimental beds based on these designs is found in Chapter 5. These two alternate designs approach the design of the adsorbent bed differently than a conventional system and offer different advantages and disadvantages that are discussed here. The first is a cylindrical design where heat is introduced in the center of the adsorbent bed and cooling delivered on the external surface. The second is a design that operates using thermal switches and leverages thermal masses to increase the speed of heat transfer into and out of the bed. Both systems are directly convection coupled to the surrounding air and utilize natural convection for cooling, eliminating the cooling loop typically found in adsorption systems. The second system has no coupling fluid for the bed at all. The baseline model developed for a conventional adsorbent bed was used as a starting point for modeling the CHEC and Flat Bed designs. The differences from the baseline model are discussed below.

Table 3.2 Different beds modeled

Feature	**Baseline**	**CHEC**	**Flat Bed**
Heating location	Center	Center	First surface
Heating method	Liquid coupled	Liquid coupled/electric heater	Solid contact to heat source
Cooling location	Center	External	Opposite surface
Cooling method	Liquid coupled	Air coupled	Solid contact to air coupled cooler
Control	Switching of coupling fluid temperature	Periodic heating	Bed movement at specified conditions

3.3.1 CHEC Design

The CHEC system uses a central heating tube, surrounded by adsorbent particles enclosed in an outer cylindrical shell. The central heating tube can be a fluid channel, an electrical heater (as is used in the experiments) or a heat pipe. Figure 3.21 shows a schematic of the CHEC design with an electrical heater. Unlike the baseline system, the adsorbent is not insulated from the outer bed wall and the cooling is provided by fins on the external structure of the adsorbent bed. The outer bed wall then provides direct convection coupling of the adsorbent to the surrounding air to provide cooling. This type of system is best suited for an adsorption system that can be applied to coolant piping to recover the waste heat useful to provide cooling and could use thermally activated valves to control the fluid flow. The fluid heated system assumes circulation from an existing waste heat source to provide the needed heat to the bed. Heat is supplied cyclically for the process while the bed is cooled continuously. Figure 3.22 shows the heat flow during heating and cooling.

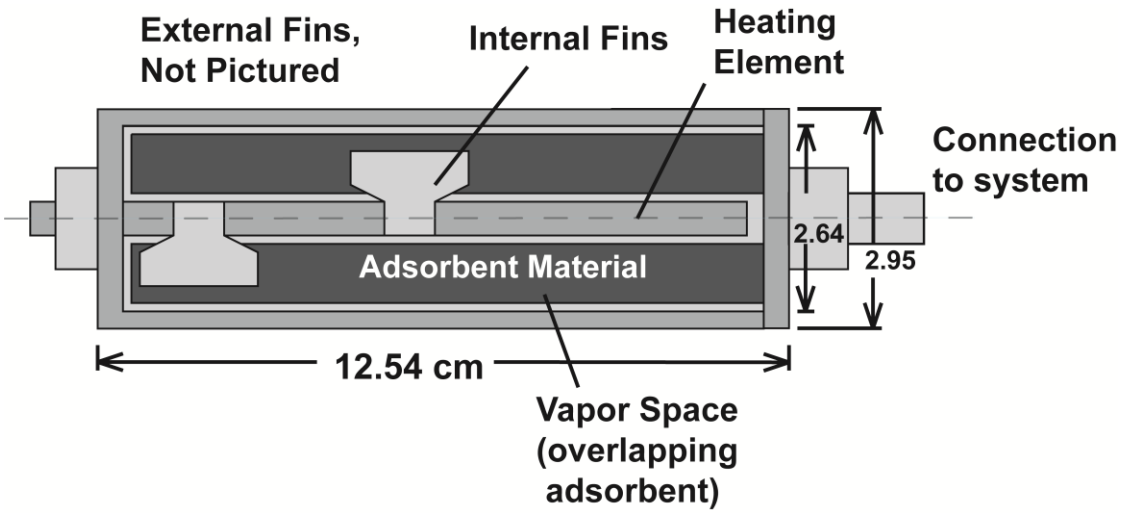

Figure 3.21 CHEC design schematic

The advantage of the CHEC design is its relative simplicity and the ease with which it may be coupled to existing heat sources. The simple design, however, leads to significant thermal shorts that leads to high thermal losses and a lower percentage of the heat input is used in the desorption process. These higher losses lead to lower system efficiencies and cooling capacities.

3.3.1.1 CHEC Model

The CHEC model is very similar to the baseline model. The primary difference between the two models is the UA values between certain nodes and the mass of the nodes. The nodes and equations are the same everywhere in the model, outside of the heating channel in the bed. The CHEC model is developed for a central fluid heat transfer channel, as well as for, an electric heater. The electric heater was used in the experiments, because it yields better uncertainties in heat inputs, making measurement of COP easier and more accurate. The fixed heat input tends to yield faster desorption rates towards the end of the desorption phase, which would otherwise experience decreasing heat input due to lower driving temperature differences between the heating fluid and the bed with time. The more consistent heat input may yield better performance. The CHEC model described here is matched to what was achievable for the experimental system fabrication. In the experiments, the walls of the bed were significantly thicker than in the model, because the bed was assembled from available materials. In a commercially fabricated system, thinner walls could be used and better performance is expected.

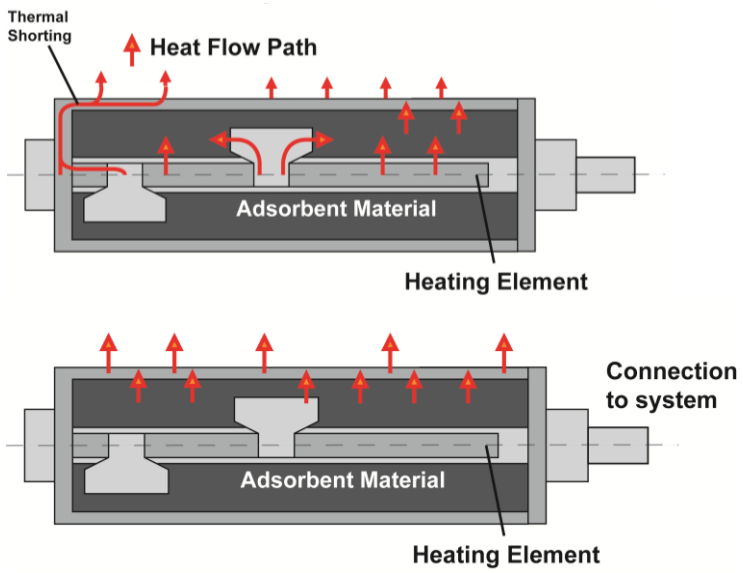

Figure 3.22 CHEC heat flow top) during desorption and bottom) during adsorption

For the electrical heater, the fluid channel nodes are removed and the heat transfer rate into the internal structure nodes is fixed. The internal structure nodes are assumed to be magnesium oxide, which makes up a large portion of the electric heater used in the experiments. The new mass within each of the internal structure nodes is 4 g and the specific heat for these nodes is assumed to be 1000 J K^{-1} kg^{-1}. Because the heater is magnesium oxide, the thermal conductivity of the heater nodes is assumed to be 40 W m^{-1} K^{-1}. In the baseline model, the adsorbent was assumed to transfer heat equally well through its mass as with heat transfer surfaces. It was found that the adsorbent materials did not pack well and contact the heater effectively and therefore, the heat transfer conductance from the internal structure to the first adsorbent node is estimated to be 0.0459 W K^{-1} instead of the previously used value because of the increased contact resistance. The heat transfer conductance down the internal structure length in the axial direction, $UA_{is,is}$, is 0.0725 W K^{-1}. This is higher than it was for the stainless steel heat transfer case and slightly lower than the value for an aluminum internal structure.

The end structure and outer structure are both much thicker for the experimental system than in the baseline model, because threaded connections were used. Therefore, the CHEC model has end structure and outer structure nodes with masses of 13 g and 40.5 g, respectively. These structures are assumed to be made of aluminum and have the same aluminum properties as those in the baseline model. The new UA values used in the CHEC model are shown in Table 3.3 with the baseline values. Most of the structure UAs have increased due to greater area for heat transfer. The heat transfer from the outer surface to the surroundings is increased by the addition of extended surfaces. UAs not listed in the table have remained the same. The insulation between the adsorbent and outer structure was removed, hence the higher heat transfer coefficient to allow faster cooling. The electrical heater does not extend the full distance to connect to the other end of the channel, therefore the UA on the outlet end of the bed is decreased by a factor of four to account for this low contact.

Table 3.3 UA values from the baseline model and the CHEC model

Name	Base [W K^{-1}]	CH [W K^{-1}]	Name	Base [W K^{-1}]	CH [W K^{-1}]
$UA_{fl,is}$	0.201	N/A	$UA_{os,os}$	0.773	1.63
$UA_{is,ad}$	0.0918	0.0459	$UA_{os,inf}$	0.050	0.20
$UA_{is,is}$	0.089	0.0725	$UA_{ad,sp}$	0.100	0.070
$UA_{is,es}$	2.125	11.5	$UA_{es,os}$	2.125	11.5
$UA_{ad,os}$	0.005	0.112			

The adsorbent nodes are treated the same for heat transfer as in the baseline model with the same intra-adsorbent heat transfer coefficients and losses to the end, but the total adsorbent loading is decreased to 35 g for the model because the packing in the CHEC bed was not as tight as initial packing estimates indicated. The mass of the adsorbent nodes were decreased proportionately.

The evaporator and condenser are identical in both models. In some of the models, a change is made to the mass transfer portions of the models by implementing delays that allow pre-cooling and pre-heating before the mass transfer with the evaporator and condenser begins. The delayed opening was done for comparison with experimental results. The delay allows greater peak cooling rates that are easier to measure in experiments. Appendix B discusses the impact of this delay on system performance. It was found that as long as the delay length is chosen, appropriately the system performance is not significantly decreased.

In addition to the differences in UA values, the system operation is different in the CHEC design. In the baseline case the system control is achieved by changing the incoming fluid temperature for mass transfer into the fluid nodes. For the fluid heated system, the flow rate is set to zero during the cooling process. The electrically heated CHEC design accomplishes this by setting the heat input to the structural nodes during the desorption phase and setting the heat input to zero during the cooling phase. The cooling of the adsorbent is achieved in this system and model by transferring heat through the outer structure to the surroundings.

A comparison is also made between the baseline model and the CHEC design, where the masses are held the same. The heat transfer conductances to and out of the end structure and axially are also held the same. Only the heat transfer conductances between the outer layer of adsorbent material and the outer structure and the heat transfer conductances between the outer structure and the surroundings are different. This comparison was also made using the liquid heated system. In this system, the baseline model was used with only two changes. The UA between the outer adsorbent layer and

the outer structure and the UA between the outer structure and the surroundings are replaced with those used in modeling the CHEC system based on the experimental design. The second difference is that the flow rate of heating fluid through the center of the bed is controlled, rather than the temperature at the inlet. During the cooling phase, the mass flow rate of coupling fluid is set to zero, allowing the bed to cool through the outer structure.

3.3.2 Flat Bed Design

The second alternative adsorbent bed design uses a planar bed of adsorbent material in a disk-shaped flat geometry, with thermal switches on either surface of the bed. Heat is constantly supplied to the Flat Bed through a connected heating block while heat is constantly removed from a finned cooling block. Thermal switches adjust the resistance between the adsorbent bed and the heat source and sink, eliminating the need for heat transfer fluid circulation. The actuation for the thermal switch controls is performed using the change in mass of the adsorbent material. The planar shape helps heat the adsorbent evenly.

In the thermal switch system, the bed structure is planar rather than cylindrical, and the design is called a Flat Bed because of the bed shape. The planar geometry lowers the temperature gradient through the adsorbent thickness and increases the surface area for heat transfer relative to the adsorbent mass, allowing more effective cooling with direct air cooling. The Flat Bed system model differs from the baseline model more significantly than the CHEC design. To help illustrate the differing geometry, Figure 3.23 shows a schematic of the Flat Bed system, the thickness of the bed is exaggerated.

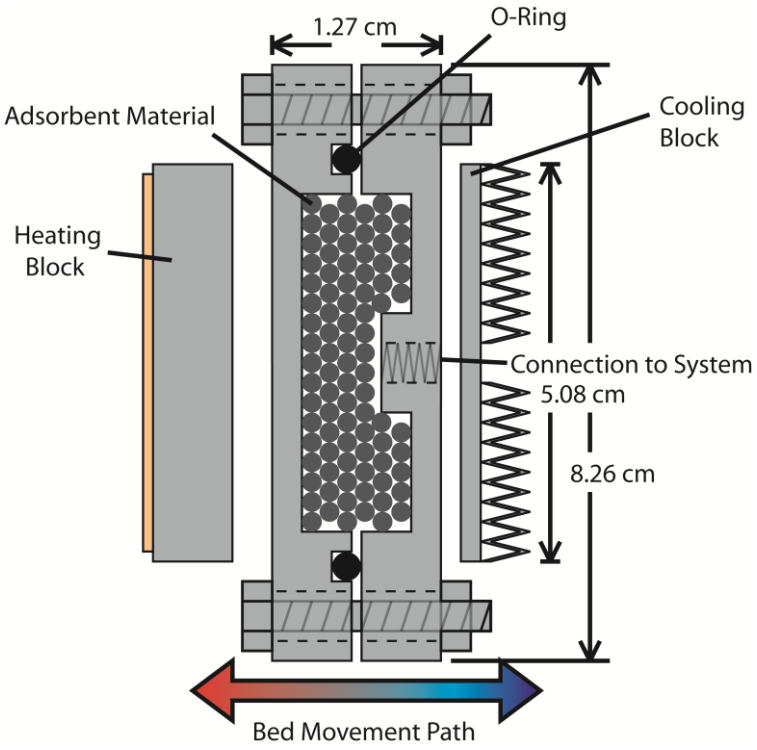

Figure 3.23 The Flat Bed adsorbent bed schematic

The bed is a cylindrical disk with a layer of adsorbent pressed between the two walls. Refrigerant is introduced into the center of the bed by a tap through the bed wall that connects to the evaporator and the condenser through tubes 3.18 mm (0.125 in.). Heat flows from the left to the right in the figure above. These heat flows for the Flat Bed system are shown in Figure 3.24. Here, the heat is assumed to be supplied by a heating pad, as is done in the experiments, with a layer of insulation backing the heater, but in actual applications, the heat source could be a hot surface or radiator lines. Heat flows from the heating pad into a heating block that stores the heat by increasing in temperature and then rapidly transfers the heat to the adsorbent bed. The heat flows into the wall of the adsorbent bed. The adsorbent is pressed between the two walls of the system and has good contact with a large contact area. The wall transfers heat to the adsorbent and to the

edges of the bed, the end structure in the model, the heat then shorts through the end structure to the other side of the bed. On the opposite side the bed, the bed wall is also transferring heat to the adsorbent and receiving heat from the edges of the structure. The adsorbent bed wall transfers heat to the cooling block, which in turn transfers heat to the surroundings. The cooling block also acts to remove heat quickly, because it continues to transfer heat to the surroundings during the desorption phase. The bed is exposed to the surrounding air on the outer surfaces and the exposed surfaces are transferring heat to the surroundings throughout the system.

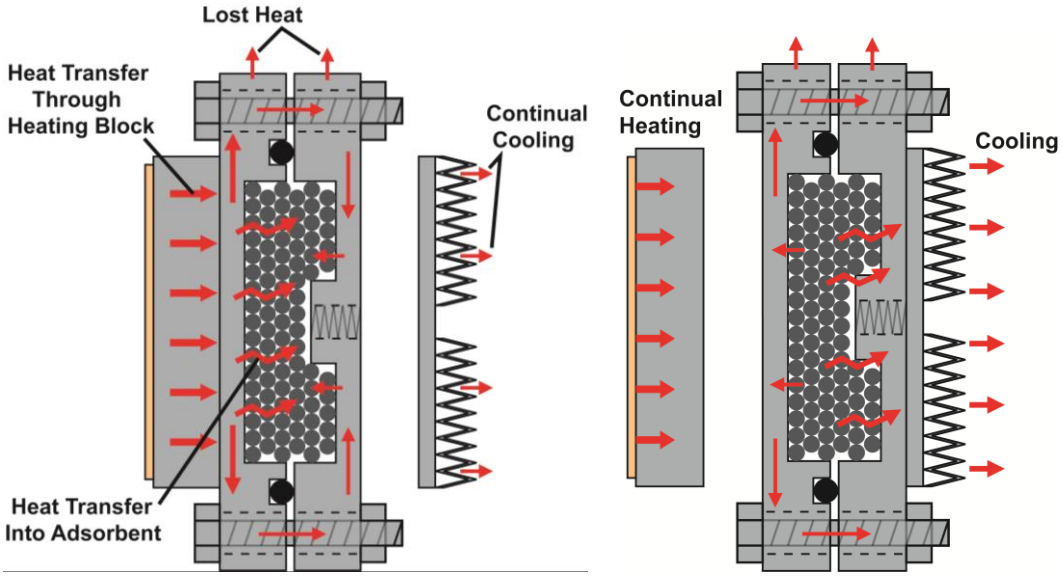

Figure 3.24 a) Heat flow path during heating and b) heat flow during cooling

The Flat Bed system changes the adsorbent bed design so that heat flow into the system is controlled by two thermal switches that operate based on the weight of the adsorbent bed. The thermal switches also take advantage of thermal mass to store energy when not in contact with the bed so that heating and cooling of the bed may be done more rapidly. The Flat Bed design also seeks to improve the heat transfer into the adsorbent by

applying direct pressure to the adsorbent particles to reduce contact resistances. This system can be scaled by increasing the radius of the disk, which has the added advantage of reducing the amount of thermal mass present in the structure.

3.3.2.1 Flat Bed Model

Even heating over the surface of the Flat Bed eliminates the need for segregation of the Flat Bed in two dimensions. Instead, the adsorbent is divided through the thickness of the bed into four nodes. The walls of the internal structure and outer structure become single nodes that represent the walls of the Flat Bed. The end node becomes the rim of the disk joining the bed. Other nodes are added for the heating block, the electrical heater, the cooling block, fittings connecting the bed to the system, and the insulation behind the heating block. The resistance network for the bed is shown in Figure 3.25 with each of the nodes named.

The UAs and masses of the nodes are shown in Tables 3.4 and 3.5. The two heat transfer conductances listed for heat transfer from the bed wall to the heating and cooling block are for when the system is connected or not connected to those components thermally by the switches. The losses for the system also change. The amount of area available for losing heat to the ambient surroundings changes as the bed is shifted. When the bed is in contact with the heating block, the area in contact between the heating block and the adsorbent system cannot transfer heat to the surroundings. The two values listed for heat loss terms correspond to these two phases of operation.

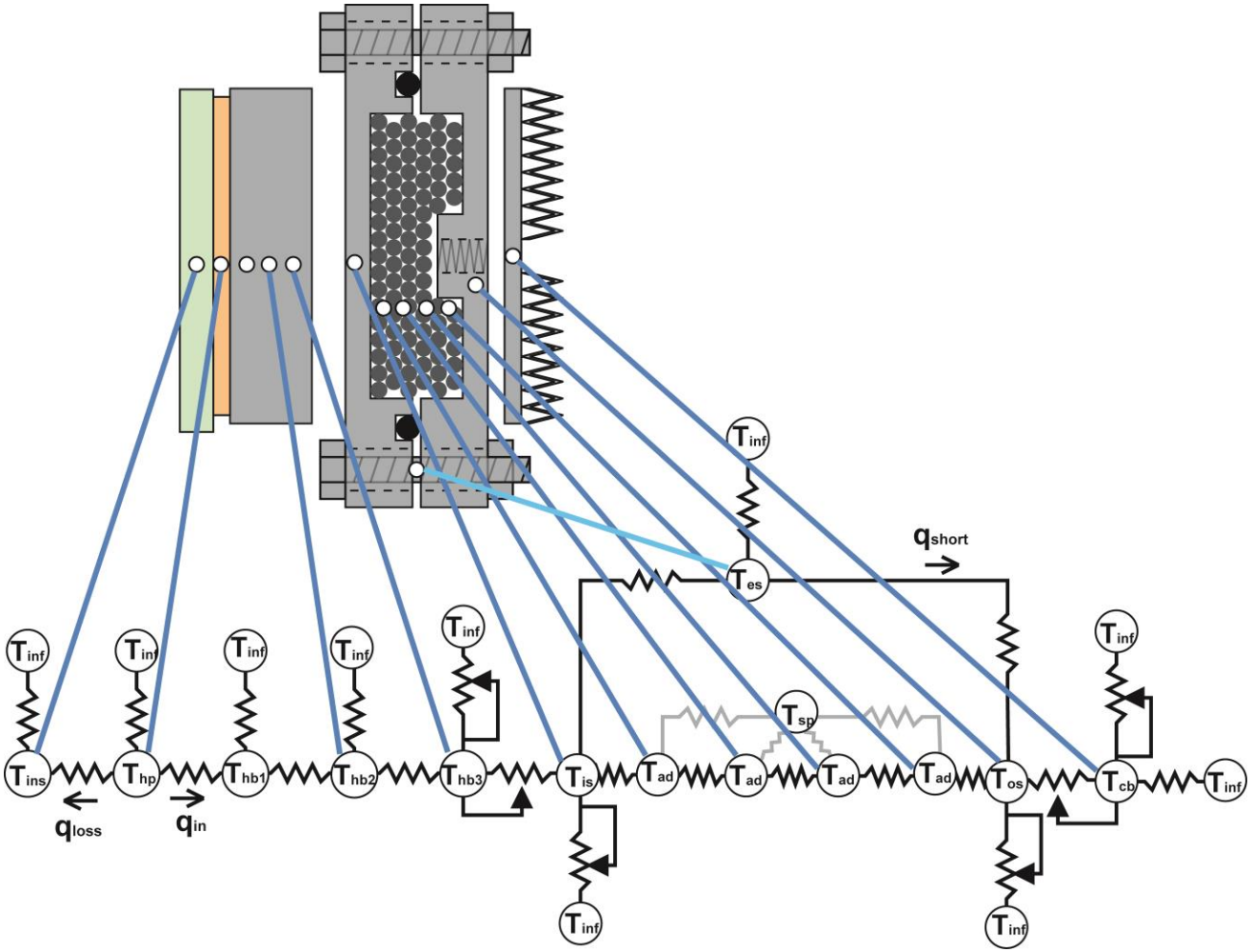

Figure 3.25 Resistance network for the Flat Bed adsorbent bed

The evaporator and condenser were modeled identically for all the systems considered initially; however, in experimental implementation, smaller coupling fluid lines were used for the Flat Bed system, and therefore this was changed in the Flat Bed models. The evaporator and condenser volume are decreased by a factor of four and the masses of the structural components are decreased by a factor of two for the evaporator and condenser.

Table 3.4 UA values for the flat bed model

Name	**UA [W K^{-1}]**	**Name**	**UA [W K^{-1}]**	**Name**	**UA [W K^{-1}]**
$UA_{hp,ins}$	0.01	$UA_{is,inf\ high}$	0.0316	$UA_{fit,inf}$	0.020
$UA_{ins,inf}$	0.0005	$UA_{is,inf\ low}$	0.0032	$UA_{os,cb\ high}$	1.067
$UA_{hp,hb}$	0.8	$UA_{is,es}$	0.395	$UA_{os,cb\ low}$	0.0246
$UA_{hp,inf}$	0.115	$UA_{es,inf}$	0.0218	$UA_{cb,inf\ high}$	0.353
$UA_{hb,inf\ high}$	0.079	$UA_{es,os}$	0.395	$UA_{cb,inf\ low}$	0.341
$UA_{hb,inf\ low}$	0.026	$UA_{ad,ad}$	0.798	$UA_{stc,inf}$	0.001
$UA_{hb,is\ high}$	1.067	$UA_{os,inf\ high}$	0.0316	$UA_{ste,inf}$	0.001
$UA_{hb,is\ low}$	0.0246	$UA_{os,inf\ low}$	0.0032	$UA_{ef,inf}$	0.001
$UA_{is,ad}$	0.798	$UA_{ad,os}$	0.798	$UA_{cf,inf}$	0.001
$UA_{hb,hb}$	0.8	$UA_{os,fit}$	0.40		

Table 3.5 Mass of each node

Name	**Mass [g]**	**Name**	**Mass [g]**	**Name**	**Mass [g]**
m_{ins}	40	m_{ad}	2.5	m_{ste}	125
m_{hp}	10	m_{es}	100	m_{stc}	125
m_{hb}	46	m_{os}	30	m_{ef}	7
m_{is}	30	m_{cb}	50	m_{cf}	7
m_{fit}	20				

The heating pad has a constant energy input over the course of operation. This is modeled as a constant heat input to the heating pad node, m_{hp}. In actual application, the system may also be used with a constant temperature source, therefore, both a constant heat input and a constant temperature for the heating pad node are also modeled. For the constant temperature source, the total transfer out of the heating pad is used as the heat for calculation of the COP.

3.4 Modeling Results

The results from the modeling of a baseline case similar in design to large scale systems are presented here first. These results are valuable for comparison with the designs proposed and investigated as part of this work. Because it is known that the masses of the structural components of the system increase relative to the adsorbent mass as the system is scaled down, a parametric study of the impact of the bed mass on the system operation was conducted. The performance predictions of the base line modeling and increased bed mass ratio systems is discussed. Models were developed for alternate system designs, and the results from these models are compared with the baseline model and presented at the end of this section.

3.4.1 Baseline Model Results

The baseline model is investigated for the case where the source temperature is 100ºC. Various cycle lengths are modeled to evaluate the conditions for maximum cooling capacity and COP can be achieved. The models assume that check valves control flow between components in all of the initial evaluations performed here. The COP here is defined using the convention for adsorption systems from the literature

$$COP = \frac{Q_{cooling}}{Q_{heat,in}} \tag{3.31}$$

The heat in $Q_{heat,in}$ is only the heat transferred from the liquid into the bed. The work required for pumping, losses in coupling fluid systems, and any exergy in the coupling fluid leaving at a high temperature is not accounted for.

Figure 3.26 shows the temperature profile throughout the adsorbent bed for the 750 s half cycle time discussed throughout this chapter. The internal structure

experiences nearly a full swing from the source temperature to the sink temperature, indicating that the dynamic losses for that portion of the bed are very large. The end structure temperature increases and decreases more rapidly than any adsorbent node temperature, which is because of the rapid heat transfer from the internal structure to the end structure. This in turn heats the outer structure rapidly, which is the primary path for losses from the system. The largest swing in the adsorbent temperature is observed in the middle of the adsorbent bed in most models. This is because the adsorbent near the inlet and the structure near the inlet transfer heat to the end which limits the peak temperature for these nodes. The adsorbent near the outlet has the lowest swing because the heating and cooling fluid temperature has changed through the length of the adsorbent bed.

The delivered cooling for this system is shown in Figure 3.27. Positive values indicate heat transfer into the system, while negative values indicate heat transfer out of the system. The peak cooling for this system is 4 watts with average cooling of 1 watt, in this set of results. The negative heat transfer rates indicate periods where heat is being transferred out of the system. Notice that during the desorption phase, there is actually heat being transferred to the coupling fluid. The heat transfer to the coupling fluid is impacted by a number of effects, such as heating of the evaporator by the ambient surroundings, but it is primarily due to fluid from the condenser coming in at a higher pressure and with a higher enthalpy heating the evaporator during the desorption phase. This effect could be eliminated with the addition of a second bed to deliver more uniform cooling. The start-up conditions can also be observed, with lower cooling being delivered on the first adsorption cycle.

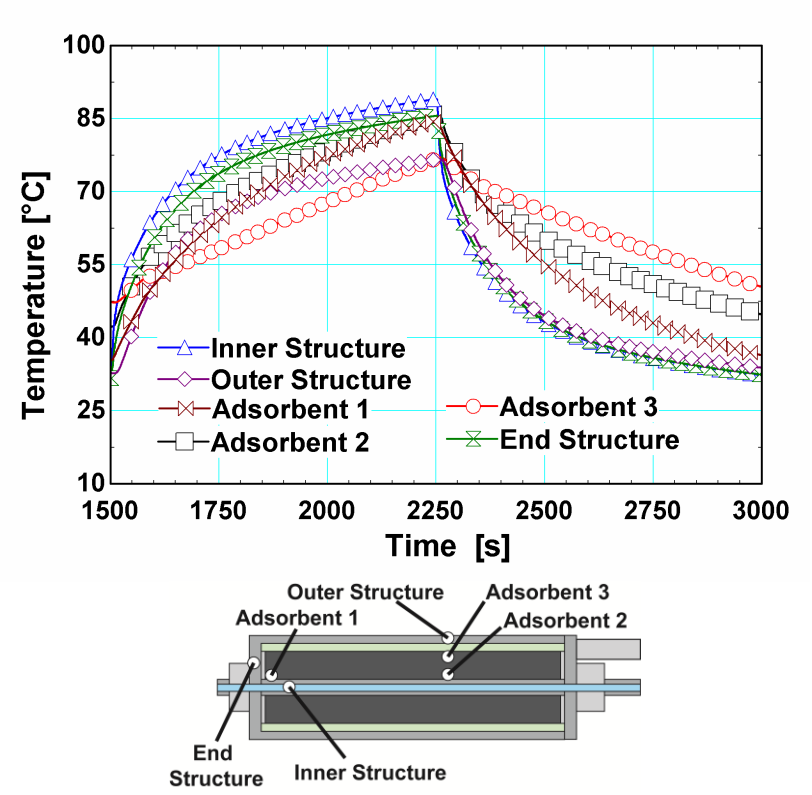

Figure 3.26 Temperature profile in the adsorbent bed for the baseline case during the second cycle

The values considered in the parametric study of the designs are shown in Table 3.5. For each of the cases, the COP and SCC are presented for each set of conditions. The COP here is defined as the amount of heat transferred from the coupling fluid stream divided by the amount of heat removed from the heating fluid stream. The pumping power and heat losses in the coupling fluid system are not taken into account.

Two bed structure materials are considered in this work. The aluminum is a higher conductivity material with a lower thermal capacity. The COPs for the different bed materials are shown in Figure 3.28 at two different source temperatures as the half-cycle time is varied. The stainless steel system has higher COPs than the aluminum bed systems. The main factor for this is that in the baseline model, the aluminum structure

allows the heat to short around the ends of the bed much faster than the stainless steel system with a thermal conductivity approximately ten times larger than that of stainless steel, which increases losses from the system. The aluminum has a thermal capacity approximately 70% of the steel. The system with a steel structure has a COP approximately 25-50% higher in most cases. The highest COPs occur at slightly shorter half cycle times for steel, because the lower thermal conductivity of the steel allows a larger percentage of the heat from the coupling fluid to enter the adsorbent material in the beginning of the cycle. A higher source temperature yields improved COPs for both materials. The COPs and SCCs peak with half cycle times of around 1000 s. SCCs and COPs commonly peak as the half-cycle time is varied in adsorption systems.

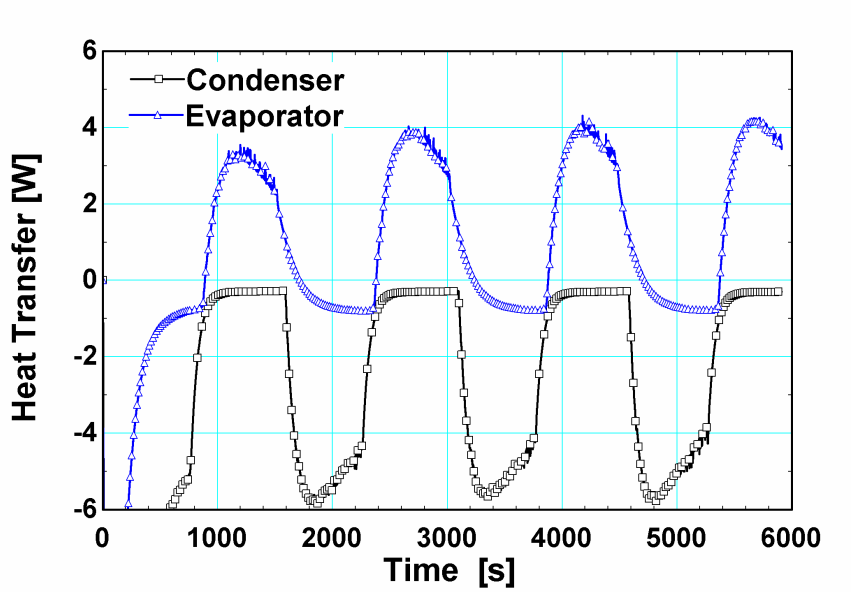

Figure 3.27 Heat transfer rates in the evaporator and condenser

At the peak COP, the swing between the high and low specific adsorption values per heat input is as large as possible for the system. Below this cycle time, the swing in specific adsorption is smaller and a larger portion of the heat input is lost to dynamic losses. When the cycle time is increased, the heat required increases for each additional

amount of refrigerant desorbed, which leads to more heat being used for each increase in the cooling. At the peak SCC, the swing in adsorption uptake per time is as large as possible for the system. When the cycle time is shorter than the SCC peak time, the adsorbent does not have sufficient heating or cooling time to experience a significant change in equilibrium adsorption. When the cycle time is longer than the SCC peak time, the heat transfer rate into/out of the adsorbent is lowered by a lower ΔT between the adsorbent and coupling fluid and the rate of mass transfer decreases, leading to lower average cooling. The half-cycle time where the COP and SCC peak depend upon a number of factors, of which the most important are: how large the dynamic losses are, the heat transfer rate, bed geometry, heat source and sink temperatures, and the adsorbent pair.

Table 3.6 Adsorption and Desorption Conditions Considered

Name	**Desorption Half Cycle Time [s]**	**Adsorption Half Cycle Time [s]**	**Source Temperature [ºC]**
Stainless Steel	500	500	100, 130
	750	750	100, 130
	1000	1000	100, 130
	1250	1250	100, 130
	1500	1500	100, 130
Aluminum	500	500	100, 130
	750	750	100, 130
	1000	1000	100, 130
	1250	1250	100, 130
	1500	1500	100, 130

The SCCs for the two different material systems at the two source temperatures are considered. The SCCs are shown in Figure 3.29 as the half-cycle time is varied. The specific cooling capacities are much closer for the two different materials. The stainless steel structure has slightly higher values. The aluminum system has a lower thermal capacity due to its much lower density and therefore has lower dynamic losses, which

improves the COP somewhat, but more strongly improves the SCC of the system, while the stainless steel has less thermal shorting, which improves both the COP and the SCC. The higher stainless steel COPs indicate that for the baseline system, the decrease in thermal shorting losses is more significant than the increase in dynamic losses. The SCCs for both materials are about 10-20 W kg^{-1} below the typical range for a large scale conventional system.

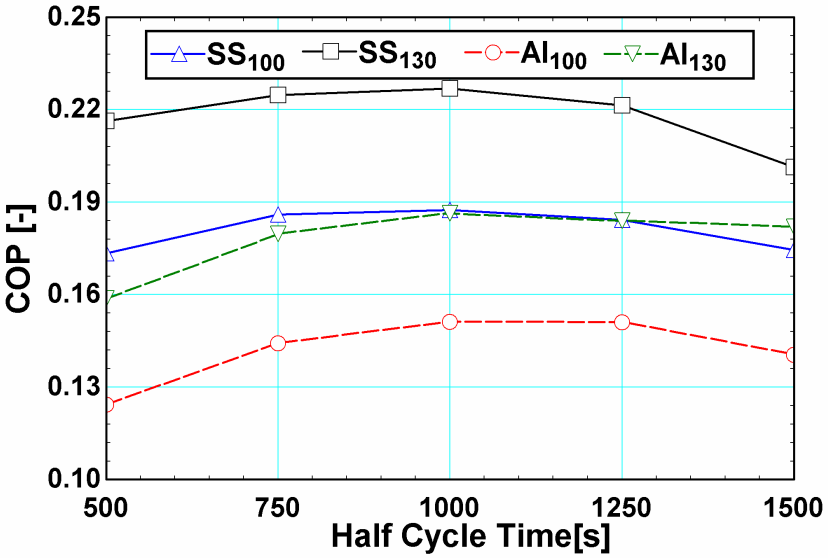

Figure 3.28 COP vs. half cycle time for an aluminum and steel structure with source temperatures of 100ºC and 130ºC

To help better understand the effect of materials, the system was modeled with the aluminum alloy 6061 that had a lower thermal conductivity, 165 W m^{-1} K^{-1}, than the default aluminum initially used in the model (k = 200 W m^{-1} K^{-1}). UAs for the system were revaluated accordingly. The alloy model was compared with the baseline aluminum model for a 750 s half cycle time and a 100ºC heat source temperature.

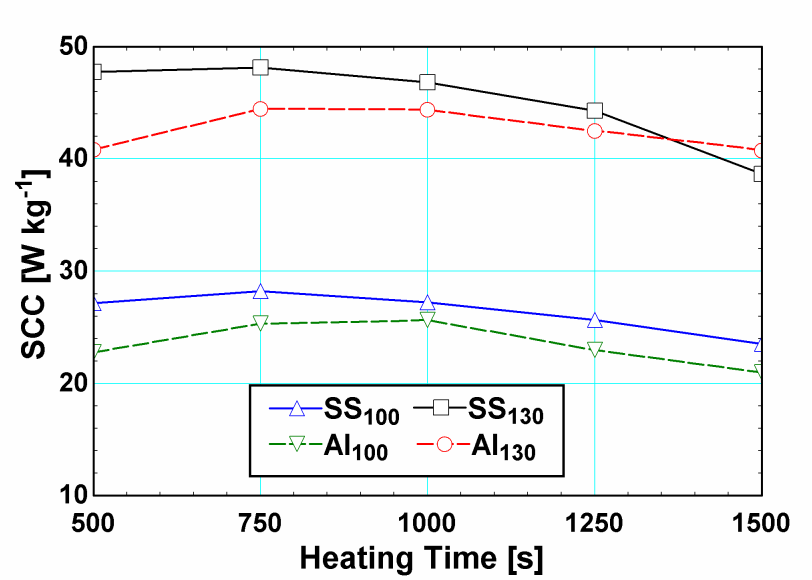

Figure 3.29 SCC vs. half cycle time for an aluminum and steel structure with a source temperature of 100ºC and 130ºC

Thermal shorting, where heat is transferred around the adsorbent materials to the outer structure of the bed without utilization for sorption, is a significant problem at this scale. One possible approach to reduce this shorting effect is to use low thermal conductivity collars around the heat transfer connections into the system that act as thermal breaks. Figure 3.30 shows an adsorbent bed with such collars. The system was also evaluated with a stainless steel collar and with a ceramic collar around the inner structure, to reduce the losses around the end. For the baseline cases, this results in new values of the heat transfer conductance between the internal structure and the end structure, $UA_{is,es}$, of 2.2 W K^{-1} for the stainless steel collar and 0.55 W K^{-1} for the ceramic collar for the experimental systems, and of 0.549 W K^{-1} for the stainless steel collar and 0.137 W K^{-1} for the ceramic collar for the baseline cases.

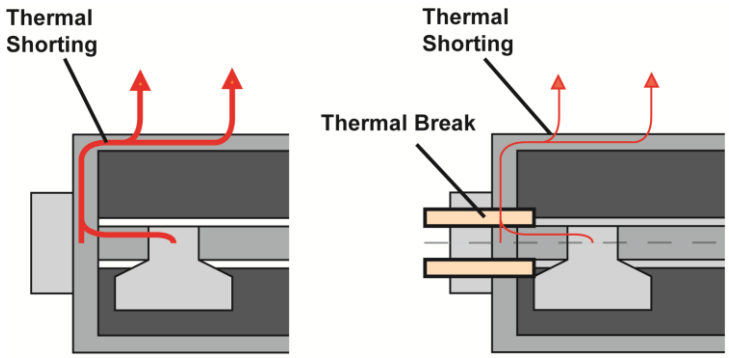

Figure 3.30 Thermal breaks applied to reduce thermal shorting effects

The results from these comparisons can be found in Table 3.6. Accounting for the reduction in heat transfer due to the lower thermal conductivity of an alloy yields only a small increase in COP and SCC, but the introduction of thermal breaks yields a significant increase in system performance, particularly the ceramic break. The introduction of breaks makes the performance comparable or better than the stainless steel system. Throughout the design process, it was found that it is easier to reduce or limit thermal losses from the bed than to eliminate thermal mass.

Table 3.7 Comparison of baseline systems with alloy and thermal breaks

Modifications	**COP**	**SCC [W kg^{-1}]**
Baseline Al	0.144	25.3
Baseline SS	0.186	28.2
Baseline Al-alloy	0.145	25.3
Baseline Al-alloy SS break	0.156	26.2
Baseline Al-alloy Ceramic Break	0.201	29.8

3.4.2 Alternate System Results

The results of the alternate system models are presented here. The CHEC system results are presented first followed by the Flat Bed system. Then a comparison is made between the performances of these systems.

3.4.2.1 CHEC

Two structural materials for the CHEC design, stainless steel and aluminum, are compared. Two methods of heating are also compared, electrically coupled and fluid coupled, for two different heat inputs, 50 W, and 75 W, and two different fluid temperatures, 100ºC and 130ºC. For each of these systems, the half-cycle time is varied and the peak COP and SCC are found. Also, because the mechanism for heating and cooling of the bed is fundamentally different for the CHEC design, the length of the heating and cooling times are varied independently for several cases to determine if a different ratio of heating-to-cooling yields better performance. The CHEC system does not perform as well as the baseline model. This is to be expected, because direct air cooling leads to increased losses throughout the entire cycle.

The COP for the fluid coupled CHEC system is calculated in the same manner as for the baseline case. The COP for the electrically coupled system is calculated as

$$COP = \frac{Q_{cooling}}{Q_{elec}} \tag{3.32}$$

The total cooling output is divided by the total electrical heat input. This system does not have any lost exergy, unlike a conventional fluid coupled system.

Figure 3.31 shows temperatures throughout the bed over the course of one system cycle for the aluminum bed with a 750 s heating time and a 50W heat input. There are several differences to note from the baseline temperature case in Figure 3.31. First, the internal structure has a much larger temperature difference from the rest of the system. The electrical heat input increases the temperature more steadily than liquid coupling with a hot fluid. Second, axial differences in the temperature of the adsorbent are significant. The temperature is highest in the middle of the adsorbent bed rather than at

the fluid inlet. The temperature profile indicates that the cooling effect due losses at the end of the structure is significant. The temperature difference axially is larger than the temperature difference radially in this bed.

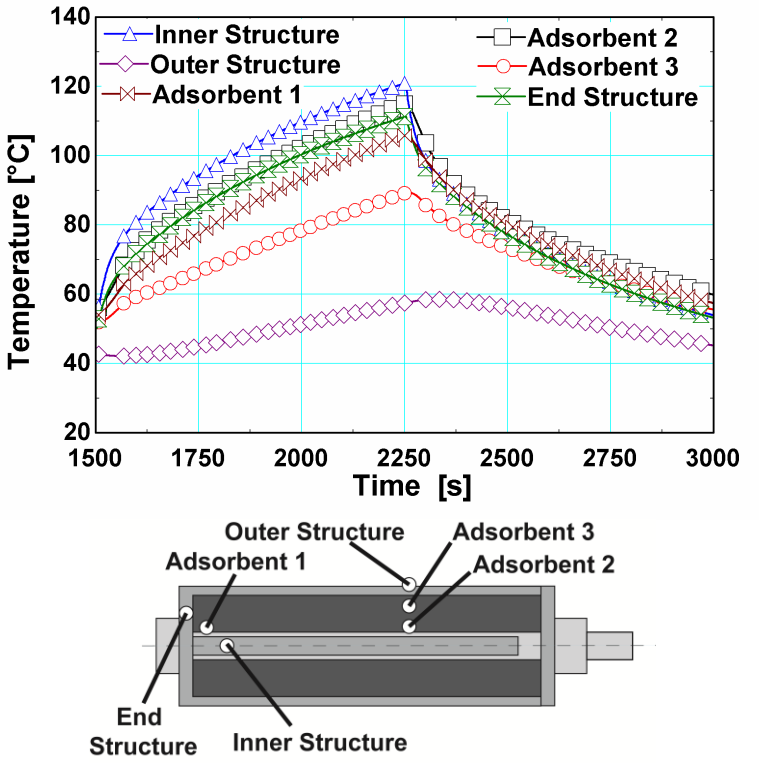

Figure 3.31 Temperature profile in the aluminum CHEC adsorbent bed with a 750s half cycle time and 50 W heat input

The results for the CHEC system with an aluminum and a stainless steel structure with a 50 W heat input as the half-cycle time is varied are shown in Figure 3.33. The peak COP and SCC are higher for the stainless steel system, but the difference in material is not as distinct as was seen in the baseline model. The peak COP and SCC differ by only about 4% between materials, the difference is the same for both parameters. The cooling capacity is also very similar for both materials. The SCCs for both systems range from 40 to 55 W kg^{-1}. The optimal cycle time lengths are also very similar, with the

stainless steel system having a peak at a slightly lower half-cycle time (750 s vs. 850 s). There is also the unexpected result that the peak COP and SCC occur at the same half-cycle time and the two parameters have the same trends in the electrically heated system. As discussed in Chapter 2, in conventional adsorption systems, the peak COP and SCC occur at different half-cycle times.

A higher heat input was also modeled and the results for the 75 W heat input are shown in Figure 3.32. For the 75 W heat input, the aluminum structure performs better than the stainless steel system. The COP improves slightly for the aluminum system and decreases for the stainless steel system. At the higher heating rate, the heat loss is limited by the convection heat transfer for both materials and the lower thermal shorting due to lower thermal conductivity plays a smaller role than the increased dynamic losses due to the higher thermal capacity of stainless steel. Therefore, the cooling capacity and COP increase for both systems, but while the stainless steel system improves only slightly, the aluminum system increases by over 50%.

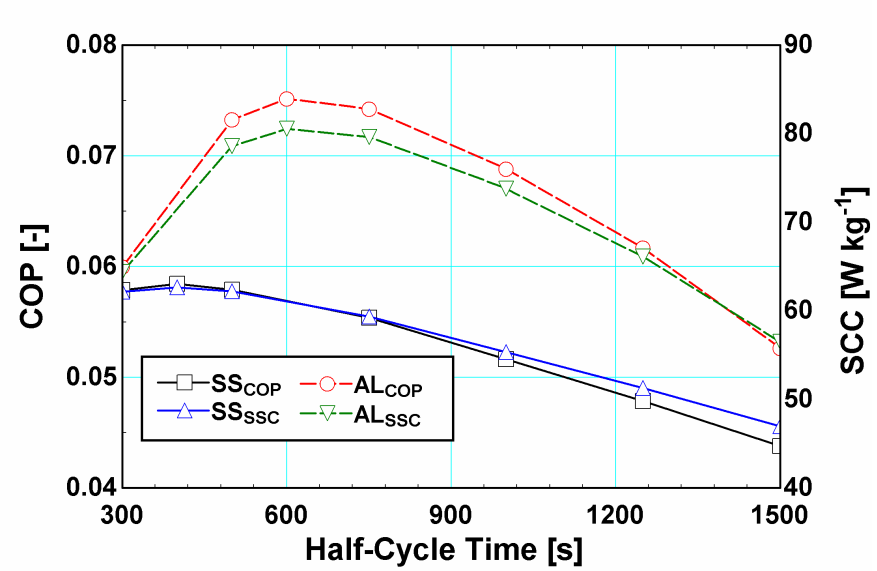

Figure 3.32 CHEC system with a 75 W heat input for a stainless steel and aluminum

Next, the performance of the fluid-coupled CHEC system with a source temperature of 100ºC with different bed structure materials is compared. The results for this temperature are shown in Figure 3.34. For both materials, the COP and SCC are very low for this source temperature. The low performance is caused by continuous cooling of the bed that prevents the adsorbent from getting hot enough to effectively desorb during the desorption phase. This implies that the CHEC system will need higher source temperatures than a conventional system to achieve similar results. The COP is much lower than what was seen for the fixed heat input case. The aluminum system performs better than the stainless steel at these conditions and the optimum half-cycle time for the stainless steel increases to be larger than the optimal value for aluminum, counter to what was observed in previous cases. Because the amount of heat being used for desorption is low, the dynamic losses are more important in this case. The peak COP and SCC occur at different half-cycle times in these cases, so that unlike the constant heat input case, it does not appear that it will be possible to optimize for both simultaneously.

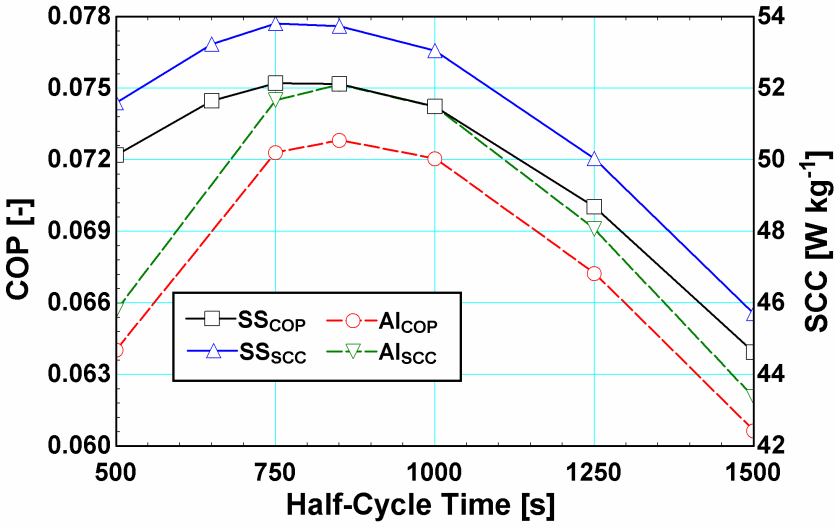

Figure 3.33 CHEC system with a 50 W heat input

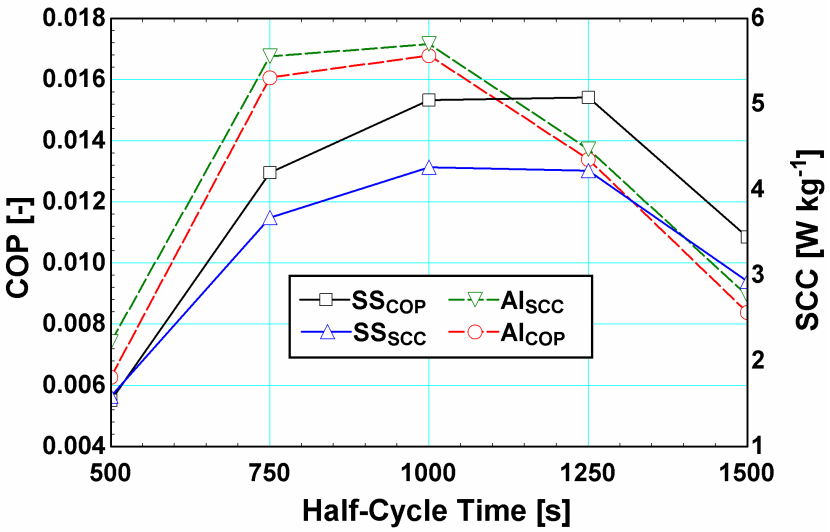

Figure 3.34 CHEC system with 100ºC source temperature

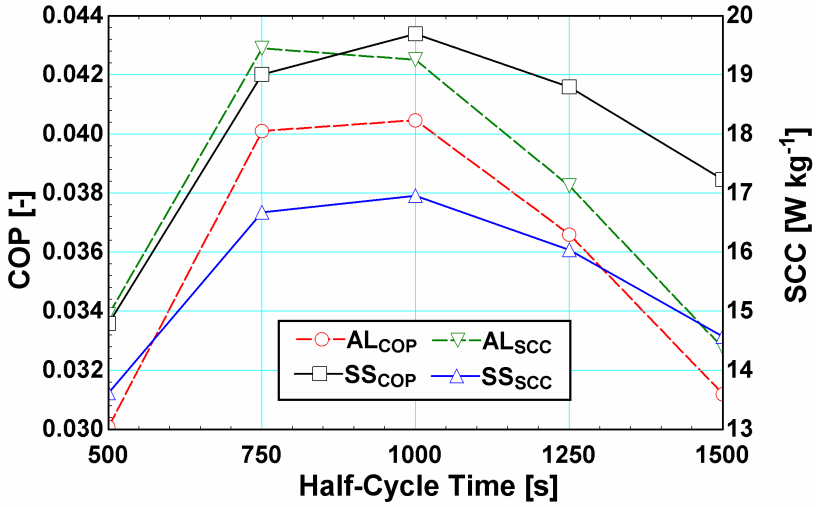

Figure 3.35 CHEC system with 130ºC source temperature

The fluid coupled system results are shown for a source temperature of 130ºC in Figure 3.35. The COP has more than doubled for both systems, and with the higher source temperature, the stainless steel system has higher performance than the aluminum system, because the reduction in losses to the surroundings has a bigger impact than the increased thermal mass at this source temperature. The SCC has increased by

approximately a factor of 3 for both systems and the aluminum system has higher cooling capacity than the steel structured system. Figure 3.36 shows the different heat flows through the adsorbent bed, including the amount of heat that shorts around the end of the bed, the amount transferred into the adsorbent from the inner structure, the amount of heat transferred into the adsorbent from the outer structure and the total heat transfer from the adsorbent bed to the surroundings. The heat flows are shown for both the stainless steel and aluminum system with a 50 W heat input. In both cases, most of the heat shorts around the end of the bed, rather than being passed from the internal structure (IS) to the adsorbent. This is the primary cause of the low COPs for this system. It can be seen in the plot that the shorting heat transfer is larger for the aluminum, which also means that heat is lost from the system during the heating phase at a faster rate and less heat is going into the adsorbent, which is why the system has a lower COP. However, it can also be seen that the heat transfer from the adsorbent to the outer structure is lower during the heating phase for the aluminum. This is because the outer structure heats more quickly and so less undesired cooling of the adsorbent occurs during the heating phase and the bed heats more rapidly for the aluminum structure. The more rapid heating is why the aluminum system has a higher SCC for fixed temperature sources. Also of note in Figure 3.36 is that shorting does not stop during the cooling phase and that as much heat is transferred out of the adsorbent through the internal structure as is transferred from the adsorbent to the outer structure directly.

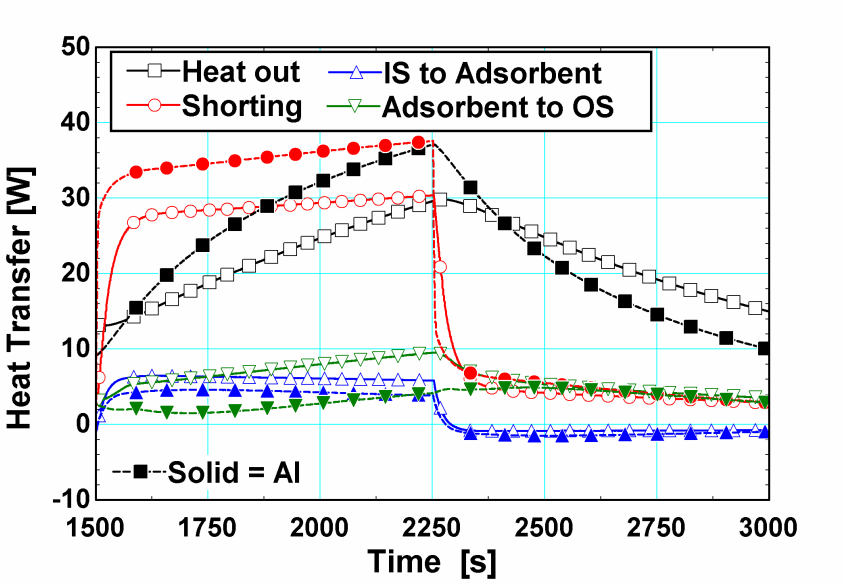

Figure 3.36 Heat flow for one cycle in the CHEC system with a 50 W heat input. (Stainless steel: hollow symbols; Aluminum: solid symbols)

Because the adsorbent bed is heated by a liquid or solid heater and cooled by natural convection, there may be an imbalance in the heating and cooling rate. To investigate the impact of heating and cooling using different paths and determine if the operation can be improved, the ratio of heating time to cooling time is varied. For the different heat inputs, the heating time for the aluminum system is fixed at 750 s and the cooling time is varied from 500-1500 s. The results for the 50 W and 75 W heat input cases are shown in Figure 3.37. Results for the 100ºC and 130ºC source temperature cases are shown in Figure 3.38.

When the cooling time is increased, the COP for the system increases while the SCC may increase slightly, but then slowly decreases. Both COP and SCC decrease when the heating time is larger than the cooling time. The COP increases because the heat input is the same for both cases, but the total amount of cooling per cycle increases for larger cooling times, at least initially. The increase is larger for the larger heat input. As the

cooling is increased more, the losses in the evaporator become significant enough to decrease the cooling and then the COP starts to decrease. Varying the cooling time for the fixed heat input decreases the SCC or leads to very slight increases, because while the amount of cooling delivered per cycle increases the total cycle time increases faster, which leads to a decrease in the cooling rate.

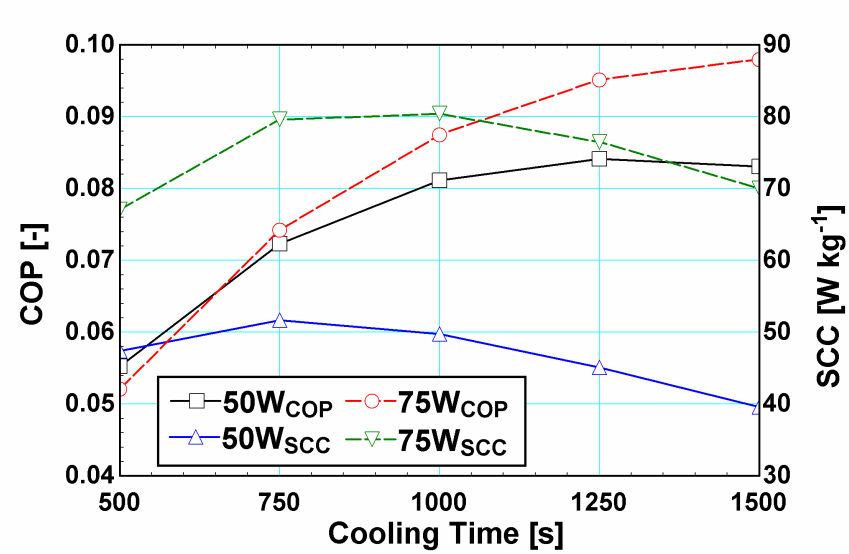

Figure 3.37 Performance of the aluminum CHEC system with a heating time of 750 s and varying cooling times for 50 W and 75 W heat inputs

The results for the liquid coupled systems with 100ºC and 130ºC follow trends similar to the constant heat input cases. The COP increases for longer cooling times until a peak is reached and decreases thereafter. The higher temperature source requires greater cooling time than the lower temperature source, because more heat must be removed in the cooling phase. The SCC appears to increase slightly and then drops below the equal half-cycle time case much sooner than the point where the peak COP is reached. The cooling per cycle increases, resulting in higher COPs, but the increase in cooling is at a lower rate towards the end of the adsorption phase so that the average cooling rate and SCC are lower.

The impact of aluminum alloys with lower thermal conductivity and the use of thermal breaks were also modeled for the electrically coupled CHEC design. The results from these analyses are shown in Table 3.8. As with the baseline model, the reduction in thermal conductivity due to using an alloy caused only a small increase in system performance. The use of thermal breaks between the internal structure and external structure of the system significantly improved performance and for both the stainless steel break and the ceramic break the aluminum system performs better than the stainless steel system. The CHEC system COP improves by 12.5% for the stainless steel break and by 38.9% for the ceramic break. The SCC improves by 5.8% for the stainless steel break and by 37.8% for the ceramic break.

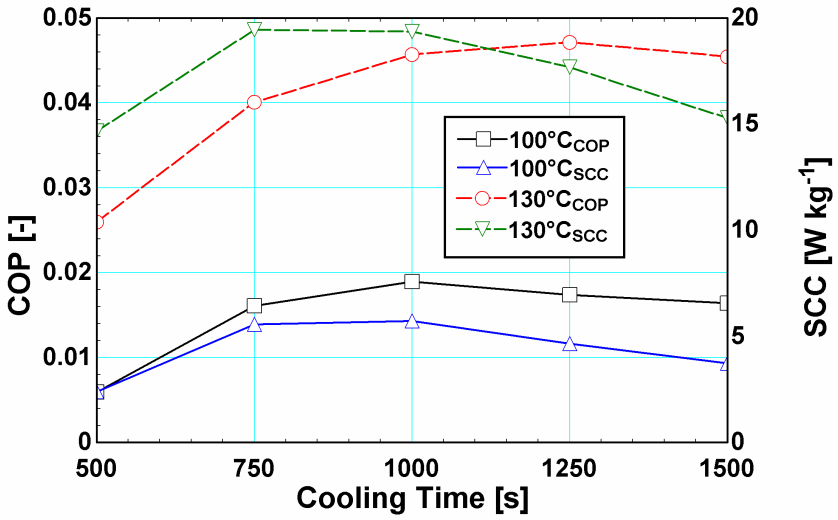

Figure 3.38 The performance of the CHEC system with an aluminum structure with a heating time of 750 s and varying cooling times for 100ºC and 130ºC source temperatures

Table 3.8 Comparison of systems with alloy and with thermal breaks for a 50 W heat input and a 750 s heating time

Modifications	COP	SCC [W kg^{-1}]
CHEC, electrically coupled Al	0.072	36.2
CHEC, electrically coupled SS	0.075	37.7
CHEC, electrically coupled Al-alloy	0.073	36.6
CHEC, electrically coupled Al-alloy SS Break	0.081	38.3
CHEC, electrically coupled Al-alloy Ceramic Break	0.100	49.9

3.4.2.2 Flat Bed

The results for the Flat Bed models are presented here. The COP for the Flat Bed system is calculated as follows

$$COP = \frac{Q_{cooling}}{Q_{hp,hb} + Q_{hp,\mathrm{in}s} + Q_{hp,\mathrm{inf}}} \tag{3.33}$$

The total cooling is divided by the total heat transferred from the heat source, including losses from the heat source and losses to the surroundings during the adsorption phase. The heat losses during the adsorption phase are significant, frequently being nearly equal to the heat transfer into the adsorbent bed. Unlike the conventional approach, no exergy losses are ignored and the losses from the source to the system have been accounted for. This yields a lower COP than if these losses were neglected, but a more realistic value for what would be achieved in an application.

Cycle time and the impact of the heating-to-cooling time ratio on system performance were investigated. Two different heating modes for the system were also been investigated: a constant heat input and a constant temperature heat source. Also investigated was the impact of thermal storage in the heating block on the performance of

the system with constant heat inputs. The primary outputs are the COP and SCC for the systems. The model design matches very closely with the experimental work and considerable attention is given to accounting for losses from the system. The losses to the surroundings for all of the exposed outer structure of the system were estimated conservatively. The total UAs for losses to the surroundings for the adsorbent bed, heater, and thermal switches are 77% of the UA for the cooling block, which is the intended primary cooling point for the system. The large fraction of the losses leads to a small COP for the system. Minimizing the losses will improve the system performance, particularly around the heating pad, which transfers more energy to the surroundings than into the system. The COP accounts for the total heat input at the pad and the system COP is much higher, usually more than twice the total COP.

The temperature profile through the adsorbent bed and in the thermal switches is shown in Figure 3.39. The system is in its third cycle and the heating phase begins at 3000 s. It transitions to the cooling phase at 3750 s, at which point the heating block is disconnected from the system and the cooling block is connected. The adsorbent temperature is taken from the middle of the bed. There is a strong temperature gradient through the heating block, which limits the temperature of the adsorbent. The heating and cooling blocks rapidly change temperature when the phase changes. The rapid temperature change is caused by the opening and closing of the thermal switches, which connects the blocks and allows the energy stored to transfer quickly. The heater node does not experience as large or rapid a temperature change because it is constantly being supplied heat, it has a larger thermal mass, and the heating block provides some delay in the response. When the heater is disconnected from the bed at 3750 s, the temperature

climbs, but then asymptotically approaches approximately 160°C. The maximum temperature is set by the losses of the heater and heating block to the surroundings. Also notice that no component goes through a full swing from the hot side temperature to the cold side temperature, so the dynamic losses should be lower for most of the components.

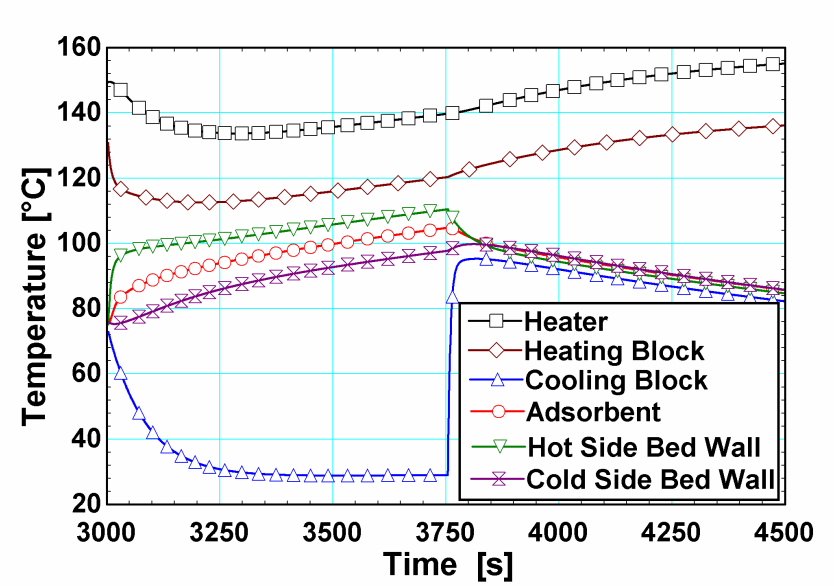

Figure 3.39 Flat Bed temperature over a single cycle with a 15 W heat input and a half cycle time of 750 s

The temperature profile in Figure 3.40 is for a 100ºC constant temperature source. The heating pad and block do not get nearly as hot, but the limit on the temperature on the hot side means that the cooling is not affected as significantly. The heating process is slower initially and the average temperature of the bed is lower, but the heating process is more continuous and for a fixed temperature source it appears that a larger swing in specific adsorption is possible. The slower continuous process would indicate that longer cycle times are better for this system. The large temperature gradient through the heating block indicates that the thermal resistance through the block is negatively impacting the performance of the system.

A constant heat input of 15 W is the first case for which the Flat Bed system performance is evaluated. In the models, this yields a temperature source for the heating pad between 140-180ºC, which represents a relatively hot temperature source. Figure 3.41 shows the COP and SCC as the half-cycle time is varied. The COPs are relatively low for the Flat Bed system in this case, but the SCCs are similar to what is seen in the literature. Peak COP occurs for a half-cycle time between 1000 s and 1250 s. Unusual for an adsorption system, the Flat Bed system appears to have peak cooling and efficiency near the same cycle time.

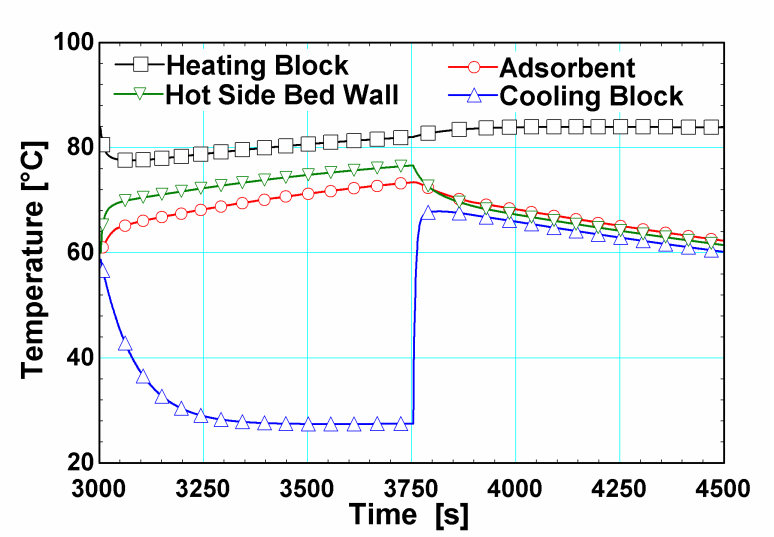

Figure 3.40 Flat Bed temperature over a single cycle with a 100ºC constant temperature source and a half cycle time of 750 s

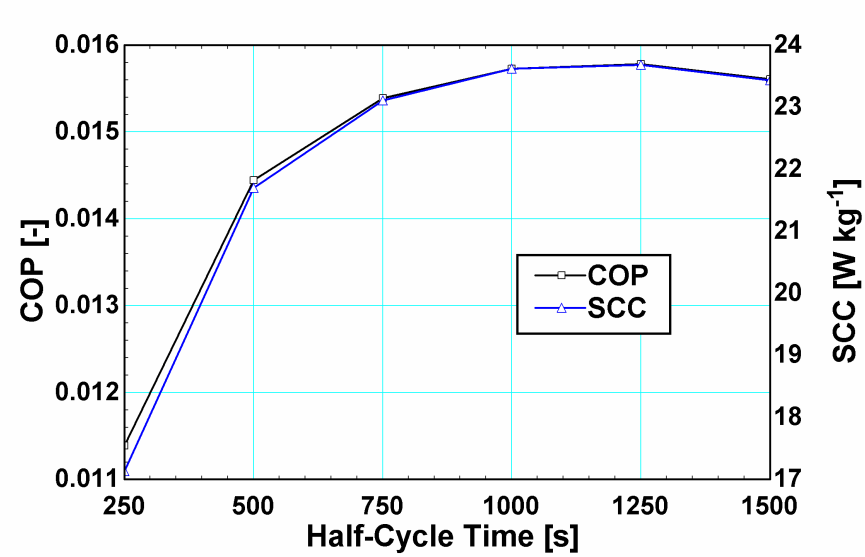

Figure 3.41 Flat Bed system performance for a 15 W heat input as the half cycle time is varied

Also investigated is the ratio of the heating time to cooling time. For the 15 W heat input, two heating times are chosen, 500 s and 750 s, and the cooling time is varied to determine the effect of the ratio of cooling to heating times on performance. The results are shown for these two cases in Figure 3.42. The peak COP occurs when the cooling time is approximately twice the heating time for this heat input. A longer cooling time yields higher cooling rates as expected because the heat transfer rate for cooling is lower than it is for heating. The highest COP of 0.0213 exhibited for this heat input occurs with a 500 s heating time with a 1250 s cooling time. This performance is even better than the best equal half-cycle times. Although the performance of the system when the heating to cooling time ratio is 1 is better for the 750 s heating time, it is possible to achieve a higher maximum performance with the shorter heating time when the cooling time is varied. These results imply that increased cooling would improve system operation and that three beds rather than two would yield greater overall system performance.

The SCCs for the fixed heating times while the cooling time is varied are shown in Figure 3.43. Similar to the COP, the peak SCC appears to occur with a cooling to heating time ratio of two or higher. The COP and SCC appear to have very similar trends even for unequal heating and cooling times. The peak specific cooling capacity for the Flat Bed system is nearly 33 W kg^{-1} and all the values are above 15 W kg^{-1} for the cycle times considered for the 15 W heat input.

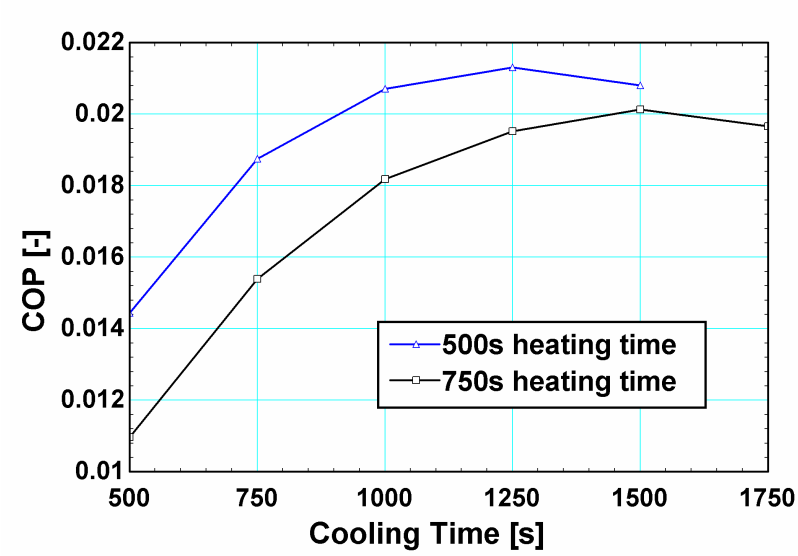

Figure 3.42 COP vs. cooling time for two different heating times with 15 W of heat input

Results for a 10 W heat input are presented next. The 10 W heat input case represents a lower temperature heat source, with the heating block temperature ranging from 100-120ºC over the course of the cycle. The COPs and SCCs as the half cycle time is varied are shown in Figure 3.44. The two values again follow the same trends and peak at the same half-cycle times, indicating that for the Flat Bed system, it may be possible to optimize for both efficiency and cooling capacity. The COP is higher for the lower heat input, which is unexpected, because higher source temperatures tend to improve COP. This can be explained by increased losses from the heating block due to the higher

temperature. The cooling capacity is lower compared to the higher heat flux case. The optimal half-cycle time is very close to the half-cycle time for the 15 W heat input case.

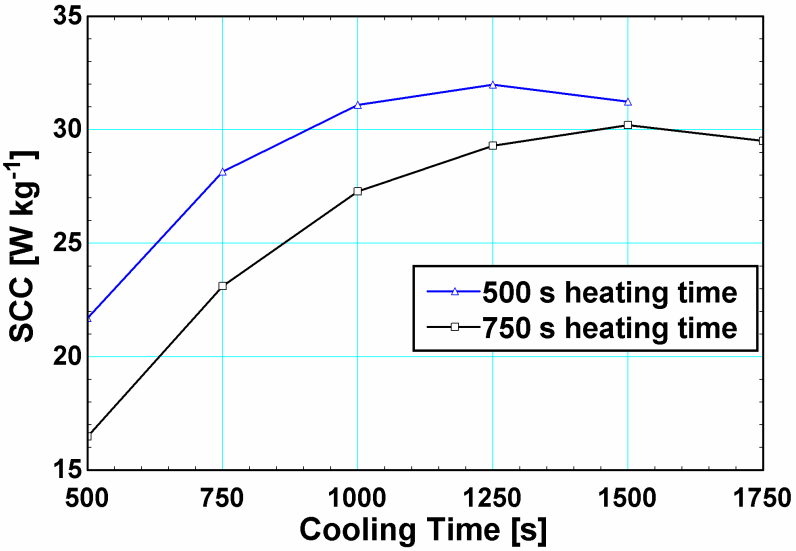

Figure 3.43 SCC vs. cooling time for two different heating times with 15 W of heat input

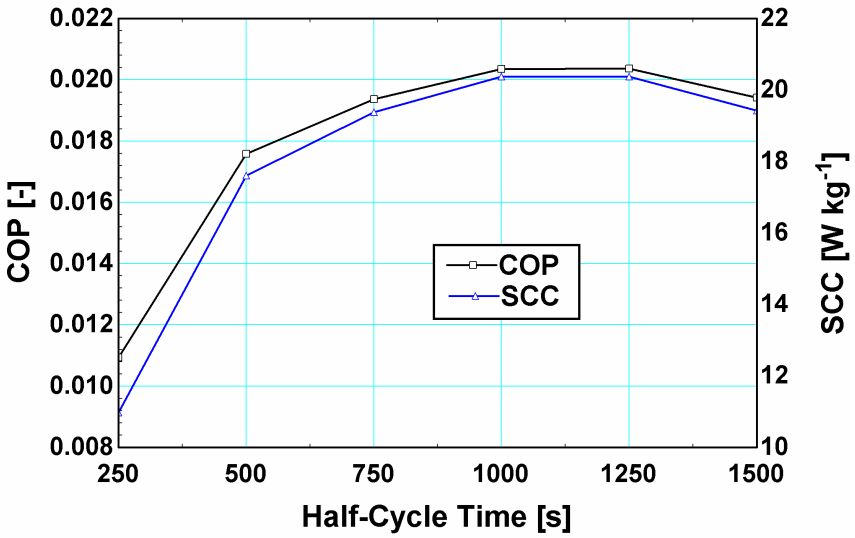

Figure 3.44 Flat Bed system performance for a 10 W heat input

Heating-to-cooling time ratio was also investigated for the 10 W heat input case. The heating time was chosen as 750 s and the cooling time was varied. The performance

results are shown in Figure 3.45. The peak performance occurs when the cooling time is one and two-thirds of the heating time for this bed; shorter than for the 15 W case. By adjusting this ratio, a ~10% increase in COP and SCC can be achieved.

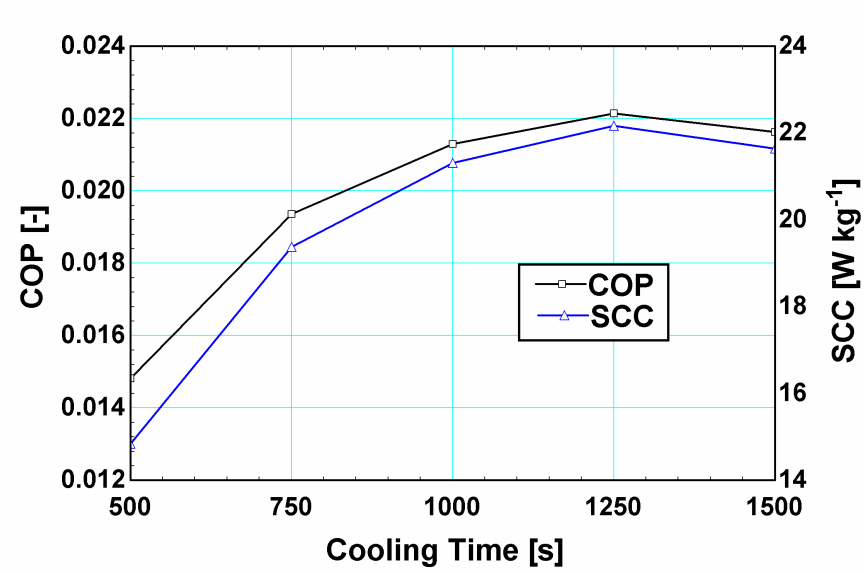

Figure 3.45 Flat Bed system performance for a 10 W heat input with a 750 s heating time

Next, a constant temperature source was examined, with the heating pad held at 100ºC. The performance for the constant temperature system is shown in Figure 3.46. The peak COP for the constant temperature source is very close to the 10 W constant heat input case, but the optimal half-cycle time is much longer for the constant temperature system. The specific cooling capacity is also lower. In the constant temperature system, the lost heat during the adsorption phase is less because the temperature of the heating pad and heating block do not increase as drastically, therefore the COP stays near the constant heat input condition, but the heating of the bed is slower, especially towards the end of the desorption phase, which leads to a lower SCC.

The heating-to-cooling time ratio was also investigated for this system. The heating time was held fixed at 750 s and the cooling time varied. The results of this

analysis are shown in Figure 3.47. Varying the ratio in this case yielded a maximum increase in performance of ~10% and the optimum ratio of cooling time to heating time is two. The constant temperature heat input system can be expected to perform better with longer cooling times because the heat losses are lower during the cooling phase than for a constant heat input.

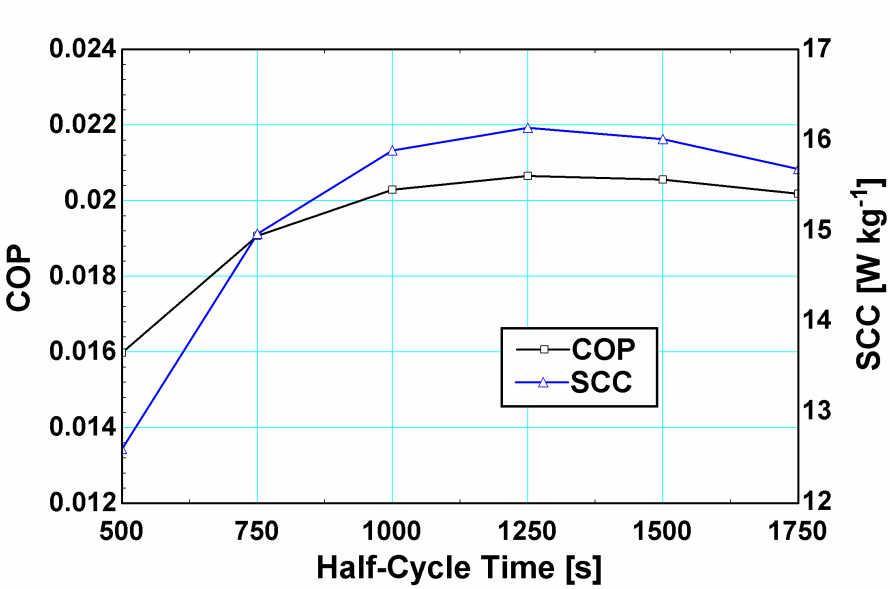

Figure 3.46 Flat Bed system performance with the heating pad held at 100ºC

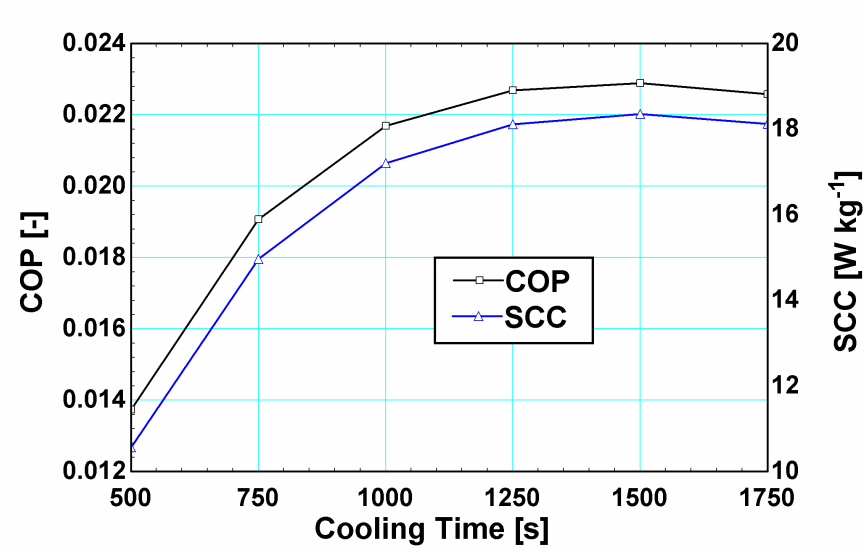

Figure 3.47 Flat Bed system performance as cooling time is varied with the heating pad at 100ºC and 750 s of heating time

The last heat input case considered is the constant temperature source held at 130ºC. As shown in Figure 3.48, the COP and SCC are both higher than for the 100ºC case and the SCC is comparable to the 15 W heat input, but the COP is higher for this case because the heating block does not increase in temperature during the adsorption/cooling phase and, therefore, has lower losses for that phase.

The COPs of the two different heat inputs and constant temperature sources are compared in Figure 3.49. The 130ºC system performs the best, as would be expected for the largest heat input, but the 100ºC and the 10 W heat input cases are very similar in terms of performance. The most efficient half-cycle time is very similar for all of the systems.

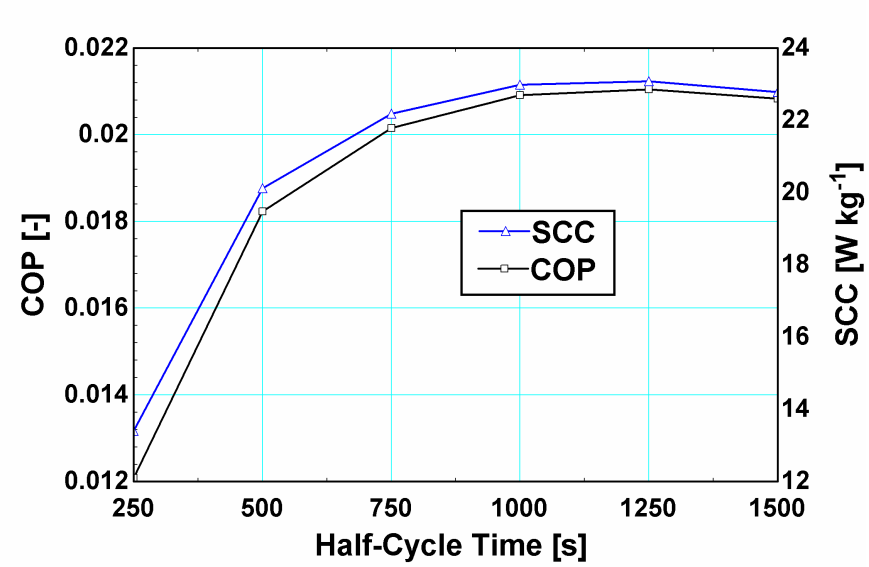

Figure 3.48 Flat Bed system performance with the heating pad held at 130ºC

The SCC is also compared for the different heating rates. These results are shown in Figure 3.50. The highest SCC occurs for the 15 W system. The higher cooling capacity is due to the faster heating allowing the bed to get higher in temperature and more

cooling to be delivered in each cycle. Similarly, the 130ºC constant temperature source delivers better SCC than the lower temperature source.

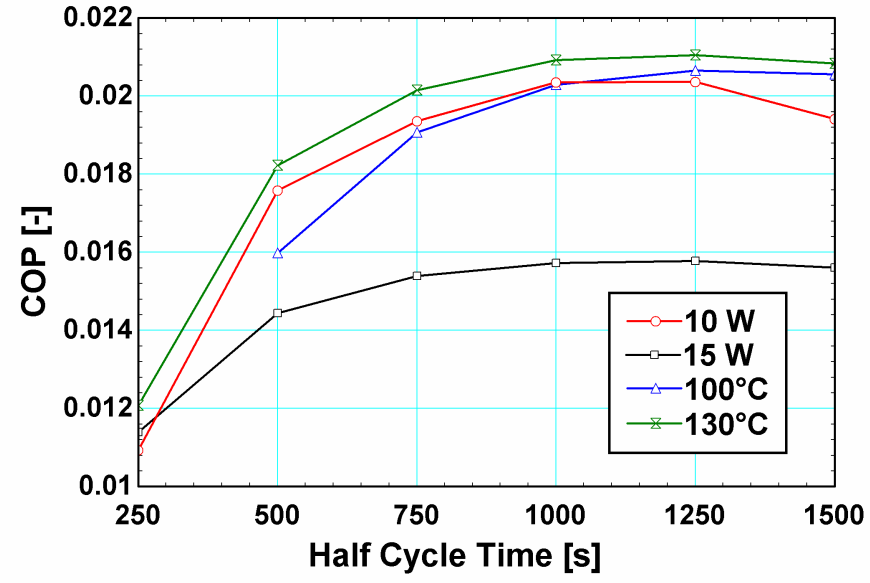

Figure 3.49 COP vs. half cycle time for Flat Bed systems considered

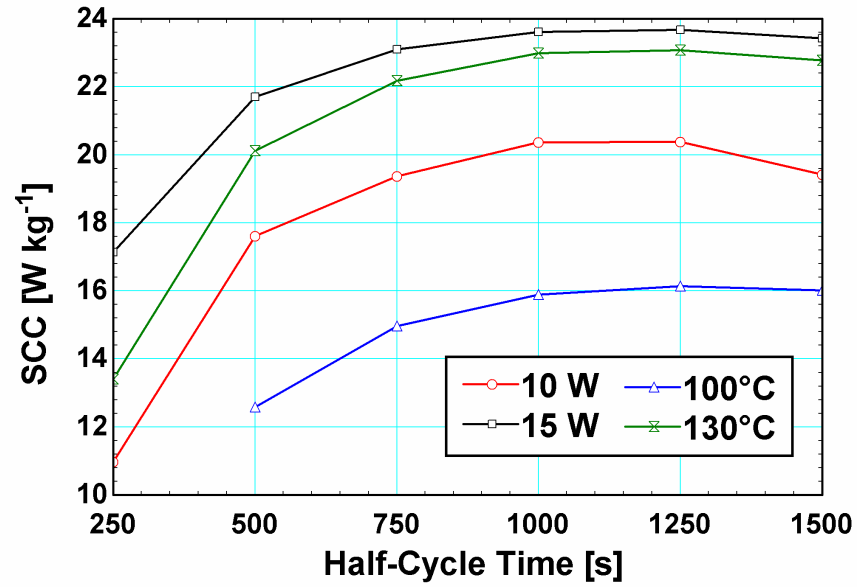

Figure 3.50 SCC vs. half cycle time for Flat Bed systems considered

The dynamic losses for these systems are very important for their operations. The thermal switches introduce a new factor into the consideration of thermal mass, because

the heating and cooling blocks store heat during the cycle that is then transferred into the bed or into the surroundings, respectively. This storage means that a larger thermal mass within a certain range may allow them to better heat and cool the bed, because their temperature will not approach the bed temperature as quickly when connected. For the heating block, additional mass also keeps the block temperature from climbing as quickly during the adsorption phase and therefore reduces the heat lost to the surroundings during that time period. To evaluate the effect of the increased thermal mass in this portion of the system, a case is modeled where the heating and cooling block masses are doubled. Consideration is also given to the dynamic losses due to excess structural mass and the models are run for an end node mass of 30 g rather than 100 g. This reduction corresponds to what could be achieved with a commercially produced system and represents a total reduction in the mass of the structure of 42%. These improvements are not implemented in the experimental validation of the design in the present study due to limitations in system fabrication. Both of these alterations are analyzed with the 15 W heat input.

The different COPs and SCCs are compared for the more massive heating and cooling blocks in Figure 3.51. The increase in mass yields a small increase in the system performance. Doubling the mass increases the COP and SCC by 1.2%. Therefore, the performance is relatively insensitive to changes in the mass of the heating and cooling blocks. The reduction in performance due to more thermal resistance being added if the block is expanded may out-weigh the benefits of increasing the mass of the heating and cooling blocks.

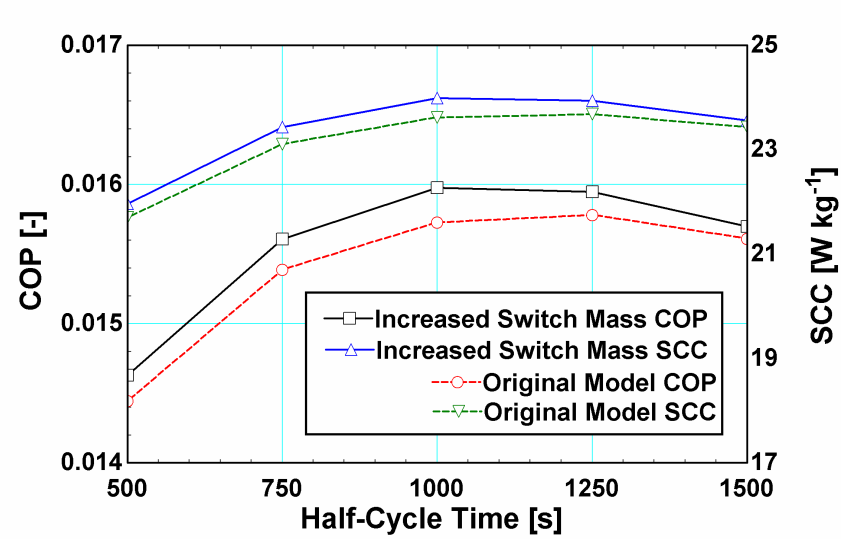

Figure 3.51 Performance comparison between the Flat Bed system with the mass of the heating and cooling blocks doubled with the original model for a 15 W heat input.

The reduction in bed mass has a much bigger impact on the system performance. The COP and SCC are compared with the normal system in Figure 3.52. Reducing the mass increases the COP and SCC by 45%. Further reductions in structural mass would continue to improve the system performance. The improvement is caused by both eliminating the dynamic loss due to heating and cooling the structure and lower bed mass reduces the thermal mass of the bed relative to the heating and cooling blocks thermal masses allowing the bed to change temperature more quickly.

Because the Flat Bed system is so different than the central heated system and the baseline system, it exhibits different trends. The Flat Bed has lower COPs. The biggest contributing factor to the low efficiency of the system is the continuous loss from the heat source during the adsorption phase. The heat loss effect is amplified for the constant heat input because energy is being stored in the heating block for only a short period of the adsorption time, then the temperature increases until the losses equal the heat input. It is expected that the COP can be nearly doubled for a two bed system, because heat that is

currently lost during the adsorption phase can be used to operate the system. Reducing losses from heating pad and heating block and other hot side components would also significantly increase the COP. However, it is apparent from the model that this system is best suited for applications where moderate SCCs are needed and where waste heat is available and the efficiency of the system is not the most important parameter. Still, the modeled COPs and SCCs are competitive with those of the much larger scale autonomous systems found in the literature, as discussed in Chapter 2.

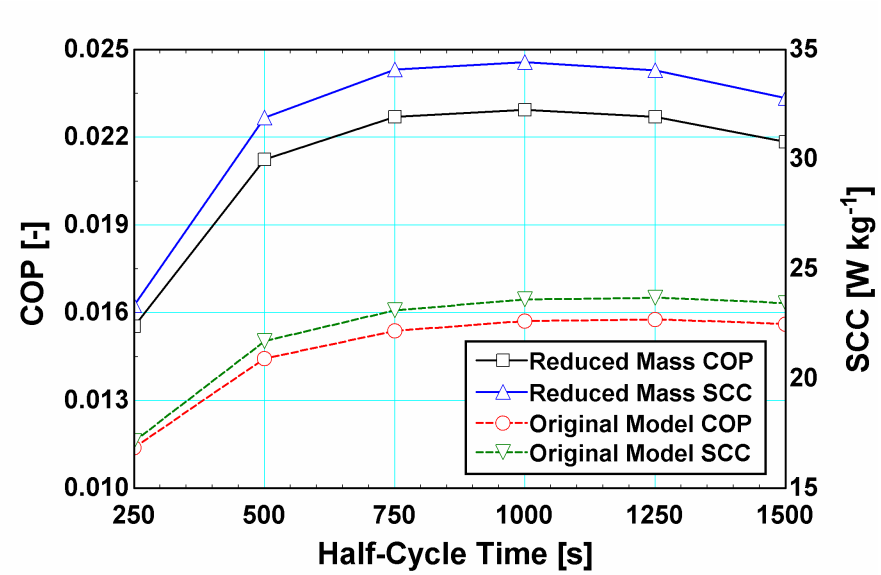

Figure 3.52 Performance comparison between the normal Flat Bed system and one with reduced structural mass for a 15 W heat input.

3.4.3 Performance Comparison

The COPs and SCCs of the baseline, the CHEC, and the Flat Bed systems are compared here. None of the systems modeled performs as well as large-scale adsorption systems because of scaling effects, as discussed in Chapter 2. However, the performance is high enough to indicate that reliable cooling at small scales using adsorption technology is feasible. The alternate approaches are also evaluated and compared with

the baseline system design to determine the trade-offs necessary to achieve simplifications in system operation. These modeling results provide a basis for the evaluation of suitable applications and the expected performance of the system.

In addition to the alternative concepts discussed above, a liquid coupled CHEC system with masses and UAs similar to the baseline system is also compared here to help determine the impact of the limits of test bed fabrication on the system performance versus the actual design. The CHEC model with baseline masses is nearly identical to the baseline model, but the insulation layer between the adsorbent and outer structure is removed and heat is removed on the external surface. Only the aluminum systems are compared here, because the stainless steel systems exhibit similar trends and little further insight can be gained by comparing the two. Because the system performances have been evaluated using the COP and SCC of the systems, the difference in the amount of adsorbent used in each type of system can largely be removed from these comparisons. The scales of all of these systems are close enough that the scaling effects are similar and the differences between the systems should be minimal.

The COP for the different systems with an aluminum structure are compared for a 100ºC source temperature in Figure 3.53. The baseline case has the highest COP for the constant temperature heat inputs, but the CHEC model with masses similar to the baseline case has COPs roughly 40% of the baseline case. The CHEC case with expected experimental masses performs the worst for this heat input, because the losses prevent the adsorbent material from heating to a high enough temperature to desorb effectively. The difference in performance strongly indicates the effect that thermal shorting can have on the performance of the CHEC system and the detrimental effect of additional thermal

mass on all adsorption systems. The Flat Bed system has significantly lower COPs than the COP of the baseline system. The COP comparison would be less distinct if pumping power and additional system losses were accounted for in the baseline system.

The SCCs for the aluminum structured systems with a 100ºC heat input are plotted in Figure 3.54. The SCCs of the alternate systems are much closer to that of the baseline system than the COPs were, indicating that although the losses from the system are greater, the amount of cooling that can be delivered is similar. The liquid coupled CHEC system again performs poorly, because of the low adsorbent temperature. The liquid coupled CHEC system with the baseline values for the end structure and outer structure delivers SCC that are slightly over 50% of the baseline designs. The Flat Bed system delivers higher cooling rates than either of the CHEC systems and achieves SCC equal to 63% of the baseline SCC.

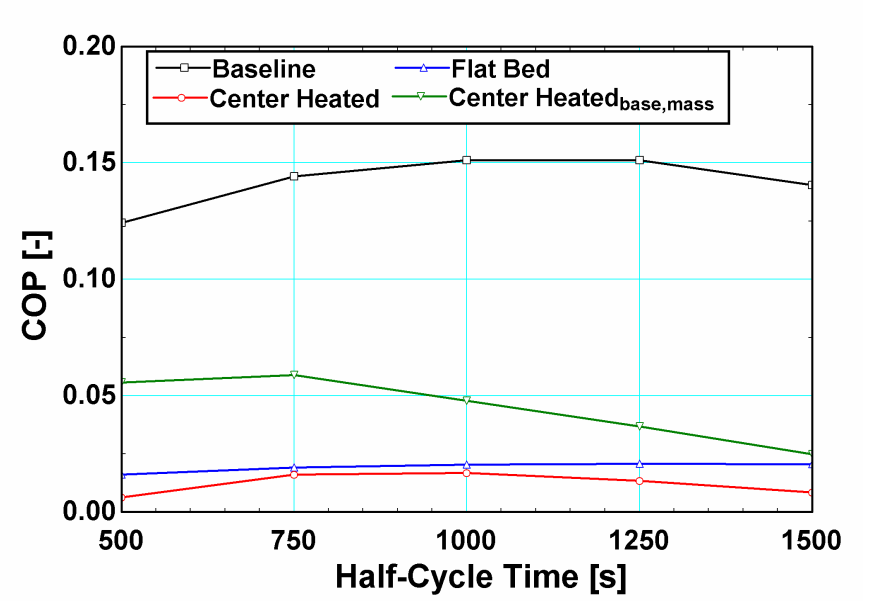

Figure 3.53 Aluminum structured systems for a 100ºC heat source and 50 W heat input

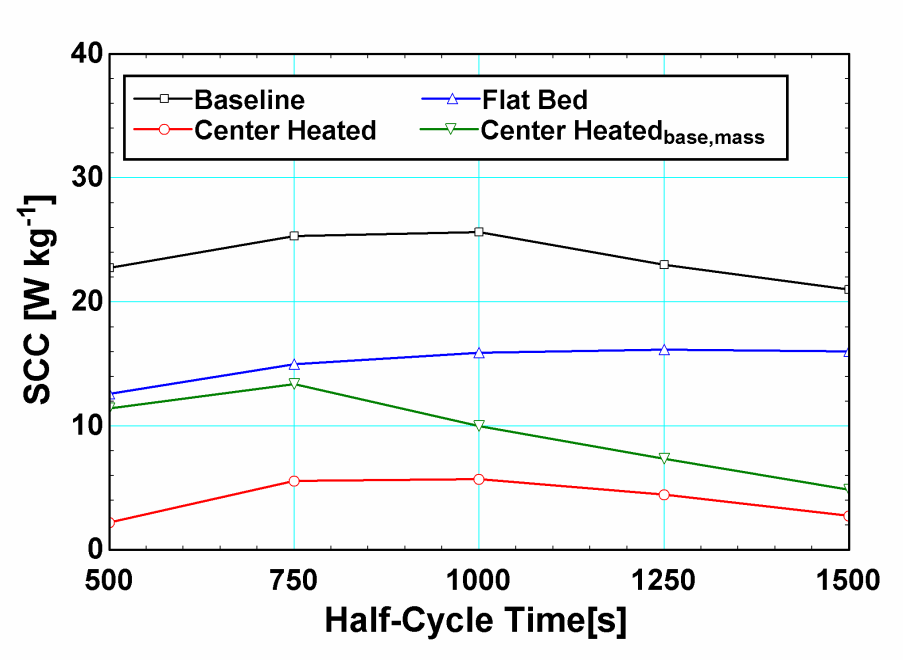

Figure 3.54 Aluminum structured systems for a 100ºC heat source

The aluminum systems are also compared with a 130ºC temperature input. For this comparison, the 50 W heat input is also compared for the CHEC system because the temperature for the heat source is near 130ºC for this case. The COP comparison is shown in Figure 3.55. The baseline system again exhibits the best COP for this temperature and the COP increases with increased driving temperature. The CHEC system achieves a higher COP than the Flat Bed system in this case, because the adsorbent is reaching the appropriate operating temperatures for the 130ºC temperature. The CHEC system with experimental masses still has less than 25% of the COP of the baseline case. The CHEC system with the baseline systems mass again performs considerably better and achieves a COP approximately 45% of the baseline system. The CHEC system with a constant heat input also performs fairly well and achieves 39% of the baseline COP, and conclusions about the systems relative to one another are difficult because of the different types of heat input.

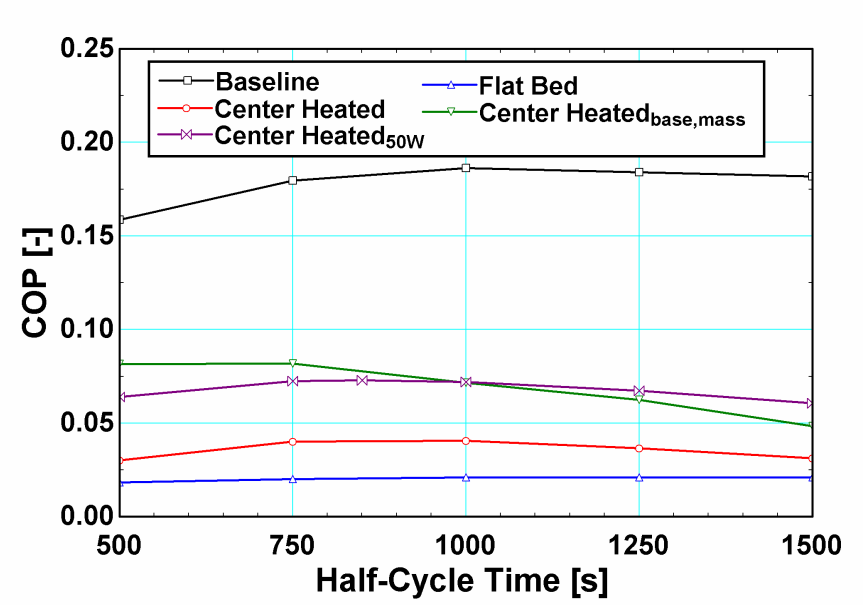

Figure 3.55 Aluminum structured systems for a 130ºC heat source

The SCCs for the aluminum systems are compared in Figure 3.56. Again, the SCCs are much closer to the baseline for these systems than the COPs were. The liquid coupled CHEC system has the lowest performance and delivers between 15-20 W kg^{-1}, depending on the half-cycle time. The Flat Bed system performs slightly better, delivering between 20 and 23 W kg^{-1} over the full range of half-cycle times tested. The CHEC system with baseline system masses comes close to matching the baseline performance and the peak SCC is 86% of the corresponding value for the base line system. The CHEC system with a 50 W heat input actually delivers better SCCs than the baseline system over all half-cycle times, but again the difference in heating mode makes comparisons difficult.

The comparison shows that the baseline system generally has higher efficiencies and higher cooling capacities than the alternate systems. A reduction in system performance was expected for the alternate systems and appears to be acceptable for applications where simplicity is more important than efficiency. Having explored

adsorbent bed designs and modeled them to evaluate their performance, the performance of prototype systems were investigated to validate the models described here. These experimental and prototype development aspects are discussed in the following chapters.

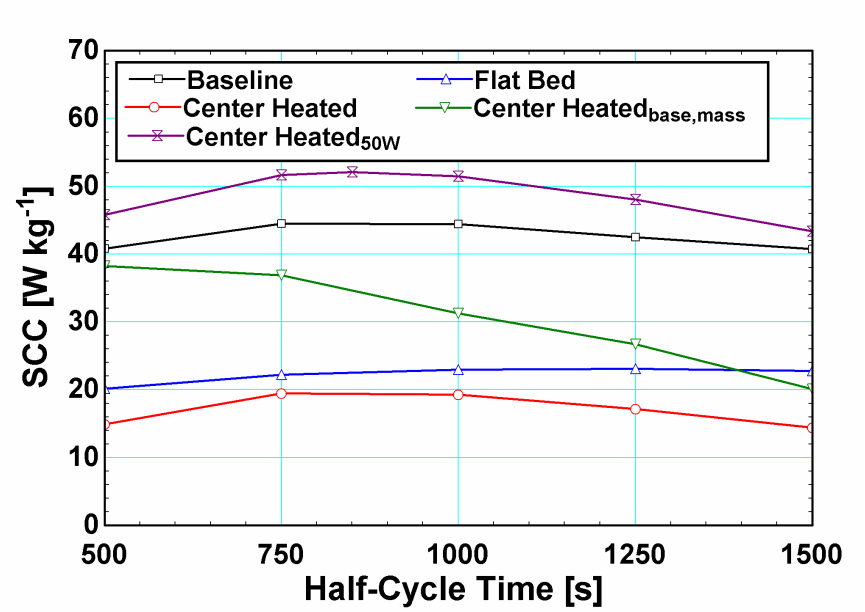

Figure 3.56 SCC comparison for the aluminum systems for a 130ºC heat source

CHAPTER 4.

EXPERIMENTAL FACILITY

The small-scale designs proposed in the present study were evaluated experimentally. The experimental facility and instrumentation used in this work is described here.

4.1 Test Facility

A diagram of the experimental set-up is shown in Figure 4.1. The primary focus of the facility is on testing and assessing the adsorbent bed. System pressures are measured in the evaporator and condenser. Temperatures are measured at the evaporator, the condenser, the adsorbent bed, and in the coupling fluid inlets and outlets. Heat duties are calculated from the experimentally measured temperature differences and volumetric flow rates. The instrumentation used in the experimental facility is discussed in the following section.

Table 4.1 Equipment List

Measurement	**Equipment**	**Accuracy**
Pressure	Wika- Eco-1 (0-300 PSI range)	± 20 kPa
Temperature	Type-T, Sheathed	± 0.1ºC
Temperature	Type-K, Unsheathed	± 0.2ºC
Data Acquisition	USB-2416	

Because the adsorbent bed is the focus of the experiments, the facility is designed to allow adsorbent beds to be easily swapped to test the performance of different modifications. A single connection to the bed (point 1) ties it to the rest of the system and the heating element (point 2) and temperature measurements (point 3) are set up before

the bed is connected. There are no liquid coupling lines for the adsorbent bed because all adsorbent beds are directly air-cooled. The surrounding air was quiescent in some cases and circulated in some cases, as discussed in detail later. The cooling surface varies according to the adsorbent bed design, but is enhanced with the addition of extended surfaces to the bed. Heat is provided to the bed with an electrical heater (point 2). For the CHEC design, a 6.35 mm (¼ in.) diameter 15.2 cm (6 in.) 150 W McMaster-Carr cartridge heater (model number 3618K419) is used, and for the Flat Bed system, an Omega 5.08 cm (2 in.) by 7.62 cm (3 in.) 1.55 W cm^{-2} (10 W in^{-2}) silicone rubber heating blanket is used. The voltage supplied to the heating element is controlled using a Staco 3PN1010B variable transformer and measured in each test. The temperature of the adsorbent bed is monitored using a 1.58 mm (1/16 in.) type K thermocouple throughout the testing. The bed temperature varies with time as well as spatially and the temperature is measured at a point on the external surface, 2.54 cm axially from the connection to the system (point 3). The bed temperature measurement helps to gauge the system progress through the adsorption and desorption cycles.

Refrigerant flow between the adsorbent bed and evaporator and condenser was originally controlled using check valves, but these valves were replaced with manually controlled ball valves for the final testing. The system valves are discussed at the end of this chapter. The adsorbent bed is connected to the evaporator and condenser by 1/8 in. (3.18 mm) stainless steel tubing.

The system was evacuated to at least 1 kPa for at least one hour using a McMaster-Carr Model Number 4396K41 Compact Electric Extreme-Vacuum Pump capable of achieving 0.002 kPa to remove humidity and non-condensable gases before

charging the system with ammonia. The actual pressure is lower than 1 kPa, but the exact pressure was unknown because the system pressure gauges were designed to measure gauge pressure and sub-atmospheric measurements were not accurate below 1 kPa. In the worst case scenario, the fraction of non-condensable gases by mass in the system is 7.35×10^{-4}. The adsorbent bed was heated during this process to help desorb contaminants from the adsorbent material. When charging the system, all lines and connections were also evacuated to remove moisture and other contaminants. To prevent the system from being flooded during the charging process, only the evaporator and connections are charged with liquid ammonia. When the connections are opened, the ammonia redistributes throughout the system.

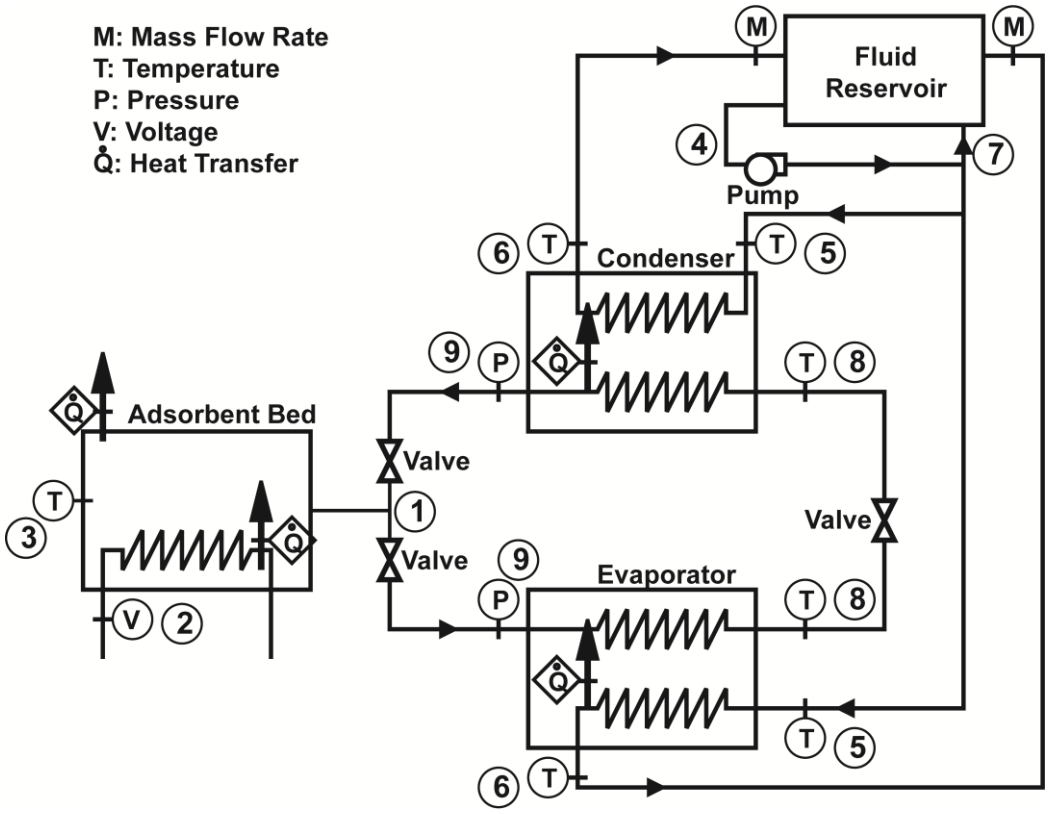

Figure 4.1 Schematic of the experimental facility. The values in circles are measured. The values in diamond are calculated based on measured values.

In a small-scale application, the evaporator and condenser would most probably be directly air coupled, but because the focus of the experimental facility is on the adsorbent bed, the evaporator and condenser are tube-in-tube heat exchangers to ease measurement of heat transfer rates. A schematic of the evaporator component is shown in Figure 4.2.

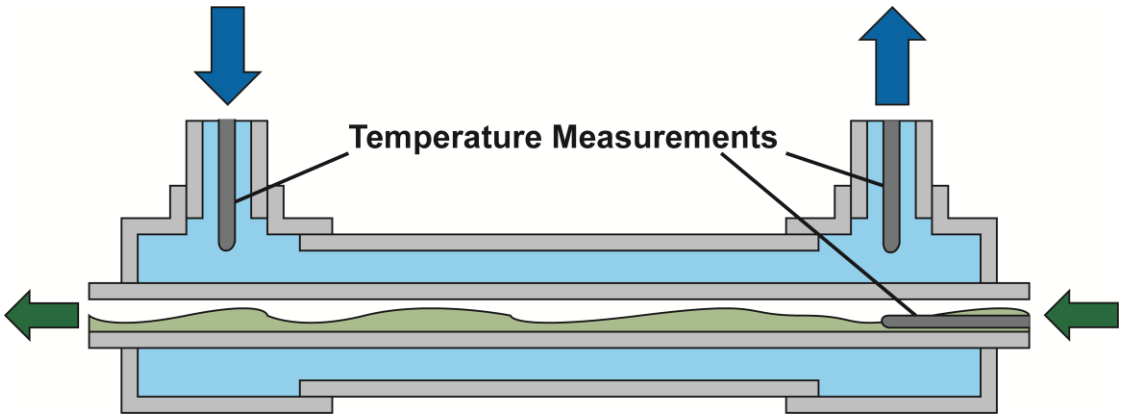

Figure 4.2 Evaporator and condenser schematic

The temperature is measured at the inlets (5) and outlets (5) of these heat exchangers using 3.18 mm (1/8 in.) Type T thermocouples. These tube-in-tube heat exchangers are fabricated from stainless steel with a wall thickness of 0.794 mm (1/32 in.) For testing of larger beds, the inner tube O.D. is 6.35 mm (1/4 in.), while the outer tube O.D. is 12.7 mm (1/2 in.). For smaller test beds, the tube sizes are reduced to 3.18 mm (1/8 in.) and 6.35 m (1/4 in.) O.D., respectively. The inner tube carries refrigerant while the outer tube carries water as the heat transfer fluid. Both heat exchangers measure 0.41 ± 0.012 m (16 in.) in length. The *UA* value of these heat exchangers varies over the length of the cycle. The change in *UA* is caused by the refrigerant evaporating quickly during the first part of the adsorption phase, when there is a large pressure change and adsorption is occurring quickly. For the first part, the heat transfer occurs as two-phase boiling and the resistance is limited by the external flow convection coefficient, and in

the second part, the refrigerant is quiescent and the flow of ammonia from the evaporator or into the condenser is slow, resulting in a low convection coefficient. The heat transfer coefficient in the external tubes is determined using the hydraulic diameter for concentric tubes (Incropera and DeWitt, 1996)

$$Dia_h = \frac{4(\pi/4)\left(Dia_o^2 - Dia_i^2\right)}{\pi Dia_o - \pi Dia_i} = Dia_o - Dia_i \tag{4.1}$$

For the CHEC heat exchangers, this yields a hydraulic diameter of 4.76 mm, and for the Flat Bed, it yields a hydraulic diameter of 1.58 mm. The ratio of inner diameter to outer diameter is 0.57 and 0.66, respectively. The Reynolds number for a flow rate of 1 g s^{-1} at a temperature of 50°C is 145 and 320 for each system; therefore, the flow is considered to be laminar for all testing conditions. The adjusted laminar Nusselt numbers for concentric tubes from (Kays and Perkins, 1972) are 5.74 on the inner surface and 4.43 on the outer surface of the outer fluid volume for both cases. This results in convection coefficients for the heat transfer from the inner tube to the coupling fluid of 735W m^{-2} K^{-1} and 2200 W m^{-2} K^{-1} for the CHEC and Flat Bed systems, respectively.

For the heat transfer internally, because the fluid transitions rapidly between boiling phase heat transfer to quiescent fluid in the channel, the heat transfer coefficients were estimated using expected ranges for convection coefficients (Incropera and DeWitt, 1996). During the boiling phase, the boiling coefficient is assumed to be 10,000 W m^{-2} K^{-1} and while the fluid is stationary, the convection coefficient is estimated to be only 1,000 W $m^{-2}K^{-1}$. This change in *UA* causes a sharp peak in in heat transfer and some of the observations made in Chapter 7. To minimize heat losses and gains in the evaporator and condenser during testing, they are insulated using Buna-N/PVC ¾ in (1.91 cm) pipe insulation with an R value of 0.5 m^2 K W^{-1}. The temperature of the refrigerant within the

evaporator and condenser components (8), and the pressure, are also measured (9). The temperature and pressure can be used to determine whether the component is experiencing two-phase conditions or is operating in a dry-out/flooding condition. The temperatures measurements can also indicate when heat transfer is occurring at rates that are too low to measure accurately.

Ball valves separate the evaporator and condenser from the test adsorbent bed and the evaporator and condenser are separated by a needle valve, which functions as an expansion valve for the system. Control of the valves allow the adsorption and desorption phases to be controlled and also allows the refrigerant level to be rebalanced throughout the system operation.

The orientation of an adsorbent system is important for operation and fluid control. The expansion valve is located at the lowest point of the system because flow through the system is slow enough that gravitational effects play a large part in fluid movement. By placing the expansion valve at the low point, liquid refrigerant in the condenser flows to it and only fully condensed refrigerant passes through the expansion valve to the evaporator. Additionally, the adsorbent bed is elevated to ensure that only refrigerant vapor is exchanged between the adsorbent bed and the rest of the system. If the adsorbent bed is not elevated, liquid will flow into the in connections between the adsorbent bed and the rest of the system. Accumulated fluid is adsorbed and desorbed first, negatively affecting system performance. The total change in elevation from the center of the adsorbent bed to the expansion valve is approximately 10 cm (4 in.). The final adsorption system experimental facility is shown in Figure 4.3 with the Flat Bed installed.

Figure 4.3 Photograph of the experimental facility. The adsorbent bed is in the lower left-hand corner. The ball valves are the black handled connections next to the insulation.

4.1.1 Instrumentation

The instrumentation used to perform tests in the experimental facility as well as the accuracy of the measurements are described here. The derivation of uncertainty values is presented in Appendix A. Table 4.1summarizes the equipment used in this work.

4.1.1.1 Pressure

The pressure was measured in both the evaporator and condenser using a Wika Eco-1 pressure gauge with a range from 0-300 psi (0-2070 kPa). The measurements are expected to be accurate within 1% of the pressure gauge span. The readings are used alongside the temperature measurements in the evaporator and condenser to assess the refrigerant purity. When refrigerant is contaminated, the pressure in these components drops below what is expected for saturated conditions. With the pressure and temperature

reading, it is also possible to identify superheated or subcooled conditions indicating that one of the components has flooded or dried out.

4.1.1.2 Temperature

Type T sheathed thermocouples are used for measurement of temperature in fluid streams in the coupling fluid lines and in the evaporator and condenser. Type K unsheathed thermocouples are used for measurement of the adsorbent bed temperature. The thermocouples are calibrated at 22ºC, 25ºC and 28ºC. The temperature readings are normalized to the average equilibrium readings at these three points with a linear correction factor applied after data acquisition. Before the corrections, individual thermocouples disagreed by as much as 0.3°C at the temperatures of interest, but these disagreements stayed relatively constant (< 0.05°C) as the temperature varies. The absolute temperature measurement is not as important as the differential temperature measurements, because it is necessary to measure the temperature changes in the fluid streams. The maximum disagreement between the thermocouple measurements in the temperature values after calibration is approximately 0.1ºC, which is primarily due to noise in the gathered data, which causes temperature measurements to fluctuate to ±0.05ºC of the average temperature value.

4.1.1.3 Mass Flow Rate

The coupling fluid flow rate was determined by measuring the amount of time it took for a fixed amount of fluid to flow through the heat exchanger. This measurement was performed before testing began and throughout the course of testing. The heat exchanger outflow was collected into a container with a fluid volume scale. The time

required for 500 ml of outflow to accumulate in the container was measured. The flow rate was determined by dividing the amount of fluid pumped by the time required. This was repeated three times and the average was used for the coupling fluid flow rates. Based on the uncertainty of the volume and time measurements, the uncertainty of the fluid flow rate is ±0.04 ml s^{-1}. The volumetric flow rate was converted to a mass flow rate, using the density of water at 25ºC. The fluid flow rate is controlled using a shunt path that redirects part of the flow back to the reservoir (point 7 in Figure 4.1).

4.1.1.4 Heat Transfer

The heat transfer into the evaporator and condenser is measured using the temperature change of the heat transfer fluid as it passes through the component. Appendix A discusses the uncertainty in the heat transfer measurements. The heat duty is assumed to be 0 W unless the measured heat transfer rate is 30% or larger than the uncertainty value. Figure 4.4 shows the cooling duty in the evaporator with the cut-off for when the cooling can be measured. In effect, only the peak cooling for the cycle can be measured accurately and the lower cooling rates achieved during the desorption phase and at the end of the adsorption phase are neglected. This assumption biases the data to lower COPs and SCCs, and depending on testing conditions, could underestimate the cooling by 50%, but underestimating performance is preferable to inflating the system performance by using possibly erroneous data that is of a similar magnitude as the uncertainty in the data. The system performance during the peak period can be matched with model data and the amount of cooling in the lower region estimated. The estimation of the cooling that could not be measured is discussed further in Chapter 7.

The input heat to the adsorbent bed is calculated using the measured resistance of the heating element and the voltage input. Both are measured with a multi-meter accurate to within ± 0.1 Ω (resistance) and ± 0.1 V (voltage). This leads to a maximum uncertainty in the heat input of ± 0.04 W.

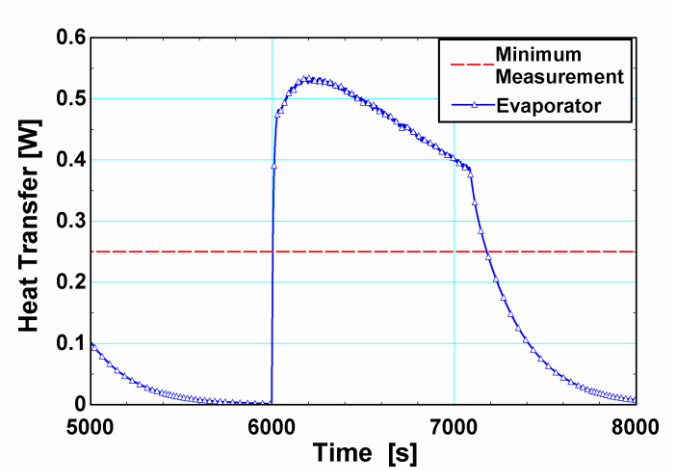

Figure 4.4 Cooling rate over the course of the cycle compared with the minimum measurable cooling rate

4.1.1.5 Data Acquisition

Data acquisition is performed using a Measurement Computing USB-2416 Series system and the information is collected using the Tracer-DAQ program. The DAQ system automatically converts the voltage measurements of the thermocouples to temperatures and corrects for environmental temperature changes using an internal temperature measurement. Data were gathered at a sampling rate of one point per second.

4.1.2 Environmental Chamber

The test facility is placed in a Vollrath Refrigeration 27410-S environmental chamber for testing. The environmental chamber allows the surrounding temperature to be controlled to ±0.55°C (±1°F). The chamber air temperature is kept uniform by a set of

circulation fans rated at 1400 CFM. These fans run continuously whenever the chamber is set. Tests were run both at ambient temperatures without the fans running and at various temperatures with the fans running. These fans are located approximately 1 m above the test facility and the air flow is not directed towards the test facility as shown in Figure 4.5. Even though the flow is not directed at the facility, the increased air movement in the chamber increases the convection coefficient for the system. The actual air flow rate over the test facility is hard to measure, because there are obstructions to air flow around the test facility. If the flow is assumed to be uniform velocity through the cross sectional area of the chamber that the test facility occupies, the air velocity would be 0.6 m s^{-1} which yields a Reynolds number around 1000-2000 for the adsorbent beds being tested. Using a correlation from Zukauskas (1973), the convection coefficient for the CHEC system is found to be approximately 12 W m^{-2} K^{-1}. It is expected that the actual air velocity over the test facility will be lower than in a uniform flow case and the forced convection coefficient found here is the upper bound of what is expected for the test facilities.

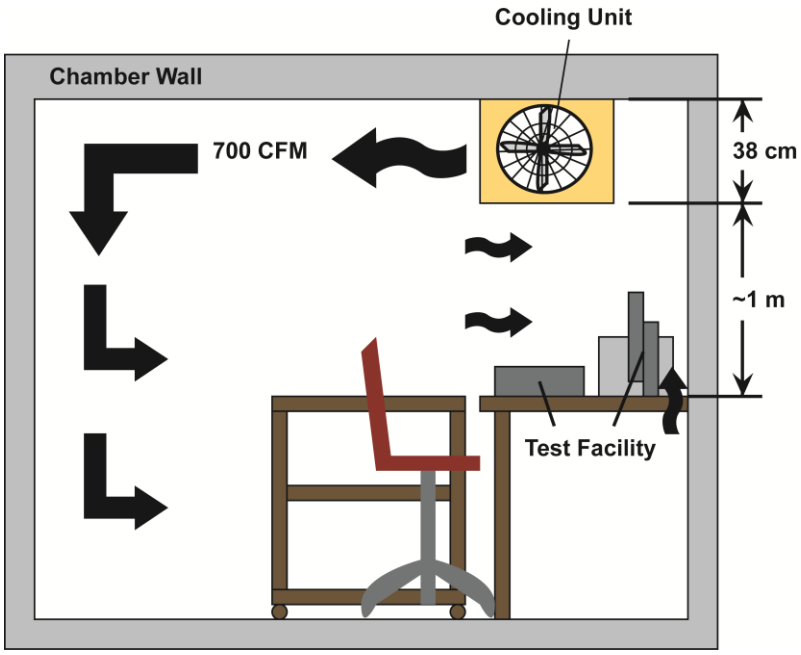

Figure 4.5 Air Flow in the Environmental Chamber

4.2 Test Facility Evolution

The test facility evolved over the course of testing as issues were addressed and measurements were improved. Early test beds were tested with a slightly different configuration than the final adsorbent beds discussed later.

The heat transfer rates were too low to measure in initial tests, even when it was clear from evaporator measurements that the refrigerant temperature was much below ambient. To improve the measurement, the coupling fluid flow rate was reduced. The required flow rates to get measureable temperature differences are discussed in Chapter 7, because they varied from bed to bed.

Originally, check valves were used to control the flow of refrigerant within the system. The check valves prevented backflow into the evaporator during the desorption phase and prevented flow from the condenser into the adsorbent bed during the

adsorption phase. However, the rate of cooling for much of the system operation was too low to measure accurately. Therefore, to increase the cooling rate to measureable levels, it was necessary to change system operation. The increase in cooling was accomplished by implementing a long pre-cooling phase during which the adsorbent bed was allowed to cool before being opened to the evaporator. This led to faster adsorption and increased cooling rate but over a shorter period of time. The total cooling for the system is similar to what would be delivered with the check valves but over a shorter period of time to make measurement easier. This was accomplished by introducing ball valves that were manually operated at the end of the pre-cooling phase rather than when the pressure in the evaporator had risen above that in the adsorbent bed.

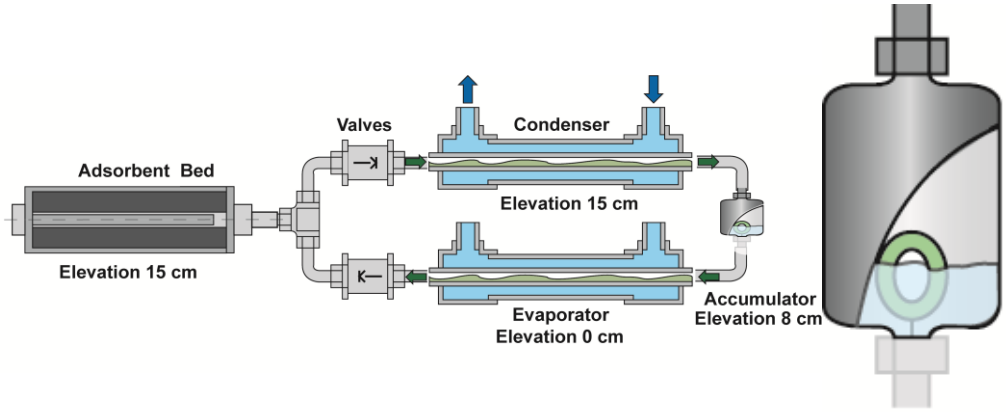

Figure 4.6 Float valve schematic

A float valve control was incorporated in one iteration of the test facility to manage the fluid levels in the condenser component. Figure 4.6 shows a float valve schematic. The float valve only opens when a sufficient volume of refrigerant has accumulated to lift the float and open the valve. It was necessary to remove the float valve from the system because of the large volume of liquid required in commercially available float valves and the difficulty in obtaining a float valve made of materials

compatible with ammonia. Modeling of system performance over many cycles with and without float valves, discussed in Appendix C, showed that the measured performance with just an expansion valve will be similar to a system with an appropriately sized float valve system for several cycles. Due to the build-up of refrigerant in the condenser, it is necessary to rebalance the refrigerant level in the system periodically, but individual tests are not affected. Because the system performance could be measured without the float valve, it was determined that the time and expense required to have an experimental float valve developed at the appropriate scale was unnecessary. A needle valve was used as an expansion valve in the system instead.

4.3 Test Procedures

Start-up and testing procedures are described here. Before testing begins, the system and surroundings are brought to testing conditions. Testing occurs in an environmental chamber that maintains the surrounding temperature within ±2ºF (1.11ºC) of the set point. For start-up, the chamber temperature is set and the environmental chamber begins to heat or cool to the testing conditions. Fans in the environmental chamber circulate air to limit the spatial variations in air temperature. The coupling fluid pump is turned on at the same time that the chamber is turned on. The coupling fluid lines help bring the insulated parts of the system to equilibrium conditions with the surroundings more quickly. The temperature of the facility is measured and is allowed to come to equilibrium, defined as a change in the average temperature in the evaporator and condenser of less than 0.1ºC for a period of ten minutes. The system typically takes one hour to come to an equilibrium temperature.

The valve between the condenser and the adsorbent bed is opened to allow adsorption. The adsorbent material during start-up is close to the ambient temperature and is at a lower pressure than the rest of the system. Ammonia tends to build up in the condenser throughout testing. Opening the valve helps to remove some of the built up ammonia while heating the adsorbent bed and equalizing the pressure. At the same time, the adsorbent bed heating element is turned on. The valve is closed when the pressure in the condenser starts to rise. At this point, a full system cycle is run with a desorption and adsorption phase. The initial heating of the bed in this first cycle requires more heat input than is used in normal operation, because the bed structure starts cold. The data from this first run are not analyzed. Once this first cycle is completed, the system start-up procedure is finished and testing begins.

Testing begins with the heating/desorption phase for the system. The adsorbent bed is heated using an electric heater delivering a constant amount of heating power. Pressure increases in the adsorbent bed as the adsorbent bed temperature increases. When a fixed period of time has passed, for the CHEC bed, or a temperature condition is met, for the Flat Bed system, the valve is opened to the condenser and desorption begins. Initially ammonia transfers quickly into the condenser and begins condensing, increasing the condenser temperature. Heating continues until either an adsorbent bed temperature is met or the cycle time length is met, depending on the test. Then the heat is removed from the bed by natural convection transfer to the surroundings and the bed begins to cool. The valve to the condenser is left open until the pressure begins to drop, because desorption continues for a short period of time after the cooling of the bed begins while the adsorbent is still hot. When the switching conditions have been met, the valve is opened

to the evaporator and adsorption begins. Cooling continues until another temperature condition or time condition has been met. Then the valve to the evaporator is closed and heating of the bed begins the next system cycle. The evaporator is still below the ambient temperature at this time and continues to deliver cooling into the heating phase. The data used for determining the cooling delivered for a cycle includes the cooling performed during the cooling/adsorption phase and in the following heating phase, although the cooling in the heating phase tends to be too low to measure accurately.

CHAPTER 5

ADSORBENT BED DEVELOPMENT

Several different adsorbent beds were evaluated with the test facility described in the previous chapter. The evolution of the adsorbent bed design is discussed below. Two final adsorbent beds were investigated based on preliminary experimental results.

5.1 Adsorbent Bed Design

The adsorbent bed here refers to the entire system component containing the adsorbent material as well as the connections and materials used for heating and cooling the adsorbent material. A simple schematic of a conventional adsorbent bed is shown in Figure 5.1. In this work the chamber wall that contains the pressure is considered part of the bed, a single port is used for transfer of refrigerant into and out of the adsorbent bed, and heating and cooling of the adsorbent is achieved with different heat transfer paths.

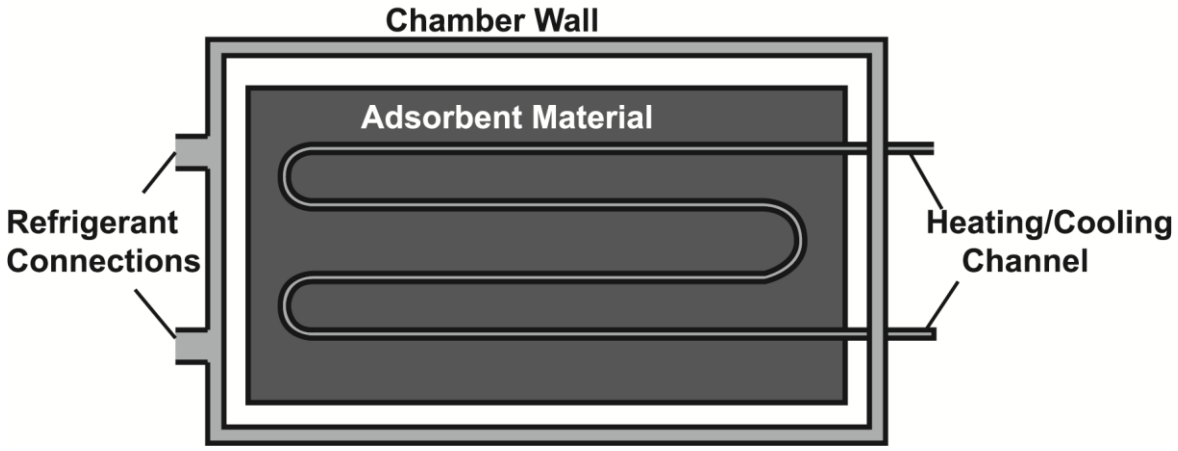

Figure 5.1 A conventional adsorbent bed with important parts labeled.

The adsorbent used for this work is Norit RB3 activated charcoal. This adsorbent is a steam activated carbon designed to balance pressure drop through an adsorbent bed with good diffusion into the material. The Norit RB3 has a pore volume of 4.1×10^{-4} m^3 kg^{-1}(Norit, 2008) and a D-A constant of 1.82×10^{-7} (Critoph, 1988). The activated carbon is shaped in cylindrical pellets 2.75 mm in diameter with lengths ranging from 3 mm-10 mm.

The adsorbent bed design was developed using insights from the modeling of adsorption systems described in Chapter 3 as well as from the literature. The selection of the adsorbent bed materials is discussed below. Heat transfer considerations for the bed and methods used to address the difficulties in direct air coupling of the bed are discussed here. Then the bed design approach is discussed.

5.1.1 Material Selection

In choosing the materials for an adsorbent bed, there are several competing concerns: material compatibility, heat capacity, and heat transfer properties. In this system, the bed material also acts as a pressure vessel and therefore, the tensile strength is also important. Material compatibility is necessary to ensure system reliability and safety. Corrosion and leaks are possible if the bed is constructed of inappropriate materials. The heat capacity depends on both the specific heat and density of the material, and contributes directly to the dynamic losses of the system, because a portion of the bed structural material is heated and cooled on each cycle. The heat capacity of the bed material should be as low as possible. The bed material must be strong enough to contain the working pressure of the cycle. At the scales being investigated in this work, the available materials and the sizing required for connections mean that tensile strength is

not the limiting factor on the component sizes. Finally, heat must be transferred through the adsorbent bed materials into the adsorbent. For adsorbent heating and cooling, a high thermal conductivity is desirable, although at the scales being considered, there is a trade-off between more rapid system heating and increased system losses. In practice, the thermal resistance of the adsorbent is much higher than the resistance of the most appropriate adsorbent bed material, and increased thermal conductivity has a small impact on system performance compared to other properties.

The materials available for the bed were greatly limited by the refrigerant, ammonia, under consideration here. Ammonia is a highly corrosive fluid and reacts with a large number of materials. The following materials were considered: stainless steel, aluminum, epoxy, Teflon, PVC, alumina, and silica glass. Table 5.1 compares the heat capacity related properties of these materials. Stainless steel has the best resistance to ammonia, and can be machined to make a variety of system components. While the corrosion resistance of stainless steel is good, it has the highest heat capacity of the materials considered. Various polymer compounds were also considered, but high diffusion rates of ammonia and water through the polymers made them unworkable as bed materials. Refrigerant would diffuse out of the system over time and the water would diffuse into the system. The ceramic materials: alumina and silica glass, were also considered for the bed. Ceramics offer good corrosion resistance and thermal properties close to aluminum, but they are harder to machine and more brittle. They were ruled out due to the difficulty of machining, although may be appropriate for future consideration. Aluminum was chosen as the structural material for the final beds. Aluminum has lower heat capacity than steel, but is more susceptible to corrosion by ammonia if there is a

small amount of water present; therefore, precautions had to be taken to avoid corrosion. The adsorbent, all system components, and charging lines are evacuated and heated to remove water to prevent corrosion, as described previously.

Table 5.1 Material Properties

Material	**Density [kg m^{-3}]**	**C_p [J kg^{-1} K^{-1}]**	**ρC_p [kJ m^{-3} K^{-1}]**	**ρ C_p % of SS**	**Pros**	**Cons**
Stainless Steel (304)[1]	7900	480	3770	100%	Corrosion resistant	Higher thermal capacity
Aluminum[1]	2700	900	2440	65%	Moderate thermal capacity, Machinability	Corrosion prone
Epoxy[2]	1200	500	600	16%	Lowest thermal capacity	Permeable
Teflon [2]	2160	1000	2160	57%	Moderate thermal capacity, Machinability	Permeable
PVC [2]	1300	900	1170	31%	Low thermal capacity	Permeable
Alumina[3]	4000	880	3520	93%	Corrosion resistant	High thermal capacity
Silica Glass[3]	2200	740	1630	43%	Moderate thermal capacity	Poor machine-ability

1 Incropera and DeWitt (1996)
2 Engineering Toolbox (2013)
3AZoNetwork (2013)

5.1.2 Heat Transfer

In the adsorbent bed design, the goal is to maximize the heating and cooling rates of the adsorbent. Fast heating and cooling rates of the adsorbent yield larger cooling duties from the system, and heat transfer rates are the primary limiting factor for the cooling capacity of the system. The heat transfer rates also indirectly affect the COP of the system by changing the system losses for each cycle, although this is less significant than the effect on cooling capacity. The thermal conductivity of the adsorbent material is

low, 0.5-0.3 W m^{-1} K^{-1} for monolithic carbon (Tamainot-Telto and Critoph, 2000) and 0.15-0.25 W m^{-1} K^{-1} for packed beds (Critoph and Turner, 1995). The thermal conductivity is generally the limiting factor in heating of the system and it is necessary to develop strategies for transferring heat into the material as quickly as possible. Increasing heat transfer in the bed is usually in conflict with limiting the bed mass and thermal capacity, because heat spreading surfaces increase the system mass. In the first set of beds, reduction in the heat transfer resistance into the adsorbent was achieved by minimizing the thickness of the adsorbent layer. There is a trade-off between the adsorbent volume and the thickness of the adsorbent layer. To help reduce this impact, fins were added to improve the heat transfer rate through the adsorbent. In one of the final beds, the contact resistance from the bed wall to the adsorbent was minimized by increasing the contact pressure. This approach is discussed in more depth for the flat bed configuration at the end of this chapter.

One of the goals of this work is to make the system a widely useful drop-in device and eliminate pumping requirements; therefore the beds considered here are direct air coupled to the surroundings. In most conventional systems, cooling is achieved through a cooling fluid pumped through the bed, and then the heat is transferred to the surroundings in a cooling tower or radiator system. Directly convectively cooling the adsorbent bed eliminates the external heat exchanger and coupling pump and plumbing; however, because the surrounding air has a much lower convection coefficient than the heat transfer fluids used in most systems (<5% of liquid), the cooling rates for the designs discussed here can be expected to be much lower than those for a comparable liquid coupled system. The lower heat transfer rate can be overcome somewhat by increasing

the heat transfer surface area. The convection coefficients are compared to assess the additional surface area required to achieve comparable cooling rates. Representative values are used to make a comparison and the actual convection coefficients in the work can be expected to be slightly different.

A representative comparison is made between the two coupling fluids here to assess the impact on heat transfer rates. The convection coefficient in the surrounding air is estimated using the Churchill and Chu (1975b) correlation, assuming that natural convection is occurring on a vertical flat plate 0.06 m in length at 70ºC, a temperature comparable to that of the adsorbent system bed, with the surroundings at 20ºC. This yields an estimated convection coefficient, h_{nat}, of 7.0 W m^{-2} K^{-1}. Radiation from the surface improves the heat transfer to the surroundings and assuming an aluminum surface with moderate oxidation, the emissivity is estimated at 0.2, has an effective convection coefficient of 1.5 W m^{-2} K^{-1} for these conditions. The effective heat transfer coefficient is then 8.5 W m^{-2} K^{-1}. Meanwhile, the convection coefficient for a conventional system is estimated assuming a 9.53 mm (3/8 in.) hydraulic diameter with laminar fluid flow and constant wall surface temperature. In this case, the convection coefficient for the fluid is estimated to be 230 W m^{-2} K^{-1}. Radiation heat transfer is neglected in this calculation. Therefore, to achieve comparable convection resistance for cooling this system, approximately 30 times as much external surface area is required. Another important consideration for the heat transfer rate is the low thermal conductivity of the adsorbent. The low thermal conductivity means that the adsorbent normally dominates the thermal resistance and although the heat transfer coefficient ratio is 1:30, the total resistance only differs by a factor of 1:3. This implies that the cooling time would be approximately

tripled for the air-coupled system assuming similar heat capacities, before extended surfaces are used to improve the cooling rates. With appropriate extended surfaces, it is expected that the cooling rates could be increased to 50% or more of those achieved by liquid-coupled systems.

5.1.3 Additional Considerations

In this work, there were a number of additional considerations for the adsorbent bed beyond those found in conventional adsorption systems. The first was the convection coupling discussed in the heat transfer system. Second was the goal of operating the system autonomously by heat alone. To achieve this, the bed design had to take into consideration the methods that could be used to achieve this. The actual control methods are discussed in the following chapter. An adsorbent bed design was developed to take advantage of the developed control systems.

5.2 Preliminary Test Beds

To develop the best adsorbent bed possible, progressively improved designs were developed as insights were gained from experimental and analytical findings during the course of the work. The first test bed (Bed #1) was a stainless steel center-heated design. A drawing of the bed is shown in Figure 5.2, while a photograph is shown in Figure 5.3. This bed was the first to implement the center-heated design. Heat is introduced through a central heating channel and heat removed on the external surface (CHEC). Heat removal occurs from the external surface of the bed. This bed also implemented a form of thermal switching.

Bed #1 is 7.94 cm (3.125 in.) in length with a 3.81 cm (1.5 in.) inner diameter and a center heating channel 1.905 cm (0.75 in.) in diameter. The design does not incorporate heat transfer fins to spread heat into the adsorbent; instead, the thickness of the adsorbent was limited to 0.953 cm (0.375 in.) The outer dimensions are 4.445 cm (1.75 in.) by 4.445 cm (1.75 in.) and 10.2 cm (4 in.) This bed holds 0.030 kg of adsorbent material. The bed structure has a mass of 0.60 kg. With fittings, it increases to ~0.70 kg. A schematic of the bed is shown in Figure 5.2. The bed is heated by a center post with a McMaster-Carr model 3618K293 6.35 mm (0.25 in.) diameter, 5.08 cm (2 in.) length, 200 W high temperature cartridge heater. The heat input is modulated using a variac to control the voltage to the cartridge heater. The center channel through the bed is tapered and the post inside is similarly tapered. The post is actuated by a solenoid that moves the post up and down to make and break contact between the heating post and the adsorbent bed. When the post is in contact, heat is transferred much more quickly to the adsorbent than it can be removed and the temperature of the adsorbent material increases. When the post is out of contact, an air gap increases the resistance from the heating post to the adsorbent and the adsorbent cools. Based on the conventional assumptions found in literature, the axial effects and heat transfer through the bed structure are assumed to be negligible in this design, although subsequent versions of the models showed that axial effects are important at this scale with the short resistance being approximately 45% of the thermal resistance through the adsorbent.

The adsorbent is loaded from the top and sealed with two neoprene O-rings. Two 1/8 in. NPT threaded connections allowed a thermocouple to be fed into the adsorbent and a connection for refrigerant transfer. This bed was tested under a range of heat inputs.

The cooling achieved with this system was too low to measure, as discussed in Appendix A, and the adsorption cycle was excessively long. The poor performance was due to a flaw in the construction of the central post discussed below. It seemed probable that there would be continued difficulty with the central post, which necessitated a change in system design. A photograph of Bed #1 is shown in Figure 5.3.

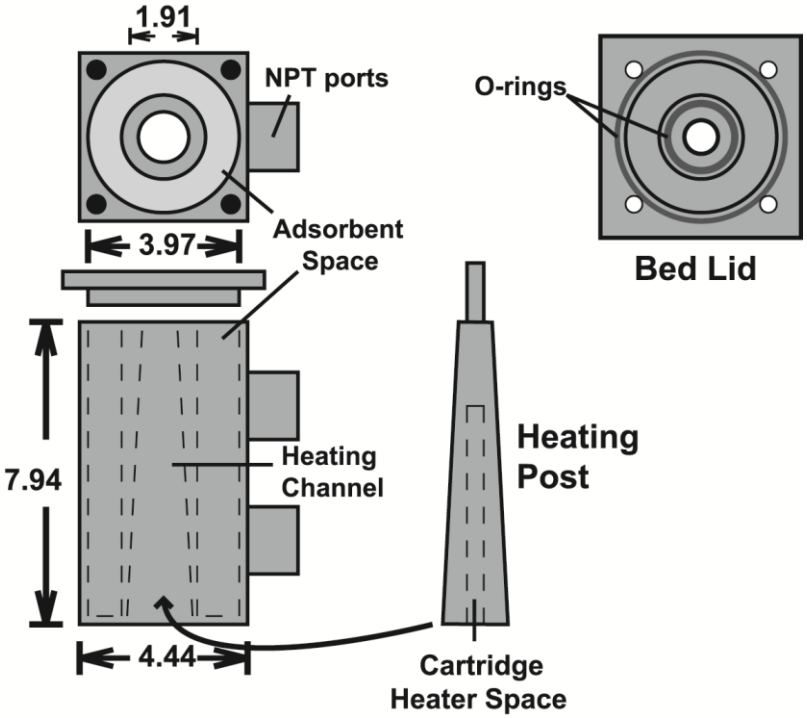

Figure 5.2 Drawing of Bed #1 Design

The change in resistance from the center post to the adsorbent is fundamental to the operation of this system. From the heating element to the center of the adsorbent material, the thermal resistance was predicted to be 4.94 K W^{-1} when the bed is heating. This resistance is dominated by the adsorbent resistance, which makes up 96% of the resistance. The contact resistance was estimated based on literature values for stainless steel surfaces in contact with grease interface material (Fried, 1969) and was multiplied by a factor of 25 to account for the decreased contact pressure. When the bed is cooling,

the resistance from the heating element to the adsorbent was predicted to be 19.08 K W^{-1}. This resistance is dominated by the air gap between the heating post and adsorbent bed. The resistance from the adsorbent to the surroundings is estimated to be 8.08 K W^{-1}. For a heating element temperature of 100ºC, the maximum swing in temperature of the adsorbent achievable is 25.9ºC, while the maximum adsorbent temperature is 73.3ºC. However, when the thermal shorting effect is accounted for, this swing in temperature increases to 32.0ºC with a maximum bed temperature of 84.7ºC. In this case, the thermal shorting around the ends of the bed increases the temperature of the adsorbent due to the temperature of the outer shell increasing and the adsorbent being heated from both sides. However, the losses to the environment due to the thermal shorting are significant, with 60% or more of the heat being lost without heating the adsorbent.

The predicted resistances were not achieved, and a temperature swing of only 5ºC was achieved. The center post did not make full contact with the bed when in the heating position because the taper of the post and the center heating channel were slightly different (~0.2°). Because of the design, very tight tolerances were required to ensure good contact. The post also had a tendency to shift off center and make partial contact with the adsorbent bed during the cooling phase. Thus, resistance was neither as high as desired during the cooling phase nor as low as desired during the heating phase. An attempt was made to eliminate the thermal switching portion of this bed and just test the CHEC design by providing additional heat transfer grease and increasing the heat input to make up for the poor heat transfer properties while cycling the heat input. Unfortunately, the post also made contact with the bed lid and the increased heat input caused the bed lid to increase in temperature around one of the O-rings. The heating of the O-ring caused

leakage and it was determined that modifications would be necessary. The decision was made to separate the thermal switching concept from the CHEC design in subsequent tests to explore each aspect independently.

Figure 5.3 Bed #1 constructed of stainless steel.

The thermal mass of the structure relative to the adsorbent material was reduced in the subsequent systems to reduce the dynamic losses. A shift was made to aluminum to further reduce the thermal mass of the system. The sealing for the system was simplified to decrease the chance of failure due to thermal break-down of the seal. A drawing of Bed #2 is shown in Figure 5.4, and a photograph of the fabricated bed is shown in Figure 5.5.

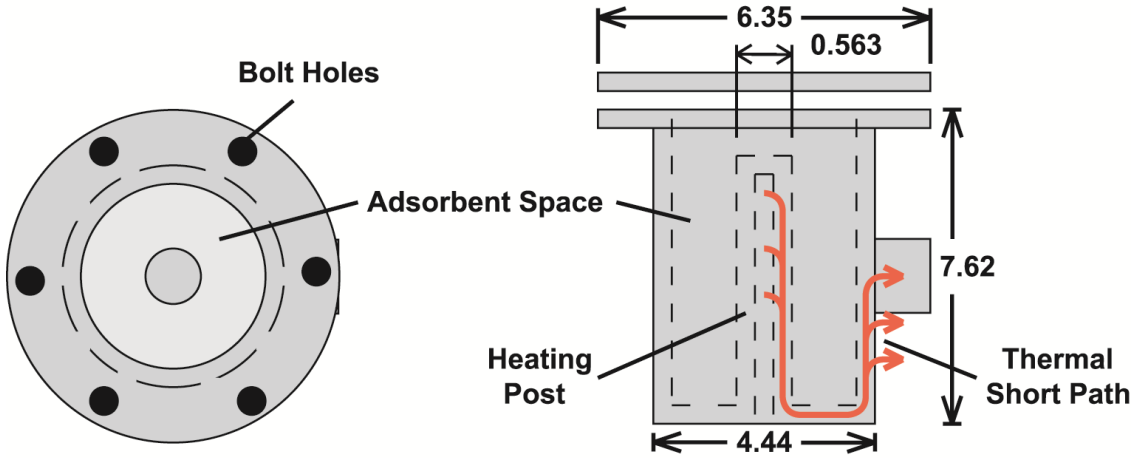

Figure 5.4 Schematic of Bed #2

Bed #2 increased the adsorbent volume by 33% and decreased the bed structure heat capacity by 50%. Bed #2 contained 40 grams of adsorbent material, 30% more than the first bed with approximately half the thermal capacity. One end is sealed with an o-ring and plate bolted to the bed. The O.D. of the flange is 6.35 cm (2.5 in.) while the adsorbent chamber has an I.D. of 4.13 cm (1.63 in.) with walls that are 1.59 mm (1/16 in.) thick. The absorbent space is 7.62 cm (3 in.) tall. A heating post runs through the center of the bed to allow the heat to be transferred into the adsorbent material and a cartridge heater is placed in the post. The post is 6.35 mm (1/4 in.) from the top of the lid to prevent the O-ring heating problems encountered in Bed #1. The reduced thermal mass of this system allowed it to heat and cool more rapidly than the Bed #1 during heating and cooling tests conducted before the system was charged. However, contamination of the refrigerant caused corrosion of the bed that pitted the wall and prevented the system from being sealed. The bed was corroded before testing could be completed and the system could not be fully characterized. Corrosion of the bed can be seen in Figure 5.6.

Better adsorbent cleaning techniques and system charging procedures were developed to prevent this from occurring in future tests.

Figure 5.5 Bed #2, Aluminum, larger capacity, lower thermal mass

The resistance from the heater to the center of the adsorbent material was estimated to be 8.40 K W^{-1}, while the resistance from the adsorbent to the surroundings without fins on the outer surface was 25.95 K W^{-1}. Fins would have been added to the outer surface of the bed if testing had continued, reducing the resistance between the adsorbent and the surroundings by approximately a factor of 3. In modeling of the bed, axial conduction through the bed structural materials had been neglected; however, the switch to aluminum made the thermal shorting around the ends of the adsorbent bed significant. The resistance from the center heating post around the ends to the outer surface was only 1.32 K W^{-1}. The thermal shorting in this case caused heat to be lost to the surroundings at a much faster rate and decreased the amount of heat reaching the adsorbent material. To illustrate the scale of the losses, at equilibrium conditions, with a heater temperature of 100ºC, only 6% of the heat from the heater goes into the adsorbent while the rest shorts around the adsorbent through the path shown in Figure 5.4. The actual losses were less significant, because the energy required for desorption keeps the temperature of the adsorbent from increasing as fast as the structure and increases the

heat transfer to the adsorbent. A maximum adsorbent temperature of 95.3ºC can be reached for this bed, although again with very low loss rates. The loss in efficiency problem would have been exacerbated by the addition of fins. In the following beds, the center post was eliminated and the heating cartridges were placed directly into contact with the adsorbent. This provided less cross-sectional area for thermal shorting heat transfer and the cartridge heaters have lower thermal conductivity than the aluminum structural material (approximately 200 W m^{-1} K^{-1} vs. a maximum of 60 W m^{-1} K^{-1} (Konoshima, 2010)). The subsequent beds were also lengthened to increase the path length, which also reduced the thickness of the adsorbent layer, which in turn increases the heat transfer into the adsorbent. The lengthening does increase the thermal mass of the bed, however.

Figure 5.6 Corrosion within the bed due to contamination of ammonia with water

A modification in approach was made to more easily produce adsorbent beds using off-the-shelf components. The Bed #3 was sealed with NPT connections and produced using off-the-shelf components rather than customized components. This decreased the cost of producing the bed and made it easier to make changes to the

adsorbent bed system. This bed could not be tested because of a faulty cartridge heater. The cartridge sheath was defective and allowed ammonia to diffuse into the heating element. This quickly led to contamination of the ammonia as well as electro-chemical corrosion within the bed. Electrical shorting through the adsorbent bed also occurred and the shorting affected system measurements, preventing testing. The final CHEC bed design is very similar to this bed in design and construction.

A schematic of Bed #3 is shown in Figure 5.7. Bed #3 has a central chamber made of aluminum piping with an O.D. of 2.54 cm (1 in.) and an I.D. of 1.91 cm (0.75 in.). The ends are fitted with threaded NPT fittings that connect to caps that are each 2.86 cm (1.13 in.) long. The ends of the cap are 6.35 mm (1/4 in.) thick. Drilled through the end caps are 1/8 in. NPT taps for a cartridge heater to be placed into the adsorbent bed and for connections to the system. A McMaster-Carr 6.35 mm (1/4 in.) diameter, 15.24 cm (6 in.) stainless steel sheathed 150 watt cartridge heater model number 3618K419 was used for this bed. Fins would have been attached to the outer surface of this bed, if it had not been damaged. A view of the assembled bed is shown in Figure 5.8.

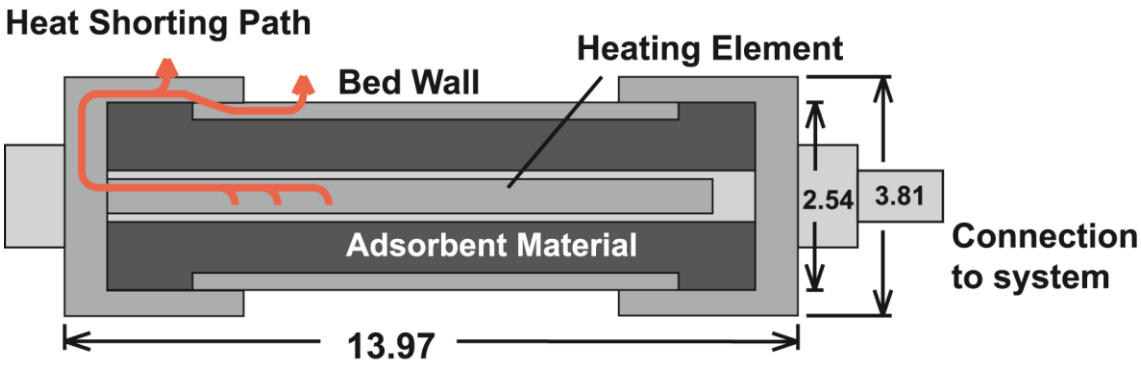

Figure 5.7 Schematic of Bed #3 without external fins attached.

The total resistance into the center of the adsorbent material was 4.78 K W^{-1}, while the total resistance from the adsorbent to the surroundings was 10.29 K W^{-1}. The

short resistance for this bed is 10.22 K W^{-1}. The maximum temperature for this bed at equilibrium when the cartridge heater is at 100ºC is 82.6ºC. The lower temperature than Bed #2 is due to the decreased convection resistance due to more surface area and less heating of the outer wall through thermal shorting. In Bed #3 at equilibrium, approximately 56.6% of the heat from the cartridge heater goes into the adsorbent, although the actual portion varies significantly over the course of the cycle.

Figure 5.8 Bed #3 without the external fins attached. This bed damaged by a faulty heater.

The adsorbent beds are summarized in Table 5.2 with a comparison of their mass and heat capacities. The heat capacities are found assuming that the whole system is of the same material as the bed structure. For the aluminum beds, this over estimates the heat capacities because the fittings have lower specific heats than aluminum.

A limiting factor in the effective construction of a small bed is the amount of material required for measurements and for connections to the small-scale components. These test beds are connected to the system using Swagelok compression fittings. The Swagelok connections allow the beds to be installed and removed quickly and easily. The mass of these connections to the system as well as the NPT adapters that thread into the bed are of a similar order of mass as the bed structural material. In production systems,

the mass can be addressed with welded connections. Welded connections were not viable for the test bed because the ability to disassemble and examine the inside of the bed was necessary to access and modify the bed. Additionally, in a production system, detailed instrumentation will not be necessary, as it is with these test systems. This additional weight negatively impacts the performance of the system, reducing both the SCC and COP of the system.

Table 5.2 Preliminary Test Beds

Test Bed	**Bed + Connection Mass (g)**	**Adsorbent Mass (g)**	**Heat Capacity Bed (J K^{-1})**	**Heat Capacity Refrigerant (J $cycle^{-1}$)**	**Comments**
Bed #1	700	30	350	4100	Stainless Steel, Mass too large and too much thermal resistance between the adsorbent bed and heater
Bed #2	200	40	175	54800	Aluminum, Corroded by contaminated refrigerant testing was not finished
Bed #3	400	40	350	54800	Aluminum, Faulty heater caused leaking and contaminated refrigerant

5.3 Final Adsorbent Beds

Using the lessons learned from the preliminary bed designs, two final adsorbent beds were designed and were tested in this work. The first employs the CHEC design described in the modeling section, while the second uses the thermal switching control technique with a Flat Bed.

5.3.1 CHEC Design

A CHEC test section was constructed to evaluate this design for use with the periodic heat supplies or a thermal flow control system. In the CHEC design concept, as described in Section 3, heat in introduced in the center of the bed and cooling of the bed

is achieved on the outer surface of the bed. The final bed is of the same design as Bed #3 described above with minor modifications.

The CHEC test section structure is made of aluminum with NPT connections. It is connected to the adsorbent system with stainless steel Swagelok fittings. The center section is 10.2 cm (4 in.) in length with an O.D. of 3.18 cm (1.25 in.) and an I.D. of 2.54 cm (1 in.). End caps add an additional 3.81 cm (1.5 in.) of internal length to the bed and have outer diameters of 4.45 cm (1.75 in.). The total internal length is 13.9 cm (5.5 in.) and the overall bed length is 15.24 cm (6 in.). At either end is a ¼ in. NPT tapped hole. The first connection converts the threading to a ¼ in. Swagelok tubing. Between the adsorbent bed and the outlet connection, a polyethylene filter material is placed to prevent migration of the adsorbent material from the adsorbent bed. The other threaded tap allows a 15.24 cm (6 in.) long, 0.635 cm diameter (1/4 in.) stainless steel cartridge heater to be fed into the center of the adsorbent bed and sealed with a Swagelok compression fitting. The adsorbent material is packed directly around the cartridge heater and fills the empty volume of the adsorbent bed. To improve the heat transfer from the heater to the adsorbent bed, a series of aluminum fins is affixed to the cartridge heater using epoxy. Aluminum fins are epoxied to the cartridge heater using JB Weld to efficiently transfer heat input the adsorbent. The epoxy is applied in a thin layer, less than 0.5 mm thick. The thermal conductivity of the epoxy is assumed to be 0.2 $W\ m^{-1}\ K^{-1}$, the lowest reported value for epoxy (Engineering Toolbox, 2013). The resulting thermal resistance due to the epoxy in each section of the heater is at most 4.58 K^{-1} W. This thermal resistance increases the thermal resistance into the fin by 40% or less compared to a fin integrated into the heater material with no adhesive resistance. The fins are

arranged in a "butterfly" pattern with the fins wrapped around the cartridge heater and then spreading through the adsorbent. This pattern was used to allow the adsorbent material to be loaded into the bed without leaving large voids. A schematic of the design is shown in Figure 5.9, the CHEC bed is shown in Figure 5.10, and a picture of the fin arrangement inside the adsorbent bed is shown in Figure 5.11. The total structural mass of the bed, fittings and heater is 0.358 kg. The bed is loaded with 35 g of adsorbent material. A thermocouple is affixed to the outer surface of the bed 1 in. from the end of the bed that connects to the system.

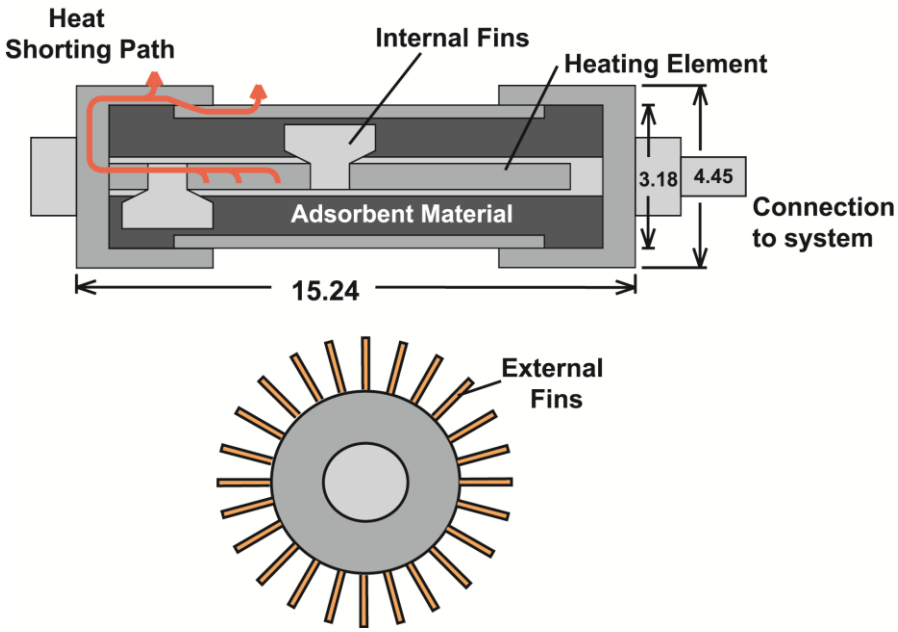

Figure 5.9 CHEC without external fins attached

Figure 5.10 The central heater and fins of the CHEC adsorbent bed.

The outer surface of the bed provides cooling for the bed by transferring heat to the surroundings. To improve the heat transfer to the surroundings, the bed is fitted with multi-louvered fins to increase the surface area of the bed. These fins are 0.953 cm (3/8 in.) tall and 3.81 cm (1.5 in.) wide. A total of 97 fins are added to the outer surface. The starting convection surface area is approximately 0.020 m^2 and the fins increase this to 0.080 m^2. When the surrounding air is still, the convective resistance is estimated to be 1.95 K W^{-1} and when the surrounding air is circulating, the convective resistance is estimated to be 0.622 K W^{-1}. The conduction resistance through the whole of the adsorbent thickness is estimated to be 3.96 K W^{-1}. Axial conduction through the adsorbent material is neglected, because it is very small compared to the axial conduction through the other components (< 1%). The maximum equilibrium temperature is 68.6ºC when the cartridge heater is surface is at 100ºC, and at equilibrium conditions, 83.6% of

the heat goes into the adsorbent. The thermal conduction resistance in the radial direction through the adsorbent is the dominant resistance. This bed has much lower resistance overall than the other beds considered, and therefore, heats and cools faster. This is largely due to the internal and external fins improving heat transfer.

The CHEC design was tested over a range of thermal inputs and conditions. The tests conducted for the CHEC bed are described in Table 5.3. The testing results are discussed in Chapter 7. The heating rate was tested at 50 W, 75 W, and 100 W ±1 W to test different heating rates for the system. The ratio of heating to cooling time was also varied. The nominal heating-to-cooling time ratios were 1:1, 1:2, 1:3, 1:4 and 1:5. Longer cooling times were used, because the cooling heat transfer rates were lower than the heating heat transfer rates. The heating times were set at 500 s, 720 s, and 1000 s. Different surrounding conditions were tested as well, including different surrounding temperatures and whether the air is still in the environmental chamber or being circulated.

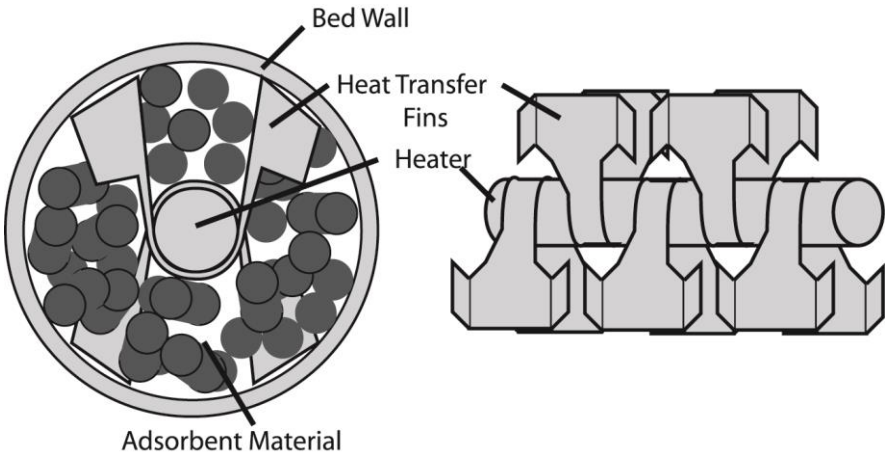

Figure 5.11 Central heater and fins of the CHEC adsorbent bed.

Table 5.3 CHEC Bed Test Matrix

Input heat [W]	**Heating time [s]**	**Nominal t_c:t_h ratio**	**Surr. Cond.**	**Nominal Surr. Temp [°C]**
50	500	1	Still	24
		2	Still	24
	1000	1	Still	24
		1	Circulation*	29
		1.5	Still	24
		2	Still	24
75	300	5	Still	24
	500	1	Circ.	29
		2	Circ.	29
		2	Still	24
		3	Circ.	29
		4	Still	24
	750	1	Circ.	29
	1000	1	Circ.	29
100	500	2	Circ.	29
	750	1	Circ.	29
		2	Circ.	29
		2	Circ	19
	1000	1	Circ	19

*Circulation is with the environmental fans on as described in Chapter 4

5.3.2 Flat Bed Design

The second bed is constructed of two aluminum plates joined together with an O-ring to seal the bed. The joining of the plates also serves to compress the plates against the adsorbent and ensure good thermal contact with the adsorbent, which is compressed between the plates. The adsorbent within the bed is aligned to ensure better thermal contact than would be achieved in a randomly packed bed. A diagram of the bed is shown in Figure 5.12 and a photograph of the fabricated bed is shown in Figure 5.13. The plates have a diameter of 8.255 cm (3 ¼ in.). A 6.985 cm (2 ¾ in.) groove is cut into one plate approximately 1 mm deep to allow an O-ring seal to be placed between the plates. The

area outside the O-ring on the plate acts as a bolt ring with 0.317 cm (1/8 in.) bolts holding the plates together. Each plate is 0.635 cm (1/4 in.) thick and has a circular impression cut into the plate that is 4.76 mm (3/16 in.) deep and 6.35 cm (2 ½ in.) in diameter. This creates a center area for the adsorbent between the two plates. The connection to the system is performed by a ¼ in. NPT connection run through the center of the cold side plate. The connection to the system is fitted with a polyethylene filter material to prevent adsorbent migration from the bed. The total mass of the plates, O-ring, bolts, and fittings for the bed is 159 g. The bed is loaded with 10 g of Norit II activated carbon.

Heat transfer into and out of this bed is controlled by thermal switching. Heat is transferred into the bed on one side and transferred out of the bed on the other side. On the hot side, a thermal mass is used to store heat between desorption cycles. An electric heat pad is attached to the hot side thermal mass, which supplies heat to the system. The heat transfer block has a mass of 0.138 kg and is approximately 5.08 cm (2 in.) in diameter. The back of the thermal mass is insulated to prevent heat losses to the surroundings. On the opposite side of the bed, cooling fins are attached to another heat transfer block with a mass of 0.050 kg. This block constantly transfers heat to the surroundings so that it can quickly cool the bed when connected. There is approximately 300 cm^2 of cooling surface for the cold side block, with multi-louvered fins that are 1.27 cm (0.5 in) in height and 2.54 cm (1 in.) wide (shown in Figure 5.14). Both blocks have 7.92 cm^2 of heat transfer area to the bed and silicone grease is applied to their surfaces to improve heat transfer. The bed translates from one thermal block to the other to make contact. During the desorption phase, the adsorbent bed is in contact with the hot thermal

mass, and during the adsorption phase, the adsorbent bed is in contact with the cold side thermal mass.

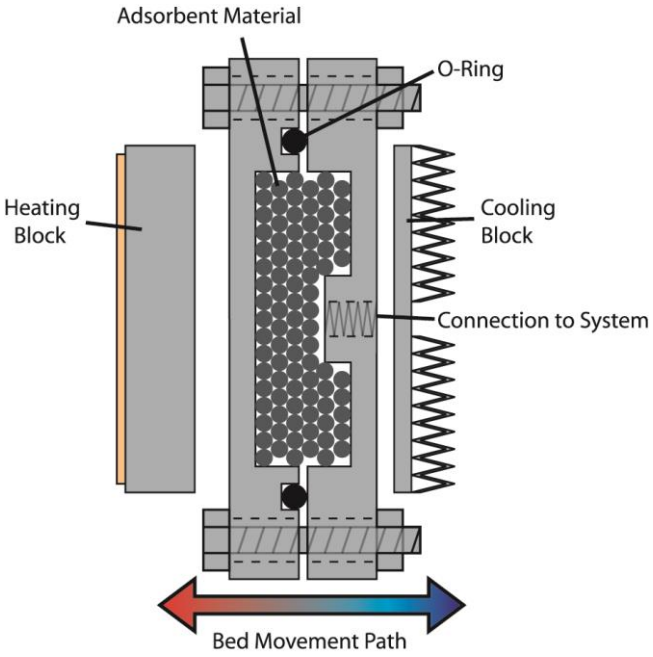

Figure 5.12 Flat Bed adsorbent bed. The bed moves between the cooling block on the right and the heating block on the left.

The total resistance from the heat into the adsorbent is 6.82 K W^{-1} and out of the adsorbent during the heating phase is 68.1 K W^{-1}. The total resistance from the heat source into the adsorbent is 66.5 K W^{-1}, and to the surroundings, the resistance is 8.36 K W^{-1}. The thermal shorting resistance is 2.53 K W^{-1}, although in this system, because the thermal shorting does not have as significant an effect on the losses because the external thermal switch limits heat transfer to the surroundings. The bed loses some heat due to convection throughout the whole cycle, the thermal resistance for the transfer from the bed surface to the surroundings is 23.0 K W^{-1}. These representative resistances do not account for all losses, particularly heat transfer through the connection to the system which may also be significant. The contact resistance is estimated using the contact

resistance for aluminum surfaces with grease found in Fried (1969) and a factor of safety of 100 is assumed to account for the low contact pressure and the estimated contact resistance is approximated as 1 K W^{-1}. For a 100 ºC heat source the maximum temperature for the adsorbent is 89.8ºC during heating. This bed also has a relatively low temperature gradient with maximum temperature difference of 7.30ºC and the minimum bed temperature is 28.8ºC. Therefore, this bed can deliver a large temperature swing effectively.

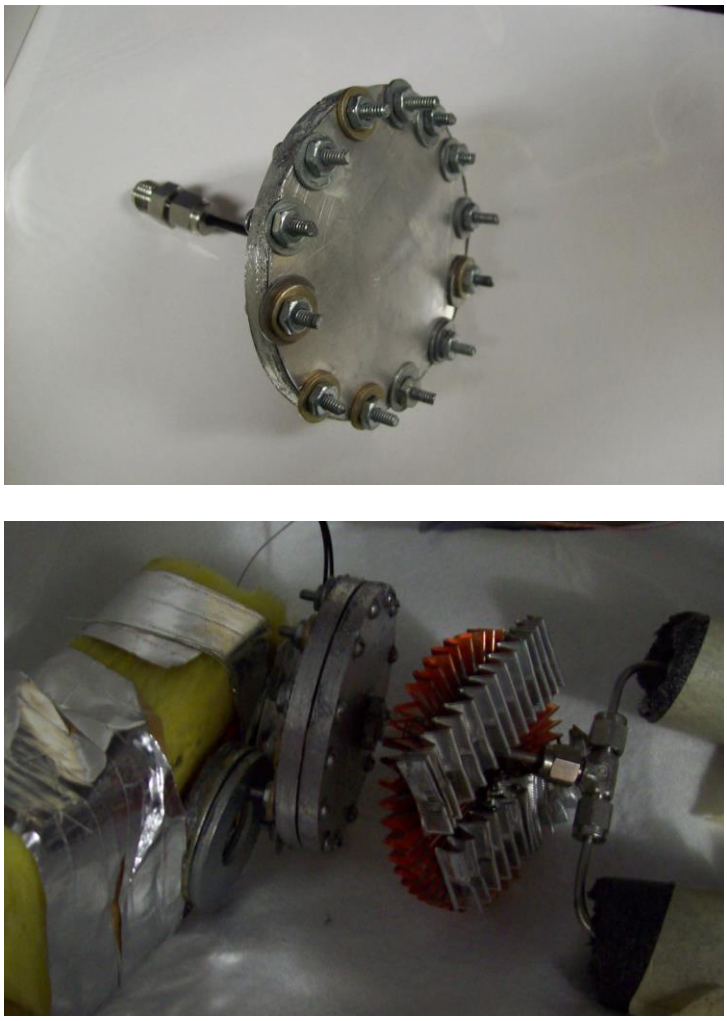

Figure 5.13 Photographs of the tested Flat Bed system.

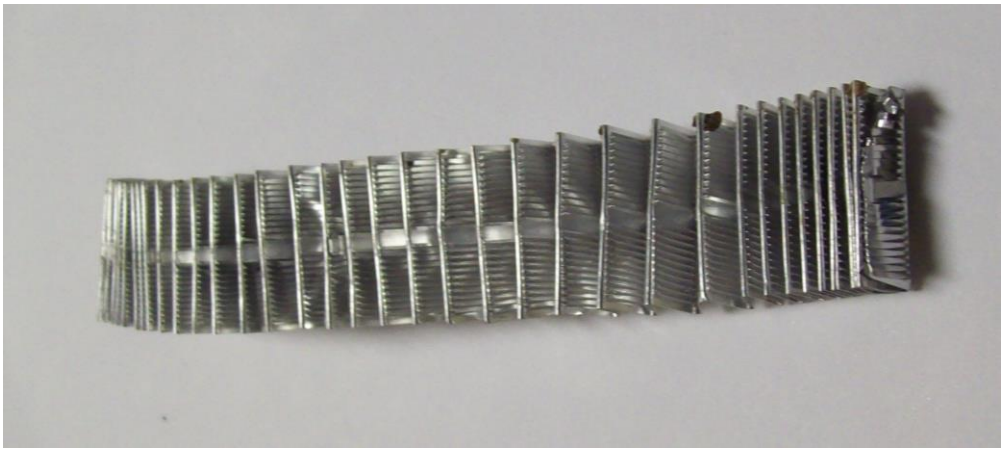

Figure 5.14 Fins used to transfer heat to the surroundings.

During adsorption, the temperature of the hot side heat transfer block increases and when put in contact with the bed, the heat can be transferred quickly into the adsorbent bed. The hot side block temperature is maintained within 2 degrees of a target temperature by controlling the heating pad. Similarly during the desorption phase, the cooling heat transfer block temperature drops so that heat can be removed from the bed quickly. Heat is lost from the bed throughout both cycles on the disconnected side of the bed, but this is small compared to the amount of heat transferred between the adsorbent bed and the heat transfer blocks.

The Flat Bed system was tested at different heating conditions as well as different thermal switching conditions. Table 5.4 shows the tests conducted for the Flat Bed adsorbent system. Two heat inputs were explored, 10 W and 20 W, with different initial heating block temperatures. Additional tests were run at 5 W of heat input, but the bed temperature did not rise above 60ºC and no cooling was measured. The Flat Bed system used temperature switching conditions rather than fixed heating and cooling phase times, so that the ratio of heating and cooling phases was not actively controlled. The hot side

temperature reached before switching was varied from 60ºC to 100ºC. The bed was switched when the temperature of the cooling block had reached 35ºC or 40ºC. The bed temperature is expected to follow these temperatures closely. The control conditions yielded heating-to-cooling time ratios ranging from 1:1 to 1:2. Another factor affecting testing is the initial temperature of the heating and cooling blocks when they are connected to the system. These affect the heat transfer rates and the ratios of the heating and cooling times, as well as the average cooling rate for the system. The initial temperatures of the heat transfer blocks depend on previous system operation and could not be controlled directly, which is why an initial cycle or cycles are required to allow the bed to come to periodic steady state.

Table 5.4 Flat Bed Test Matrix

Input heat [W]	**Switching Temperature (high)**	**Switching Temperature (low)**	**Surr. Cond.**	**Nominal t_h:t_c ratio**	**Nominal Surr. Temp [ºC]**
10	65	35	Still	2	25
	70	35	Still	1.75	25
	80	45	Still	1.25	25
	80	40	Still	1.5	25
	60	35	Circ.*	1	25
	65	35	Circ.	2.75	25
	70	35	Circ.	1.5	25
20	85	35	Circ.	2.25	25
	90	40	Circ.	1.75	25
	95	35	Circ.	2.75	25
	100	35	Circ.	1.25	25

*Circulation is provided by the environmental chamber fans as described in Chapter 4

CHAPTER 6

CONTROL SYSTEM DEVELOPMENT

Due to the transient and cyclic nature of an adsorption system, a control system is required to regulate the adsorption/desorption switching behavior. To have an entirely thermally driven system, it is necessary that the operation not depend on an electronic control system. By developing a control system that can operate utilizing the system behavior itself to achieve actuation, it is possible for the adsorption system to be entirely thermally driven and to operate autonomously without an external control device. To achieve a drop-in waste heat driven adsorption system at a small scale, it is necessary to eliminate the heat transfer coupling fluid systems currently used for regulation of system operation.

6.1 Autonomous Control

The standard control scheme for an adsorption system is to use timed valves to control the flow of the hot and cold fluid through the adsorption bed heat exchanger loop. The heat exchanger coupling fluid is circulated by electrically driven pumps. This approach is inadequate for a small-scale adsorption system that is driven entirely by heat. The valve system and controls require electrical energy, necessitating another input beyond the heat supplied to the system. The electrical requirements for the valves and pumps are usually small enough that it may be feasible to design a photovoltaic or thermoelectric device to provide electrical power. However, both of these options are relatively expensive and increase system complexity. Including the cost of the valves,

pumps, additional heat exchangers, and connections, the system could become uneconomical. If the electrical power requirements can be eliminated entirely, the adsorption system can be made less expensive and the range of possible applications increases.

To address this need, a number of alternative control methods are proposed here to enable cyclic system operation with only the primary heat input. The control methods under consideration were modeled at a system level to predict their performance using the earlier iterations of the system model described in Chapter 3. Then, the systems were modeled at a component level, and the systems with the highest predicted performance were investigated experimentally at the component level to evaluate their operation.

6.1.1 Concept Overviews

To develop an autonomous control method, consideration was given to the behavior of components throughout the cycle. Means of actuation for this autonomous system must provide the physical action that changes the system operation, but also must do so in a way that responds to the system conditions to achieve cyclic operation. Ideally, the control method would act as both a sensor and actuator. The means of actuation identified for the controls include: physical expansion of the adsorbent during the adsorption process, variations in physical properties that are dependent on temperature, and fluctuation in the weight of the adsorbent bed due to refrigerant transfer. Systems were proposed to take advantage of each of these physical phenomena. These systems are described in Sections 6.2 and 6.3.

Although the proposed designs differ in operation, they can be grouped into two broad control criteria. The first considers the temperature of the adsorbent, and the cycle

switches when the adsorbent bed has reached some maximum or minimum temperature. The adsorbent expansion and physical property based systems both use this control criterion. The second group depends on the mass of the refrigerant adsorbed, and the system has some maximum and minimum adsorption conditions at which switching occurs. The adsorbent temperature and refrigerant uptake are strongly related. Using either of these conditions as the control criterion is expected to lead to similar tends.

6.1.2 Control Criteria Modeling

To investigate whether the proposed control criteria are appropriate for system control and to assess their performance, the criteria under consideration were modeled using an approach similar to what is described in Chapter 3. The baseline model was modified so that the system no longer used fixed cycle times for the heating and the cooling of the bed. Instead, the switching temperature and uptake were chosen from the conditions at the switching times for a fixed cycle time system that had been optimized for cooling capacity. One of the requirements for allowing an adsorption system to be a drop-in for various applications is that it must be able to operate over a range of input heat conditions. To account for this need, the source temperature was varied to evaluate the way the proposed criteria operated outside of their design condition.

Alternate control criteria were evaluated early in the system development process. Therefore, the assessments were done using a different iteration of the model. The differences are discussed here. The system model was developed assuming a single gram of adsorbent with the masses of other components scaled accordingly. The system masses, *UA* values and other properties that differ from the final model described in Chapter 3 are shown in Table 6.1. The bed was modeled without end nodes; therefore,

thermal shorting was not accounted for. The masses were chosen based on the ratios of adsorbent to inert masses found in conventional systems. The UA values were scaled to a single gram of adsorbent from a larger system. The alternative control criteria were modeled for a conventional system with fluid coupling for both heating and cooling to establish if these alternatives were effective. Losses from the evaporator and condenser were considered negligible. Although the model parameters are different, the general conclusions hold true for the adsorption systems considered.

Table 6.1 Modeling Parameters

Parameter	**Variable Name**	**Value**	**Parameter**	**Variable Name**	**Value**
Evaporator/condenser	UA_{evap}	0.095 W K^{-1}	Internal structure-to-adsorbent	$UA_{is,ad}$	0.009 W K^{-1}
Outer structure-to-ambient	$UA_{os,inf}$	0.0006 W K^{-1}	Adsorbent-to-space	$UA_{ad,sp}$	0.003 W K^{-1}
Adsorbent-to-adsorbent	$UA_{ad,ad}$	0.003 W K^{-1}	Fluid-to-internal structure	$UA_{f,is}$	0.09 W K^{-1}
Mass flow rate	$\dot{m}_{cf}$	0.00003 kg s^{-1}	Source temp	T_h	130°C
Mass internal structure	m_{is}	6 g	Mass outer structure	m_{os}	6 g
Mass evaporator structure	m_{evap}	6 g	Mass condenser structure	m_{cond}	6 g

The *COP* and *SCC* results from this modeling are shown in Figures 6.1-6.2. The first case is for a source temperature design condition of 100ºC, while the second case is for a source temperature design condition of 130ºC. It was observed that the alternative control criteria operate with performance comparable to the fixed cycle time performance except when far outside of the system design conditions. Thus, it was concluded that the control criteria used by the alternative system designs are appropriate for system control, and further investigation was justified.

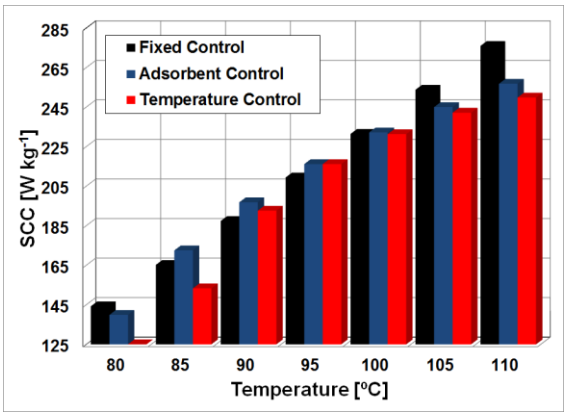

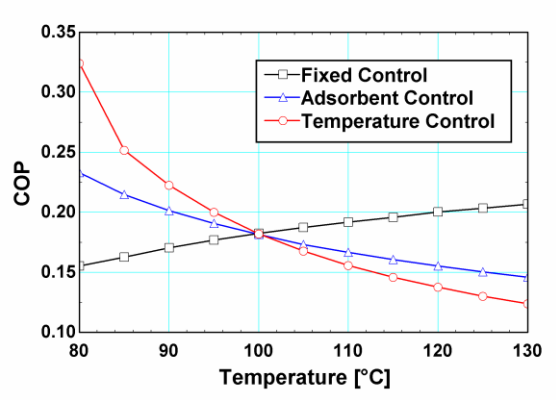

(*a*) (*b*)

Figure 6.1 (*a*) *SCC* of the system and (*b*) *COP* of the system for the different control methods when the source temperature is varied from 100°C

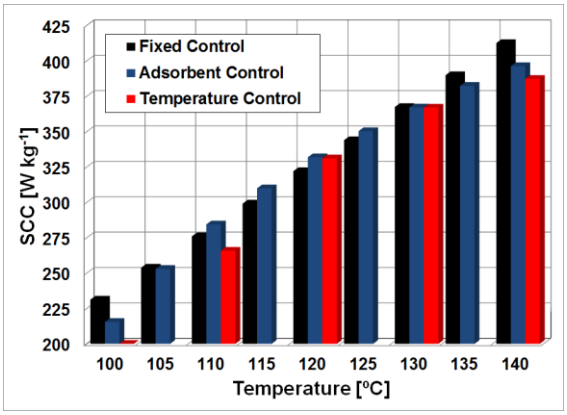

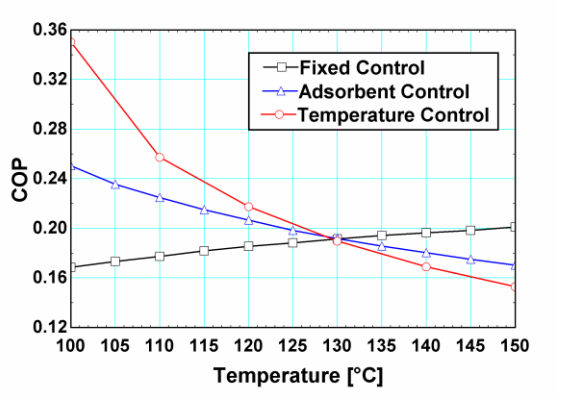

(*a*) (*b*)

Figure 6.2 (*a*) *SCC* as the system and (*b*) *COP* of the system is varied from the design condition of 130°C

6.2 Adsorbent Expansion Actuation

One means of actuation considered was the expansion of the adsorbent during the adsorption process, implemented using a piston-cylinder design described here.

6.2.1 Concept Description

Chemical adsorbents are known to exhibit large expansion during adsorption. Metal chloride chemical adsorbents in particular can demonstrate increases in volume of

2-3 times the original volume. In metal chloride systems, this can lead to problems because expansion of the adsorbent clogs beds or causes consolidation problems (Wang *et al.*, 2005b). Figure 6.3 shows a metal chloride bed before and after adsorption. Drastic volume changes were observed and the volume can double for some the adsorbent and refrigerant pairs. Studies of metal chlorides have shown that the adsorption is nearly independent of the pressure exerted on the adsorbent (Wang *et al.*, 2009b). This implies that the expansion process should exert a large force. To determine if the expansion could be used for actuation, a piston was set up with adsorbent material to convert the expansion to linear motion.

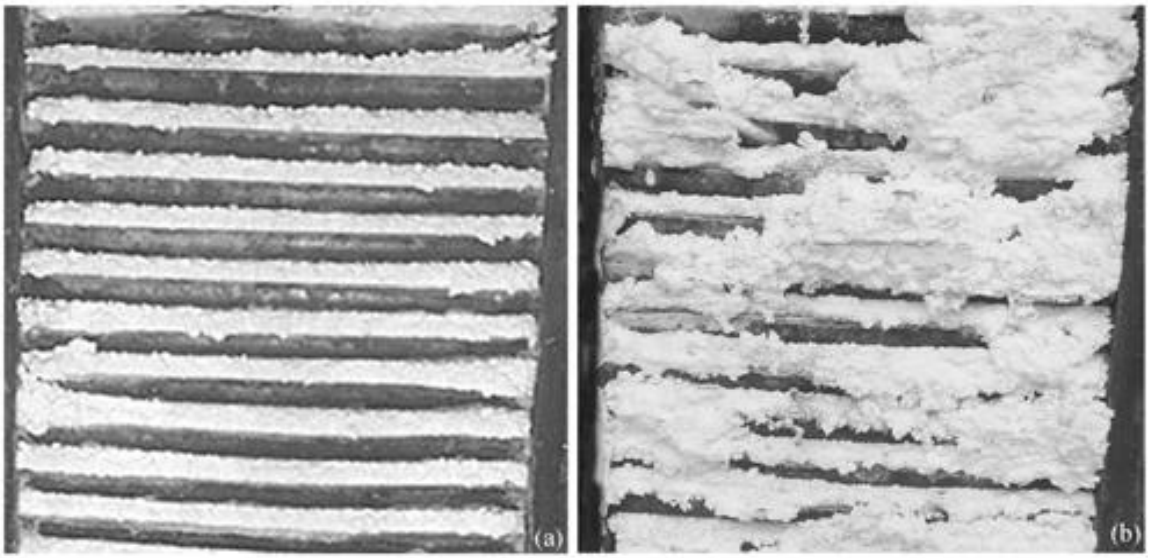

Figure 6.3 Photo of a metal chloride bed before and after adsorption from Wang et al. 2005, Science in China, Series *E* Engineering and Materials Science Vol. 48

The proposed mechanism consists of a piston-cylinder with gas ports to allow refrigerant vapor to enter the cylinder. Within the cylinder is a pellet of adsorbent that is pressed against the piston. As refrigerant vapor is adsorbed into the adsorbent, it expands and displaces the piston. Figure 6.4 shows a diagram of the adsorbent expansion switch and the proof-of-concept test piston.

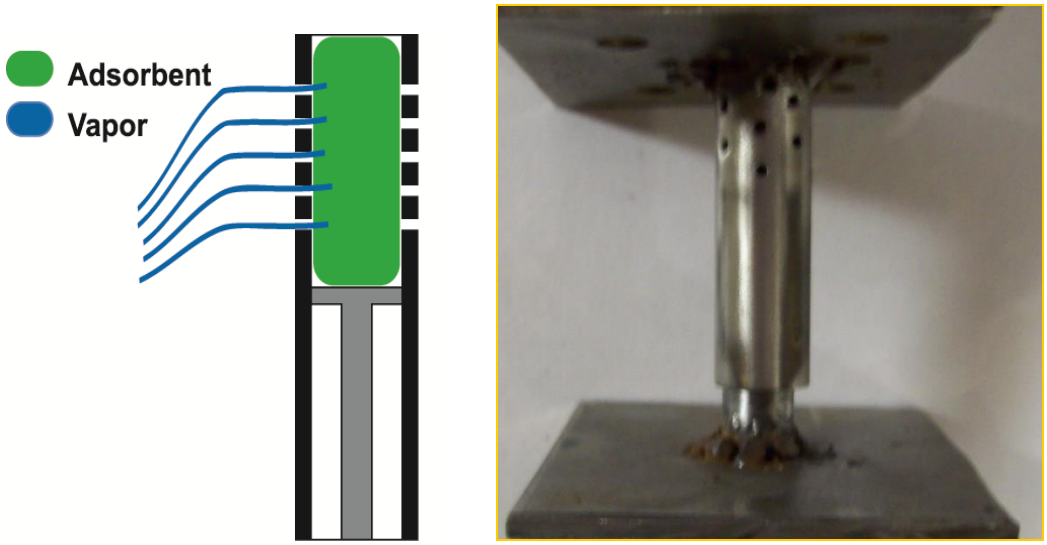

Figure 6.4 Expansion actuation piston (left) and the proof-of-concept testing apparatus (right)

6.2.2 Concept Testing

An adsorbent expansion switch was constructed using stainless steel. Calcium chloride was used as the adsorbent with water vapor as the refrigerant. The piston system was weighted with a 7 kg block exerting a force of approximately 69 N on the piston. The area of the piston was 0.78 cm^2 so that the resulting pressure on the adsorbent due to the piston weight was approximately 900 kPa. The piston was exposed to water vapor to expand the salt, although not to the point of dissolving the adsorbent. Then, the piston was heated to drive the water vapor out of the salt, and the process was repeated several times. The piston was filled with approximately 1 cm of adsorbent material occupying the entire piston cross-section. The piston position was tracked along a measuring stick with 1 mm resolution using the top edge of the piston plate. The maximum movement of the piston observed in testing this concept was a 1 mm expansion above the starting position, followed by a 2 mm contraction so that the final position was 1 mm below the initial position. A large hysteresis was observed throughout all tests of the piston concept. The

adsorbent material expanded through the vapor ports during testing and after two cycles, more than 20% of the adsorbent material had migrated to the outside of the piston. It was determined that a selectively porous material that only allowed the diffusion of the refrigerant gas would be required to allow the piston to operate over a large number of cycles. An adequate material compatible with the system could not be identified, and the expansion actuation concept was eliminated as a possible means of system control.

6.3 Thermal Switch

A thermal switch was considered next to control the flow of heat into and out of the adsorbent material. The thermal switch changes the thermal resistance in the system. By varying the thermal resistance, the temperature of the bed can be controlled along with the operation of the system.

6.3.1 Concept Descriptions

Two thermal switching concepts were considered. The first concept uses the change in density with temperature in a thermal reservoir connected to the adsorbent bed. The second method uses the variation in weight of the adsorbent bed as adsorption occurs, which causes a physical contact to be made or broken in the system. Both concepts have the advantage of storing energy in a hot-side thermal mass and removing heat continuously in a cold-side thermal mass. The designs of the two systems are described, and the modeling of each of these is discussed in the following section. Based on the results of the modeling, one of the concepts will be chosen for further investigation.

6.3.1.1 Float-Style Switch

The float-style thermal switch system takes advantage of the movement of a floating heat transfer material as a result of changes in fluid density with temperature. The system utilizes the transient nature of a heating process to control the heat flow into an adsorption bed. Figure 6.5 shows the layout of the float control system. A fluid reservoir is connected to a narrow fluid gap separating two surfaces through which heat is transferred. For the adsorption system, the two surfaces are the adsorbent bed and either a heat sink or heat source. The fluid channel is filled with ethanol, chosen for its heat transfer and thermal expansion properties. The narrow fluid-filled gap contains a rectangular block of floating material made of 25% aluminum and 75% polymer foam by volume. The two materials are segregated in the floating block to create two regions of differing conductivity. The ratio of the two materials gives an average density for the floating block very similar to that of ethanol, and the ratio of the block materials can be adjusted to match different fluid densities. The floating block is narrower than the fluid gap so that it can move freely. When the fluid reservoir is at a low temperature, the fluid density is higher and the block floats because its density is less than that of the fluid. While floating, the lower section of the block is in position between the heat transfer sections of the channel walls. As the fluid reservoir is heated, the ethanol expands until its density becomes less than that of the floating block. The higher density of the block causes it to sink, and the upper section of the float moves into the heat transfer section. The two sections of the float differ in thermal conductivity by a factor of approximately 1000 ($k_{aluminum} \approx 200$ W m^{-1} K^{-1}, $k_{polymer} \approx 0.2$ W m^{-1} K^{-1}), and the theoretical maximum change in thermal resistance is equal to the ratio of the two thermal conductivities. The

achievable change in resistance is limited by the small fluid-filled gap between the heat transfer section and the floating material as well as the thermal resistance in the two heat transfer sections. The gap is necessary to allow the movement of the floating material but should be minimized to make the thermal switch effective. In this study, the fluid-filled gap length is assumed to be 0.075 mm on either side of the floating section, which is 1.5% of the total distance between the two heat transfer sections. Additionally, thermal energy short circuits through the walls of the switch limit the performance of this system.

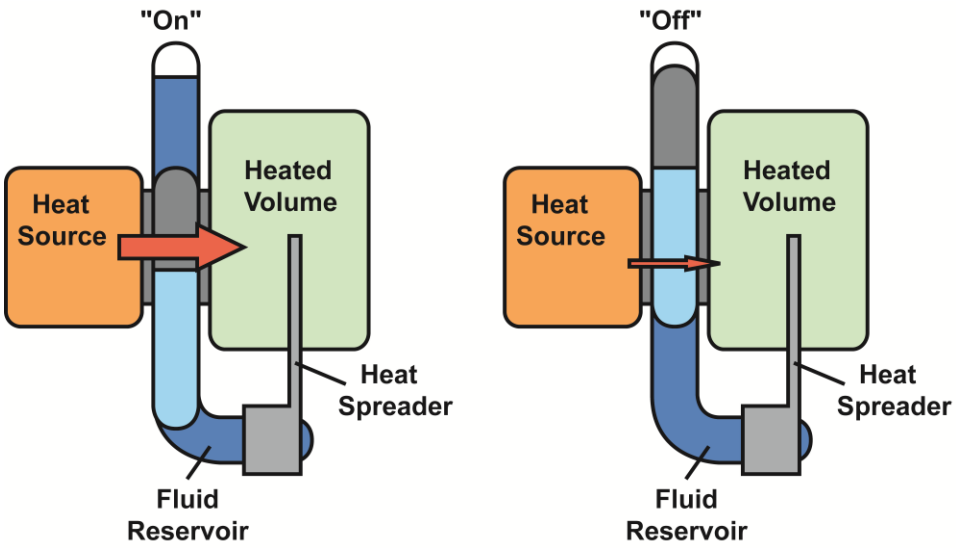

Figure 6.5 The float-style thermal switch arranged for the heat-source side

This type of thermal switch can be arranged in a number of different configurations based upon the location of the fluid reservoir. Other configurations are shown in Appendix C. Figure 6.5 shows a negative feedback loop, in which the thermal switch maintains the heated volume, the adsorbent bed in the proposed system, within a set temperature range. The heat spreader that transfers heat to the fluid reservoir is in thermal contact with the heated volume. The amount of temperature swing the adsorbent bed experiences can be set by adjusting the thermal resistance and thermal mass of the spreader. On the heat-sink side, the thermal switch is arranged in the opposite manner,

with the fluid reservoir in the adsorbent bed and the floating material arranged in the opposite orientation. As a result, the thermal resistance changes out of phase with the hot side thermal switch.

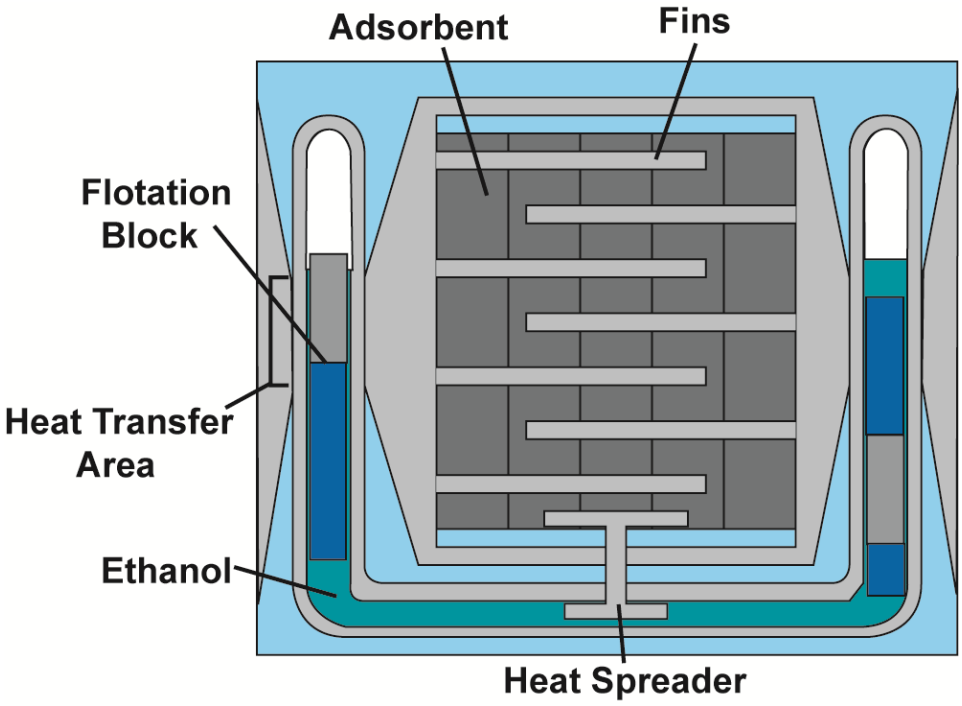

Figure 6.6 The arrangement of the adsorbent bed with the thermal switches applied

The fluid reservoir is connected to the middle of the adsorbent bed through a heat spreader. When the fluid reservoir is at a low temperature, the bed has a relatively low resistance on the hot side and a high resistance on the cold side. Heat is transferred first to the bed and then to the fluid reservoir. Due to the thermal capacity of the heat spreader and the fluid reservoir, the fluid reservoir is heated out of phase with the middle of the adsorbent. When the fluid reservoir reaches the set point, the resistance changes on both sides of the bed. The change in resistance causes the bed to cool. Simultaneously, the hot-side heat transfer surface increases in temperature, storing energy to more rapidly transfer heat to the bed on the next cycle. This arrangement allows the temperature to cycle from high to low in a regular timed pattern. The bed arrangement is shown in Figure 6.6.

6.3.1.2 Thermal Contact Style Switch

The thermal switching method utilizes two parallel plates with opposing triangular fins that come into contact to control the thermal resistance between the plates. One surface is fixed in position, and the other is allowed to move parallel to it. The movement of the second surface completes or breaks contact between the fins. While the contacts are "on", the thermal resistance across the fin assembly is low, and while the contacts are "off", the thermal resistance across the fin assembly is high. Although only one fourth of the total switch area is in contact, the high thermal conductivity of the metal fins compared to the low thermal conductivity of the air gap allows a large change in the thermal resistance between the plates. Figure 6.7 illustrates the arrangement of the fin structures in the “on” and “off” positions. The effectiveness of the thermal switch is dependent upon the contact resistance between the sets of fins, the difference between the thermal conductivity of the materials, and the air in the gap.

In an adsorption system, the weight of the bed increases during adsorption and decreases during desorption processes as refrigerant moves in and out of the bed. The movement of the bed surface is actuated by this change in weight. As the mass of the refrigerant increases, the bed slides down and makes contact on one side of the adsorbent bed. As the mass of the refrigerant decreases, a spring returns the bed to its original position and completes contact on the opposite side of the adsorbent bed while breaking contact with the other set of fins. The arrangement of the thermal switches applied to an adsorbent bed is shown in Figure 6.8.

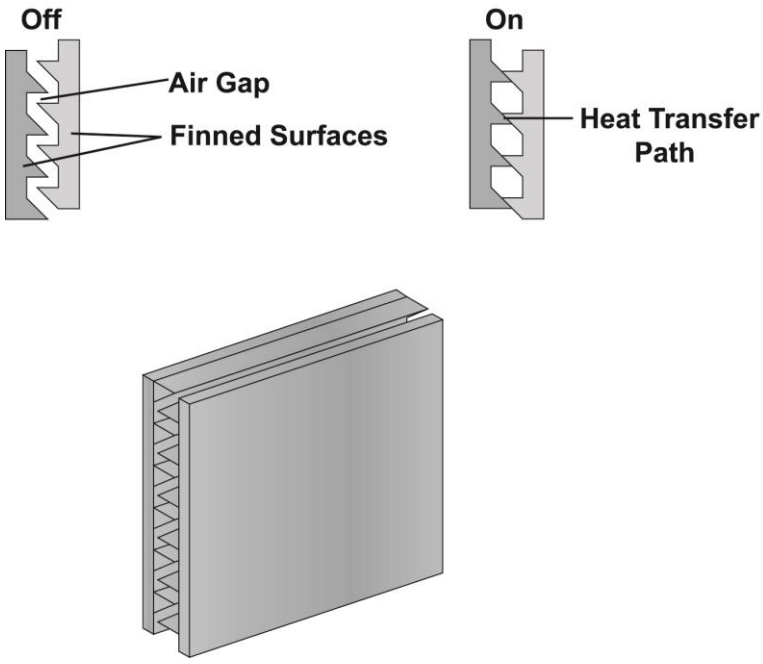

Figure 6.7 Fin structure

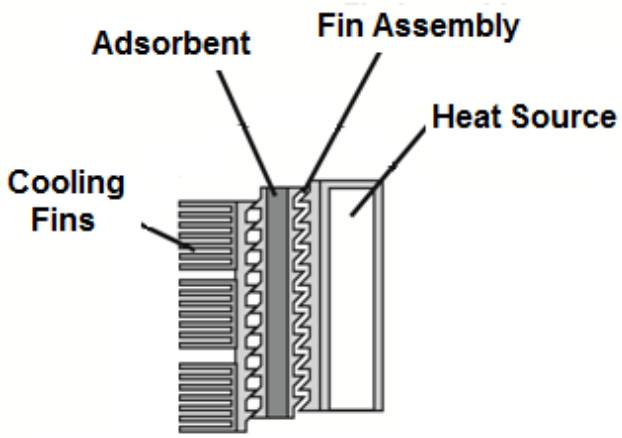

Figure 6.8 The arrangement of the adsorbent bed with the contact switches

6.3.2 Concept Modeling

Modeling of the two concepts was used to compare the methods before testing. The thermal contact style method was chosen for testing based on these modeling results.

6.3.2.1 Float-Style Switch Modeling

A model of the float switch system is used to predict its ability to control the bed temperature. The bed is divided into nodes as shown in Figure 6.9. The contribution of each node to the thermal resistance between each node is calculated by using half of the thickness of the node in the direction of heat transfer and the average cross-sectional area of the node through that thickness. Equation 6.1 is the thermal resistance between two nodes of dimensions (l_1,y_1,z_1) and (l_2,y_2,z_2) in the l direction

$$R_{node1,node2} = \frac{l_1 / 2}{k_{node1} y_1 z_1} + \frac{l_2 / 2}{k_{node2} y_2 z_2} \tag{6.1}$$

Heat transfer to the surroundings were estimated assuming a 2.54 cm (1 in.) layer of polymer insulation for all nodes, between the nodes and the surroundings. Improved heat transfer due to heat spreader fins is modeled as the adsorbent conductivity being doubled to (0.4 W m^{-1} K^{-1}) based on improvements in heat transfer rates when using fins seen in literature (Zhang and Wang, 1999; Rezk and Al-Dadah, 2012).

To create a heat transfer area that only transfers heat through the intended part of the float switch, tapered heat transfer plates are used shown at Points A, D, H, and I in Figure 6.9. These plates have a maximum cross-section of 10 cm by 10 cm and a minimum area of 8 cm by 3 cm, highlighted at Point A in Figure 6.9. The gap between these heat transfer areas is 0.5 cm, and the floating block is 0.485 cm wide (Point B and

C). The heat capacities of the system components are provided in Table 6.1. In the area outside the tapered heat transfer plates, the space is filled with an insulation material to prevent heat transfer to the float switch outside of the heat transfer area Point J in Figure 6.9. The system is arranged so that the heat source is on one side of the adsorbent bed and the heat sink is on the other, which means that heat always enters on one side of the system and leaves on the opposite side. There are two float switches in this system, one on the hot side of the adsorbent bed, and one on the cold side. Heat transfer plates are positioned on both sides of the adsorbent bed and allow for connection to the heat source and sink.

The floatation block (B and C) lies in fluid in the gap between the heat transfer plates. The gap has a 10 cm wide by 16 cm high cross-section and is connected to the fluid reservoir. There is a vapor volume at the top of the gap to allow the fluid to expand. The floating material, composed of aluminum (B) and polymer foam (C), is 0.485 cm thick. The aluminum portion has a 3 cm by 8 cm cross-section while the polymer portion has a 9.5 cm by 7.5 cm cross-section. The volumes of the aluminum and polymer are 0.0012 m^3 and 0.0036 m^3, respectively. The float is identical on both sides, but the aluminum portion is oriented upward on the hot side and downward on the cold side. On the hot side, cold fluid in the reservoir has a high density and forces the aluminum portion of the block to rise into the heat transfer area. On the cold side, low temperatures cause the insulated portion of the block to rise into the heat transfer area. When the float switch is “on”, the thermal resistance from the heat transfer area to the aluminum portion is 0.27 W K^{-1}. When the float switch is “off”, heat is transferred primarily into the insulated region, and the thermal resistance reaches 10.3 W K^{-1}.

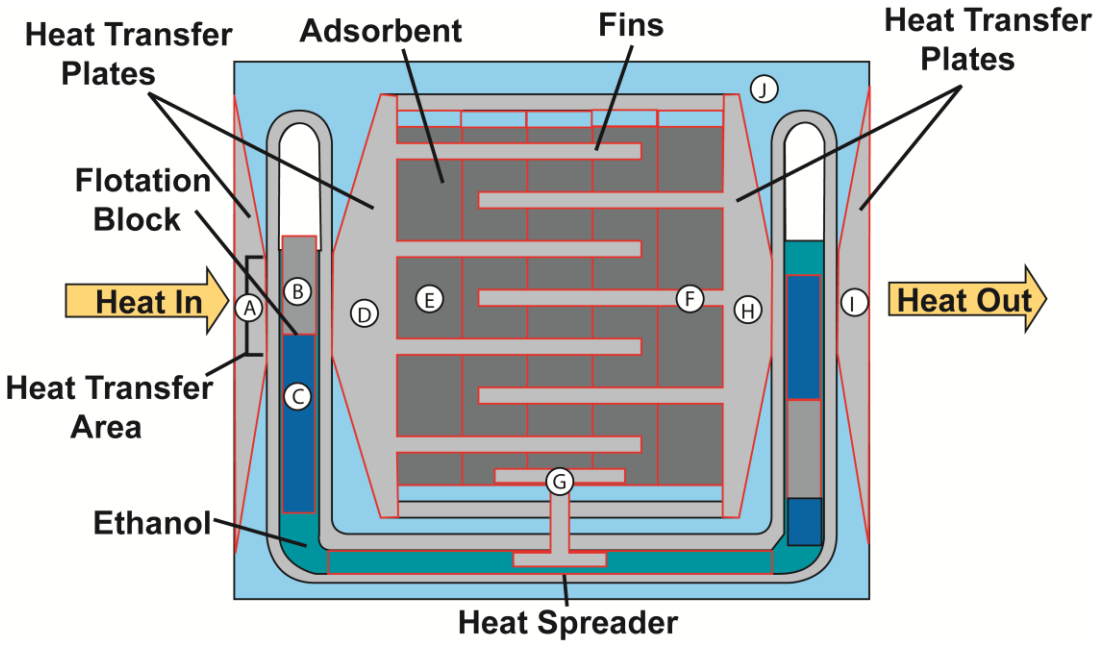

Figure 6.9 Adsorbent bed using float switches with nodes outlined in red

The fluid used in this system is ethanol. At the desired switching temperature of 60ºC, ethanol has a density of 0.7544 g cm^{-3} and an expansion rate of 0.001 g cm^{-3} K^{-1}. The average floating material density must be equal to the density of ethanol to function as designed. The aluminum considered here has a density of 2.696 g cm^{-3}, and the expanded foam has a density of 0.1 g cm^{-3}. To achieve an average density of 0.7544 g cm^{-3}, the volume of the block composed of aluminum must be 25.21% of the total floating material volume. For the dimensions of the block considered here, the average density is 0.7541 g cm^{-3}, and the switching temperature will be slightly above 60ºC. The ratio of the materials must be controlled very precisely or the switching temperature will vary significantly. A 1% change in the float density results in an 8 K change in the switching temperature.

The adsorbent material and heat transfer plates are in contact via a 10 cm by 10 cm area through which heat is transferred. The rate of heat transfer is improved using fins that extend from the plates into the adsorbent material (Point F).

The bed is divided into 5 sections across its width, as shown in Figure 6.9. In Figure 6.9 Point E marks the first adsorbent node. Each adsorbent section is 0.5 cm thick and has a 10 cm by 10 cm cross-section. The adsorbent bed is composed of activated carbon with a density of 600 kg m^{-3} at a packing density of 0.60. The bed has a resulting total density of 360 kg m^{-3}, and the total mass of adsorbent is 18 g. To account for the adsorption and desorption energy that would be exchanged in a full system, the adsorbent material was given a large specific heat, 8.6 kJ kg^{-1} K^{-1}. The total resulting heat capacity for each of the adsorbent nodes is 155.1 J K^{-1}. The adsorbent material is insulated along the walls to minimize the loss of heat from the adsorbent to the outer surface of the adsorbent bed, referred to as the shell. The shell is a thin metal enclosure that primarily serves to contain high-pressure refrigerant vapor. The center adsorbent node transfers heat to the heat spreader that is used to heat the fluid reservoir (Point G).

The heat spreader connects the center of the adsorbent bed and extends down into the fluid reservoir. The spreader provides effective heating of the fluid to enable the switching of the system. The fluid volume is nominally 89 cm^3. The reservoir volume is smaller than the fluid volume, because fluid in the gap must also be heated during the switching process.

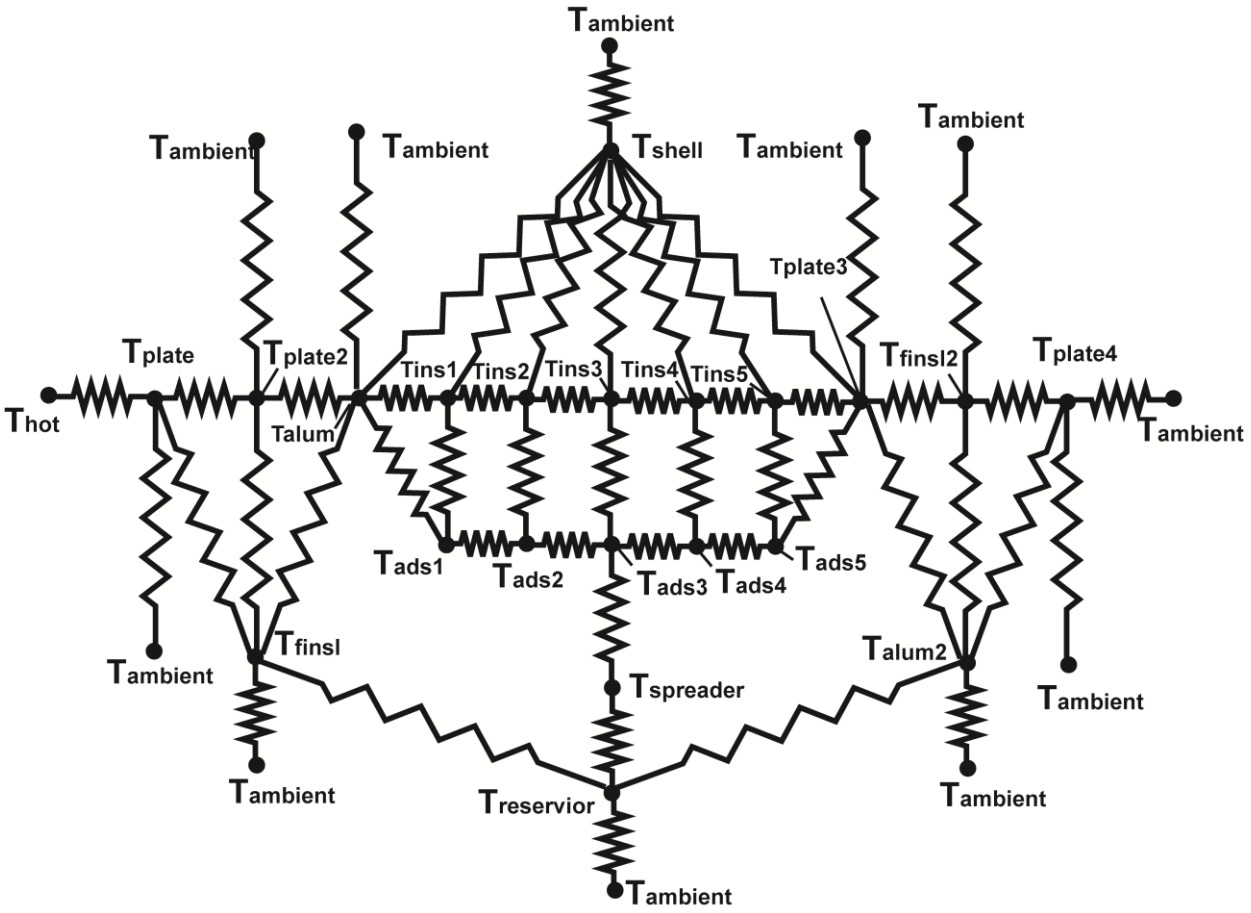

Figure 6.10 The resistance network used to model the float switch system

Table 6.2 The heat capacities of nodes used in thermal switching models

Node Name	Volume (cm^3)	Heat Capacity ($J\ K^{-1}$)	Mass (g)	Description
T_{hot}	-	-	-	Heat source temperature, set to 100°C
T_{amb}	-	-	-	The temperature of the surroundings, set to 25°C
T_{plate}	62	76.2	167	The plate between the source and the float switch
T_{plate2}	62	76.2	167	The plate between the hot-side float switch and the absorbent bed
T_{plate3}	62	76.2	167	The conducting plate between the adsorbent bed and the cold-side float switch
T_{plate4}	62	76.2	167	The conducting plate between the cold-side float switch and the ambient, acts as the heat dissipator
T_{alum}	12	29.5	32.4	The aluminum portion of the float in the first switch
T_{alum2}	12	29.5	32.4	The aluminum portion of the float in the second float switch
T_{finsl}	36	8.64	3.6	The foam portion of the float in the first switch
T_{finsl2}	36	8.64	3.6	The foam portion of the float in the second switch
T_{ad1}-T_{ad5}	50	155	18	The adsorbent material nodes
T_{ins1}-T_{ins5}	21	5.0	2.1	Insulation between the adsorbent and shell
T_{shell}	15	37.0	41.2	The shell of the adsorbent bed
$T_{spreader}$	21	50.0	55.7	The heat spreader connecting the adsorbent to the reservoir
$T_{reservoir}$	89	164	67.2	The fluid reservoir

Each external node is separated from the ambient by insulated material, and heat losses through the insulation are accounted for in the modeling. Shown in Figure 6.10, a resistance network is developed between these nodes to determine system behavior. The node names and heat capacities are given in Table 6.2, and the thermal resistance values are given in Table 6.3. The heat source in this model is set to a temperature of 100ºC, and the heat sink is set to 20ºC.

Table 6.3 Resistance values in the thermal switching models

Resistor Name	**Node 1**	**Node 2**	***R* Value (K W^{-1})**	**Description**
R_{hp}	T_{hot}	T_{plate}	1	From hot liquid to the connection plate, assumed convection coefficient 100 W m^{-2} K^{-1}
R_{pc}	T_{plate4}	T_{cold}	1	From the fourth plate to the heat sink
R_{pins}	$T_{plate\#}$	$T_{fins\#}$	0.27 / 50	Resistance to the insulation of the float
R_{pal}	$T_{plate\#}$	$T_{alum\#}$	60.5 / 10.3	Resistance to the aluminum of the float
R_{pamb}	$T_{plate\#}$	T_{amb}	100	Resistance to the environment for the plates
$R_{finsamb}$	$T_{fins\#}$	T_{amb}	100	Resistance for losses to the environment for the float
R_{alamb}	$T_{alum\#}$	T_{amb}	100	Resistance for losses to the environment for the float
R_{alins}	$T_{alum\#}$	$T_{fins\#}$	100	Resistance within the float
$R_{inslres}$	T_{ins1}	$T_{reservoir}$	20	Resistance from the insulation to the reservoir
R_{pad}	$T_{ad\#}$	$T_{plate\#}$	0.225	Resistance between the chamber wall plates and the adsorbent
R_{pins}	$T_{plate\#}$	$T_{ins\#}$	2.5	Resistance between the chamber wall plates and the adsorbent bed insulation
R_{pshell}	$T_{plate\#}$	T_{shell}	0.5	Resistance between the chamber wall plates and the shell of the adsorbent bed
R_{insad}	$T_{ad\#}$	$T_{ins\#}$	10	Resistance between the adsorbent material and the adsorbent bed insulation
R_{adsads}	$T_{ad\#}$	$T_{ad\#}$	0.45	Resistance between the adsorbent material nodes
R_{insins}	$T_{ins\#}$	$T_{ins\#}$	5	Resistance between the insulation nodes in the adsorbent bed
$R_{shellins}$	$T_{ins\#}$	T_{shell}	2.5	Resistance between the bed insulation and the bed shell
$R_{shellamb}$	T_{shell}	T_{amb}	34	Resistance between the bed and the surrounding insulation
R_{adsp}	T_{ad3}	$T_{spreader}$	9	Resistance between the adsorbent and the spreader
R_{spres}	$T_{spreader}$	$T_{reservoir}$	21	Resistance between the spreader and the fluid reservoir

After modeling the adsorbent bed, it was determined that a temperature swing of 40 K can be expected for the adsorbent bed. This temperature swing is approximately 50% of the temperature difference between the source and sink. This is a large enough swing to perform adsorption and desorption for the investigated temperature difference between the sink (20°C) and the source (100°C). It is expected that the time taken for the bed to heat and cool can be reduced by increasing the mass of the first (Point A) and fourth plate (Point I) allowing them to store more thermal energy. The temperature output for the model is shown in Figure 6.11. The temperature in the outer plates approaches the source and sink temperatures when the switches connecting them to the adsorbent bed have high resistances. When the switch changes to the low resistance condition, the

temperatures of these plates drop quickly as heat is transferred to the bed from the outer plates. The temperature gradient through the adsorbent material is relatively small throughout the process, with a maximum temperature difference of less than 5 K through the bed thickness.

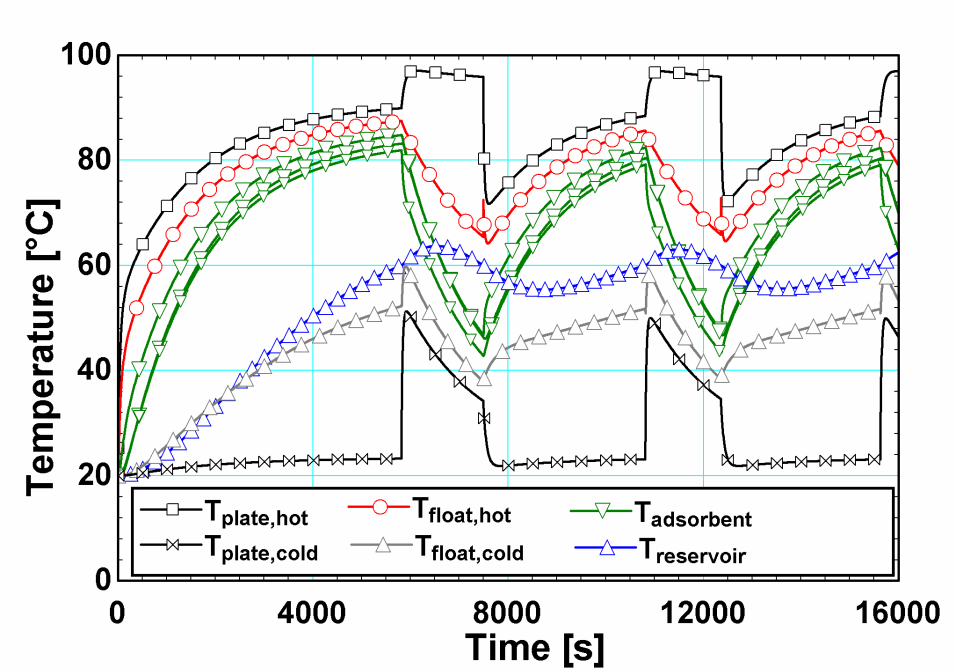

Figure 6.11 Temperature profile in the float valve controlled bed

6.3.2.2 Contact Design Modeling

The expected thermal resistance was modeled for an ideal system in which no thermal contact resistances are present. In an ideal system, the thermal resistance in the "off" state is approximately 40 times larger than the resistance in the "on" state. The contact resistance is neglected in the calculation of the thermal resistances, and actual changes in thermal resistance are expected to be lower due to contact resistance between the plates. When the fins are in the "off" position, there is a 1.6 mm gap between the tips of the fins and the next surface. The bases of the fins are separated by 4.76 mm.

A 2D model is used to calculate the expected thermal resistance per unit area in both the "on" and "off" positions. The model is based on an ideal heat switch in which there is no contact resistance. The thermal conductivity of the air, k_{air}, is assumed to be 0.03 W m^{-1} K^{-1}, and the conductivity of the stainless steel in the heat switch is set to 15.5 W m^{-1} K^{-1}. This gives a unit area thermal resistance of 0.067 m^2 K W^{-1} for the "off" position and a value of 0.0017 m^2 K W^{-1} for the "on" position. The model predicts a ratio of the “off” thermal resistance to the “on” thermal resistance of 39. The position of the fins relative to one another in the "off" position is important. If the fins are 0.4 mm (1/64 in.) closer together in the direction of movement, the "off" thermal resistance is reduced by 6%, and the ratio falls to approximately 36. The spacing between the bases of the fins is also important. Increasing the spacing between the fin surfaces by 0.4 mm decreases the ideal ratio to 36. Decreasing the spacing by 0.4 mm increases the "on"/"off" thermal resistance ratio slightly to 40. The distance between the plates is less important than the spacing of the fins in the direction of movement for the performance of the switch.

The modeled thermal switch was then applied to an adsorption system with similar characteristics similar to those of the system for which the float switch was modeled. A factor of 10 change in resistance was assumed for this model to account for the non-ideal operation of the switch. The nodes of the floatation block were removed from the model and they were replaced by the contact switches. Besides the flotation block nodes, the rest of the resistances and nodes were kept the same as shown in Table 6.2 and 6.3. The resulting temperatures are shown in Figure 6.12. The transition temperatures for these results were 75ºC and 45ºC.

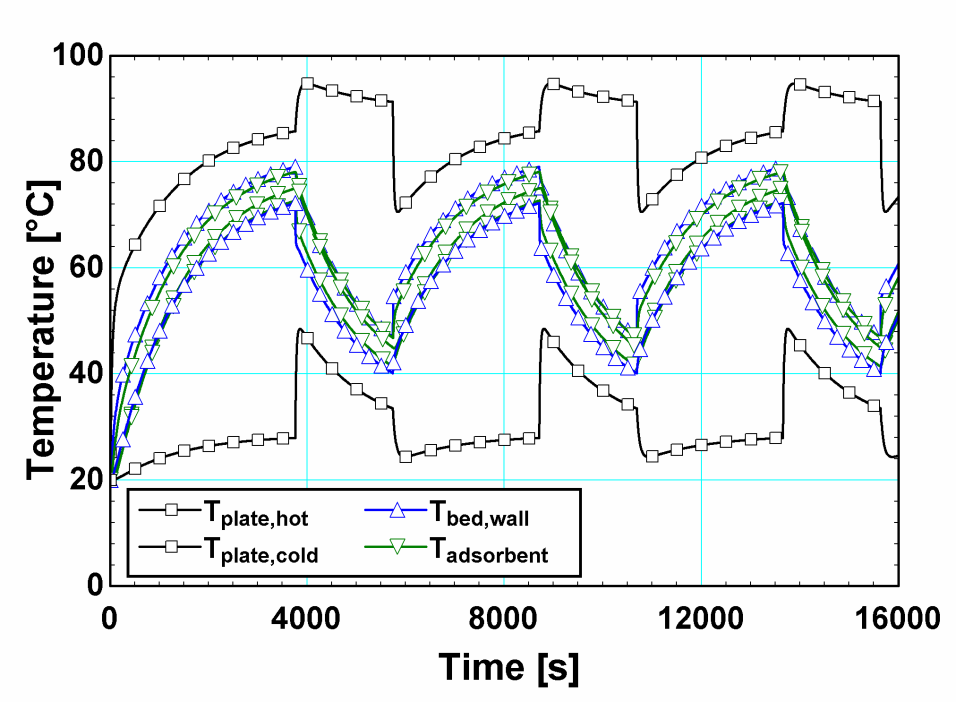

Figure 6.12 Temperature profile in the contact switch controlled bed

6.3.3 Thermal Switching Testing

Based on the concept modeling results, the contact-style switch was less complex and yielded similar temperature swings with faster response times than the float-style switch. Therefore, the contact-style thermal switch was chosen for experimental investigation.

To test the performance of the proposed switching system, two thermal switching devices were constructed. One device was machined using electric discharge machining (EDM) from 304 stainless steel, and the other was milled. The two fabrication techniques yielded different surface roughnesses. The milled surface has distinct mill marks while the EDM surface is smooth and homogeneous. The thermal resistance between plates was recorded when the fins were in contact and when the fins were not in contact with fixed

heat transfer rates through the surfaces. The EDM surface was also tested dry and wetted with 10W-30 SAE oil to reduce contact resistances. The surfaces were 5.08 cm by 7.64 cm with 6.35 mm edge areas without fins to allow movement of the surfaces in tracks. The total projected heat transfer area was 29.1 cm^2.

A diagram of the test set-up is shown in Figure 6.13. The two heat transfer surfaces were positioned in a track opposite one another. An electric McMaster-Carr ultra-thin 100 W sheet heater (model number 35475K723) was attached to the plane side of one surface with thermal grease to enhance thermal contact. The back side of the heater was insulated with a 76 mm thick section of fiberglass insulation. In addition, the edges of the system were insulated with 50 mm of fiberglass insulation. The track material was PVC and was approximately 9.5 mm wide and 15.9 mm thick. The track had grooves for the edges of the fin surfaces. The surfaces were moved manually, and a blockage in the track is used to stop the movement in the correct position. The test section was heated at a fixed heat input rate until it reached a steady state condition in both positions.

The dimensions of the test surface are shown in Figure 6.14. The finned surfaces were 3.18 mm high with an angle of $\theta = 45^o$, and the fin pitch was 6.35 mm. The fin surfaces were spaced 4.76 mm apart, which results in a 1.59 mm overlap between the tops of the fins (approximately half the fin height). In the "on" position, one fourth of the total vertical area was transferring heat through direct contact. When the fins were in the "off" position, the minimum distance between the fin surfaces was 1.59 mm, and the average air gap was approximately 2.4 mm. The 2.4 mm value was used to approximate the expected air gap resistance. The temperature was measured in the middle of the

finned surfaces using thermocouples. Taps in the heat switch surfaces allow the thermocouples to be positioned in the middle of the plate.

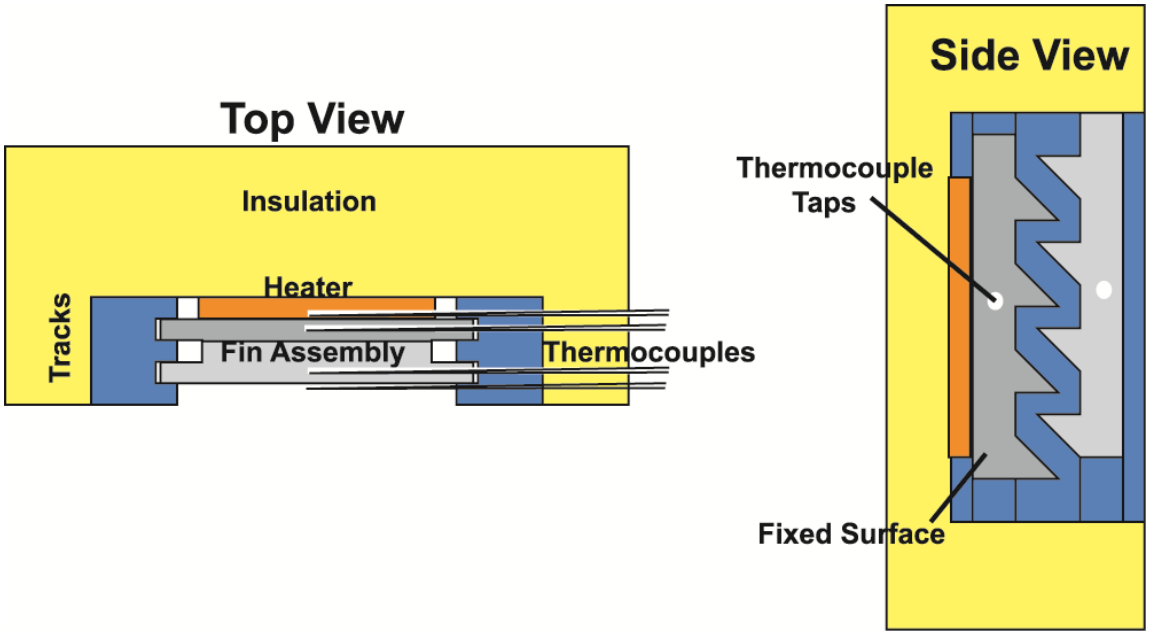

Figure 6.13 The test section in which two finned surfaces are held in tracks with an electric heater applied to the back of the inner finned surface

The steady state temperatures for the surfaces ranged between 50 and 100ºC. The power input for the surface was varied from 1-5 watts, and the thermal resistance was determined. In the tests conducted, the thermal resistance was shown not to depend strongly upon the heat flux through the test section. The results are shown in Figure 6.15.

The dry milled surface demonstrated the poorest performance with a thermal resistance ratio of only 2-2.7. The "off" resistances were slightly lower than the dry EDM surface, and the "on" resistances were slightly higher than the dry EDM surface. This was likely due to the roughness of the milled surface preventing complete contact between the surfaces. The resulting high contact resistances limited the effectiveness of the rough surfaces as a thermal switch.

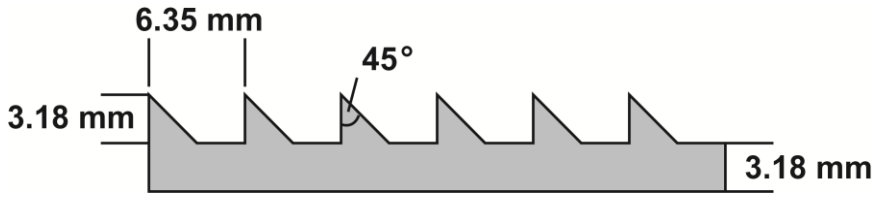

Figure 6.14 The dimensions of the finned surface used for testing the contact switch

The dry EDM surfaces yield "off" resistances at 75-90% of the predicted values and “on” resistances higher than predicted. The thermal resistance ratio between "off" and "on" for the dry surfaces was 2.9-4.5. This was approximately one tenth of the ideal ratio for the design in consideration. The poor performance was likely caused by high contact resistances between the surfaces and imprecise positioning of the surfaces in the "off" position.

When the EDM surfaces were wetted with oil, both the "off" and "on" thermal resistances decreased. For the "on" position, this was due to a decrease in contact resistance and enhanced heat transfer. For the "off" position, this was most likely due to the oil on the surface of the fins reducing the size of the air gap between the two plates. The lowest observed resistances for the "off" position were near those for the "on" position for the milled and dry EDM surfaces. The change in thermal resistance for the switch was a ratio of 6.2-13.3. The change in resistance was better than for the other surfaces, but was still lower than predicted due to the low "off" position resistance. The variability in the results is due to the track not holding the plate in the same position for all of the "off" positions. As a result, there were variations in the size of the air gaps.

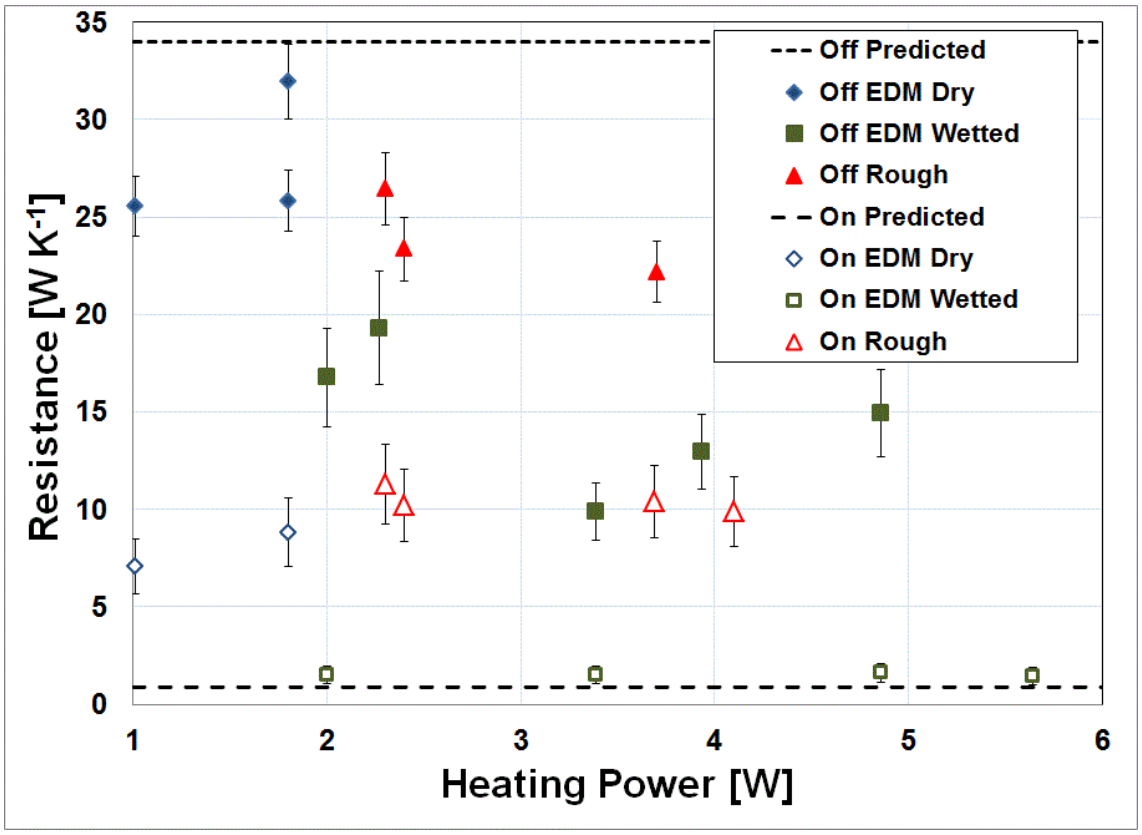

Figure 6.15 The thermal resistance vs. the heating power delivered to the system

Table 6.4 shows the minimum, average, and maximum thermal resistance ratios observed for each of the different surface conditions investigated. With appropriate thermal interface materials and accurate fin positioning, the thermal contact switching approach was determined to be feasible for the control of adsorption systems.

Table 6.4 Ratio of thermal resistances for on/off position for various surface configurations

	Minimum Ratio	**Average Ratio**	**Maximum Ratio**
Dry EDM	2.9	3.5	4.5
Wet EDM	6.2	9.8	13.3
Rough	2.0	2.3	2.7

CHAPTER 7

SYSTEM INTEGRATION AND TESTING

The components of the system and controls presented in previous chapters were installed into the experimental facility for testing. The results from those tests are presented here and comparisons are made with the predictions of the design models and also with values from the literature. Modifications are made to the models where appropriate to account for differences using one set of experimental results. The models were then validated with another set of experimental results to confirm that the refinements were appropriate.

7.1 Final Bed Testing

Results from the control system proof of concept tests, described in Chapter 6, were integrated with the modeling efforts, described in Chapter 3, to develop adsorbent bed designs for testing. Initial test beds were improved through iterations addressing issues, as described in Chapter 5. Construction of the beds helped establish the masses and the heat transfer coefficients that could be achieved for the bed. It was found in the experimental adsorbent beds that the structural masses are higher than those expected at the smaller scales, because the connections into the bed and the limits on material thicknesses mean that the ratio of structural material to adsorbent material is larger at these scales. This is even beyond the inability to thermally isolate the adsorbent from the bed wall. Conduction heat transfer through the structure of the bed was also found to be very important at this scale and losses were larger than expected. The two final bed

designs explore active control of the heating of the bed versus utilizing the thermal switching technique tested in Chapter 6. These two beds are tested using the experimental facility described in Chapter 4 and the results are presented here. Based on the modeling results for system performance in Chapter 3, several system operation variables are considered for each bed to assess the system performance.

In these tests, the thermal switching mechanism was applied with manual control based on the measured temperatures rather than fully autonomous control. The proof of concept testing had previously demonstrated that autonomous control is feasible, but manual control allowed a broader range of conditions to be tested without system modification and allowed testing to focus on system performance rather than fine tuning of the control mechanism.

Cooling in adsorption systems tends to occur primarily in a peak time period and then taper off to almost nothing during the desorption phase. Due to the long tail on the delivered cooling, some portion of the cooling is in a range too low to measure adequately. The models accounted for the cooling tail and in addition to predicting the total delivered cooling, the delivered cooling in the measureable range was modeled. In most cases, more than 80% of the delivered cooling is expected to be measureable. Appendix B, explains the immeasurable cooling and the experimental techniques employed to minimize its impact. Modeling comparisons are presented after the experimental results for each bed and both the predicted cooling and predicted measureable cooling are presented.

For the system testing procedures, there are transient effects and artifacts of the testing facility that must be accounted for. Some issues were addressed in Chapter 4

through the testing procedure, but further consideration is given here to the experimental demonstrations of these effects. Specifically, lower performance on start-up cycles, the accumulation of refrigerant through multiple cycles, and the amount of precooling time allowed before valve opening are discussed here and shown with experimental results.

7.1.1 Start-up Performance

At the start of the test, the first cycle runs with different performance than later cycles, depending upon the initial conditions of the system. The impact of start-up cycles was accounted for by recording performance of the second cycle once the system was able to reach normal operating conditions. To illustrate the start-up effects, the COP and SCC for the first and second cycle runs with a 75 W heat input, 500 s heating time, and 500 s cooling time with air circulation as described in Chapter 4 are compared. In the first cycle, the system delivers 163 J of cooling for a COP of 0.0043 and a SCC of 4.1 W kg^{-1}. The second cycle only delivers 133 J of cooling for a COP of 0.00355 and a SCC of 3.3 W kg^{-1}. In this case, the first cycle delivers more cooling, because the previous test had left the adsorbent with a lower refrigerant loading than is observed at the end of the adsorption phase for these conditions.

7.1.2 Refrigerant Accumulation

Because the volumes of available float valves and other refrigerant level control mechanisms were too great to be used at this scale, refrigerant slowly accumulates in the condenser during successive cycles. Appendix B shows that the accumulation has a relatively minor impact (<2%) on system performance until a single-phase state is reached in either the evaporator (dry-out) or condenser (flooding). The refrigerant levels

were allowed to rebalance between successive tests to prevent this from impacting the evaluation of the system performance. However, the system was also run through enough cycles to demonstrate this effect for one test case. The CHEC system was run for a 50 W heat input with a 1000 s heating time and a 1000 s cooling time, until dry-out of the evaporator occurred. For the case where system dry-out occurs, no cooling is measured for the cycle. Figure 7.1 shows the pressure and temperature profiles in the evaporator for a normal operation and during dry-out conditions when the valve is opened between the evaporator and the adsorbent bed. It can be seen from the swing in pressure that in both cases, the evaporator pressure quickly falls to the pressure of the adsorbent bed. In normal operation, the pressure drop is accompanied by a drop in temperature as the saturation temperature also drops. During dry-out, the pressure and temperature drop initially, but the drop is much smaller and likely due to remaining liquid evaporating away.

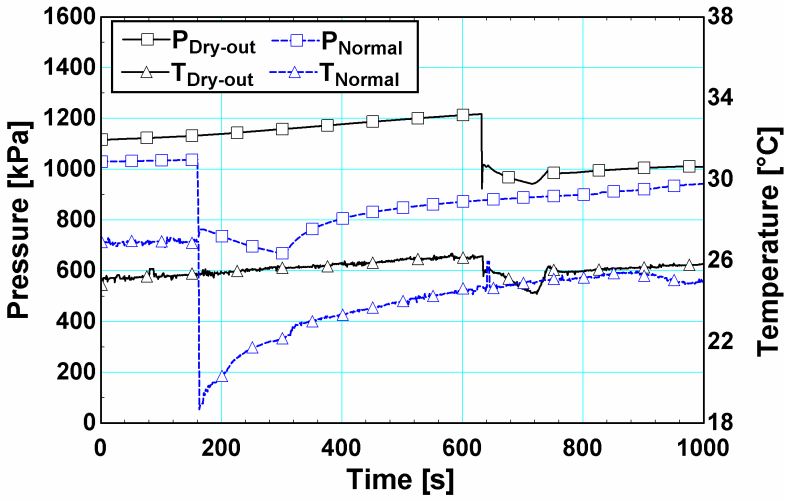

Figure 7.1 Pressure and temperature in the evaporator when the valve is opened, during normal operation and dry-out conditions

7.1.3 Pre-cooling Time

Because the check valves were removed from the system, the pre-cooling phase was manually controlled. The lower flow rates and lower structural masses for these tests mean that cooling can be measured at lower rates than in the CHEC design. The pre-cooling is controlled to try to push more of the cooling into the measureable range, as is done with the CHEC system. Two runs were conducted at the same conditions with different pre-cooling times to compare the amount of cooling that is lost due to being too low to measure and validate the improvement in performance measurements due to pre-cooling. Appendix C shows that within appropriate bounds, the length of the pre-cooling time does not largely influence the total cooling provided by the system, because much of the cooling phase is spent cooling the adsorbent and structure to the point where the pressure in the surrounding space is low enough to draw refrigerant from the evaporator.

Both tests were run with a 10 W heat input with the surrounding air still and at 24ºC. The upper switching condition is set at 80ºC with a lower switching condition of 45ºC. In the first case, the system is allowed 645 s (~11 min) of pre-cooling time. In the second, the system is allowed just 250 s (~4 min) of pre-cooling time. Both are allowed approximately 1350 s (~22.5 min) of cooling time total. A measured total of 517 J of energy are removed from the coupling fluid stream in the first case, but only 259 J of cooling is measured in the second case. The performance of these two runs should be nearly identical, but because a large portion of the cooling is at a rate too low to measure, it is lost. This changes the measured average cooling and the COP of the system by nearly a factor of two. It is clear that the measured system performance represents the lower bound of the actual system performance.

The limitations of the cooling rate measurements were recognized, and efforts were taken to decrease their impact on the cooling. For this reason, the pre-cooling time was held longer than modeling predicted to be necessary to achieve measurable cooling rates. The immeasurable cooling for each operation is estimated through comparison with model predictions, shown in Section 7.5. This comparison provides a more accurate estimate of the actual system performance.

7.2 CHEC Bed Results

The CHEC bed was tested over the range of conditions shown in Table 7.1. Investigated for this bed were different input heat rates, the impact of surrounding conditions including surrounding temperature and air circulation, and the ratio of cooling-time to heating-time were investigated for this bed. A standard set of test conditions was assumed for comparison of different variables. The standard heat input was 75 W, with a 500 s heating length time, and a nominal ratio of cooling time to heating time of 1. When possible, parameters were varied around the standard configuration to assess their impact and the results for the system performance are shown here. The uncertainty analysis may be found in Appendix A.

7.2.1 Cooling time to Heating time

The ratio of cooling-time to the heating-time was varied during the tests. This ratio is important for the beds considered here, because heat is being introduced through conductive heat transfer and removed through natural convection. Therefore, it is expected that the heating rates will be different for heating than the heat transfer rate for cooling of the bed. The best cooling and COP are usually achieved when the swing in

temperature is as large and as fast as possible. The largest temperature swing with the shortest possible cycle time achieves the best performance. The average temperature of the bed will shift until the heat transfer in the two phases is equal. To ensure good performance it is expected that the adsorbent cooling time should be longer than the heating time. Therefore, the nominal ratios of cooling-to-heating time of 1, 2, 3, and 4.5 were tested for 75 W heat input with the heating time held at 750 s. Other heating rates investigated included 50 W and 100 W, but only for ratios of 1 and 2. The 50 W case used 1000 s of heating time because the lower heat input was expected to take longer to reach desorption temperature. Figures 7.2 and 7.3 show the COP and SCC, respectively, for the CHEC system as the ratio varies for the 50 W, 75 W and 100 W heating cases.

Table 7.1 CHEC Bed Test Matrix

Input heat [W]	**Heating time [s]**	**Nominal t_c:t_h ratio**	**Surr. Cond.**	**Nominal Surr. Temp [ºC]**
50	500	1	Still	24
		2	Still	24
	1000	1	Still	24
		1	Circulation	29
		1.5	Still	24
		2	Still	24
75	300	5	Still	24
	500	1	Circ.	29
		2	Circ.	29
		2	Still	24
		3	Circ.	29
		4	Still	24
	750	1	Circ.	29
	1000	1	Circ.	29
100	500	2	Circ.	29
	750	1	Circ.	29
		2	Circ.	29
		2	Circ	19
	1000	1	Circ	19

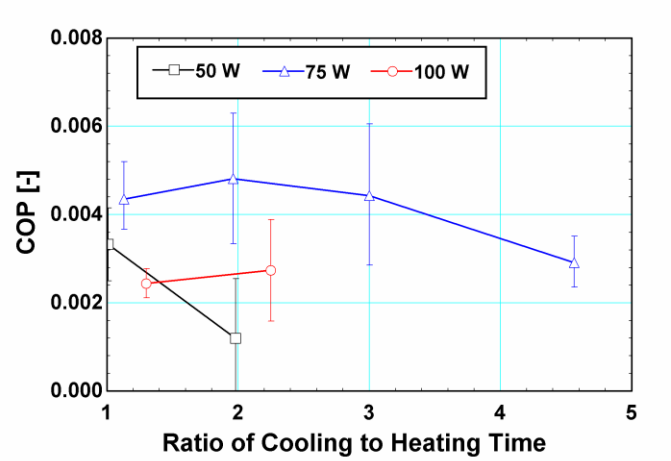

Figure 7.2 Effect on COP of varying the ratio of cooling to heating time

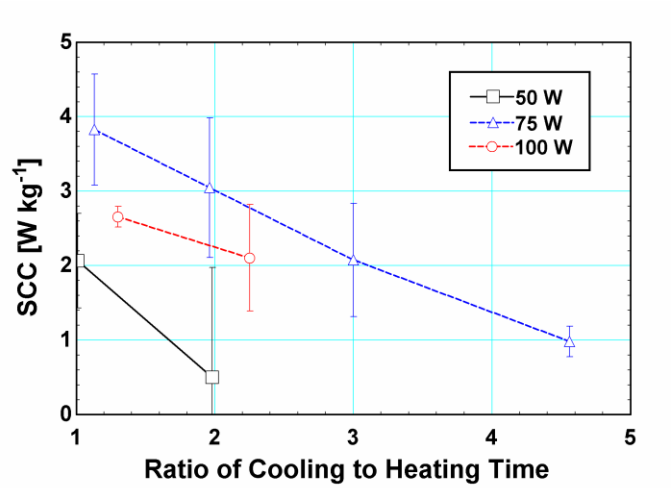

Figure 7.3 Effect on SCC of varying the ratio of cooling to heating time

The SCC of the system decreased with increasing ratio of cooling to heating time for every heating rate. The amount of cooling achieved in each cycle increases, but not at a rate commensurate with the increased time required for further cooling of the bed. The peak cooling also increases with increased cooling time. The COP meanwhile reaches a peak around a ratio of 2 for the 75 W case. For the 50 W case, increasing the cooling time reduces the COP as well, because the bed does not heat effectively for the 50 W case and excess cooling lowers the average temperature when the system has reached periodic

steady state conditions. The lower average temperature decreases the amount of desorption that can occur in the heating phase and the adsorbent cannot perform effectively. For the 75 W heating case, the COP is higher when the bed cooling time is twice the bed heating time and the COP is nearly the same when the ratio is 3-to-1. The improved COP is caused by longer time for adsorption allowing more cooling to be achieved in a single cycle, while the heat input for the cycle remains constant. Increasing the cooling time further reduces the performance, because the average temperature of the system decreases too much to allow effective desorption, as is seen in the 50 W heating case. The 100 W heating case also shows an increase in COP when the ratio is increased.

7.2.2 Heating Rate

The heating rate was varied to examine the effect on the system performance. Normally, the effect of increasing the heating rate of the adsorbent is to increase the cooling capacity of the system. Increased heating rate also usually leads to higher adsorbent temperatures, which can lead to better COPs until around 120 ºC for activated carbon. However, for the CHEC design, the direct convection coupling can lead to increased losses to the surrounding with increased heating rates. Therefore, it is expected that different trends will be observed for this bed with heating rate than those observed in a conventional bed design. Based on the modeling, it was expected that there would be an optimal heating temperature that would heat the adsorbent quickly and efficiently without overheating. Above this optimal heating temperature, the bed will be heated above the critical temperature of the refrigerant and increased heating will not yield further desorption. Below the optimal heating rate, the refrigerant will not desorb effectively.

The experimental results for the different heating rates are shown in Figure 7.4. The cooling-to-heating ratio is 1 for each of these heating rate cases. The system performance is best for the 75 W case. The 50 W case does not desorb effectively and so has a lower SCC, but the lower heat input means that the COP does not decrease as significantly. Increasing the heat input to 100 W decreases the COP and SCC. For the 100 W case, the temperature of the bed increases much higher than necessary and the excess heat does not contribute to desorption. The excess heat just contributes to dynamic losses and prevents the bed from cooling low enough to adsorb effectively during the adsorption phase and decreasing the delivered cooling.

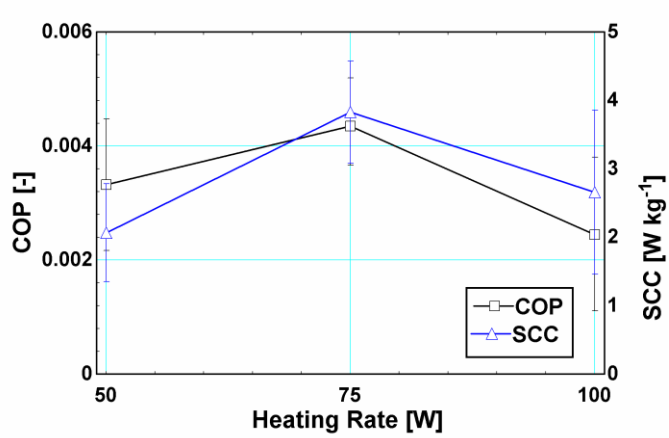

Figure 7.4 Experimental performance for different heat input rates

The heating time is also considered for the system. The ideal heating time is expected to be different depending upon the heat input rate and other system factors; therefore, several heat input rates and heating-to-cooling time ratios are investigated. Figure 7.5 shows the COP vs. the heating time for 50 W, 75 W, and 100 W heat inputs, where the ratio of cooling-to-heating time and other system conditions are the same and the heating time is varied. As the heating time is increased, the COP tends to decrease for the higher heating rates. This indicates that there is sufficient heating with the shorter

heating time for higher heat inputs. The temperatures in the bed are higher than predicted by the models for these experimental cases, indicating lower cooling than expected. The lower cooling explains why the longer heating times reduce performance. The COP for the 50 W case is higher with longer heating times, because the heat input rate is lower and therefore, the longer heating time allows the total heat input to the bed to be higher and more desorption to occur. The longer heating time has an even more appreciable effect when the cooling-to-heating time is increased for the 50 W case, because the long cooling time and low heat input may be preventing the adsorbent from reaching the necessary desorption temperatures.

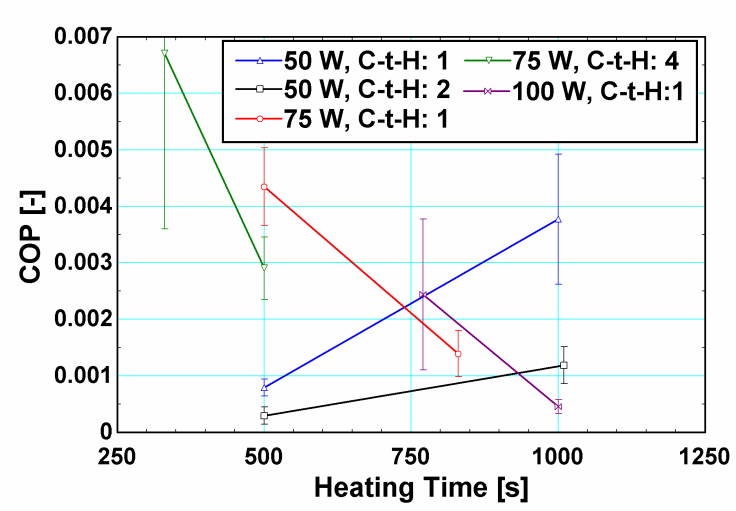

Figure 7.5 Effect on COP of varying the heating time

The SCC vs. the heating time is shown in Figure 7.6. The trends for the SCC are similar to those for the COP. As the heating time is increased, the SCC decreases for higher heating rates and increases for lower heating rates, just as the COP does. The 100 W heating rate especially loses capacity quickly with increased heating time, because the increased heating time not only decreases the effectiveness in the adsorption phase, but it also increases the length of the cycle so that what cooling does occur, happens over a

shorter period of time. The 50 W heating case experiences a large increase in cooling capacity again because the larger heating times allow more desorption to occur. The optimal heating time will depend on the other operating conditions.

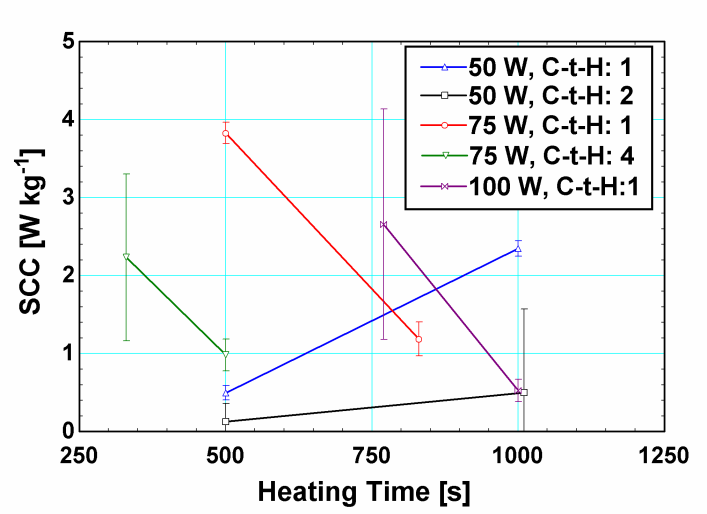

Figure 7.6 Effect on SCC of varying the heating time

7.2.3 Surroundings Effects

Two factors were considered for the surroundings of the system; the surrounding temperature of the air and whether the air was circulating or still in the environmental chamber. The nominal standard testing condition was 24ºC for the heating of the system. The air temperature is increased and decreased by 5ºC.

7.2.3.1 Air Circulation

In modeling the adsorbent system, convection around the system was assumed to be free convection. In the test chamber, to maintain surrounding temperatures, the chamber fan had to be running. The air circulation in the chamber changes the convection coefficient for the system and so the system is tested with still air and the surrounding air circulating in the environmental chamber driven by fans. These fans are not directed at

the bed, but do act to improve the convection heat transfer from the outer surface of the bed. The bulk movement allows two different convection cases to be explored and mimics the system operating in both a calm environment and one where air currents are common. The convection coefficient value for the air circulation case is then estimated from the experimental temperatures, starting with the convection coefficient estimation from Chapter 4, which gives a convection coefficient approximately twice as large as for the free convection case. Surrounding conditions in applications may vary.

The experimental results for air circulation around the adsorbent bed and when the air in the test chamber is stationary are shown in Figure 7.7. The results in Figure 7.7 are plotted against the total heat input per cycle, allowing the heating rate and heating time to be aggregated. Air circulation around the bed improves both the COP and the SCC for the system. The higher heat transfer rate on the external surface cools the bed more quickly allowing the system to adsorb more heat from the evaporator and deliver more cooling for the same energy input. The specific cooling capacity is more than twice as high with air circulation as for the still air cases. For both conditions, as the total heat input per cycle increases, the COP for the system decreases. The SCCs for the system are more varied and the trend of decreasing SCC with heat input per cycle is less pronounced than the COP. The cases with circulation had conductance values that were 40-120% of the design conductance, while for still air, the conductance is only 15-55% of the design conductance. This is likely due to the fins not being spaced effectively and obstruction of air flow by the experimental facility.

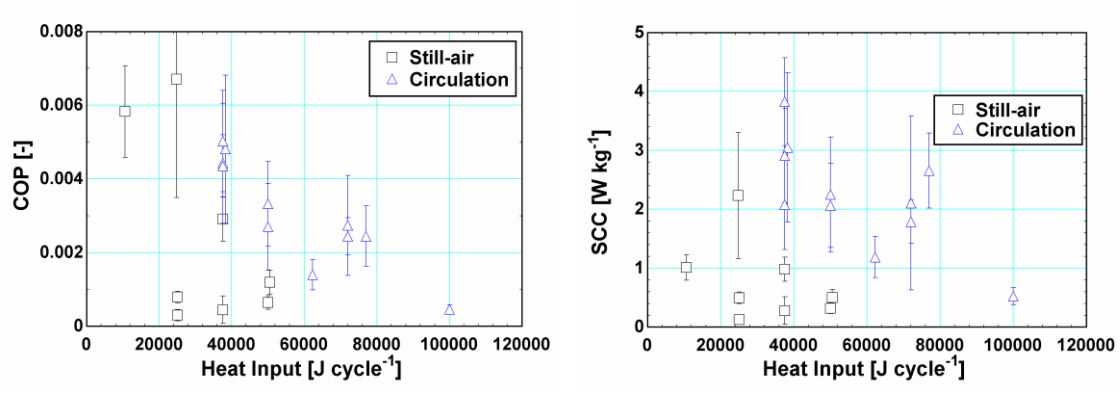

(a) (b)

Figure 7.7 The experimental performance with and without surrounding air circulation vs. the total heat inputs per cycle (a) COP and (b) SCC

7.2.3.2 Surrounding Temperature

Changing the surrounding air temperature changes the heat sink temperature for the adsorbent bed. Lowering the surrounding air temperature is expected to improve the system performance by increasing the temperature difference between the adsorbent bed and the surroundings. The greater temperature difference allows heat to transfer from the bed more quickly and the bed can reach a lower minimum temperature. The opposite trend is expected for an increased in surrounding air temperature. For many adsorption systems, the heat sink for the adsorbent bed and the condenser are at the same temperature, but there is no inherent reason this must be true. For the current system, the fluid reservoir acts as a thermal mass and maintains its temperature near the average ambient temperature throughout testing. There is some temperature change in the coupling fluid inlet temperatures due to heat transfer in the coupling fluid lines from the reservoir to the system, but the change in heat sink temperature for the condenser is less than 1°C.

The convection cooling was not as effective as predicted in the models and therefore, the temperature differences between the adsorbent bed and surroundings is of the order of the 50-80°C, higher than expected throughout the entire cycle. Thus, the change of 5°C in the surrounding air temperature results in a ~10% change in the driving temperature difference. The high bed temperature is contrary to what is observed in conventional adsorption systems, where at least part of the adsorbent bed structure approaches the heat sink temperature during the adsorption phase and a large change in performance is observed. For this system, unlike for a conventional system, the surrounding air temperature also impacts the temperature the bed can reach during desorption, because the bed continues to transfer heat to the surroundings while being heated. The heat transfer during desorption is expected to have a contradictory effect on system performance because a lower surrounding temperature causes a lower desorption temperature, which would be expected to decrease system performance. As a result of the slower than design cooling and the impact on desorption temperature of the surrounding air temperature, for the CHEC system increasing and decreasing the surrounding air temperature by 5°C did not result in measurable differences in system performance. Figure 7.8 shows the system performance 5 degrees above and below the standard testing conditions with circulating air. The differences in COP and SCC are within the experimental uncertainty for these values.

The effective temperature lift for this system is hard to define, because the temperatures of the evaporator and the condenser vary over time. The coupling fluid lines both enter at the temperature of the fluid reservoir, which is slightly below the average surrounding temperature of 24°C (in the experiments a temperature 0.3-0.4°C lower was

observed) because of evaporation from the reservoir surface. The minimum evaporator temperature was typically around 3°C below the coupling fluid inlet temperature and the maximum condenser temperature was typically 5°C above the coupling fluid inlet temperature. During the cycle phase where no mass transfer was occurring, both components approached the coupling fluid inlet temperature.

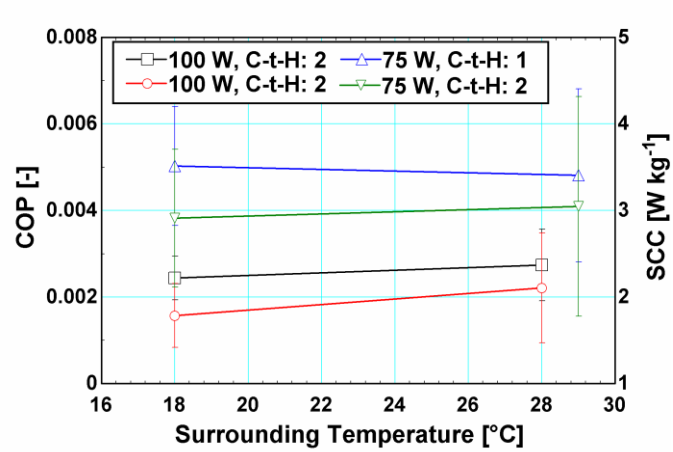

Figure 7.8 System performance as the temperature changes

7.2.4 CHEC Model Comparison

The predictions of the CHEC system model are compared with the experimental results here. The CHEC model is run with the same heating and cooling times, the same delay in valve openings, and the same environmental conditions for each of these comparisons. The temperature measurements and system performance are compared with the predictions of the model. The experimental system does not perform as well as the model predicted. The experimental results achieve COPs and SCCs from 2-20% of those predicted by the models, with the average results being 6% of the predicted performance. The recorded temperatures also differ somewhat and help identify the discrepancies between the initial system model and the experiments. It is clear that some factors not

identified in the original model affect the system performance significantly. Although the performance is much lower, the trends predicted by the models match closely with the experimental results, indicating that the fundamental basis of the model is correct. Based on differences between the experimental operation and the predicted operation, corrections to the model are proposed and implemented to yield better accuracy. Several factors are considered to account for the low performance, including additional losses, lower than predicted UAs, particularly the convection cooling of the outer wall, connection volumes, and conduction transfer within the system. Each of these factors was found to contribute to the decreased system performance and in some cases, they interacted to cause a greater decrease in performance than either of them would separately. The model is corrected based on the experimental results for a few of the data sets and then compared with the full set of experimental results.

The corrected model predicts performance within 60% on average compared to experimental results. The experimental temperature measurements of the bed and in the evaporator agree well with the modified model. The largest errors are for the 50 W heating case where even the corrected models show significantly higher performance than observed in the system. This may indicate that the adsorption equilibrium equation used for the adsorbent is not accurate in the lower temperature region. The corrections made to the model are discussed below.

The first factor considered to correct the model was accounting for additional losses from the system. The bed and heat exchangers had both been modeled with losses, but other areas where heat could be transferred with the surroundings were identified. These areas included, convection heat transfer from the connection lengths for the

pressure gauges and the charging ports, convection losses from the valves, and increased losses from the heat exchangers. Considering additional heat losses at these points by accounting for additional evaporator volume with a heat transfer coefficient of $UA_{evap,loss}$ = 0.04 W K^{-1} and increasing the losses from the evaporator by a factor of 10, decreases the system performance by less than 5%, showing that this additional heat transfer with the surroundings is not the primary cause of the lower than predicted performance.

Because the bed temperatures do not agree with the experimentally observed temperatures, the UAs are adjusted to match the experimental results. The bed cools more slowly and reaches higher temperatures than those predicted by the models, indicating that the convection cooling UA was likely incorrect. The model conductance values were varied iteratively to try to achieve the temperature profiles observed in the experiments. Adjustment of model parameters found that the heat transfer coefficient between outer surface and the surroundings, $UA_{os,inf}$, was between 20-80% of the initial model value. In the model, a fixed value for $UA_{os,inf}$ had been used, but it was determined that this was inadequate to represent the system and $UA_{os,inf}$ was made to vary linearly with surface temperature. The full correlation originally used to estimate the convection coefficient was not implemented because of stability issues with the code. The $UA_{os,inf}$ was 0.2 W K^{-1} with still air in the original model and 0.4 W K^{-1} with circulation in the original model and in the corrected model, it was found to be between (0.028-0.112) W K^{-1} for still air and (0.08-0.24) W K^{-1} for circulating air. Error in the convection cooling UA was insufficient by itself to explain the difference between the measured bed temperature and the predicted bed temperature. The heat transfer coefficient between the outer wall of the bed structure and the adsorbent material, $UA_{ad,os}$, is found to be a factor of approximately

two times larger than initially estimated. Better heat transfer between the outer wall and the adsorbent explains the faster than predicted temperature response in the outer structure to the opening of the valves. Axial conduction along the wall of the chamber, $UA_{os,os}$, was also found to be approximately half of what was predicted. This is likely caused by the modeling assumption of a continuous piece of aluminum rather than the fitted pipe sections from which the bed was constructed. Collectively, these changes decreased the temperature swing and average temperature significantly. As a point of comparison, for the 75 W, 500 s heating time, 1000 s cooling time, with still air, the original model predicted a temperature swing of approximately 65ºC and an average temperature of approximately 60ºC while the corrected model has a temperature swing of approximately 60ºC and an average temperature of approximately 100ºC. The impact of this change in average temperature depends on the specific case, but generally shifts the adsorption swing into a less favorable temperature range.

The heat transfer rates in the evaporator and condenser are also different from the predictions of the model. In the experiments, heat transfer initially occurs very rapidly when the valve is opened and mass transfer from the evaporator is fast, but quickly drops even when the evaporator temperature is still low. The heat transfer coefficient was found to be more dependent upon the mass transfer rate into or out of the component than on the temperature difference or absolute temperature in the component. By matching the experimentally observed changes in heat transfer rate, the heat transfer conductance was estimated to be linearly dependent upon the rate of mass transfer. Therefore, UA_{ev} was changed to:

$$UA_{ev} = \left|\dot{m}_{ev}\right| K_{ev} + 0.01 \frac{W}{K} \tag{7.1}$$

Where K_{ev} is 2.35 x 10^{-4} W s K^{-1} kg^{-1}. This better reflects the actual heat transfer observed in the system. This change does not significantly impact the system performance (<1%), but it affects how much of the cooling is measurable.

Next, the connection volumes connecting the adsorbent bed to the evaporator and the condenser are considered. These volumes were neglected in the model, but in the experimental facility, a length of piping is required as well as valves. The volume of the connections is larger than the void space around the adsorbent and has significant surface area with the walls that are considerably lower in temperature than the bed. The low temperature pipe walls mean that condensation can occur on the connection during the desorption phase. Most of this ammonia eventually transitions to the condenser, but some remains into the adsorption phase. The remaining refrigerant is then readsorbed as the pressure drops in the adsorbent bed, while the bed is still higher in pressure than the evaporator. The readsorbed refrigerant reduces the amount of adsorption that can occur from the evaporator. This is the most significant single error in the model. Approximately 20-50% of the ammonia mass that is desorbed/readsorbed each cycle is trapped in the connection sections and the cooling delivered by the system is decreased by an amount commensurate with the trapped refrigerant. This has the additional effect of minimizing the peak cooling that can be achieved in the system, by reducing the heat transfer rate in the evaporator, which stretches out the cooling. This lower cooling is harder to measure accurately. The reduction in performance is amplified by the relatively small volume of the adsorbent bed, so that the connection volume is roughly equal to the volume of the bed. Increasing the bed's volume relative to the connection length would decrease the impact. The mass of ammonia in the connections fluctuates for each cycle depending

upon the initial distribution of ammonia in the system and means that successive tests run under the same conditions can yield different results.

The final source of error identified was conduction along the walls of the connections with the heat exchangers and the bed, which played a part in decreasing system performance. As with losses from the bed leading to lower performance in small scale systems, the conduction effects here are partially a result of the system scale. Although the conduction heat transfer coefficients between the bed and the other components are small compared with other heat transfer coefficients for the system (~2% of the heat transfer coefficient through the adsorbent for example), but the conduction transfer into the evaporator was amplified by the accumulation of refrigerant in the connection volume. The connections acted like a heat pipe, carrying heat to the valves and pipe section close to the evaporator through refrigerant condensation and those components in turn heated the evaporator. This reduced the effective length that heat had to be conducted to approximately 1 in. rather than 8 in. the heat would otherwise have to travel. The heat transfer coefficient from the connection walls to the evaporator, $UA_{cv,ev}$, was modeled as 0.00625 W K^{-1}. On average for the different conditions tested, the heat conducted into the evaporator is equal to approximately one-fourth of the total cooling per cycle and reduced the delivered cooling by an equal amount. If the system were operating as intended, this heat would be only 2.6% of the total cooling delivered by the cycle.

In the experiments there is a portion of the cooling that is too low to measure accurately, the model predicts both the total cooling and the amount of cooling that will be measured in the experiments. All of the experimental trials are plotted in Figure 7.9,

the total predicted cooling and the measurable cooling from the corrected model are plotted with the corresponding experimental measured cooling. The amount of measureable cooling is predicted to be 70% or greater of the total cooling in almost all of the different trials. Because the amount of refrigerant in the connections changes with each cycle and is not easily measured, the amount of refrigerant in the connections at the start of testing has an adverse and unpredictable effect on system performance. Much of the error in model predictions is expected to come from the refrigerant distribution and there is no way to account for the accumulation in the model without knowing the initial conditions. The predictions are most accurate for the 75 W heat input cases (Case #1-9 in Figure 7.9) and least accurate for the 50 W heat input cases (Case #10-15).

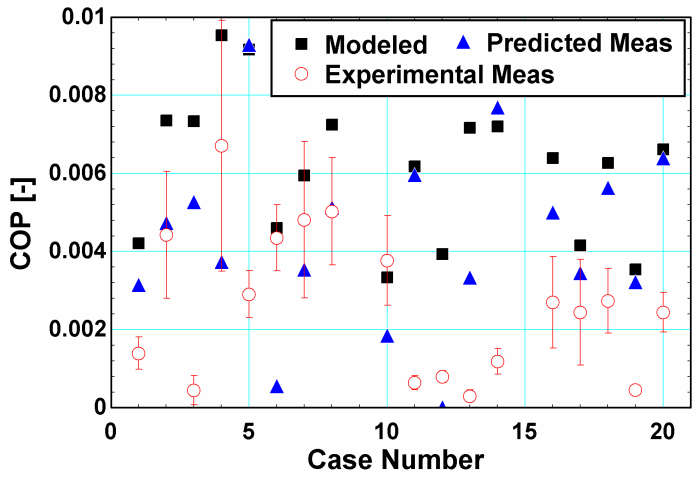

Figure 7.9 Model predicted performance and the predicted cooling measurement, compared with the experimental results.

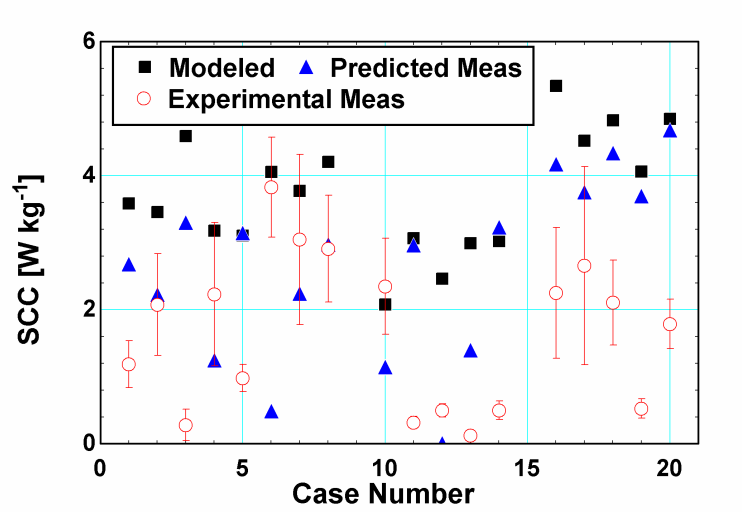

Figure 7.10 Comparison of the SCCs from the experiments and the corrected model

The results for the Specific Cooling Capacity from the corrected models are compared with the experimental results in Figure 7.10. The results are very similar to the COP results. The 75 W heat input cases match fairly well with the experimental results. The 50 W heat input cases are predicted to perform just slightly worse than the 75 W heat input cases, but perform much worse in the experiments. It is impossible at this point to further differentiate how much of the error is due to refrigerant distribution uncertainty and what may be due to other factors not considered in the model.

7.2.5 Comparison of Performance with Literature

The system performance is compared here with the performance of other small-scale systems reported in the literature. The performance for the CHEC bed is very poor compared with the values in the literature for conventional adsorption systems. The COP is significantly lower than that of conventional systems and the SCC is also low compared to that of conventional systems. Conventional systems typically exhibit COPs between 0.2-0.6 (Wang *et al.*, 2009b) and the COP obtained here is approximately 1% of

the other systems. However, when scaling trends are considered, the performance of the system is consistent with what is expected at this scale. From the literature, a trend of approximately a 0.07 reduction in COP for each decrease in order of magnitude for the system is expected, as shown in Figures 2.1 and 2.2 in Chapter 2. The systems investigated here are 3-5 orders of magnitude smaller than conventional systems, and therefore, a decrease of 0.21-0.35 in COP is expected. Additionally, this work only considered single bed systems, and the improvement offered by heat and mass recovery approaches were not possible for this system. The reduction in system performance is due to several factors: thermal shorting, increased inert masses, refrigerant condensation, and increased interaction with the adsorbent bed wall.

Thermal shorting is caused by heat conduction from connections through the adsorbent bed wall. In Chapter 3, it was seen that as much of 80% of the heat introduced into the system can be transferred through thermal shorting. The thermal shorting is a heat diffusion process driven process that depends upon how much of the surrounding material interacts with the connection. If the system operated at steady state like an absorption system for example, eventually surrounding material would reach a steady state condition and the thermal shorting impact would be reduced. It is because of the cyclic operation that this effect is so significant. The amount of material that interacts with the connection can be estimated using the Fourier Number. At Fo = 0.2, the distance the heat from the connection has traveled through the wall, L_{short}, is approximated by

$$Fo = \frac{\alpha t_{half,cycle}}{L_{short}^{2}} \tag{7.2}$$

Where α is the thermal diffusivity of the wall material and $t_{half,cycle}$ is the half-cycle time, which is approximately 500 s for the systems considered. For an aluminum

wall, the thermal diffusivity is 97.1×10^{-6} m^2 s^{-1} and for a stainless steel wall, it is 3.95×10^{-6} m^2 s^{-1} (Incropera and DeWitt, 1996). This yields distances for thermal shorting of 0.49 m and 0.10 m, respectively, so that chamber wall material within those distances can be expected to be heated and cooled during each cycle. These values are independent of the system scale and the additional dynamic losses they represent are nearly constant, but as the system size is decreased, the size of these losses compared to the adsorbent mass increases. At the system size being considered here, essentially the entire bed wall is being heated and cooled during each cycle due to thermal shorting.

As the bed is scaled down, it also becomes harder to fabricate components at the same size relative to the adsorbent volume. For example, to have the same wall mass-to-adsorbent mass ratio as a large-scale system, the present system would need a wall < 0.1 mm thick. Therefore, as the system is scaled down, the inert mass relative to the adsorbent mass increases. In conventional systems, ratios of 2:1 inert mass-to-adsorbent mass or better are often achieved (Miyazaki *et al.*, 2010). In the present work, the ratio was 10:1 and with improvements in fabrication, this could get as low as 4:1. In addition, in conventional systems, much of that mass can be considered non-interacting, but the thermal shorting at this scale leads to all of the thermal mass contributing to dynamic losses.

Another effect that becomes important at this scale is condensation of the refrigerant in undesired areas of the system, particularly in connections between components. This effect is particularly detrimental because it directly decreases the amount of cooling that can be delivered at the evaporator, rather than requiring a higher heat input to the adsorbent. The beds tested in the present work were not designed to

address this issue, as it had not been previously been identified in the literature to the best of the author's awareness. This is likely because the effect is so small as to be negligible at the scale where most systems operate. During the desorption phase, the high pressure refrigerant condenses on any surface that is below its condensation temperature, which is most likely to be connection walls and areas near the connections to the evaporator. This condensation reduces the delivered cooling by the fraction of the total desorbed refrigerant that condenses on these connection walls. As the system is scaled down, the amount of refrigerant being transferred scales with the adsorbent volume while the surface area scales with the characteristic length of the adsorbent volume squared. This means that the surface area available for condensation decreases more slowly than the total amount of refrigerant being transferred. This was exacerbated by increasing the length of the connections to minimize the amount of conduction heat transfer that was possible between the CHEC bed and the evaporator/condenser components.

Finally, interaction between the adsorbent volume and the chamber wall is increased. The adsorbent transfers heat to the chamber wall through radiation and convection from the outer surface of the adsorbent bed volume. The amount of heat transferred from the adsorbent to the wall then depends upon the outer surface area of the adsorbent mass while the total heat required for the cycle and the total cooling both depend on the volume

$$Q_{\text{interaction}} = Q_{cooling}^{2/3} \tag{7.3}$$

Therefore, the interaction heat transfer does not decrease as fast as the cooling and the interaction becomes increasingly important. For both the CHEC and Flat Bed systems, this interaction heat transfer is not as important as the other scaling effects,

because the designs placed the adsorbent material directly in contact with the bed wall to reduce the overall system size. For a conventional system made at this scale, insulation of the bed wall would be necessary to minimize this effect.

The SCC is also approximately 1% of those achieved by conventional large scale systems. However, the scaling effects are expected to reduce the system performance compared to these conventional systems. The scaling reduction in the SCC has different causes than the reduction in COP. The SCC is determined by Equation 7.4

$$SCC = \frac{Q_{cooling}}{m_{ad} t_{half-cycle}} \tag{7.4}$$

The COP is reduced due to increased losses, increased interaction with inert masses that increases dynamic losses, and increased inert masses relative to the adsorbent. As can be seen in Equation 7.4, the SCC decreases due to the increased time required to heat and cool the adsorbent material represented by increased half-cycle times. The heating/cooling time is not directly dependent upon the amount of additional heat required and depends more on the heat transfer rates, which may be improved by additional masses that decrease COP. If the heat transfer rate is constant (as with an electrically heated system,) increases in dynamic losses increase the cycle time proportionally, and the SCC follows the same trend as the COP. Because SCC is not as widely reported as COP, there was insufficient data to establish a trend in the scale of the reduction, but the physical mechanisms imply that the reduction in SCC should be of the same order as the reduction in COP, but with a fast enough heat transfer rate, it is conceivable that SCCs approaching large scale systems could be achieved. Regarding the interaction of specific scaling effects with the SCC, thermal shorting prevents heat flow into the adsorbent, which increases the cycle time and reduces the SCC. The SCC is

reduced by the same fraction as the COP by refrigerant condensation in undesired locations, because this is a direct reduction in the delivered cooling.

Experimental results from the present study are compared here with the performance of the smallest adsorption systems from the literature. The smallest conventional system found in the literature is an activated carbon/ammonia system employing 800 grams of adsorbent material delivering approximately 50-100 W of cooling (Tamainot-Telto and Critoph, 1997). This system has a COP ranging from 0.06-0.12 and SCC ranging from 30-60 W kg^{-1}. The initial models from the present study predicted performance competitive with Tamainot-Telto and Critoph's work, despite this system being one to two orders of magnitude larger than the one developed in the present work. However, during model refinement, it was found that the CHEC system has limitations that only allowed it to achieve approximately 10% of the performance seen in their work.

Other systems that deliver cooling <1 kW utilize much larger adsorbent masses and systems than those investigated here. Critoph (1994a) investigated a system that delivered 10-100 W of cooling on average, but did so with 17 kg of adsorbent material. Yang (2005) investigated a system that delivered 500-800 W of cooling with 10 kg of silica gel. These systems function more like conventional systems operating far outside the optimal design conditions than a true small-scale system. It is unclear how valid a comparison with these systems is, because they have three orders of magnitude more adsorbent than the amount used in the present work, but they are some of the only systems investigated close to the cooling ranges of interest here.

The results from the present work are compared with the results from these three studies in Figure 7.11. These comparisons are made on the basis of desorption temperature as a common variable where similar systems would be expected to perform equally, even when the cycle time and other factors may vary. The COP of the CHEC design is only 10% of the results reported by Critoph (1994a) and Tamainot-Telto and Critoph (1997), and roughly 2-3% of those seen by Yang (2005). Each of these alternative systems is more complex than the system explored here and would be expected to have higher performance values, as much as 50% higher than the current system. Even when scaling trends are considered, the CHEC design does not compare favorably with COPs from literature and should have delivered COPs in the range of 0.03-0.08.

The specific cooling capacity of the system developed here is in the same range as the corresponding value for Critoph (1994a) despite the much lower COP. The higher SCC means that despite the small size and lower than expected UAs, the heating and cooling of the adsorbent material is at least as fast as Critoph (1994a). The other two small-scale systems have SCCs approximately 10 times higher than the value from the present work. Scaling effects are a part of the decrease in SCC, and the air-coupled cooling with the longer associated cycle times is also a large factor. The system developed by Tamainot-Telto and Critoph (1997) has an SCC that is lower than most conventional systems, despite being designed along similar lines.

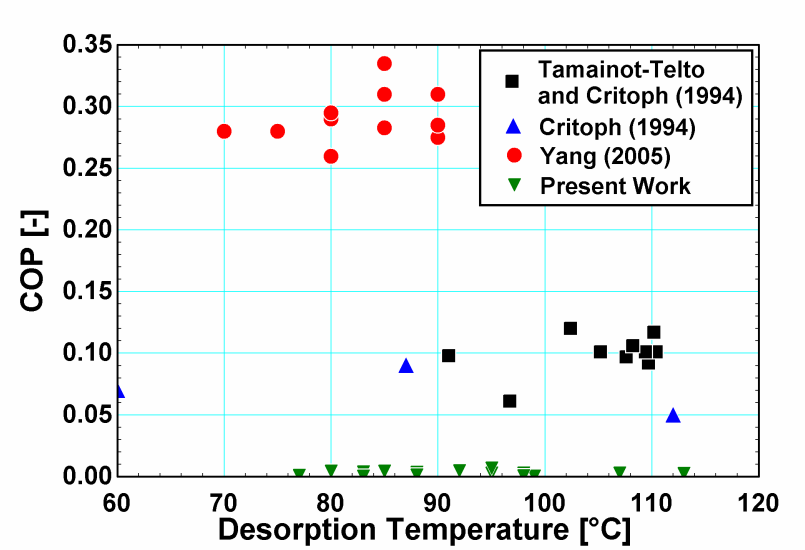

7.11 Comparison of the CHEC system with other small scale systems from literature

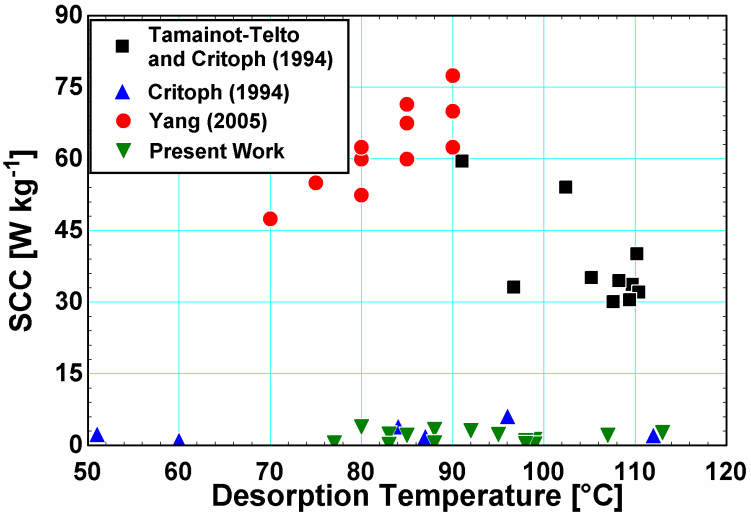

7.12 Comparison of the CHEC system with other small scale systems from literature

7.3 Flat Bed System

Experimental results for the Flat Bed system are discussed here. For this system, the factors considered were the heat input and switching conditions. The thermal switch was also assessed on the system to verify that it was working as designed. The test matrix for the Flat Bed system is shown in Table 7.2.

Table 7.2 Flat Bed Test Matrix

Input heat [W]	**Switching Temperature (high)**	**Switching Temperature (low)**	**Surr. Cond.**	**Nominal Surr. Temp [ºC]**
10	65	35	Still	25
	70	35	Still	25
	75	40	Still	25
	80	40	Still	25
	80*	40	Still	25
	60	35	Circ.	25
	65	35	Circ.	25
	70	35	Circ.	25
20	85	35	Circ.	25
	90	40	Circ.	25
	95	35	Circ.	25
	100	35	Circ.	25

*This case was run twice with different precooling times to demonstrate the effect of precooling time on the amount of measureable cooling.

7.3.1 Heat Input

The different heat inputs investigated lead to very different results in the system. The 20 W heat input yields much higher adsorbent bed temperatures and faster heating than the 10 W heat input. Figure 7.13 shows the temperature curves for each test condition with the bed starting at 50ºC for 200 s. For the 20 W heat input, the heating block increases in temperature much faster than the 10 W heat input case.

Figure 7.14 shows the temperature of the heating block as it is connected to the system for each case when the heating block is at a temperature of 100 °C. The temperature of the block drops rapidly as it transfers heat into the adsorbent bed. After the initial rapid temperature drop, the heat transfer slows as the heating block and bed temperature approach each other. Then the temperature begins to rise again as the heat input from the heating element becomes higher than the heat transfer into the system. The

20 W heating case reaches the point where the temperature starts increasing again much sooner than the 10 W heating case, but the initial temperature drop is very similar for both cases, showing that the stored heat is similar for both heating conditions.

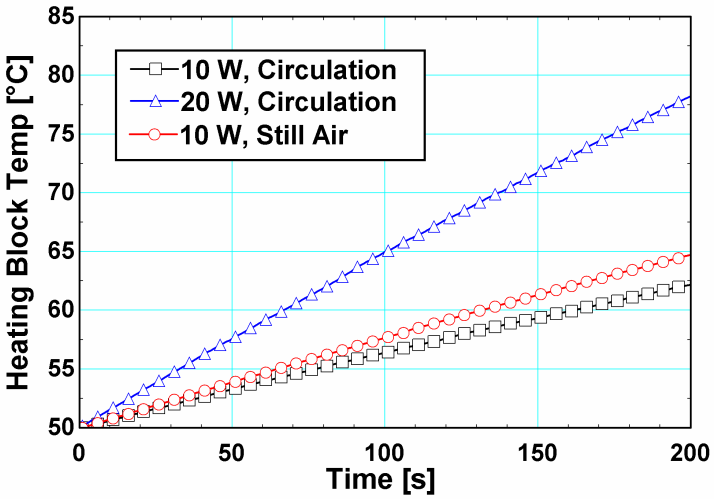

Figure 7.13 Temperature of the heating block as it is heated for the different test conditions

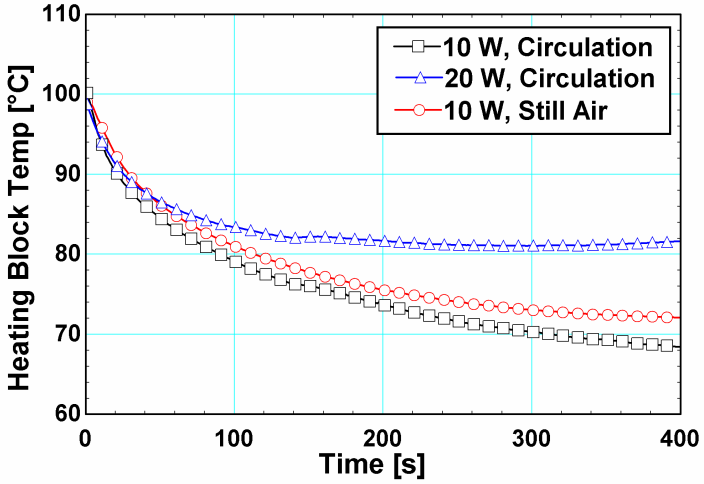

Figure 7.14 Temperature of the heating block when it is connected to the system

The performance of the Flat Bed system for the 10 W heat input is shown in Table 7.3 and the performance for the 20 W heat input is shown in Table 7.4. The highest COP

is observed for the 10 W heat input while the 20 W heat input delivers higher SCCs. In both cases, the bed reaches high enough temperatures to desorb effectively and cools to low enough temperatures to adsorb effectively. The 10 W heat input has lower losses throughout the cycle which is why the COP is higher. The losses are higher for the 20 W heat input, but the heating time is shorter; therefore, the SCCs are higher.

Table 7.3 Experimental Flat Bed Results for the 10 W heat input

Switching Temperature (high)	**Switching Temperature (low)**	**Surr. Cond.**	**Nominal Surr. Temp [°C]**	**COP [-]**	**SCC [W kg^{-1}]**
65	35	Still	25	0.014	14
70	35	Still	25	0.023	23
75	40	Still	25	0.030	30
80	40	Still	25	0.022	22
80*	40	Still	25	0.012	12
60	35	Circ.	25	0	0
65	35	Circ.	25	0.006	6
70	35	Circ.	25	0.002	2

*Demonstration of pre-cooling effects.

Table 7.4 Experimental Flat Bed Results for the 20 W heat input

Switching Temperature (high)	**Switching Temperature (low)**	**Surr. Cond.**	**Nominal Surr. Temp [°C]**	**COP [-]**	**SCC [W kg^{-1}]**
85	35	Circ.	25	0.006	14
95	35	Circ.	25	0.015	30
100	35	Circ.	25	0.014	28

7.3.2 Switching Conditions

The switching conditions determine the extent of the adsorption and desorption phases. By setting the switching conditions at which the bed is shifted to the cooling position to a higher temperature, it is possible to make the bed go to a lower specific adsorption value. This can lead to greater adsorption during the cooling phase and therefore greater cooling, but the higher temperature requires a longer heating time,

which can lead to a lower cooling capacity on average. Similarly, the switching condition from adsorption to desorption states determines the higher bounds of the specific adsorption. During the cooling phase, heat is lost from the hot side to the surroundings. Initially, the heat from the heat source is stored in the heating block, but as the cooling phase increases in length and the heating block increases in temperature, the heat loss increases. In the experimental facility, because a constant heat input is supplied, heat is lost at a nearly constant rate to the surroundings during the adsorption phase, much faster than would be expected from a constant temperature source waste heat supply. If the cooling phase goes on too long, the lost heat can decrease the efficiency. Increasing the cooling phase can increase the amount of cooling done during that phase, which can increase the cooling capacity of the system.

The temperature is measured on the heating and cooling block, but a good picture of the temperature of the bed can be achieved from these measurements. The relative heating and cooling times become dependent on the switching conditions that are specified, rather than being chosen as in the CHEC system. The high side switching temperature is varied. Figure 7.15 shows the results for the 10 W heating case with still air and the 20 W heating case with circulating air. Different trends are observed for the two heat inputs, but for each the COP and SCC reach a peak value. Below this value, the performance drops quickly and decreases more slowly when the switching temperature is above this peak value. The same trend is observed in system models.

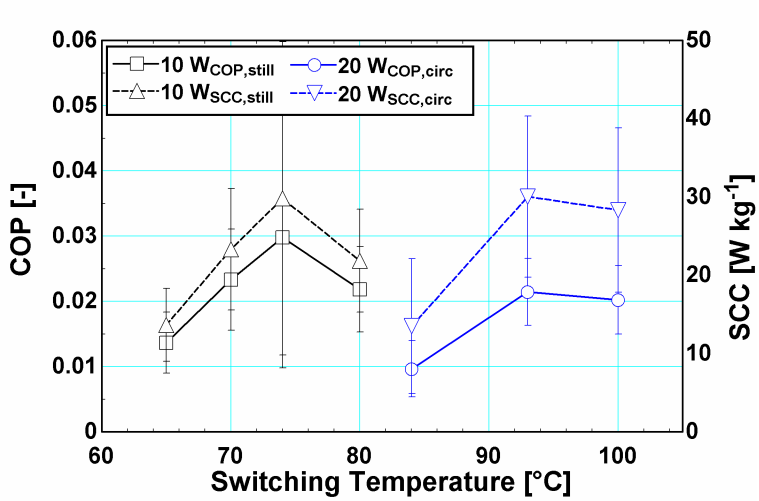

Figure 7.15 The COP and SCC for the flat bed system as the switching temperature is varied

7.3.3 Air Circulation Effects

The Flat Bed was tested under the two different air circulation conditions in the environmental chamber. In one case, the air was circulated by the chamber's fans and in the other, the only circulation was caused by natural convection. Initially, testing of both heat inputs was planned with and without air circulation in the chamber, but for the 20 W case without air circulation, the heating block temperatures were higher than the operating temperature of the O-ring used to seal and these tests were not conducted for safety reasons. With air circulation, the heating block temperature increases approximately 15% more slowly and the temperature falls approximately 15% more slowly in the heating block. The rest of the system also loses heat more quickly throughout the entire cycle with air circulation. The slower heating and losses from the system lead to lower temperatures for the system with circulation. To reach the same peak temperatures, longer cycle times are required, which reduces the SCC and the COP in the Flat Bed system.

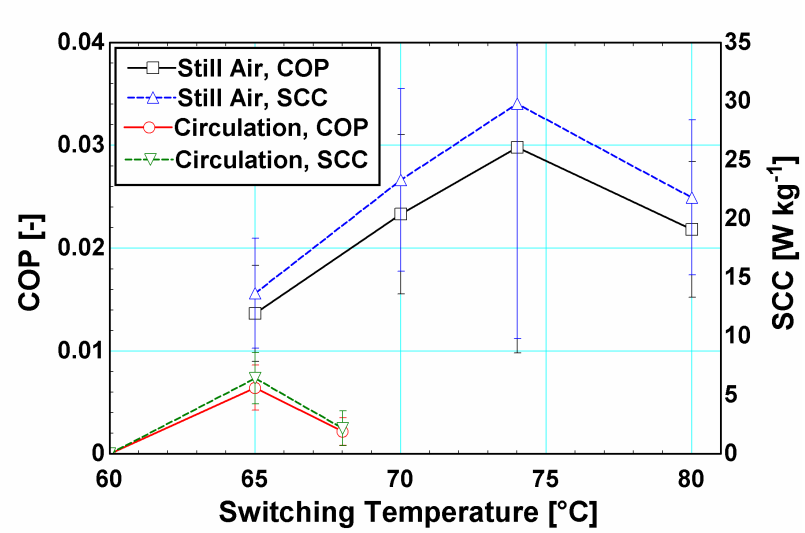

Figure 7.16 The COP and SCC for a 10 W heat input with and without the chamber air circulating.

The results comparing the performance of the 10 W heat input with and without air circulation are shown in Figure 7.16 as the switching temperature is varied. The still air system achieves its peak performance at a higher switching temperature than with circulating air. The COP for the still air case is 2-6 times higher, and the SCC is similarly higher. The circulating temperature case could not reach higher switching temperatures, indicating that the bed could not reach the necessary desorption temperature to operate effectively.

7.3.4 Thermal Switch Operation

The experimental results show that the thermal switch operates as designed for the adsorption system. Figure 7.17 shows temperature data for a 10 W heating case in the heating and the cooling blocks for both the experimental and modeled systems. The switching behavior can be seen clearly in the experimental results. The heating block increases in temperature, storing energy during the adsorption phase and then rapidly transfers heat to the adsorbent bed. The cooling block likewise rapidly increases in

temperature during the start of the adsorption phase and then cools with the adsorbent bed. During the desorption phase, the cooling block is transferring heat to the surroundings, so that it will more effectively cool the bed during the adsorption phase.

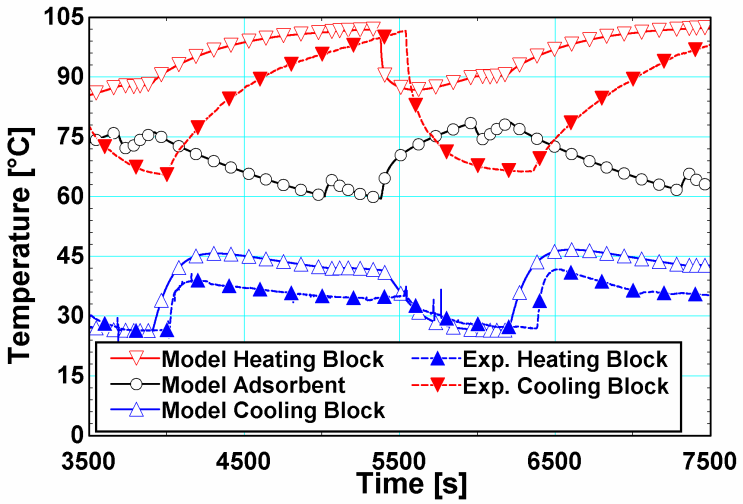

Figure 7.17 The temperature profile in the heating and cooling block in the experiments (solid) and in the models (hollow)

The modeling results are shown beside the experimental results in 17.7. It can be seen that the experimental temperature on the heating block actually drops lower and faster than in the model. The heating block temperature also recovers faster when removed from the experimental bed. The difference in temperature is likely caused by two things. First, the heating block was assumed as a uniform piece of steel in the models, while in the experimental set-up, it is comprised of three layers of steel joined by JB weld epoxy. The thermocouple is placed between layers and epoxied into place. Therefore, the modeled heat transfer rate through the block and from the block is likely overestimated compared to the experimental system. The lower heat transfer rate would cause the back part of the block to be higher in temperature than the section being measured and modeled; therefore, the temperature recovery is largely caused by heat

transfer within the heating block. The faster drop in temperature indicates that the assumed contact resistance was too conservative in the model and that the heating block is actually transferring heat more effectively than indicated. The thermal capacity of the bed is larger than the value used in the model, because the masses of the fittings and connections also participate in the thermal processes and represent additional thermal mass.

The cooling block temperatures are also slightly different from the values predicted by the model. The modeling results are higher in temperature by about 7ºC for most of the adsorption phase and the block also experiences a faster rise in temperature when connected. The higher model temperature may be due to the temperature measurement being done on the cooling fin, rather than the center of the block in the experiments. The fin is expected to be at a lower temperature than the portion of the cooling block in contact with the bed. The faster rise in temperature again indicates that the contact resistance assumed for the switch is too conservative. The adsorbent temperature predicted by the model shows a swing of approximately 15ºC; however, lower contact resistances with the thermal switches may be yielding slightly higher temperatures in the experiments. These results confirm that the thermal switch operates as intended and yields the desired swing in adsorbent temperature.

7.3.5 Comparison of Experimental and Modeling Results

The experimental results were compared with model prediction to help validate the models and to yield insight into the actual processes. The predicted temperatures are compared with the experimentally observed temperature as well as the system performance to evaluate the model. It is only possible to measure cooling above a certain

rate depending on the test conditions. This means that when the cooling rate falls below the measureable rate, the cooling cannot be measured. The immeasurable cooling is predicted using the system models. The models are compared with the experimental results by setting the model times for each phase equal and using similar precooling and preheating times.

The Flat Bed system did not experience as much thermal shorting, because the bed was not being constantly cooled so that heat that shorted around the bed was not lost to the environment as quickly. Additionally, the connection sizes were reduced to help minimize undesired condensation effects by shortening the connection length by several inches and using 3.18 mm (1/8 in.) tubing rather than 6.35 mm (¼ in.) tubing.

7.3.5.1 System Temperature Comparisons

The temperature measurements throughout the system during the experimental operation are compared with the corresponding values from the models. Together with the cooling, the temperature comparisons can be used to validate the accuracy of the system models developed for system design. With validated models, reliable insights, understanding, and conclusions can be drawn. The temperatures of the heating block and cooling block have already been compared in section 7.3.4 in validating the thermal switching control. The evaporator temperature is compared here. Figure 7.18 shows the temperatures of the evaporator from the experiments and the model predictions.

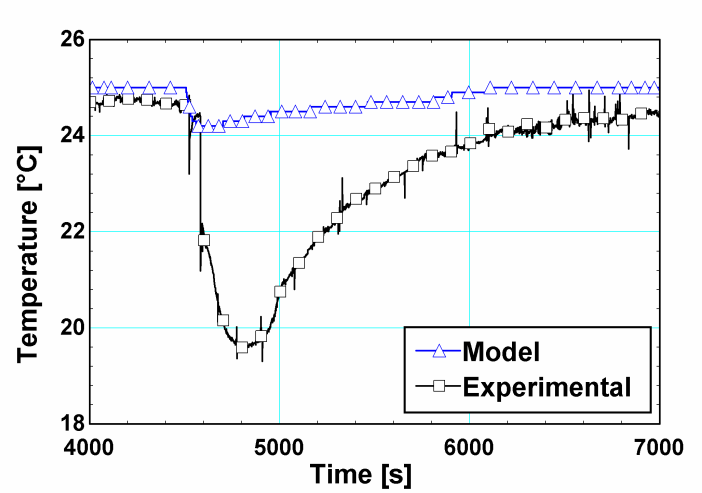

Figure 7.18 The temperature profile in the evaporator during the adsorption phase from the model and the experiments

The minimum temperature of the evaporator seen in the experiments is approximately 4°C lower than predicted by the models. The general shape of the temperature curves is similar, but the experimental temperature change has a much larger magnitude. This could indicate that the heat transfer conductance between the refrigerant and the coupling fluid stream is lower than expected, and a larger temperature difference is needed to transfer the same amount of heat. In the model, the convection coefficient depends upon the temperature difference between the coupling fluid stream and the evaporator temperature. In the experiments, it appears as if the convection coefficient depends more upon the mass transfer rate. When the valve first opens and the mass transfer from the evaporator is high, the convection coefficient is high, but as the mass transfer drops, the convection coefficient drops. The lower convection coefficient causes the evaporator temperature to get lower and the larger temperature difference causes the heat transfer to be similar to what was predicted by the model. Adjustment of the convection coefficient in the models showed that the performance was relatively

insensitive to the evaporator and condenser convection coefficients. Changing the convection coefficient by a factor of 10 changes the performance by only about 10%.

7.3.5.2 Estimated Performance

The experimentally observed COPs and SCCs are compared with those predicted in the models. The cooling rate for much of the cycle is too low to measure in the experimental facility. The limits on these cooling measurements are described in Appendix A. However, although the cooling cannot be measured in parts of the cycle, it is known from evaporator temperature measurements that cooling is occurring during these periods. When the measured cooling is of the same order as the experimental uncertainty, it is assumed to be zero, which underestimates the system performance. The system performance was intentionally underestimated, to avoid overly optimistic claims of the system performance. By using the lower bound, the conclusions drawn about applicability and feasibility are conservative; however, it is useful to know the safety margin that has been assumed by neglecting the lower cooling rate measurements and to form a realistic assessment of the system. The model is used to predict measureable cooling, as well as the portion of the cooling that is not measureable. When the model has been validated based upon the predicted measureable cooling, an estimate can be made of the cooling that is missed by the experimental set-up.

Figure 7.19 shows predicted cooling per cycle from the model as well as the predicted cooling that will be measurable per cycle for the Flat Bed system operating under the same conditions as the experimental systems. The experimentally measured cooling is also shown. For most of the system runs, the measured cooling is approximately 80% of the total predicted cooling. For lower cooling rates, a larger

portion of the cooling is immeasurable. The 80ºC testing cases with different precooling conditions demonstrates that the model can predict the cooling even when the total cooling is the same, but the fraction of the cooling that is measurable has changed.. The results agree well for each of the modeled cases and all of the experimental results are within the experimental uncertainty of the measurements except the 10 W case with circulation and the 68ºC switching condition (nominally 70ºC).

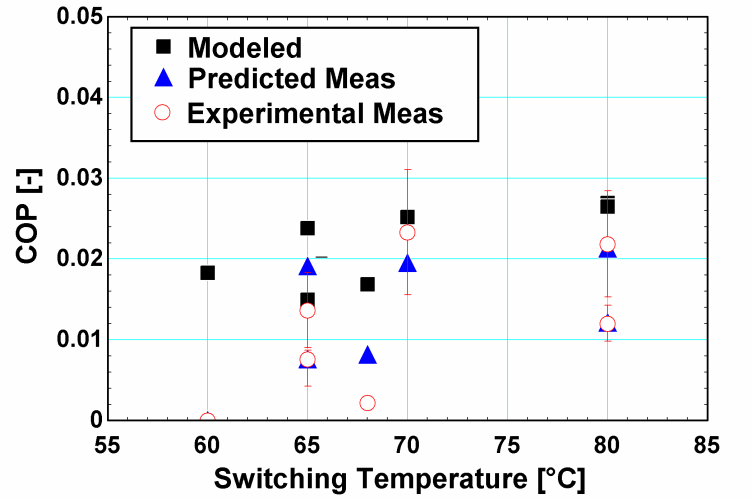

7.19 Comparison of the Flat Bed experimental and modeling results with a 10 W heat input

No modifications of the Flat Bed model were made based on the experimental results to achieve the good agreement observed between the two. The Flat Bed system avoided the connection volume and conduction problems of the CHEC system by having lower volume connections. The convection cooling of the Flat Bed system was more effective than the CHEC convection cooling and reached the modeling design values. The experimentally validated model can be expected to reliably serve as a tool for design and evaluation of similarly designed adsorption systems.

7.3.6 Comparison with Literature

The Flat Bed system performs better when compared with literature than the CHEC system. Figures 7.20 and 7.21 show the COPs and SCCs from the present work compared with the performance of other autonomous systems from the literature. Similar to the other autonomous systems, the COPs for the Flat Bed system are lower than those of large scale conventional adsorption systems, but the COP for the present system is similar to the results of Headley *et al.* (1994) results and not much lower than the values Critoph (1994a) obtained. Both of these competing systems were much larger than the present system with Headley's system having 2.6 kg of adsorbent and Critoph's system using 17 kg of adsorbent material compared with 10 g of adsorbent used in the Flat Bed system developed here. Despite the greatly reduced size, the present system has higher SCCs than either of the autonomous systems found in the literature. Peak SCCs are nearly 5 times larger for the present system than those of other autonomous systems and are in the same range as the SCCs of smaller conventional silica-gel/water systems (Wang *et al.*, 2009b).

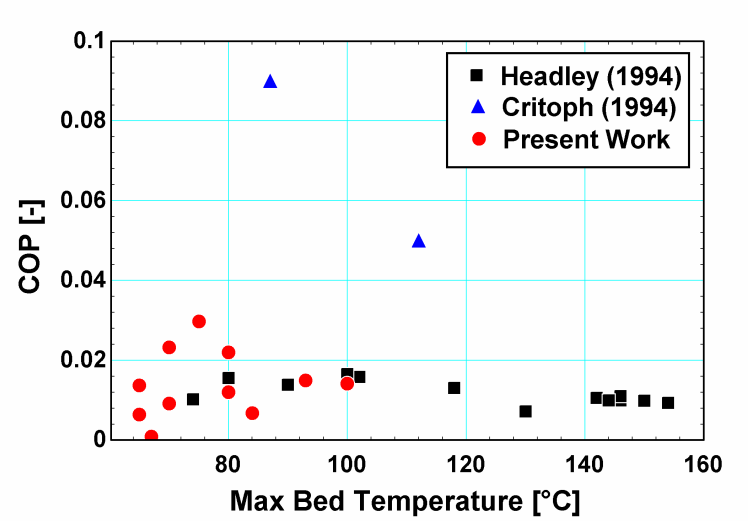

7.20 Comparison of the Flat Bed experimentally observed COPs with other autonomous systems from literature

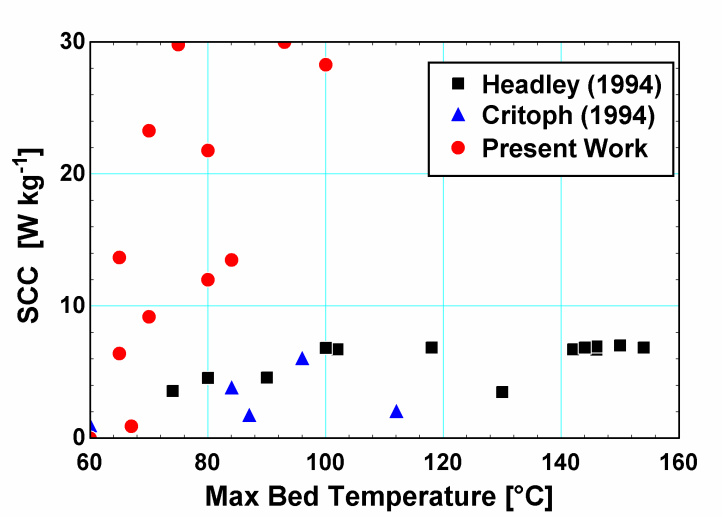

7.21 Comparison of the Flat Bed experimentally observed SCCs with other autonomous systems from literature

CHAPTER 8

CONCLUSIONS AND RECOMMENDATIONS

8.1 Conclusions

The applicability of small-scale adsorption systems for distributed cooling utilizing waste heat sources was investigated. This study explored the smallest adsorption heat pump systems to date. New control strategies and mechanisms for the implementation of those strategies were developed. The design, fabrication, and testing of adsorption systems specifically designed to utilize heat sources less than 100 W were performed for the first time.

In the process, design methodologies for this scale and important scaling factors were identified. Detailed computational analyses of the system were conducted and the effect of adsorbent bed mass, heat input rates, and cycle time lengths were investigated. The design method and experimentally validated tools can be used with modifications to bed geometry for future work in small-scale adsorption systems.

A bread board test facility was designed and fabricated for the evaluation of adsorbent beds. The testing facility allowed a wide range of heat inputs and surrounding conditions to be tested. Pressure, temperature, and heat transfer measurements allowed the characterization of adsorption system operation. Several early designs were tested on this facility, of which two small-scale adsorbent beds were chosen and tested as adsorption heat pumps.

The first small-scale adsorption system utilizes a CHEC adsorbent bed with direct air coupled cooling to eliminate the cooling coupling fluid loop and to reduce the system footprint. This bed demonstrates one of the fundamental issues with scaling adsorption technology: as the scale of the system is decreased, the conduction length from the feed through to the adsorbent bed shell decreases and conduction losses become significant compared to the adsorbent mass. At the scales considered in this work, it is impossible to isolate the external structure from the adsorbent material as is done in large-scale systems. Heat from the connections through the walls tends to penetrate a distance on the order of 0.1 m, which means that almost the entire external structure is interacting thermally and contributing to dynamic losses at small scales. The external structure decreases system performance by both increasing the dynamic losses in the system and increasing the amount of heat lost to the environment rather than heat being used in the desorption process.

Figure 8.1 shows the distribution of heat that enters the adsorbent bed for a large and small adsorption system. The heat is divided between thermal shorting, transferred directly into the adsorbent, transferred into fins to pass deeper into the adsorbent, and used as dynamic losses in the structure. In the large scale system, the major fraction of the heat goes into the bed fins to be transferred throughout the adsorbent or transferred directly into the adsorbent. The loss is dominated by dynamic losses in the internal heat transfer structure and shorting losses are a small fraction. In the small-scale system, the shorting losses become dominant, using more than half the heat going into the system. The dynamic losses continue to play an important role. The heat transfer into the fins and adsorbent only makes up about one-third of the total heat rather than three-quarters of the

total heat for a large scale system, which means that ~2.25 times as much heat must be added to the system to achieve the same cooling. The CHEC system attempts to overcome not being able to thermally isolate the bed wall by leveraging the heat losses to provide cooling to the adsorbent material allowing the bed to be simplified. Thermal breaks modeled in Chapter 3 present an effective path for reducing the impact of the shorting effects. The Flat Bed system heats and cools the whole bed so that even though the dynamic losses are still high, the heat transfer rates into the adsorbent are improved.

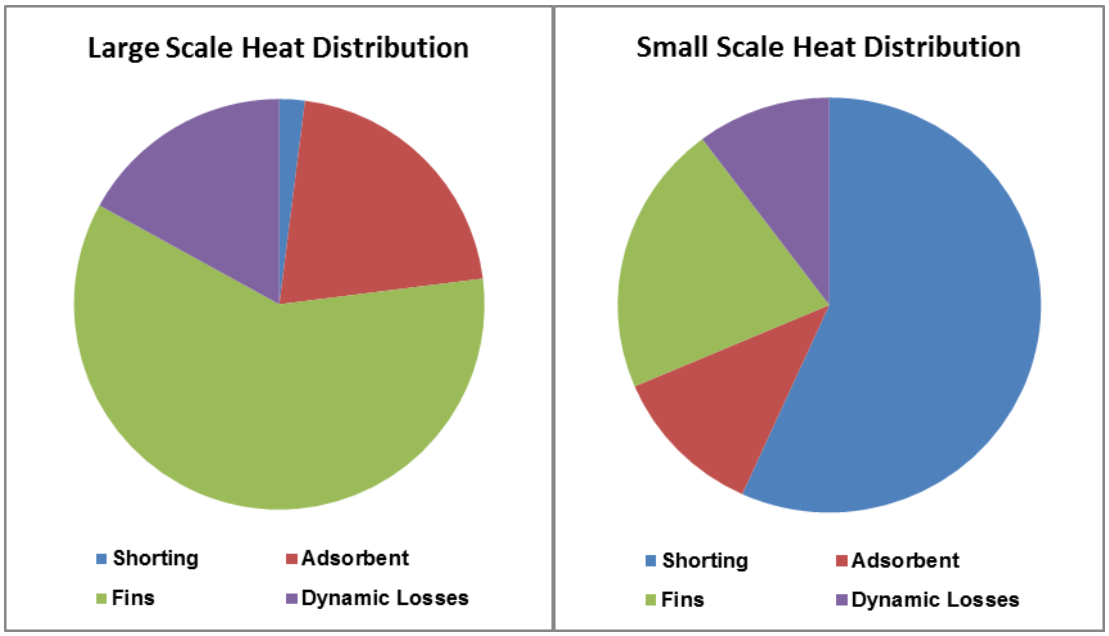

Figure 8.1 Heat distribution in a) a large system and b) a small system

In testing the CHEC bed, another issue not seen in large scale systems was identified in the connection sections. In a large system, the amount of connection length between the evaporator, condenser, and adsorbent bed is small compared to the total refrigerant transferred in each cycle. At the smaller scales, this volume becomes significant and the refrigerant trapped in this section significantly decreases system performance. Additionally, the bed is not effectively cooled by natural convection, and

radiation and conduction around the adsorbent decreased the amount of heat reaching the adsorbent material. The bed delivers only 10% of the predicted cooling and is not competitive with the smallest systems identified in literature, having lower COPs and SCCs that match only one other system. Therefore, the CHEC design was ruled out as viable for use in distributed cooling applications. The decreased system complexity does not justify the trade-offs in decreased performance. Possible modifications are discussed in the recommendation section to address the identified issues, but based on the better performance of the more compact Flat Bed geometry, continued investigation of this bed design is not advisable.

The second system utilized two hollowed circular disks with the adsorbent material contained between them and used the thermal switching approached developed in this work for system control. Because of the flat profile, this bed was referred to as the Flat Bed throughout the work. The adsorbent material is held in four layers between the two disks and the pressure used to seal the adsorbent bed also ensures that the adsorbent material is in good thermal contact with the bed structure and is tightly packed. The thermal switching technique physically completes and breaks thermal contact between the bed and the heat source and heat sink. Because the housing structure is used to heat and cool the adsorbent material, there are no connections going through the bed to allow conduction losses and the only path of loss is the connection to the system for transferring ammonia. The sizes of the connections were smaller in this system (3.18 mm vs. 6.35 mm diameter tubes), which, combined with the tighter packing of adsorbent material, allowed for the losses in cooling due to refrigerant trapped in the connections to be largely eliminated. The thermal switching technique used for control also allows the

adsorption system to operate only on heat, opening up a wider range of distributed cooling applications. The Flat Bed performed as designed, delivering a peak COP of 0.03 and a peak SCC of 30 W kg^{-1}, with peak cooling rates approaching 4 W with heat inputs as low as 10 W. The design of the bed allows effective operation on any heat source at a temperature above 80ºC and the system can be scaled with little modification to match heat sources ranging from 10 W to 1 kW. The COP falls in the same range as the COPs for autonomous systems that utilize more than 100 times more adsorbent material. The SCC is approximately 2-4 times higher than the values reported for other autonomous systems. The total weight for this system is only approximately 1.5 kg and removal of the measurement devices and fittings would allow this to be reduced further to less than 1 kg. The bed has a total volume of less than 70 cm^3 and the total system volume excluding the charging port and measurement coupling lines is approximately 300 cm^3. This bed represents a pathway to future utilization of diverse heat sources.

8.2 Thermal Control for Adsorption Systems

In addition to the scaling effects and system design investigated in this work, adsorption system controls were investigated. Alternative adsorption system control criteria were identified, rather than using just heating and cooling time for system control. The adsorbent temperature and amount of refrigerant adsorbed were both identified for use in monitoring the progress of the cycle of a phase. These adsorption system control criteria are broadly applicable to adsorption systems of any scale. By using these alternative criteria, it was found that more consistent performance was possible with less variation in COP and SCC as the source temperature is varied compared with conventional control techniques.

A number of novel control mechanisms were proposed to implement these control criteria, including actuation by adsorbent material expansion, a float controlled thermal switch, and a physical thermal switch. The adsorbent material expansion process was put through a proof of concept test. Large hysteresis effects in the adsorbent caused adsorbent expansion to be ruled out as a means of system control. Both the physical and float controlled thermal switches were modeled. The physical thermal switch was found to deliver better changes in thermal resistance and was less complex, and was chosen for testing. Testing showed that changes in thermal resistance by a factor of 10 was possible with this type of thermal switch and this type of switching was applied for the heating and cooling of the Flat Bed system. The thermal switch control technique was successful and functioned better than predicted in the Flat Bed experiments. The thermal switch is not only applicable to distributed small-scale controls, but is also well suited for large-scale autonomous adsorption systems, offering a better alternative to the diurnal control methods investigated by other researchers. Autonomous systems at large scales are particularly appealing for solar heat driven applications where reliable electrical sources are limited for control and operation of the system. For large-scale autonomous solar heat driven systems, higher COPs and SCCs can be achieved without significant increases in system complexity.

8.3 Recommendations

To address the key fundamental scaling issues identified in this work, the following methods are proposed for small-scale systems. Then recommendations are made for future improvement of the absorbent bed concepts tested in this work.

The increased ratio of structural material to adsorbent material leads to larger dynamic losses at small-scales. This is unavoidable, as it is nearly impossible to thermally isolate the chamber walls or to otherwise reduce the structural material size. Future work on adsorption at this scale should investigate alternative structural materials for the adsorbent bed. Lower thermal capacities will reduce the contribution of the material contribution to dynamic losses in each cycle. A composite structure made of fiberglass or polymer backing with a metal film coating the inside of the adsorbent bed, as is used in lightweight pressurized canisters, would be appropriate for combining both the desired properties with low diffusion refrigerant losses from the system. Alternatively, ceramic materials or high density polymers with low refrigerant diffusivity could also be useful. These alternatives also have the positive effect of reducing the total system weight. Materials with lower thermal conductivities or an adsorbent bed made of several materials may also reduce thermal shorting that allows heat input to bypass the adsorbent material and be lost to the surroundings.

As the bed is scaled down, connection volumes become significant compared to the adsorbent bed volume. These volumes offer the opportunity for undesirable condensation and then re-adsorption to occur from the connections rather than from the evaporator. The connection volumes must be limited as much as possible. Insulating connections and using low thermal capacity materials for these lines will also help reduce this effect. If a conventional bed design is to be used at this scale, insulation should be used to isolate the adsorbent from the chamber. The vapor gap employed in large scale systems is not viable at this scale as it can increase the bed footprint by a factor of 2 or

more. The insulation should be a fully solid material; a foam material may trap non-condensable gases that can poison system operation.

At this scale, it is also necessary to consider the pumping power and auxiliary component power use. In large systems, such power draws represent ~1% of the total power use for the system, but as the system is scaled down the ratio of the pumping power required for coupling fluid lines to the total power usage in the system increases.

Conduction heat transfer lengths between components also begin to play a part in small scale-adsorption systems. This factor is in competition with limiting the connection lengths. If the connection length is eliminated entirely, the conduction heat transfer from the bed will heat the evaporator and negate any cooling delivered by the system. The conduction heat transfer between components was mitigated in this work by having oversized evaporator and condenser components with long connection lengths to isolate the adsorbent bed from the other components.

The CHEC concept has been ruled out as viable with the current design. The losses due to refrigerant accumulation in connections are too great to allow the system to operate efficiently and convection cooling was lower than what was expected through modeling. A new arrangement of connections to mitigate these effects would improve the system efficiency. Better fin arrangement would allow better convection cooling. The fins also prevented the adsorbent material from packing as tightly as they could have otherwise. The reduction in adsorbent material is more significant than the increased heat transfer in the bed. Removal of the fins with tighter packing of adsorbent material would allow better performance. Lowering the thermal mass through welded rather than threaded connections would help the system, but addressing the connection volume issue

is more important. Thermal breaks to reduce the thermal shorting would improve the COP for the system, as shown in Chapter 3, but this requires identifying a compatible machinable material for use in creating these thermal breaks.

Future pathways for improvement of the Flat Bed concept are described here. The present work investigates a single adsorbent bed system. Two beds will allow more consistent cooling and because of the way heat is lost when the heating block is not connected to the adsorbent bed, adding a second bed utilizing the same heat source could be expected to nearly double the COP for the system. The concept could also be scaled up to utilize heat sources larger than 20 W. The air-coupled convection cooling approach may start to be limiting for systems with 1 kW or more heat input, but a range of lower heat input applications exist. The bed tested here was constructed so that it could be easily disassembled for examination. A future system could eliminate approximately 30% of the bed mass by eliminating the accessibility features. Similar reductions in the evaporator and condenser could be gained by eliminating the compression fittings, which could bring the total system weight below a kilogram with a total system volume of less than 250 cm^3. Recent research has characterized a number of composite adsorbent materials. A similar system constructed with activated carbon and alkali metal chlorides should be able to achieve increases in COPs and cooling capacities of at least 50% and may even double the system performance (Wang *et al.*, 2005a; Tso *et al.*, 2012). Combining a two bed system using the Flat Bed concept with composite adsorbents, COPs as high as 0.1 and SCCs as high as 150 W kg^{-1} could be achievable without increasing the system complexity.

APPENDIX A UNCERTAINTY ANALYSIS

Uncertainty propagation for the heat transfer measurements is discussed here. The heat transfer measurement depends upon the measurement of the temperature change of the water and the mass flow rate of the water flowing through the heat exchanger

$$\dot{Q}_i = c_p \dot{m}_i \left(T_{in} - T_{out}\right) \tag{A.1}$$

The uncertainty in both temperature measurements is ±0.1ºC and the uncertainty in the mass flow rate is ±0.04 mg s^{-1}. The specific heat for the water is taken from literature values and is assumed to be equal to that of water at 25ºC at atmospheric pressure. The error associated with the specific heat assumption is less than 0.1% or 0.005 kJ kg^{-1} K, due to the relatively small change in temperature of the coupling fluid in these tests. The uncertainty in the heat transfer rate is then determined by

$$U_{\dot{Q}} = \sqrt{\left(\left(\frac{d\dot{Q}}{d\dot{m}}\right)U_{\dot{m}}\right)^2 + \left(\left(\frac{d\dot{Q}}{dT_{in}}\right)U_{T_{in}}\right)^2 + \left(\left(\frac{d\dot{Q}}{dT_{out}}\right)U_{T_{out}}\right)^2 + \left(\left(\frac{d\dot{Q}}{dc_p}\right)U_{c_p}\right)^2} \tag{A.2}$$

When the differential terms are simplified in equation (A.2) the equation becomes

$$U_{\dot{Q}} = \sqrt{\left(c_p\left(T_{in} - T_{out}\right)U_{\dot{m}}\right)^2 + \left(\left(c_p\dot{m}\right)U_{T_{in}}\right)^2 + \left(\left(c_p\dot{m}\right)U_{T_{out}}\right)^2 + \left(\left(\dot{m}\left(T_{in} - T_{out}\right)\right)U_{c_p}\right)^2} \tag{A.3}$$

For our sample calculation, the mass flow rate is 1.25 g s^{-1}, the inlet temperature is 26.3ºC and the outlet temperature is 25.9ºC. Applying these representative values yields an uncertainty in the heat transfer measurement of

$$\begin{aligned} U_{\dot{Q}} &= \sqrt{\begin{array}{l}\left(4.181\frac{kJ}{kg-K}\left(26.3°C - 25.9°C\right)0.04\frac{g}{s}\right)^2 + \left(\left(4.181\frac{kJ}{kg-K}1.25\frac{g}{s}\right)0.1°C\right)^2 + \\ \left(\left(4.181\frac{kJ}{kg-K}1.25\frac{g}{s}\right)0.1°C\right)^2 + \left(\left(1.25\frac{g}{s}\left(26.3°C - 25.9°C\right)\right)0.005\frac{kJ}{kg-K}\right)^2\end{array}} \\ U_{\dot{Q}} &= \sqrt{\left(0.004475\,\mathrm{W}^2\right) + \left(0.273\,\mathrm{W}^2\right) + \left(0.273\,\mathrm{W}^2\right) + \left(6.25\times10^{-6}\,\mathrm{W}^2\right)} \\ U_{\dot{Q}} &= \pm 0.74\mathrm{W} \end{aligned} \tag{A.4}$$

The measured heat transfer for this sample point is 2.09 W, which results in a heat transfer measurement uncertainty of 35%. The uncertainty in the temperature measurements dominates the uncertainty in the heat transfer measurement and the uncertainty due to the mass flow rate measurement and the specific heat assumption may be neglected. In estimating the cycle cooling duty, when the measured heat transfer is not at least 30% larger than the uncertainty value, the heat transfer is assumed to be 0. For this sample case, only heat transfer duties of greater than 1 W are considered for determining the heat transfer in this case. When the flow rate is reduced, the uncertainty in the measurement decreases and it is possible to measure cooling duties as low as 0.3 W.

For the CHEC system, the volume of fluid in the tube-in-tube heat exchanger is approximately 12 mL, and a flow rate of 1.25 mL/s, the fluid in the channel stays in the channel for approximately 9 seconds. This allows the coupling fluid time to transfer heat with the refrigerant tube and create a measurable temperature difference. For the Flat Bed system, the volume of fluid in the tube-in-tube heat exchanger is approximately 4 mL, so that at a flow rate of 1 mL/s, the fluid in the channel stays in the channel for approximately 4 seconds. Due to the relatively low temperature difference throughout much of the process, there is insufficient time for the fluid to be heated in the heat exchanger. For this reason, the flow rate was lowered to 0.34 mL s^{-1}. This allows 9 seconds for the fluid to transfer heat with the fluid and the temperature change in the fluid stream is larger and can be more easily measured. This was accomplished by implementing a shunt valve into the fluid source that redirects a portion of the flow back to the fluid reservoir rather than through the heat exchanger.

To help visualize the time-dependent profile of the delivered cooling and the cooling that can be measured, Figure A.1 shows the measured heat transfer in the experiments for a Flat Bed test with a 20 W heat input and the predictions for the same modeling case. The red line shows the cut off, below which the cooling is assumed to be zero to avoid measuring noise as cooling. The peak cooling is similar, but is reached less rapidly and then the cooling falls below measureable levels more quickly. Noise in the data also results in a less smooth cooling shape. Some of the difference in cooling may be caused by difference between the actual convection coefficient and the assumed convection coefficient in the model.

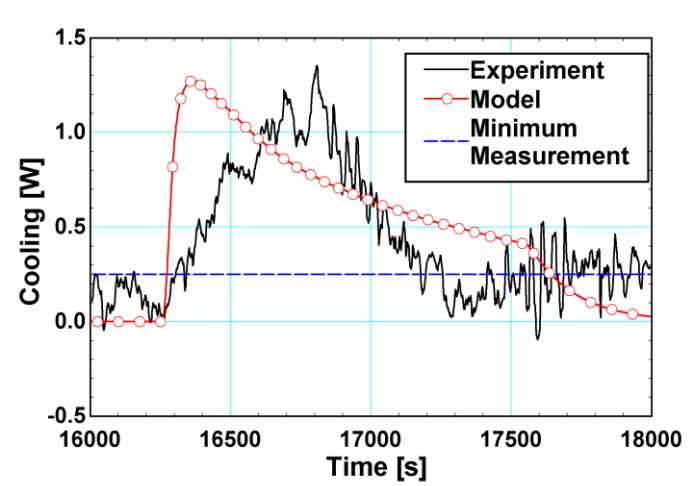

Figure A.1 Comparison of the modeled and the experimentally recorded cooling

APPENDIX B EFFECT OF PRECOOLING ON SYSTEM PERFORMANCE

When the system is operated using check valves to control refrigerant flow, the delivered cooling is consistent throughout the adsorption cycle. The cooling throughout the adsorption phase is on the verge of being measureable, resulting in large uncertainties, and the cooling is too low to be measureable at the start and end of the cooling phase. To mitigate this effect, a precooling time is allowed in the bed before the valves are opened. Because the adsorption process is limited by the heat transfer rate into the adsorbent and not the mass transfer, the precooling time allows the adsorbent to cool and when the valves are opened, the same amount of adsorption for the cycle occurs. If this is done correctly, the same amount of adsorption should be achievable in a shorter period of time, thereby increasing the cooling rate. This reduces the uncertainty and increases the amount of cooling that is in the measureable range. If the precooling time is too large, however, there will not be enough time for the refrigerant to be adsorbed regardless of the cooling of the bed and the total cooling will be reduced. There will be a slight decrease in heat removal rate, because the adsorption process heats the bed. Without the heat of adsorption being introduced, the bed temperature drops fasters and the driving temperature difference for cooling will be lower with precooling. In the precooling phase, heat is removed from the inert masses that contribute to dynamic losses and adsorption from the void space occurs, heating the adsorbent, minimizing the reduction in cooling rate due to lower temperature differences between the bed and surroundings.

A case study is performed to assess the impact on the measured cooling when a precooling phase is used to improve the measureable cooling rates. The Flat Bed system is heated for 10 W with cooling by natural convection with a 750 s heating time and 1250 s cooling time. The precooling time is modeled with no delay in valve openings, so that when the pressure has decreased below the evaporator pressure, the valve opens, after approximately 100 s. Figure B.1 shows the plotted cooling of several cycles and Table B.1 shows the COP for the system with the different precooling times. The start of the cooling phase is at 4750 s for the system without delays and the valve opens after approximately 50s. Cooling of the bed continues until 6000 s, when the bed begins heating for the desorption phase. There is some continued mass transfer for 10-20 seconds after this and then the valve closes. After 6000 s, most of the cooling is due to latent heating of the refrigerant and evaporator structure and not evaporation. It can be seen that with a 200 s precooling time, the initial cooling is truncated, and the cooling rate when the valve is first opened, at 4950 s, is about 0.05 W larger compared to the system without delays. The cooling rate stays larger throughout the cycle, but by 5500 s, cooling rates are within 1-2% of each other. There is almost no increase in peak cooling with the 200 s precooling time. As the precooling times are increased, the time where the cooling occurs is decreased and once cooling begins, the cooling rate is larger than it is for the cases without delays. With longer precooling times, the peak cooling rate increases by between 50-75% and the cooling is concentrated into approximately 50-70% of the time span.

Table B.1 summarizes the analysis of the system performance with varying precooling times. The SCC changes at the same rate as the COP for the Flat Bed system;

therefore, a comparison is not necessary. The change in COP is less than 3% for all of the precooling times less than 500 s. Beyond this precooling time the COP decreases because there is not enough time during the adsorption phase for all of the refrigerant to be adsorbed. Meanwhile, the percentage of the cooling that can be measured increases from 58.3% of the cooling with no delay to 76.8% at 500 s. It decreases again as the precooling time is increased, because the lower total cooling means a larger portion of the cooling is occurring in the desorption phase at a level too low to measure. It was decided that the ability to measure a larger portion of the cooling and the reduced uncertainty was worth the slight decrease in system performance.

Table B.1 Measureable vs. Predicted Cooling

Input Heat [W]	**Heating Time [s]**	**Cooling Time [s]**	**Precooling Time [s]**	**COP**	**COP Measured**	**Percent Measureable**
10	750	1250	No Delay	0.028	0.016	58.3%
			200	0.028	0.020	70.5%
			400	0.028	0.021	76.6%
			500	0.027	0.021	76.8%
			600	0.025	0.019	75.4%

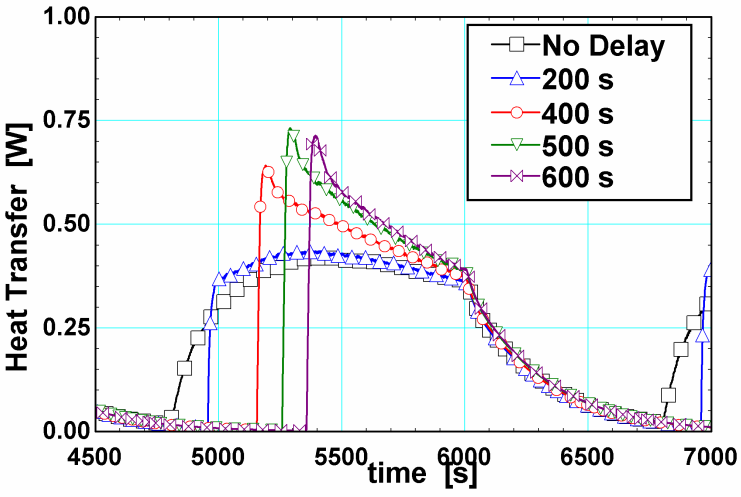

Figure B.1 Cooling rate for the system with different precooling times

APPENDIX C MODELING OF A SYSTEM WITH AND WITHOUT FLUID LEVEL CONTROL

In an adsorption system, the pressure difference in the evaporator and the condenser are not constant. The amount of refrigerant in each of these components fluctuates throughout the cycle. If a fixed expansion valve is used, refrigerant will tend to accumulate in either the evaporator or the condenser, which can severely impact system performance. Figure C.1 below shows the cooling over time for the conventional system model used as a baseline in Chapter 3 without a refrigerant level control and the refrigerant levels within the components over time. Three different modes of operation are shown. The first case (a and b in Figure C.1) is refrigerant accumulation in the condenser. (a) shows that with each cycle, the amount of refrigerant in the condenser increases and the rate of accumulation increases until the evaporator dries out. Notice that for many cycles, the cooling in the system appears to be at a steady state condition. Accumulation in the condenser is the most detrimental form of operation, because it leads to drying out of the evaporator during the adsorption phase. Without refrigerant in the evaporator, cooling cannot occur for much of the cycle, drastically reducing the cooling capacity of the system. The COP and SCC can easily be reduced by 75% or more in this mode of operation. The second case (c and d) is refrigerant accumulation in the evaporator. Accumulation in the evaporator occurs when refrigerant flows too quickly from the condenser to the evaporator because the expansion valve is not constrictive enough. Again, there are several cycles with good performance before a problem is encountered. Accumulation of refrigerant in the evaporator has less impact upon the peak

cooling of the system and the reduction in SCC and COP is nowhere near as drastic as for the first case, but performance is still reduced. Notice that the heat transferred into the evaporator is negative for a large portion of the cycle indicating that heat is being transferred out of the evaporator to the environment. Because the condenser has dried out, the refrigerant flowing from the adsorbent bed does not condense before being passed to the evaporator, the refrigerant vapor is at a temperature higher than that of the conditioned space and the evaporator transfers heat to the conditioned space for a brief period of time. Often, the necessity of regulating the refrigerant level is left unmentioned in the literature, despite being a fundamental part of an adsorption system.

Refrigerant accumulation is important to consider for this work, because a materially compatible float valve of an appropriate size could not be found for the experimental facility. But using model comparisons, it was possible to show that the cooling for the system with refrigerant level control can be predicted accurately without valve controls, until a dry-out or flooding condition is reached. The refrigerant level is rebalanced between cases to prevent the off design conditions from being tested. For the dry-out case modeled, the dry-out case delivers 108% of the cooling in the cycles before dry-out conditions are reached. This is primarily due to the slower flow of warm refrigerant from the condenser which would increase the temperature in the evaporator during the evaporation phase. For the flooding case modeled, the system delivers 98% of the cooling for a case with active control. In the long term, these modes of operation are undesirable, but in the absence of an appropriately sized control valve, the performance with a fixed expansion valve will be sufficiently similar to the system operation to provide evaluation of system operation using the experimental results.

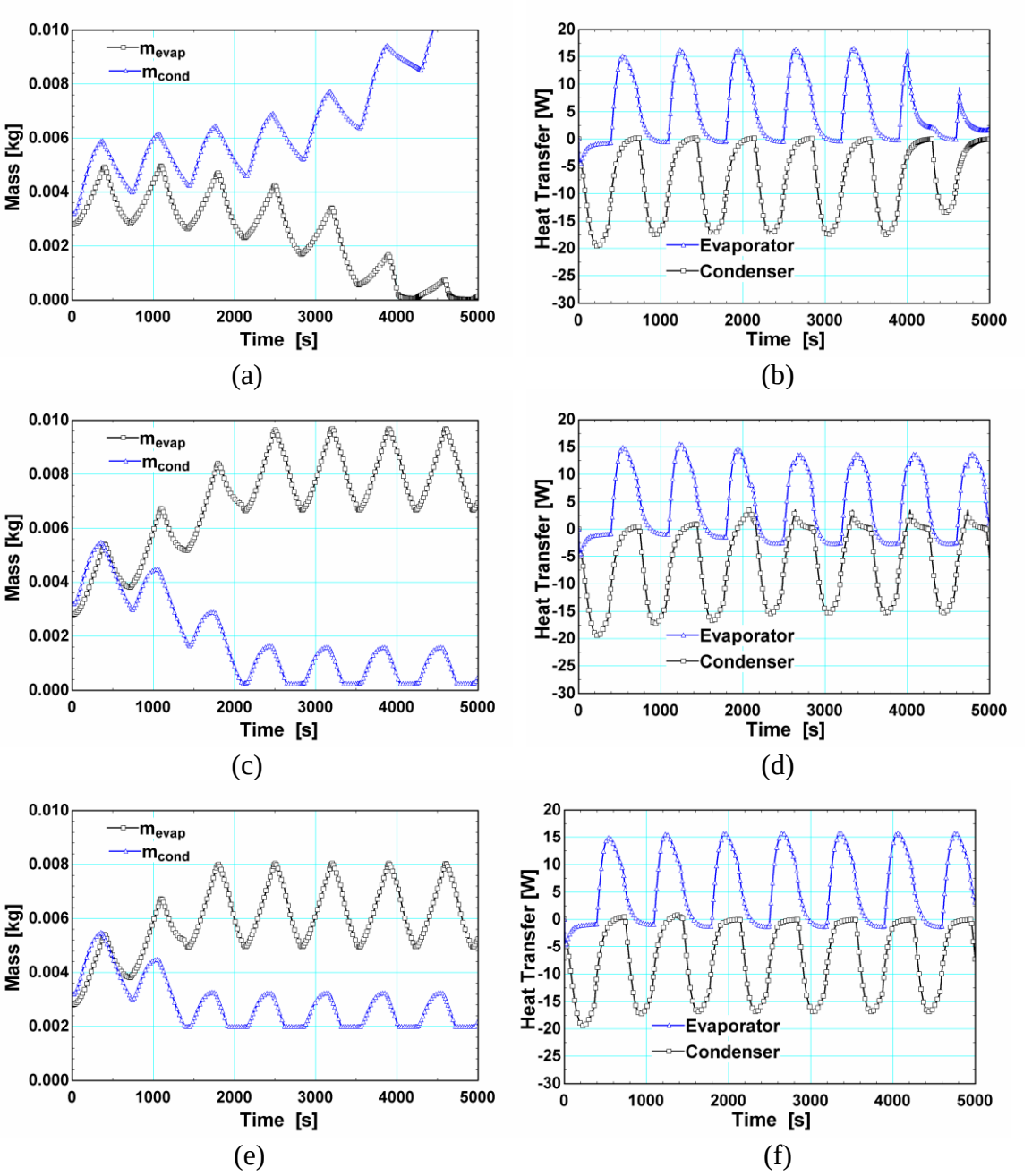

Figure C.1 (a) Shows the accumulation of refrigerant over time in the condenser of the system and (b) shows the heat transfer into the evaporator and out of the condenser. Notice that there is a critical point where the performance of the system drastically decreases. (c) shows the accumulation of the refrigerant in the evaporator over time and (d) shows the heat transfer into the evaporator and out of the condenser for the system. (e) shows the refrigerant levels with a float valve control regulating the refrigerant level and (f) shows the performance of this system.

REFERENCES

Akahira, A., K. C. A. Alam, Y. Hamamoto, A. Akisawa and T. Kashiwagi (2005), "Mass Recovery Four-Bed Adsorption Refrigeration Cycle with Energy Cascading," *Applied Thermal Engineering* Vol. 25 p. 15.

Al-Ghouti, M. A., I. Yousef, R. Ahmad, A. M. Ghrair and A. A. Al-Maaitah (2010), "Characterization of Diethyl Ether Adsorption on Activated Carbon Using a Novel Adsorption Refrigerator," *Chemical Engineering Journal* Vol. 162(1) pp. 234-241.

Alam, K. C. A., B. B. Saha, Y. T. Kang, A. Akisawa and T. Kashiwagi (2000), "Heat Exchanger Design Effect on the System Performance of Silica Gel Adsorption Refrigeration Systems," *International Journal of Heat and Mass Transfer* Vol. 43(24) pp. 4419-4431.

Alyousef, Y., A. A. Antukh, A. P. Tsitovich and L. L. Vasiliev (2012), "Three Adsorbers Solar Cooler with Composite Sorbent Bed and Heat Pipe Thermal Control," *Applied Thermal Engineering* Vol. 38(0) pp. 124-130.

Aristov, Y. I., B. Dawoud, I. S. Glaznev and A. Elyas (2008), "A New Methodology of Studying the Dynamics of Water Sorption/Desorption under Real Operating Conditions of Adsorption Heat Pumps: Experiment," *International Journal of Heat and Mass Transfer* Vol. 51(19–20) pp. 4966-4972.

Aristov, Y. I., G. Restuccia, G. Cacciola and V. N. Parmon (2002), "A Family of New Working Materials for Solid Sorption Air Conditioning Systems," *Applied Thermal Engineering* Vol. 22(2) pp. 191-204.

Askalany, A. A., B. B. Saha, K. Kariya, I. M. Ismail, M. Salem, A. H. H. Ali and M. G. Morsy (2012a), "Hybrid Adsorption Cooling Systems–an Overview," *Renewable and Sustainable Energy Reviews* Vol. 16(8) pp. 5787-5801.

Askalany, A. A., M. Salem, I. M. Ismail, A. H. H. Ali and M. G. Morsy (2012b), "A Review on Adsorption Cooling Systems with Adsorbent Carbon," *Renewable and Sustainable Energy Reviews* Vol. 16(1) pp. 493-500.

Attan, D., M. A. Alghoul, B. B. Saha, J. Assadeq and K. Sopian (2011), "The Role of Activated Carbon Fiber in Adsorption Cooling Cycles," *Renewable and Sustainable Energy Reviews* Vol. 15(3) pp. 1708-1721.

AZoNetwork, U. L. (2013). *Physical, Mechanical, Thermal, Electrical and Chemical Properties*, The A to Z of materials

Boatto, P., C. Boccaletti, G. Cerri and C. Malvicino (2000), "Internal Combustion Engine Waste Heat Potential for an Automotive Absorption System of Air Conditioning Part 2: The Automotive Absorption System," *Proceedings of the Institution of Mechanical Engineers, Part D: Journal of Automobile Engineering* Vol. 214(8) pp. 983-989.

Cacciola, G. and G. Restuccia (1995), "Reversible Adsorption Heat Pump: A Thermodynamic Model," *International Journal of Refrigeration* Vol. 18(2) p. 7.

Catarino, I., G. Bonfait and L. Duband (2008), "Neon Gas-Gap Heat Switch," *Cryogenics* Vol. 48 pp. 17-25.

Chan, K. C., C. Y. H. Chao, G. N. Sze-To and K. S. Hui (2012), "Performance Predictions for a New Zeolite 13x/Cacl2 Composite Adsorbent for Adsorption Cooling Systems," *International Journal of Heat and Mass Transfer* Vol. 55(11–12) pp. 3214-3224.

Chang, W. S., C. C. Wang and C. C. Shieh (2009), "Design and Performance of a Solar-Powered Heating and Cooling System Using Silica Gel/Water Adsorption Chiller," *Applied Thermal Engineering* Vol. 29(10) pp. 2100-2105.

Chen, C. J., R. Z. Wang, Z. Z. Xia, J. K. Kiplagat and Z. S. Lu (2010), "Study on a Compact Silica Gel–Water Adsorption Chiller without Vacuum Valves: Design and Experimental Study," *Applied Energy* Vol. 87(8) pp. 2673-2681.

Chua, H. T., K. C. Ng, W. Wang, C. Yap and X. L. Wang (2004), "Transient Modeling of a Two-Bed Silica Gel–Water Adsorption Chiller," *International Journal of Heat and Mass Transfer* Vol. 47(4) pp. 659-669.

Churchill, S. W. and H. H. S. Chu (1975a), "Correlating Equations for Laminar and Turbulent Free Convection from a Horizontal Cylinder," *International Journal of Heat and Mass Transfer* Vol. 18(9) pp. 1049-1053.

Churchill, S. W. and H. H. S. Chu (1975b), "Correlating Equations for Laminar and Turbulent Free Convection from a Vertical Plate," *International Journal of Heat and Mass Transfer* Vol. 18(11) pp. 1323-1329.

Clausse, M., K. C. A. Alam and F. Meunier (2008), "Residential Air Conditioning and Heating by Means of Enhanced Solar Collectors Coupled to an Adsorption System," *Solar Energy* Vol. 82(10) pp. 885-892.

Critoph, R. E. (1988), "Performance Limitations of Adsorption Cycles for Solar Cooling," *Solar Energy* Vol. 41(1) pp. 21-31.

Critoph, R. E. (1989a), "Activated Carbon Adsorption Cycles for Refrigeration and Heat Pumping," *Proceedings of the Conference on Porosity and Carbon materials: Measurements and applications* Vol. 27(1) pp. 63-70.

Critoph, R. E. (1989b), "Activated Carbon Adsorption Cycles for Refrigeration and Heat Pumping," *Carbon* Vol. 27(1) pp. 63-70.

Critoph, R. E. (1994a), "An Ammonia Carbon Solar Refrigerator for Vaccine Cooling," *Renewable Energy* Vol. 5(1–4) pp. 502-508.

Critoph, R. E. (1994b), "Forced Convection Enhancement of Adsorption Cycles," *Heat Recovery Systems & CHP* Vol. 14(4) p. 8.

Critoph, R. E. (1996), "Evaluation of Alternative Refrigerant-Adsorbent Pairs for Refrigeration Cycles," *Applied Thermal Engineering* Vol. 16(11) pp. 891-900.

Critoph, R. E. (1998), "Forced Convection Adsorption Cycles," *Applied Thermal Engineering* Vol. 18(9–10) pp. 799-807.

Critoph, R. E. (2002), "Multiple Bed Regenerative Adsorption Cycle Using the Monolithic Carbon–Ammonia Pair," *Applied Thermal Engineering* Vol. 22(6) pp. 667-677.

Critoph, R. E. and S. J. Metcalf (2004), "Specific Cooling Power Intensification Limits in Ammonia-Carbon Adsorption Refrigeration Systesm," *Applied Thermal Engineering* Vol. 24 pp. 661-678.

Critoph, R. E. and L. Turner (1995), "Heat Transfer in Granular Activated Carbon Beds in the Presence of Adsorbable Gases," *International Journal of Heat and Mass Transfer* Vol. 38(9) pp. 1577-1585.

Danica, M. H. and K. S. W. Sing (1961), "The Surface Properties of Silica Gels. Iii Adsorption of Benzene and Ethanol Vapours," *Journal of Applied Chemistry* Vol. 11(9) pp. 313-317.

Delano, A. (1997). *Analysis of the Einstein Refrigeration Cycle*. Mechanical Engineering, Georgia Institute of Technology, Vol. Masters.

Delano, A. (1998). *Design Analysis of the Einstein Refrigeration Cycle*. Mechanical Engineering. Atlanta, Georgia Institute of Technology, Vol. Doctorate.

Demir, H., M. Mobedi and S. Ülkü (2008), "A Review on Adsorption Heat Pump: Problems and Solutions," *Renewable and Sustainable Energy Reviews* Vol. 12(9) pp. 2381-2403.

Demir, H., M. Mobedi and S. Ülkü (2010), "The Use of Metal Piece Additives to Enhance Heat Transfer Rate through an Unconsolidated Adsorbent Bed," *International Journal of Refrigeration* Vol. 33(4) pp. 714-720.

Deng, J., R. Z. Wang and G. Y. Han (2011), "A Review of Thermally Activated Cooling Technologies for Combined Cooling, Heating and Power Systems," *Progress in Energy and Combustion Science* Vol. 37(2) pp. 172-203.

Determan, M. D. and S. Garimella (2010). *A Microscale Monolithic Absorption Heat Pump*. International Refrigeration and Air Conditioning Conference. Purdue University.

DiSalvo, F. J. (1999), "Thermoelectric Cooling and Power Generation," *Science* Vol. 285(5428) pp. 703-706.

Do, D. D. (1998). *Adsorption Analysis: Equilibria and Kinetics*. London, Imperial College Press.

Dubinin, M. M. and V. A. Astakhov (1971), "Development of the Concepts of Volume Filling of Micropores in the Adsorption of Gases and Vapors by Microporous Adsorbents," *Bulletin of the Academy of Sciences of the USSR, Division of chemical science* Vol. 20(1) pp. 3-7.

El-Sharkawy, I. I. (2011), "On the Linear Driving Force Approximation for Adsorption Cooling Applications," *International Journal of Refrigeration* Vol. 34(3) pp. 667-673.

El-Sharkawy, I. I., M. Hassan, B. B. Saha, S. Koyama and M. M. Nasr (2009), "Study on Adsorption of Methanol onto Carbon Based Adsorbents," *International Journal of Refrigeration* Vol. 32(7) pp. 1579-1586.

El-Sharkawy, I. I., B. B. Saha, S. Koyama, J. He, K. C. Ng and C. Yap (2008), "Experimental Investigation on Activated Carbon–Ethanol Pair for Solar Powered Adsorption Cooling Applications," *International Journal of Refrigeration* Vol. 31(8) pp. 1407-1413.

El-Sharkawy, I. I., B. B. Saha, S. Koyama and K. C. Ng (2006), "A Study on the Kinetics of Ethanol-Activated Carbon Fiber: Theory and Experiments," *International Journal of Heat and Mass Transfer* Vol. 49 p. 7.

Engineering Toolbox (2013). *Material Properties*, The Engineering Toolbox, Vol. 2014.

Fried, E. (1969). *Thermal Conduction Contribution to Heat Transfer at Contacts*. London, Academic Press.

Garimella, S., A. M. Brown and A. K. Nagavarapu (2011), "Waste Heat Driven Absorption/Vapor-Compression Cascade Refrigeration System for Megawatt Scale, High-Flux, Low-Temperature Cooling," *International Journal of Refrigeration* Vol. 34(8) pp. 1776-1785.

Glaznev, I. S. and Y. I. Aristov (2010), "The Effect of Cycle Boundary Conditions and Adsorbent Grain Size on the Water Sorption Dynamics in Adsorption Chillers," *International Journal of Heat and Mass Transfer* Vol. 53(9–10) pp. 1893-1898.

Goetz, V., B. Spinner and E. Lepinasse (1997), "A Solid-Gas Thermochemical Cooling System Using Bacl2 and Nicl2," *Energy* Vol. 22(1) pp. 49-58.

Gräber, M., C. Kirches, H. G. Bock, J. P. Schlöder, W. Tegethoff and J. Köhler "Determining the Optimum Cyclic Operation of Adsorption Chillers by a Direct Method for Periodic Optimal Control," *International Journal of Refrigeration* Vol. In Press, Corrected Proof.

Gräber, M., C. Kirches, H. G. Bock, J. P. Schlöder, W. Tegethoff and J. Köhler (2011), "Determining the Optimum Cyclic Operation of Adsorption Chillers by a Direct Method for Periodic Optimal Control," *International Journal of Refrigeration* Vol. 34(4) pp. 902-913.

Gupta, Y., L. Metchop, A. Frantzis and P. E. Phelan (2008), "Comparative Analysis of Thermally Activated, Environmentally Friendly Cooling Systems," *Energy Conversion and Management* Vol. 49(5) pp. 1091-1097.

H.T. Chua, K.C. Ng, A. Malek, T. Kashiwagi, A. Akisawa and B. B. Saha (1999), "Modeling the Performance of Two-Bed, Sillica Gel-Water Adsorption Chillers," *International Journal of Refrigeration* Vol. 22 pp. 194-204.

Habib, K., B. B. Saha, A. Chakraborty, S. Koyama and K. Srinivasan (2011), "Performance Evaluation of Combined Adsorption Refrigeration Cycles," *International Journal of Refrigeration* Vol. 34(1) pp. 129-137.

Habib, K., B. B. Saha, K. A. Rahman, A. Chakraborty, S. Koyama and K. C. Ng (2010), "Experimental Study on Adsorption Kinetics of Activated Carbon/R134a and Activated Carbon/R507a Pairs," *International Journal of Refrigeration* Vol. 33(4) pp. 706-713.

Hajji, A. and S. Khalloufi (1996), "Improving the Performance of Adsorption Heat Exchangers Using a Finned Structure," *International Journal of Heat and Mass Transfer* Vol. 39(8) pp. 1677-1686.

Hassan, H. Z., A. A. Mohamad and R. Bennacer (2011), "Simulation of an Adsorption Solar Cooling System," *Energy* Vol. 36(1) pp. 530-537.

Headley, O. S., A. F. Kothdiwala and I. A. McDoom (1994), "Charcoal-Methanol Adsorption Refrigerator Powered by a Compound Parabolic Concentrating Solar Collector," *Solar Energy* Vol. 53(2) pp. 191-197.

Huangfu, Y., J. Y. Wu, R. Z. Wang and Z. Z. Xia (2007), "Experimental Investigation of Adsorption Chiller for Micro-Scale Bchp System Application," *Energy and Buildings* Vol. 39(2) pp. 120-127.

Hyeun-Su, K., L. Hsien-Hsin, S. Hyun Oh and T. W. Kenny (2008), "Variable Thermal Resistors (Vtr) for Thermal Management of Chip Scale Atomic Clocks (Csac)," *Micro Electro Mechanical Systems, 2008. MEMS 2008. IEEE 21st International Conference on*, pp. 852-855.

Incropera, F. P. and D. P. DeWitt (1996). *Fundamentals of Heat and Mass Transfer*. 4th Ed. New York, John Wiley & Sons.

Jiang-Jiang, W., Z. Chun-Fa and J. You-Yin (2010), "Multi-Criteria Analysis of Combined Cooling, Heating and Power Systems in Different Climate Zones in China," *Applied Energy* Vol. 87(4) pp. 1247-1259.

Kays, W. and H. Perkins (1972), "Handbook of Heat Transfer," *New York*.

Khan, M. Z. I., K. C. A. Alam, B. B. Saha, A. Akisawa and T. Kashiwagi (2007), "Study on a Re-Heat Two-Stage Adsorption Chiller – the Influence of Thermal Capacitance Ratio, Overall Thermal Conductance Ratio and Adsorbent Mass on System Performance," *Applied Thermal Engineering* Vol. 27(10) pp. 1677-1685.

Khan, M. Z. I., K. C. A. Alam, B. B. Saha, A. Akisawa and T. Kashiwagi (2008), "Performance Evalution of Multi-Stage, Multi-Bed Adsorption Chiller Employing Re-Heat Scheme," *Renewable Energy* Vol. 33 p. 11.

Klein, S. A. (2009). *Engineering Equation Solver*, F-Chart Software.

Kong, X. Q., R. Z. Wang, J. Y. Wu, X. H. Huang, Y. Huangfu, D. W. Wu and Y. X. Xu (2005), "Experimental Investigation of a Micro-Combined Cooling, Heating and Power System Driven by a Gas Engine," *International Journal of Refrigeration* Vol. 28(7) pp. 977-987.

Konoshima, C. (2010). *Application of Magnesium Compounds to Insulating Heat-Conductive Fillers*, Konoshima Chemical, Vol. 2013 p. A chemical company materials property page.

Kubota, M., T. Ueda, R. Fujisawa, J. Kobayashi, F. Watanabe, N. Kobayashi and M. Hasatani (2008), "Cooling Output Performance of a Prototype Adsorption Heat Pump with Fin-Type Silica Gel Tube Module," *Applied Thermal Engineering* Vol. 28(2-3) pp. 87-93.

Lambert, M. A. and B. J. Jones (2006), "Automotive Adsorption Air Conditioner Powered by Exhaust Heat. Part 2: Detailed Design and Analysis," *Proceedings of the Institution of Mechanical Engineers, Part D: Journal of Automobile Engineering* Vol. 220(7) pp. 973-989.

Leong, K. C. and Y. Liu (2004), "Numerical Study of a Combined Heat and Mass Recovery Adsorption Cooling Cycle," *International Journal of Heat and Mass Transfer* Vol. 47(22) pp. 4761-4770.

Leong, K. C. and Y. Liu (2006), "System Performance of a Combined Heat and Mass Recovery Adsorption Cooling Cycle: A Parametric Study," *International Journal of Heat and Mass Transfer* Vol. 49(15–16) pp. 2703-2711.

Li, S. and J. Y. Wu (2009), "Theoretical Research of a Silica Gel–Water Adsorption Chiller in a Micro Combined Cooling, Heating and Power (Cchp) System," *Applied Energy* Vol. 86(6) pp. 958-967.

Li, T. X., R. Z. Wang, J. K. Kiplagat and L. Ma (2012), "Performance Analysis of a Multi-Mode Thermochemical Sorption Refrigeration System for Solar-Powered Cooling," *International Journal of Refrigeration* Vol. 35(3) pp. 532-542.

Lu, Z. S., R. Z. Wang, L. w. Wang and C. J. Chen (2006), "Performance Analysis of an Adsorption Refrigerator Using Activated Carbon in a Compound Adsorbent," *Carbon* Vol. 44 pp. 747-752.

Martin, J. J. and Y.-C. Hou (1955), "Development of an Equation of State for Gases," *AIChE Journal* Vol. 1(2) pp. 142-151.

Milanez, F. H. and M. B. H. Mantelli (2003), "Theoretical and Experimental Studies of a Bi-Metallic Heat Switch for Space Applications," *International Journal of Heat and Mass Transfer* Vol. 46(24) pp. 4573-4586.

Miles, D. J. and S. V. Shelton (1996), "Design and Testing of a Solid-Sorption Heat-Pump System," *Applied Thermal Engineering* Vol. 16(5) pp. 389-394.

Min, G. and N. M. Yatim (2008), "Variable Thermal Resistor Based on Self-Powered Peltier Effect," *Journal of Physics D: Applied Physics* Vol. 41(22) p. 222001.

Miyazaki, T. and A. Akisawa (2009), "The Influence of Heat Exchanger Parameters on the Optimum Cycle Time of Adsorption Chillers," *Applied Thermal Engineering* Vol. 29(13) pp. 2708-2717.

Miyazaki, T., A. Akisawa and B. B. Saha (2010), "The Performance Analysis of a Novel Dual Evaporator Type Three-Bed Adsorption Chiller," *International Journal of Refrigeration* Vol. 33(2) pp. 276-285.

Ng, K. C., X. Wang, Y. S. Lim, B. B. Saha, A. Chakarborty, S. Koyama, A. Akisawa and T. Kashiwagi (2006), "Experimental Study on Performance Improvement of a Four-Bed Adsorption Chiller by Using Heat and Mass Recovery," *International Journal of Heat and Mass Transfer* Vol. 49(19–20) pp. 3343-3348.

Norit (2008). Datasheet Norit Rb 30m, 2 p.

Phelan, P. E., V. A. Chiriac and T. Y. T. Lee (2002), "Current and Future Miniature Refrigeration Cooling Technologies for High Power Microelectronics," *Components and Packaging Technologies, IEEE Transactions on* Vol. 25(3) pp. 356-365.

Pons, M., D. Laurent and F. Meunier (1996), "Experimental Temperature Fronts for Adsorptive Heat Pump Applications," *Applied Thermal Engineering* Vol. 16(5) pp. 395-404.

Prina, M., P. Bhandari, R. C. J. Bowman, C. G. Paine and L. A. Wade (1999). *Development of Gas Gap Heat Switch Actuator for the Planck Sorption Cryocooler*. Cryogenic Engineering & International Cryogenic Materials Confence

Montreal, Canada.

Rattner, A. S. and S. Garimella (2011), "Energy Harvesting, Reuse and Upgrade to Reduce Primary Energy Usage in the USA," *Energy* Vol. 36(10) pp. 6172-6183.

Raymond, A. (2010). *Investigation of Microparticle to System Level Phenomena in Thermally Activated Adsorption Heat Pumps*. Mechanical Engineering. Atlanta, Georgia Institute of Technology, Vol. Master of Science p. 423.

Raymond, A. and S. Garimella (2009), "Use of the Linear Driving Force Approximation in Adsorption Heat Pump and Chiller Modeling," *ASME 2009 Heat Transfer Summer Conference*, San Francisco, California

Restuccia, G., A. Freni, F. Russo and S. Vasta (2005), "Experimental Investigation of a Solid Adsorption Chiller Based on a Heat Exchanger Coated with Hydrophobic Zeolite," *Applied Thermal Engineering* Vol. 25(10) pp. 1419-1428.

Restuccia, G., A. Freni, S. Vasta and Y. Aristov (2004), "Selective Water Sorbent for Solid Sorption Chiller: Experimental Results and Modelling," *International Journal of Refrigeration* Vol. 27 p. 10.

Rezk, A. R. M. and R. K. Al-Dadah (2012), "Physical and Operating Conditions Effects on Silica Gel/Water Adsorption Chiller Performance," *Applied Energy* Vol. 89(1) pp. 142-149.

Ryan, W. (2004), "Driving Absorption Chillers Using Heat Recovery," *ASHRAE Journal* Vol. 46(9) pp. S31-S38.

Saha, B. B., A. Chakraborty, S. Koyama and Y. I. Aristov (2009), "A New Generation Cooling Device Employing Cacl2-in-Silica Gel–Water System," *International Journal of Heat and Mass Transfer* Vol. 52(1–2) pp. 516-524.

Saha, B. B., A. Chakraborty, S. Koyama, S.-H. Yoon, I. Mochida, M. Kumja, C. Yap and K. C. Ng (2008), "Isotherms and Thermodynamics for the Adsorption of N-Butane on Pitch Based Activated Carbon," *International Journal of Heat and Mass Transfer* Vol. 51(7–8) pp. 1582-1589.

Saha, B. B., Elisa C. Boelman and T. Kashiwagi (1995), "Computational Analysis of an Advanced Adsorption-Refrigeration Cycle," *Energy* Vol. 20(10) pp. 983-994.

Sapienza, A., S. Santamaria, A. Frazzica and A. Freni (2011), "Influence of the Management Strategy and Operating Conditions on the Performance of an Adsorption Chiller," *Energy* Vol. 36(9) pp. 5532-5538.

Scott, D. M. (1994), "The Linear Driving Force Model for Cyclic Adsorption and Desorption: The Effect of Shape," *Chemical Engineering Science* Vol. 49(6) p. 3.

Shelton, S. V., W. J. Wepfer and D. J. Miles (1990), "Ramp Wave Analysis of the Solid/Vapor Heat Pump," *Journal of Energy Resources Technology* Vol. 112 p. 10.

Sinha, A. and Y. Joshi (2010), "Performance of Two-Step Thermoelectric-Adsorption Heat Pump for Harsh Environment Electronics Cooling," *Thermal and Thermomechanical Phenomena in Electronic Systems (ITherm), 2010 12th IEEE Intersociety Conference on*, pp. 1-9.

Srivastava, N. C. and I. W. Eames (1998), "A Review of Adsorbents and Adsorbates in Solid–Vapour Adsorption Heat Pump Systems," *Applied Thermal Engineering* Vol. 18(9–10) pp. 707-714.

Sumathy, K., K. H. Yeung and L. Yong (2003), "Technology Development in the Solar Adsorption Refrigeration Systems," *Progress in Energy and Combustion Science* Vol. 29(4) pp. 301-327.

Sun, L. M., Y. Feng and M. Pons (1997), "Numerical Investigation of Adsorptive Heat Pump Systems with Thermal Wave Heat Regeneration under Uniform-Pressure Conditions," *International Journal of Heat and Mass Transfer* Vol. 40(2) pp. 281-293.

Suzuki, M. (1993), "Application of Adsorption Cooling Systems to Automobiles," *Heat Recovery Systems and CHP* Vol. 13(4) pp. 335-340.

Sward, B. K., M. D. LeVan and F. Meunier (2000), "Adsorption Heat Pump Modeling: The Thermal Wave Process with Local Equilibrium," *Applied Thermal Engineering* Vol. 20(8) pp. 759-780.

Szekely, V. and G. Mezosi (2006). *Design Issues of a Variable Thermal Resistance*. Dans Proceedings of 12th International Workshop on Thermal investigations of ICs. Nice, France.

Tamainot-Telto, Z. and R. E. Critoph (1997), "Adsorption Refrigerator Using Monolithic Carbon-Ammonia Pair," *International Journal of Refrigeration* Vol. 20(2) pp. 146-155.

Tamainot-Telto, Z. and R. E. Critoph (2000), "Thermophysical Properties of Monolithic Carbon," *International Journal of Heat and Mass Transfer* Vol. 43(11) pp. 2053-2058.

Tamainot-Telto, Z., S. J. Metcalf and R. E. Critoph (2008), "Novel Compact Sorption Generators for Car Air Conditioning," *International Sorption Heat Pump Conference 2008*.

Tellurex (2013). *Tellurex Information Page*. Traverse City, MI, Vol. 2013 p. A manufacturer of thermoelectric devices.

Tso, C. Y., C. Y. H. Chao and S. C. Fu (2012), "Performance Analysis of a Waste Heat Driven Activated Carbon Based Composite Adsorbent – Water Adsorption Chiller Using Simulation Model," *International Journal of Heat and Mass Transfer*(0).

U.S. Energy Information Administration (2009). Residential Energy Consumption Survey. U.S. Energy Information Administration. http://www.eia.gov/consumption/residential/index.cfmp.

Wang, D. C., Y. H. Li, D. Li, Y. Z. Xia and J. P. Zhang (2010), "A Review on Adsorption Refrigeration Technology and Adsorption Deterioration in Physical Adsorption Systems," *Renewable and Sustainable Energy Reviews* Vol. 14(1) pp. 344-353.

Wang, D. C., Y. J. Wang, J. P. Zhang, X. L. Tian and J. Y. Wu (2008), "Experimental Study of Adsorption Chiller Driven by Variable Heat Source," *Energy Conversion and Management* Vol. 49(5) pp. 1063-1073.

Wang, L., L. Chen, H.L. Wang and D. L. Liao (2009a), "The Adsorption Refrigeration Characteristics of Alkaline-Earth Metal Chlorides and Its Composite Adsorbents," *Renewable Energy* Vol. 34.

Wang, L., R. Wang, J. Wu and K. Wang (2005a), "Research on the Chemical Adsorption Precursor State of $Cacl_2$-Nh_3 for Adsorption Refrigeration," *Science in China: Series E Engineering and Materials Science* Vol. 48(1) p. 13.

Wang, L., R. Wang, J. Wu and K. Wang (2005b), "Research on the Chemical Adsorption Precursor State of Cacl2−Nh3 for Adsorption Refrigeration," *Science in China Series E: Technological Sciences* Vol. 48(1) pp. 70-82.

Wang, L. W., R. Z. Wang, Z. S. Lu, C. J. Chen, K. Wang and J. Y. Wu (2006), "The Performance of Two Adsorption Ice Making Test Units Using Activated Carbon and a Carbon Composite as Adsorbents," *Carbon* Vol. 44 p. 10.

Wang, L. W., R. Z. Wang and R. G. Oliveira (2009b), "A Review on Adsorption Working Pairs for Refrigeration," *Renewable and Sustainable Energy Reviews* Vol. 13 pp. 518-534.

Wang, L. W., R. Z. Wang, J. Y. Wu and K. Wang (2004a), "Compound Adsorbent for Adsorption Ice Maker on Fishing Boats," *International Journal of Refrigeration* Vol. 27 p. 8.

Wang, L. W., R. Z. Wang, J. Y. Wu, K. Wang and S. G. Wang (2004b), "Adsorption Ice Makers for Fishing Boats Driven by the Exhaust Heat from Diesel Engine: Choice

of Adsorption Pair," *Energy Conversion and Management* Vol. 45(13–14) pp. 2043-2057.

Wang, L. W., J. Y. Wu, R. Z. Wang, Y. X. Xu, S. G. Wang and X. R. Li (2003), "Study of the Performance of Activated Carbon–Methanol Adsorption Systems Concerning Heat and Mass Transfer," *Applied Thermal Engineering* Vol. 23(13) pp. 1605-1617.

Wang, Q., X. Gao, J. Y. Xu, A. S. Maiga and G. M. Chen (2012), "Experimental Investigation on a Fluidized-Bed Adsorber/Desorber for the Adsorption Refrigeration System," *International Journal of Refrigeration* Vol. 35(3) pp. 694-700.

Wang, R. Z., M. Li, Y. X. Xu and J. Y. Wu (2000), "An Energy Efficient Hybrid System of Solar Powered Water Heater and Adsorption Ice Maker," *Solar Energy* Vol. 68(2) pp. 189-195.

Wang, R. Z. and R. G. Oliveira (2006), "Adsorption Refrigeration—an Efficient Way to Make Good Use of Waste Heat and Solar Energy," *Progress in Energy and Combustion Science* Vol. 32(4) pp. 424-458.

Wang, X. and H. T. Chua (2007a), "A Comparative Evaluation of Two Different Heat-Recovery Schemes as Applied to a Two-Bed Adsorption Chiller," *International Journal of Heat and Mass Transfer* Vol. 50(3–4) pp. 433-443.

Wang, X. and H. T. Chua (2007b), "Two Bed Silica Gel–Water Adsorption Chillers: An Effectual Lumped Parameter Model," *International Journal of Refrigeration* Vol. 30(8) pp. 1417-1426.

Wu, J. Y. and S. Li (2009), "Study on Cyclic Characteristics of Silica Gel–Water Adsorption Cooling System Driven by Variable Heat Source," *Energy* Vol. 34(11) pp. 1955-1962.

Xia, Z. Z., R. Z. Wang, D. C. Wang, Y. L. Liu, J. Y. Wu and C. J. Chen (2009), "Development and Comparison of Two-Bed Silica Gel–Water Adsorption Chillers Driven by Low-Grade Heat Source," *International Journal of Thermal Sciences* Vol. 48(5) pp. 1017-1025.

Xiaobao, G., P. Patel and D. D. Meng (2010), "A Self-Adaptive Thermal Switch Array to Stabilize the Temperature of Mems Devices," *Micro Electro Mechanical Systems (MEMS), 2010 IEEE 23rd International Conference on*, pp. 148-151.

Xu, L., R. Z. Wang, T. X. Li and L. W. Wang (2011), "Experimental Study on a Combined Double-Way Chemisorption Refrigeration System," *International Journal of Refrigeration* Vol. 34(4) pp. 914-921.

Yang, G. Z., Z. Z. Xia, R. Z. Wang, D. Keletigui, D. C. Wang, Z. H. Dong and X. Yang (2006), "Research on a Compact Adsorption Room Air Conditioner," *Energy Conversion and Management* Vol. 47(15–16) pp. 2167-2177.

Yang, J., Ed. (2005). *Materials and Technologies for Direct Thermal-to-Electric Energy Conversion : Symposium Held November 28 - December 2*. Boston.

Yao, C. and C. Tien (1998), "Application of New Rate Models to Cyclic Adsorption in Adsorbents," *Chemical Engineering Science* Vol. 53(21) p. 4.

Zhang, L. Z. and L. Wang (1999), "Effects of Coupled Heat and Mass Transfers in Adsorbent on the Performance of a Waste Heat Adsorption Cooling Unit," *Applied Thermal Engineering* Vol. 19(2) pp. 195-215.

Zhong, Y., R. E. Critoph, R. N. Thorpe, Z. Tamainot-Telto and Y. I. Aristov (2007), "Isothermal Sorption Characteristics of the Bacl2-Nh3 Pair in a Vermiculite Host Matrix," *Applied Thermal Engineering* Vol. 27(14-15) pp. 2455-2462.

Ziegler, F. (1999), "Recent Developments and Future Prospects of Sorption Heat Pump Systems," *International Journal of Thermal Sciences* Vol. 38(3) pp. 191-208.

Ziegler, F. (2002), "State of the Art in Sorption Heat Pumping and Cooling Technologies," *International Journal of Refrigeration* Vol. 25(4) pp. 450-459.

Zukauskas, A. (1973), "Heat Transfer from Tubes in Crossfiow," *Advances in heat transfer* Vol. 8 p. 93.